

Aus dem Institut für Molekulare Onkologie
Direktor: Prof. Dr. Thorsten Stiewe
des Fachbereichs Medizin der Philipps-Universität Marburg

**Establishment and characterization of preclinical
mouse models for evaluation of oncogenic and tumor-
suppressive properties of p53 family members**

Inaugural-Dissertation zur Erlangung des Doktorgrades der
Naturwissenschaften
dem Fachbereich Medizin der Philipps-Universität Marburg
vorgelegt von

Jeannette Fuchs

aus Karlsruhe

Marburg, 2017

Angenommen vom Fachbereich Medizin der Philipps-Universität Marburg am:
22.03.2017

Gedruckt mit Genehmigung des Fachbereichs.

Dekan: Herr Prof. Dr. H. Schäfer

Referent: Herr Prof. Dr. T. Stiewe

1. Korreferent: Frau Prof. Dr. U.-M. Bauer

für Ursula Bertha Elly Voss

Table of Contents

Table of Contents.....	I
Abstract	V
Zusammenfassung	VII
1 Introduction	1
1.1 Cancer.....	1
1.2 Limitations of cancer treatment	2
1.2.1 Cancer - a war on multiple fronts	2
1.2.2 Methods for monitoring and modelling of tumor heterogeneity	6
1.3 The p53 family members.....	8
1.3.1 p53.....	10
1.3.2 p73-a complicated gene	12
1.3.3 TAp73-a bird in the hand is worth two in the bush	14
1.3.4 Δ Np73-the bad apple	16
1.4 Developmental defects in mouse models of the p53 family.....	18
2 Material and Methods.....	21
2.1 Material	21
2.1.1 Mouse strains	21
2.1.2 Cell lines	21
2.1.3 Bacterial strains	22
2.1.4 Plasmids	22
2.1.5 Oligonucleotides	23
2.1.5.1 siRNAs.....	23
2.1.5.2 shRNAs	23
2.1.5.3 Primers.....	23
2.1.6 Antibodies.....	25
2.1.6.1 Primary antibodies.....	25
2.1.6.2 Secondary antibodies	25
2.1.7 Chemicals.....	26
2.1.8 Consumables.....	26
2.1.9 Hardware and devices	26
2.2 Methods	28
2.2.1 Molecular Biology	28
2.2.1.1 Genotyping PCR.....	28
2.2.1.2 Separation of nucleic acids by agarose gel electrophoresis	29
2.2.1.3 Genomic DNA (gDNA) isolation from mammalian cells	30

Table of Contents

2.2.1.4	RNA Isolation from mammalian cell culture	30
2.2.1.5	RNA isolation from tissue	30
2.2.1.6	cDNA synthesis	31
2.2.1.7	qPCR	31
2.2.1.8	Semiquantitative PCR.....	33
2.2.1.9	Two-color based Microarray.....	34
2.2.1.10	Digital PCR.....	36
2.2.1.11	Gateway cloning.....	39
2.2.1.12	Transformation of <i>E.coli</i> by electroporation.....	39
2.2.1.13	Plasmid DNA isolation from bacteria.....	39
2.2.2	Proteinbiochemistry	40
2.2.2.1	Preparation of protein lysates	40
2.2.2.2	Protein separation by SDS Page.....	41
2.2.2.3	Protein detection by Western Blot	41
2.2.2.4	Chromatin immunoprecipitation	42
2.2.2.5	Histopathology and Immunohistochemistry (IHC)	43
2.2.3	Cell biology	45
2.2.3.1	Cultivation of mammalian cells.....	45
2.2.3.2	Preparation of murine embryonic fibroblasts (MEFs)	46
2.2.3.3	Manipulation of cells.....	46
2.2.3.4	Luminescent cell viability assay.....	48
2.2.3.5	Monitoring of luciferase-labeled tumor cells	48
2.2.4	Animal experiments	49
2.2.4.1	Breeding of mice.....	50
2.2.4.2	Induction of the EF1 α - Δ Np73 transgene	50
2.2.4.3	Survival analysis of transgenic mice	50
2.2.4.4	Transplantation of established tumor cell lines.....	50
2.2.4.5	Monitoring of luciferase-labeled tumor cells in vivo	51
3	Results	55
3.1	Establishment of an assay to monitor the dynamics of clonal tumor evolution in vivo using secreted luciferases	55
3.1.1	Characterization of combined applications of GLuc and CLuc in vitro	55
3.1.2	Characterization of combined GLuc/CLuc applications in vivo	59
3.1.3	Monitoring shRNA-induced heterogeneity of tumors under chemotherapy	63
3.1.4	Application of the GLuc/CLuc assay in experimental metastasis..	67

3.1.5	Expanding the GLuc/CLuc assay to an inducible system for knockdown of essential tumor genes.....	72
3.1.5.1	Knockdown of p73 reduces tumorigenicity in Hs 766T cells	72
3.1.5.2	Reintroduction of p73 isoforms identifies Δ Np73 as essential tumor factor in Hs 766T	75
3.1.6	Low immunogenicity of luciferases in immunocompetent mice	80
3.2	Characterization of a mouse model overexpressing oncogenic Δ Np73... ..	84
3.2.1	Impact of the Δ Np73-transgene on murine embryonic fibroblasts	86
3.2.1.1	Validation of the Δ Np73-transgene expression and functionality in MEFs... ..	86
3.2.1.2	Whole transcriptome analysis of Δ Np73-overexpressing MEFs.....	88
3.2.2	Expression analysis of the Δ Np73-transgene in murine organs....	92
3.2.3	Reproductive defects of Δ Np73 transgenic mice	94
3.2.3.1	Infertility of Δ Np73-overexpressing males.....	94
3.2.3.2	Embryonic lethality of Δ Np73-overexpressing offspring from rec- Δ Np73 females	95
3.2.4	Δ Np73-overexpressing mice lack a tumorigenic phenotype	98
3.2.5	Impact of the Δ Np73-transgene on the tumor phenotype of the p53-knockout mouse model.....	99
4	Discussion	105
4.1	A dual luciferase assay to monitor tumor heterogeneity in solid tumors in vivo	105
4.1.1	Limitations of imaging techniques for solid tumors in small experimental animals.....	105
4.1.2	Combined applications of GLuc and CLuc to monitor tumor composition	108
4.1.3	Endpoint analyses confirm results from luciferase activities in plasma samples.....	110
4.1.4	Application of GLuc and CLuc provide refinement and reduction of animal experiments.....	110
4.1.5	Evaluation of essential genes by tet-inducible genetic manipulation	111
4.1.6	Identification of p73 as an essential factor for cell growth in Hs 766T cells	112
4.1.6.1	An unlikely couple: growth-inhibitory TAp73 versus growth-promoting Δ Np73.....	112
4.1.7	Perspectives of the dual luciferase assay beyond transplantation experiments	113
4.1.8	Immune tolerance of GLuc and CLuc pave the way for monitoring of endogenous tumors	114

4.2 The $\Delta Np73\alpha$ -knockin model: developmental disorders, reproductive failure and tumor progression	115
4.2.1 Impaired transgene expression in organs of $\Delta Np73\alpha$ -knockin mice	115
4.2.2 ... based on epigenetic silencing?	115
4.2.3 $\Delta Np73\alpha$ aggravates tumorigenic phenotype of p53+/- mice	117
4.2.4 Dysregulation of p73 causes male infertility	118
4.2.5 p73 is essential for embryonic development	120
4.2.6 $\Delta Np73\alpha$ -overexpressing MEFs exhibit a metastatic signature....	120
4.2.7 $\Delta Np73\alpha$ induces factors involved in migration and EMT	121
References	125
Abbreviations	X
Publications	XIII
List of Academic Teachers	XIV
Acknowledgements	XV

Abstract

Cancer development is a multistep process which leads to tumors composed of diverse cell populations originating from one cell which underwent differential genetic changes over time. Within one tumor, such heterogeneity provides distinct subpopulations with selection advantages promoting metastasis as well as therapy resistance. In the course of targeted cancer therapies tumor composition is meanwhile monitored via circulating tumor DNA from blood samples during treatment and accordingly allows adjustment of therapy. In experimental models of solid tumor xenografts in mice, however, this method is not applicable as required blood volumes exceed blood volume of animals, hence limiting investigation of tumorrelevant genes in preclinical mouse models. Here, a method was developed which facilitates simultaneous monitoring of growth dynamics of two distinct tumor cell populations within one tumor xenograft. Therefore, cells were labelled by stable expression of either Gaussia luciferase (GLuc) or Cypridina luciferase (CLuc) prior to injection. Both luciferases are secreted into the blood stream of transplanted mice. This allows assessment of tumor composition by enzyme activity of both luciferases requiring only very low blood volumes. Moreover, to facilitate investigation of the impact of targeted genetic manipulations luciferases were linked with (non)-targeting shRNAs. To establish this method, shRNAs were used targeting the p53 family members p53 and p73. Whereas p53 is acknowledged as the most important tumor suppressor, p73 can occur in two N-terminally different isoforms with opposing attributes: the tumorsuppressive full length isoform TAp73 and the N-terminally truncated tumorpromoting isoform Δ Np73. The dominant negative function of Δ Np73 includes its ability to form hetero-oligomers with its family members p53 and TAp73, thereby interfering with their transcriptional activity. Linking the luciferases to (non)-targeting shRNAs, the differential growth properties of transplanted cells in presence and absence of p53 (or p73) can be monitored simultaneously. The here established method was successfully validated in a model of experimental metastasis as well as under therapeutic conditions.

Moreover, it could be demonstrated that the growth behaviour of p73-high-expressing cells Hs 766T is highly dependent on the relative abundance of both

N-terminal isoforms. The shRNA-mediated reduction of both isoforms strongly reduces tumorigenicity of these cells. In accordance with previous publications, the reintroduction of Δ Np73 rescued this growth defect, whereas ectopic expression of TAp73 further attenuates proliferation.

In order to further investigate Δ Np73's role in tumor development, an inducible Δ Np73 transgenic mouse model was characterized. Whereas mere overexpression of Δ Np73 exhibited no tumorrelevant properties, the combination with heterozygous knockout of p53 entailed earlier and accelerated tumor development particularly of lung tumors and lymphoma. The loss of the second p53 allele in lung tumors suggests that the dominant negative effect of Δ Np73 rather impacts TAp73 than p53. Accordingly, the observed fertility and embryonic developmental defects in this transgenic model rather pointed towards a TAp73-dependent effect of Δ Np73 as, in contrast to p53-deficient mice, severe and partially comparable defects have been described in TAp73- and complete p73-deficient mice.

Finally, transcriptomewide analysis of Δ Np73-overexpressing murine embryonic fibroblasts revealed positive regulation of metastasis-promoting factors like ITGB4, JAG1 and 2. This tumorpromoting property of Δ Np73 goes in line with accelerated dissemination of lymphoma into lungs of Δ Np73;p53^{+/-} mice.

Taken together, these results clearly demonstrate growth- as well as metastasis-promoting traits of Δ Np73. However, the specific virtue of Δ Np73 are largely cell context-dependent.

Zusammenfassung

Die Tumorentwicklung ist ein mehrstufiger Prozess, bei dem sich aus einer einzigen Ursprungszelle durch Akkumulierung diverser Mutationen Tumoren entwickeln, die aus mehreren Populationen unterschiedlichen genetischen Status bestehen. Diese Heterogenität führt zu Selektionsvorteilen einzelner Subpopulationen innerhalb eines Tumors, die unter anderem Metastasierung sowie Therapieresistenz begünstigen. Zur Verbesserung der gezielten Krebstherapie von Patienten kann mittlerweile während des Therapieverlaufs die Zusammensetzung der Tumoren durch im Blut zirkulierende Tumor DNA verfolgt und die Therapie dementsprechend angepasst werden. In experimentellen Ansätzen, wie Transplantationsmodellen solider Tumoren in Mäusen, kann diese Methode allerdings nicht angewandt werden, da das Blutvolumen der Versuchstiere zu klein ist. Dies limitiert die Untersuchung tumorrelevanter Faktoren in präklinischen Studien im Mausmodell.

In dieser Arbeit wurde eine Methode entwickelt, mit deren Hilfe die Wachstumsdynamiken zweier unterschiedlicher Zellpopulationen in einem einzigen Tumorzellimplantat simultan verfolgt werden können. Hierzu wurde vor der Transplantation jeweils eine Zellpopulation durch stabile Expression von Gaussia Luziferase (GLuc) oder Cypridina Luziferase (CLuc) markiert. Beide Luziferasen werden aus den Zellen sezerniert und ins Blut der Versuchstiere abgegeben. Kleinste Blutproben sind bereits ausreichend, um die Tumorkomposition mittels Messung der Enzymaktivität beider Luziferasen zu bestimmen. Um die Auswirkungen gezielter genetischer Manipulationen untersuchen zu können wurden die Luziferasen zusätzlich an (un)spezifische shRNAs gekoppelt. Zur Etablierung wurden shRNAs verwendet, die sich gegen die p53 Familienmitglieder p53 und p73 richten. Während p53 als der wichtigste Tumorsuppressor bekannt ist, gibt es von p73 zwei N-terminal unterschiedliche Isoformen, die entgegengesetzte Funktionen besitzen: das ebenfalls tumorsuppressive TAp73 und das tumorfördernde Δ Np73. Die dominant negative Wirkung von Δ Np73 liegt unter anderem in der Komplexierung seiner Familienmitglieder p53 und TAp73, wodurch diese die Fähigkeit verlieren an ihre Zielgene zu binden. Durch Kopplung der Luziferasen an unspezifische bzw. experimentelle shRNAs konnte die unterschiedliche Wachstumsdynamik

transplantierte Zellen in An- bzw. Abwesenheit von p53 (oder p73) simultan verfolgt werden. Die in dieser Arbeit etablierte Methode wurde sowohl in einem Modell der experimentellen Metastasierung als auch unter therapeutischen Bedingungen erfolgreich validiert.

Darüberhinaus konnte gezeigt werden, dass das Wachstumsverhalten p73-hochexprimierender Hs 766T Zellen abhängig vom relativen Verhältnis beider N-terminaler Isoformen zueinander ist. Eine shRNA-vermittelte Reduktion beider Isoformen hemmt die Tumorigenität dieser Zellen. In Übereinstimmung mit dem aktuellen Wissensstand wurde dieser Effekt durch ektopische Expression von Δ Np73 wieder aufgehoben, wohingegen die Wiedereinführung von TAp73 die Proliferation noch weiter reduzierte.

Um die Rolle von Δ Np73 während der Tumorentwicklung genauer zu untersuchen, wurde zudem ein induzierbares Δ Np73-transgenes Mausmodell charakterisiert. Obwohl die alleinige Überexpression von Δ Np73 keinen tumorigenen Effekt aufwies, führte die Kombination mit heterozygotem Verlust von p53 zu einer früheren und verstärkten Tumorentstehung, insbesondere von Lungentumoren und Lymphomen. Der Verlust des zweiten p53 Allels in den Lungentumoren lässt eher auf eine dominant negative Wirkung von Δ Np73 auf TAp73 als auf p53 schließen. Auch die beobachteten Fertilitäts- und embryonalen Entwicklungsdefekte dieser transgenen Mäuse weisen vielmehr auf einen TAp73-abhängigen Effekt von Δ Np73 hin, da im Gegensatz zu p53-defizienten Mäusen bereits ähnliche Defizite in TAp73- und gesamt-p73-defizienten Mäusen beschrieben wurden.

Letztlich wurde durch die transkriptomweite Analyse Δ Np73-überexprimierender muriner embryonaler Fibroblasten eine positive Regulation metastasierungsrelevanter Faktoren (ITGB4, JAG1, JAG2) festgestellt. Diese onkogene Eigenschaft von Δ Np73 geht einher mit der Beobachtung dass Lymphome aus Δ Np73;p53^{+/-} Mäusen verstärkt in die Lungen disseminierten.

Insgesamt zeigen diese Ergebnisse, dass Δ Np73 sowohl wachstums- als auch metastasierungsfördernde Eigenschaften besitzt, die genauen Wirkungsmechanismen allerdings abhängig vom Zellkontext sind.





1 Introduction

1.1 Cancer

The latest worldwide cancer statics from 2012 reveal 32.6 million patients living with cancer, 14.1 million newly diagnosed cancer patients and 8.2 million cancer caused deaths (www.globocan.iarc.fr). Apart from cardiovascular diseases and hunger, these numbers make cancer a leading cause of death. On the one hand, modern lifestyle (e.g. stress, less physical activity and wrong nutrition/obesity) steadily increases the cancer risk especially in industrial countries (Countries et al. 2007)(<http://canceratlas.cancer.org/risk-factors/>). On the other hand, the access to healthy food and common health care constantly

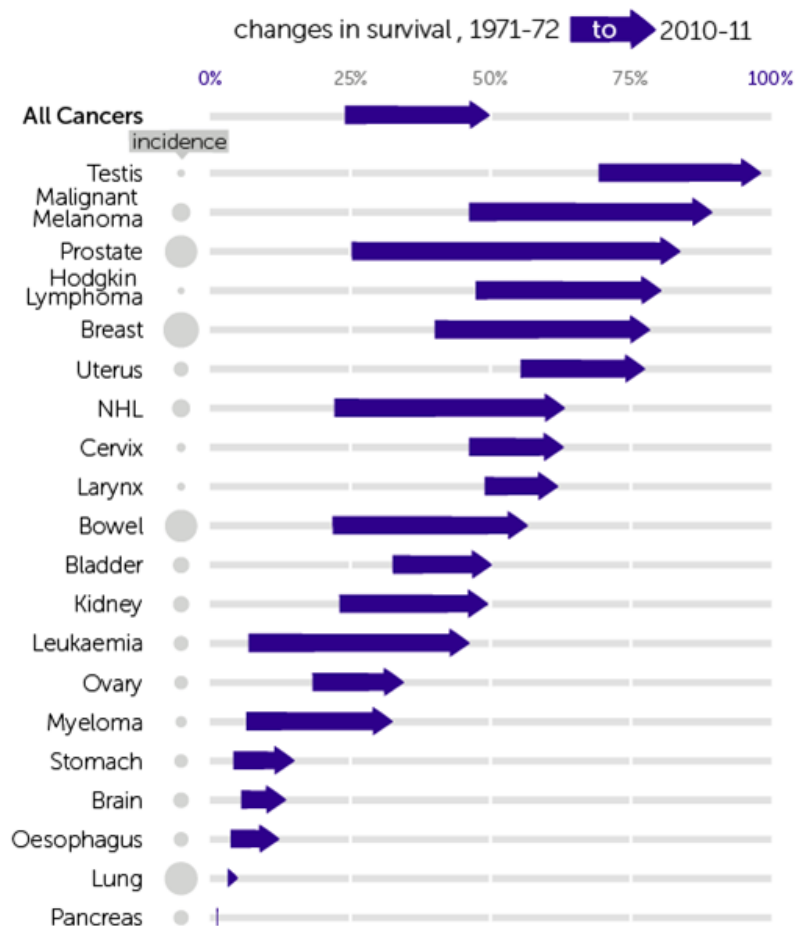


Figure 1: 40 years to improve cancer therapies: Ten-year survival rates of selected cancers in 1971 and today (2011)

Changes of ten-year net survival of selected cancers in adults (aged 15-99) from England and Wales in 1971 and 2011; data from Cancer Research UK, (<http://www.cancerresearchuk.org/health-professional/cancer-statistics/survival/common-cancers-compared#heading-Three.>)

improved cancer therapy during the last decades. Thus, despite elevated numbers of cancer patients, improved cancer therapies continuously increase their 5-year survival rate (Quaresma et al. 2015). The success of treatment is closely related to the tumor stage at which the patient is diagnosed. The later a tumor is detected, the higher is the probability of infiltrative growth, resistance and distant metastases. Apart from the tumor grade, the cancer type is also very critical. Whereas prostate cancer, testicular cancer and many lymphomas became well treatable diseases within the last years, the therapy of cancers affecting the lung or the pancreas has barely progressed (Figure1)(DeSantis et al.; Quaresma et al. 2015).

1.2 Limitations of cancer treatment

Successful cancer treatment is heavily impeded by the genetic diversity of cell populations within a primary tumor and its distant metastases. As described above (see 1.1), tumor stage and type are important factors which need to be considered when deciding for the therapeutic strategy (<http://www.cancer.org/treatment/understandingyourdiagnosis/staging>). Curative surgery is applied at early tumor stages, when the tumor mass is restricted to one part of the body and it is likely to remove the cancer by excision. This treatment can be further supported by radio- or chemotherapy (<http://canceratlas.cancer.org/taking-action/management-and-treatment>).

However, in a progressed disease with distant metastases, surgery or locally restricted irradiation are not sufficient to cure the patient. In this case, a systemic chemotherapy needs to be applied which also reaches disseminated degenerated cells. But even this treatment can fail: while the cytotoxic/cytostatic drug hits the majority of malignant cells, few cells escape treatment due to their progressed mutational status (see 1.2.1), thus leading to relapse of the disease with poor outcome for the patients as recurring tumors are virtually always therapy resistant.

1.2.1 Cancer - a war on multiple fronts

Cancer is a complex disease caused by the deregulation of intertwining pathways which control cell growth, proliferation and DNA-damage repair in order to maintain cell homeostasis. The phenotypic changes which emerge from these alterations were summarized by Hanahan and Weinberg (Figure

Establishment and characterization of preclinical mouse models for evaluation of oncogenic and tumor-suppressive properties of p53 family members

2)(Hanahan & Weinberg 2011): Sustained proliferative signalling is caused by accelerated growth factor receptor stimulation and enhanced activation of their downstream effectors. In a healthy cell, such a cellular stress leads cell cycle regulators to halt cell cycle progression. But in tumor cells, such growth suppressors are frequently lost or inactivated by other means, thus allowing hyperproliferation. Yet another safety mechanism to prevent excessive cell divisions is replicative senescence, a state in which cells remain metabolically active but undergo irreversible cell cycle arrest (Bringold & Serrano 2000). It is caused by the shortening of telomeres during each division cycle but is counteracted in malignant cells by enhanced telomerase activity resulting in telomere maintenance (Kim et al. 1994; Shay 2001).

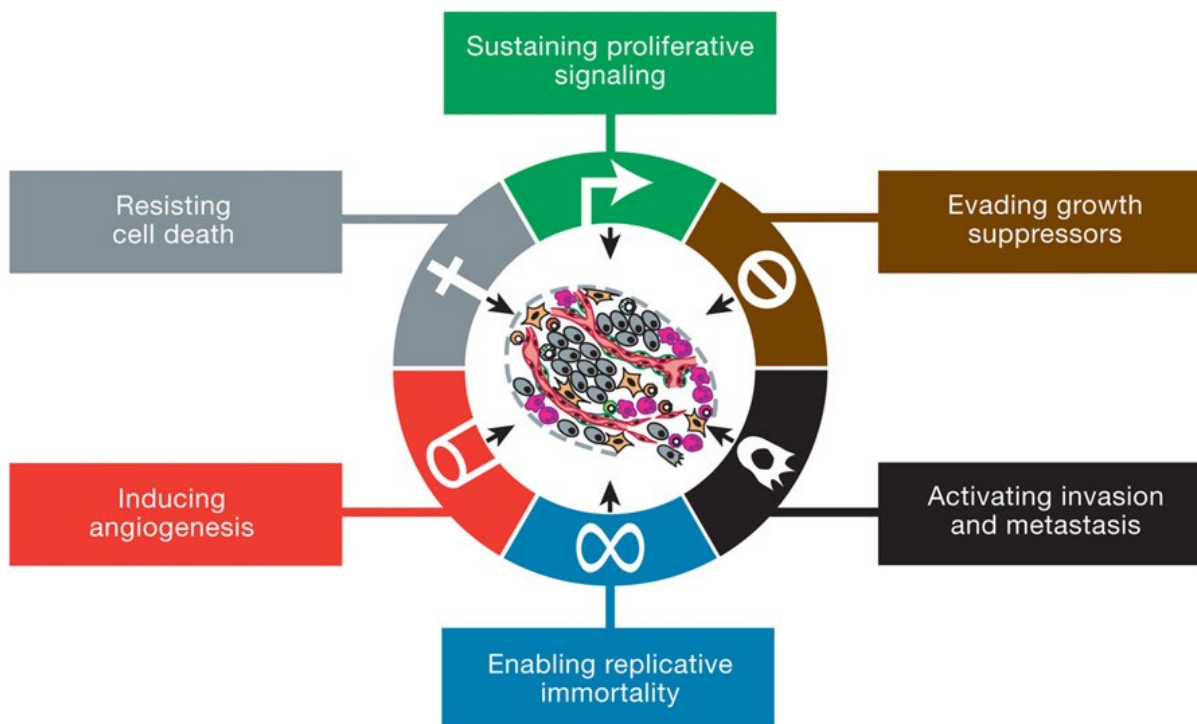


Figure 2: Hallmarks of cancer
(Hanahan & Weinberg 2011)

Finally, cell death remains as the last emergency exit to prevent erratic growth. Yet, cancer cells become also largely resistant against apoptosis by downregulation of cellular stress sensors and/or proapoptotic factors as well as by upregulation of antiapoptotic factors (Fulda 2009). As the tumor gains size, tumor cells at the centre of the tumor mass suffer shortage of oxygen- and energy supply. On the one hand, this leads to necrosis in the inner tumor mass which -at first sight- seems to be advantageous for the patient. Yet, necrosis

also attracts immune cells which secrete growth-stimulating factors further boosting tumor growth (Leek et al. 1999; Scaffidi et al. 2002; Vakkila & Lotze 2004). On the other hand, immune cells and tumor cells secrete angiogenesis-stimulating factors which lead to enhanced vascularization and thus to restoration of nourishment (Karin 2006; Mantovani et al. 2008). Additionally, metabolic changes within the cells can help to adapt to the changing environment with reduced resources (Eales et al. 2016; Vander Heiden et al. 2009). Another characteristic of progressing disease is infiltrative and metastatic growth. For example, malignant cells of epithelial origin undergo epithelial-to-mesenchymal-transition (EMT) which results in the loss of important adhesion molecules sustaining tissue integrity (E-Cadherin) and overexpression of migration-promoting adhesion molecules (N-Cadherin) (Kang & Massagué 2004; Cavallaro & Christofori 2004).

Self-evidently, a single genetic alteration is not sufficient to match all these traits characterizing malignancy. It is rather the accumulation of several genetic insults, the combination of functional loss of tumor-suppressors and sustained activation of (proto-) oncogenes, which drives malignant transformation (Nordling 1953). This is achieved by the iterative process of (epi-) genetic changes and sequential clonal selection, a model already described very early by P. C. Nowell (Nowell 1976). In a first step, a healthy cell undergoes a genetic or epigenetic change due to failure in DNA repair or methylation machinery upon intrinsic stress (e.g. ROS (reactive oxygen species), replication errors, mutagen exposure). Next, as a result of genomic instability, the proliferating neoplastic cells acquire more mutations. Most of them are silent mutations - which do not affect cell growth- or adverse mutations which reduce cell fitness leading to clearance from the tumor (Greenman et al. 2007). Still, few genetic alterations occur which provide further advantage to withstand the constant selective pressure prevailing in the tumor microenvironment: sustained competition for limited space, oxygen and energy supply as well as growth factors (Greaves & Maley 2012). Thus, the cells which adapted best, display a selective growth advantage over normal and premalignant ancestor cells, undergo clonal expansion and become the predominant cell population within the arising tumor (Figure 3). Accordingly, cells which developed metastatic properties exploit new niches in lymph nodes and/or distant organs.

Establishment and characterization of preclinical mouse models for evaluation of oncogenic and tumor-suppressive properties of p53 family members

The application of chemo- or radiotherapy applies an additional selective pressure on the heterogeneous tumor composition. As rapidly-dividing cells are particularly sensitive to DNA-damage induced by chemotherapeutic drugs and irradiation, a large proportion of the fast-proliferating cell populations becomes eradicated from the tumor, whereas quiescent and therapy-resistant cell populations might escape cell death. The surviving cells can now benefit from the rapid change in the tumor microenvironment and foster their clonal expansion claiming all resources while repopulating the tumor (Gerlinger & Swanton 2010; Morelli et al. 2015). Moreover, the application of genotoxic agents provokes enhanced genetic diversity by introduction of further mutations resulting in further progression of the disease.

Taken together, the accumulation of genetic alterations and the sequential subclonal selection lead to a clonal diversity which makes cancer treatment a war on multiple fronts as some clonal tumor cell populations may respond to chemotherapy, while others do not. Hence, there is an urgent need to understand the dynamics of the clonal diversification which promotes neoplastic progression, metastasis and therapy resistance.

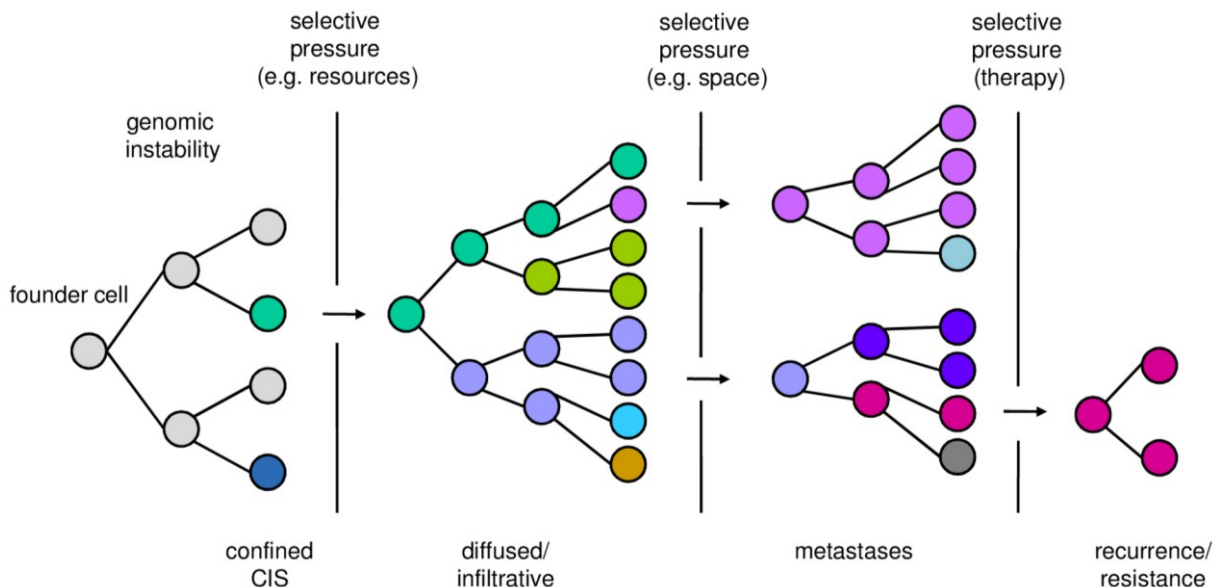


Figure 3: Sequential mutations and clonal expansions leading to tumor heterogeneity

Adapted from (Greaves & Maley 2012)

1.2.2 Methods for monitoring and modelling of tumor heterogeneity

As described above the heterogeneous nature of tumors significantly hampers successful cancer treatment. Thus, there is an urgent need to better understand the complexity and interplay of all genetic changes which cause tumorigenesis, resistance and metastatic spread. Hence, it was a huge leap forward when next generation sequencing was developed as a cost-effective method rapidly delivering a large amount of data (Shyr & Liu 2013)(see <http://cancergenome.nih.gov>). Genetic alterations as well as gene expression profiles are easily assessed in patients' tumor samples, even single cell sequencing is possible nowadays (Navin 2014). Still, there are hurdles to overcome. The profiling of formalin-fixed tissue after surgery may give insight in the heterogeneous tumor composition when samples from different tumor areas are sequenced. But this gives only a snapshot in time, it does not provide any information about the changes a tumor goes through during treatment and relapse. To pursue these changes, sequential biopsies are needed. But biopsies only represent a very restricted area of the tumor and would miss to give information about the heterogeneous composition. Therefore, the discovery of circulating nucleic acids originating from the tumor in the bloodstream was a great success. The tumor-specific genomic DNA and mRNA extracted from patients' blood samples can give valuable information about the overall tumor composition, detect rare mutations and can even be decisive for the choice of therapy (Pereira et al. 2015; Tie et al. 2015; Olsson et al. 2015; Bettegowda et al. 2014). Hence, this approach embodies a great opportunity for improving personalized treatment of cancer patients, as already few millilitres of a patients' blood sample suffice to detect specific tumor markers.

Still, experimental approaches to model and monitor the complexity of tumor progression have to be implemented. Here, mouse models are of particular importance, as the diversified influence of the tumor microenvironment can hardly be simulated in cell culture experiments. Transplantation experiments of patient-derived xenografts or established cancer cell lines are a commonly used method to assess tumorigenicity, metastatic potential or chemosensitivity in vivo (Frese & Tuveson 2007; Siolas & Hannon 2013). Moreover, targeted genetic manipulation of such cells either by RNA interference (RNAi) or gene transfer is a well-used tool to identify and validate tumor-relevant genes (Zender et al.

2008). Nevertheless, monitoring of the growth dynamics is technically restricted. The total size of a tumor which is injected close to the body surface (e.g. subcutaneous, mammary fat pad) can easily be measured with calipers. However, this method harbours a high variance of results (Ayers et al. 2010). Even more important, if the competitive growth dynamics of 2 or more distinct genetically manipulated cell populations in a mixture is to be followed, caliper measurements are not able to provide any information about tumor composition. Additionally, tumors of inner organs (e.g. induced by intravenous injection or direct application of cancer cells to the lung or pancreas) are not accessible for such measurements. Here, tumor growth has to be monitored with costly methods like MRT (magnetic resonance tomography) or ultrasound (Ayers et al. 2010).

Alternatively, cells can be labelled with fluorescent or bioluminescent markers prior to transplantation. This facilitates the monitoring of tumor growth upon repeated bioimaging of a living experimental animal and, depending on the sensitivity of the marker, can be even suitable to localize metastases (Jenkins et al. 2003; M. Yang et al. 2000). Moreover, the application of a secreted luciferase originating from the copepod *Gaussia princeps* as a marker for transplanted tumor cells improved experimental procedures and the data output a lot (Tannous 2009; Wurdinger et al. 2008; Chung et al. 2009). Beyond bioluminescent imaging, *Gaussia* luciferase activity can be assessed in small blood samples of transplanted mice as the luciferase is transported out of the cell into the surrounding milieu. Moreover, it has been shown that the number of injected cells directly correlates with *Gaussia* luciferase activity measured in the blood sample, thus enabling a reliable quantification of tumor cells (Wurdinger et al. 2008). Even though the application of a marker like *Gaussia* luciferase provides a more reliable and more sensitive quantification of tumor cell abundance than a caliper, an evaluation of a heterogeneous tumor mass as described above is still not approachable with this method. Even the previously mentioned investigation of tumor-specific genomic DNA or mRNA from blood samples is not able to address this problem, as the required blood volume exceeds the total blood volume of a mouse. To this point, the only option to evaluate the heterogeneous composition of transplanted tumors does not permit repeated measurements as it comes in form of endpoint analyses: after

sacrificing the experimental animal, the tumor is isolated and investigated by molecular biological methods (e.g. sequencing, immunohistochemistry). A solitary exception is made in the context of haematological malignancies: here, labelling of different tumor cell populations with different fluorescent markers like GFP and RFP has proven to facilitate the repeated monitoring of heterogeneous tumor cell mixtures by flow cytometry of blood samples (Zuber et al. 2011). Yet, this method addresses only a small proportion of human cancers: leukemias account for less than 5% of all malignancies (<http://globocan.iarc.fr>) whereas 95% of cancer patients suffer from solid tumors.

Hence, methods need to be established especially for solid tumors which are able to detect changes in tumor composition in mouse models of human cancer.

1.3 The p53 family members

As described above, the progression of malignant disease requires not only hyperactivation of oncogenic signalling but also disruption of tumor suppressive pathways (see 1.2.1). The p53 family is a multifaceted group of transcription factors which inherit both, oncogenic as well as tumor suppressive traits.

The most noted and likewise eponymic member p53 is known as (one of) the most important tumor suppressors protecting the organism from the aberrant growth of degenerated cells. Extrinsic as well as intrinsic cellular stresses like UV-radiation, tobacco smoke, oncogenic signalling, oxidative stress or hypoxia lead to stabilization and activation of p53 (Maltzman & Czyzyk 1984; Hermeking & Eick 1994; Lowe & Ruley 1993; Graeber et al. 1994; Serrano et al. 1997). Depending on quality and severity of the cellular stress, p53 induces a transcriptional program leading to DNA repair, senescence, cell cycle arrest or even apoptosis in order to eliminate damaged cells from the organism (Ford & Hanawalt 1997; Shay et al. 1991; Kastan et al. 1991; Yonish-Rouach et al. 1991). The other two family members p63 and p73 inherit similar tumor suppressive functions due to their high structural homology with p53 and among each other (Mourad Kaghad et al. 1997; C. A. Jost et al. 1997; Yang, Kaghad, Wang, Gillett, Fleming, Dötsch, et al. 1998). All three family members comprise an N-terminal transactivation domain (TAD), a proline rich region (PR), a central DNA binding domain (DBD) and a C-terminal oligomerization domain (OD) (Figure 4) (A. Yang et al. 2002). Additionally, p63 and p73 contain a sterile

Establishment and characterization of preclinical mouse models for evaluation of oncogenic and tumor-suppressive properties of p53 family members

alpha motif (SAM) which mediates protein-protein interactions and is known to play a role in developmental programs (Schultz et al. 1997). Likewise, the PR region is also a docking site for signalling modules (Kay et al. 2000).

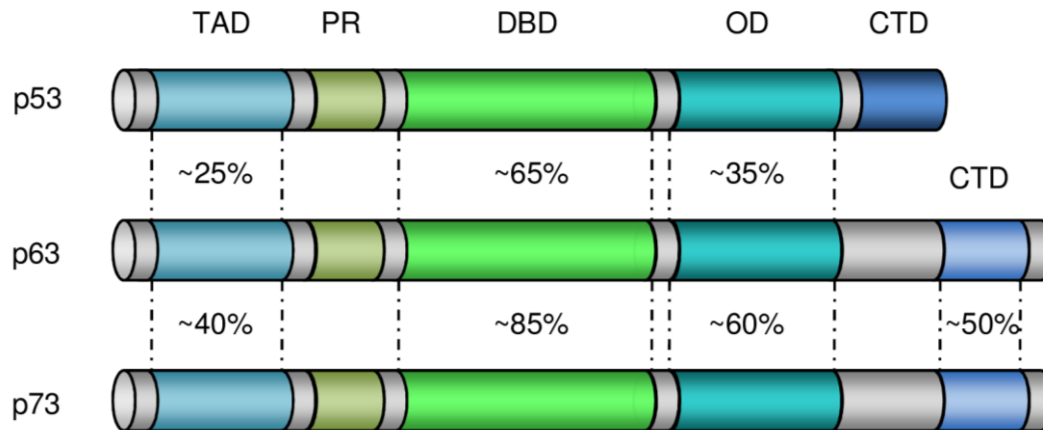


Figure 4: Structure of p53-family members

Protein domains of p53-family members p53, p63 and p73 are composed of a transactivation domain (TAD), a proline-rich region (PR), a DNA-binding domain (DBD), an oligomerization domain (OD) and C-terminal-domain (CTD) which additionally contains a sterile alpha-motif within the p63 and p73 family members. Percentages reflect homologies between family members. Adapted from (A. Yang et al. 2002).

In contrast to the aforementioned protein interaction sites, the OD serves as an interaction site for tetramerization of the transcription factors predominantly as homo-oligomers, but also as hetero-oligomers. This tetrameric conformation is essential for transcriptional activity. The highest homology is reached within the DBD which is important for recognition and binding to specific promoter or enhancer elements in the DNA. Indeed, all p53 family members can attach to p53 response elements thereby sharing many target genes (Levrero et al. 2000; Yang et al. 2010). Still, the induction of these target genes differs depending on the family member (Yu et al. 1999; Zhu et al. 1998). Thus, one family member alone is not able to compensate for the others.

The TAD acts as a binding site for co-regulatory proteins and exerts a pivotal role in cell fate decisions mediated by p53 family members as its presence or absence is largely decisive for their anti- or pro-tumorigenic function. Each family member possesses antagonistic isoforms which lack the N-terminal TA domain either due to alternative splicing or the use of a second intronic promoter (Bourdon et al. 2005; Yang, Kaghad, Wang, Gillett, Fleming, Dötsch, et al. 1998; A. Yang et al. 2000). Whereas the full length proteins p53, TAp63 and TAp73 induce cell cycle arrest, DNA repair, senescence and apoptosis

upon cellular stress, the N-terminally truncated isoforms D133p53, Δ Np63 and Δ Np73 oppose their tumor suppressive siblings in a dominant negative manner with rather antiapoptotic and oncogenic functions (Aoubala et al. 2011; Yang, Kaghad, Wang, Gillett, Fleming, Dötsch, et al. 1998; Mundt et al. 2010; Grob et al. 2001a).

1.3.1 p53

The indispensable role for p53 in counteracting neoplastic growth becomes evident regarding the fact that more than 50% of human malignancies harbour p53 mutations or even deletions (Greenblatt et al. 1994). Most mutations are located within the DBD and 75% of them are missense mutations leading to amino acid substitutions and thus to the accumulation of a defective p53 protein lacking the capacity to bind to p53 consensus sequences in the DNA (Greenblatt et al. 1994). One possible explanation for the advantage of a missense mutation over a simple deletion is the dominant effect of mutant p53: it is able to form inactive hetero-oligomers with wildtype p53 expressed from the remaining wildtype allele, thus inhibiting the transactivation of tumor suppressive target genes (Milner & Medcalf 1991). This dominant negative effect has also been shown to target TAp63 and TAp73 (Strano et al. 2002; Gaiddon et al. 2001; Como et al. 1999). Moreover, in addition to the loss of its tumor suppressive function, mutant p53 often acquires oncogenic features which promote metastasis and chemoresistance. Additionally, in line with *Knudson's Two-Hit-Hypothesis* (Knudson 1971), loss of the wildtype p53 allele (loss of heterozygosity, LOH) is frequently observed in malignant cells with mutated p53, indicating a strong selection against the merest tumor suppressive activity from residual wildtype p53. Tumors retaining wildtype p53 frequently display an inactivation of p53 by other mechanisms like nuclear exclusion, amplification of its negative regulators Mdm2 and Mdm4 (mouse double minute 2 and 4 homolog) or viral inhibition (Moll et al. 1995; Oliner et al. 1992; Hoppe-seyler & Butz 1993; Danovi et al. 2004). In addition, germline mutations in the p53 locus have been identified to be the leading cause of the Li-Fraumeni syndrome, a hereditary disease predisposing patients to cancer (Malkin et al. 1990; Li & Fraumeni 1969).

Establishment and characterization of preclinical mouse models for evaluation of oncogenic and tumor-suppressive properties of p53 family members

Ultimately, the generation of a p53-deficient mouse model delivered final evidence for p53's tumor suppressive function: half of heterozygous knockout mice (p53^{+/-}) develop spontaneous tumors within 18 months whereas the remaining half develops tumors within 2 years of age at the latest (Donehower 1996; Donehower et al. 1992; Jacks et al. 1994). In fact, the homozygous knockout (p53^{-/-}) prepones the tumor onset to the age of 6-10 months in all mice depending on the background of the mouse model. Comparable to patients' tumor samples, analyses of tumors from p53^{+/-} mice revealed a loss of the remaining p53 wildtype allele in 50-90% of all cases being accompanied with an earlier tumor onset and enhanced genomic instability (Donehower 1996; Jacks et al. 1994). Moreover, the prevalent tumor entities in p53^{-/-} mice, lymphomas and - to a lower extent - soft tissue sarcomas and osteosarcomas, closely resemble the tumor spectrum of Li-Fraumeni patients.

Based on these observations, p53 became one of the most extensively investigated tumor relevant factors during the last decades: In unstressed cells, a negative feedback loop -mediated by the p53 target gene Mdm2- is responsible for the short half-life of p53 protein. Mdm2 is an E3 ubiquitin protein ligase which ubiquitinates p53 leading to its proteasomal degradation. In addition, MDM2 as well as MDM4 interfere with p53's transcriptional activity, thereby preventing target gene activation. However, upon cellular stress p53 undergoes various phosphorylations and acetylations preventing the binding and consequently the ubiquitination of p53 by Mdm2, thereby protecting p53 from proteasomal degradation (Shieh et al. 1997). The DNA-damage induced activation of ATM (ataxia telangiectasia mutated), ATR (ATM-Rad3 related) and DNA-PK (DNA-dependent protein kinase) kinases, for example, leads to direct and indirect phosphorylation of several serines in p53 (Canman 1998; Tibbetts et al. 1999; Lees-miller et al. 1992). Further posttranslational modifications like the acetylation of several lysines by histone acetyltransferases p300 and PCAF subsequently activate p53-mediated transcription (Sakaguchi et al. 1998). Eventually, the induction of p53 target genes like Cdkn1a, Gadd45 and 14-3-3 σ prevents the cell cycle progression of damaged cells to gain time for DNA damage repair. In case the damage is too severe to be fixed, cells undergo p53-mediated apoptosis by induction of proapoptotic genes like Puma, Bax and

Noxa, thus averting corrupted cells to pass on mutations acquired by DNA damage.

The restoration of p53 function is hence a highly desirable goal for cancer therapy. Various small molecules have been developed which disrupt the protein-protein interaction of p53 and its negative regulator MDM2 by blocking the binding pockets of either p53 (RITA) or MDM2 (e.g. nutlin3a)(Issaeva et al. 2004; Vassilev et al. 2004). In fact, these compounds stabilize p53 in p53wt cancer cells resulting in an anti-proliferative and pro-apoptotic response.

1.3.2 p73-a complicated gene

The data about p73 are less conclusive than for p53, and thus TP73 is not unambiguously described as a tumor suppressor gene. Unlike p53, p73 has been found to be rarely mutated in cancer (M Kaghad et al. 1997; Ichimiya et al. 1999; Stiewe & Pützer 2002). The notion of p73 being a tumor suppressor rather arose by the finding that the chromosomal region 1p36, where the TP73 gene is located, is frequently deleted in human tumors, especially in neuroblastoma (M Kaghad et al. 1997; Schwab et al. 1996; Ichimiya et al. 1999). Moreover, p73 expression is silenced by hypermethylation of the 5' CpG island in a large proportion of Acute Lymphoblastic Leukemias and Burkitt's Lymphoma (Corn et al. 1999). Yet, in contrast to these observations, p73 has also been found to be upregulated in various tumor entities like breast, bladder, ovarian and lung cancer and even in some neuroblastoma (Casciano et al. 2002; Concin et al. 2004; Yokomizo et al. 1999; Zaika et al. 1999; Zaika et al. 2002; Tokuchi et al. 1999). Consequently, the low mutational rate and contradictive observations of either loss or overexpression in tumor samples led to the question whether TP73 can really be classified as a tumor suppressor gene or also inherits oncogenic features.

Tumorigenicity studies in a Trp73 knockout mouse model, however, also largely failed to deliver a clear answer. First of all, 75% of homozygous total-p73 knockouts (Trp73^{-/-}) die within the first two months of age due to severe developmental defects which makes it very difficult to obtain reliable results on spontaneous tumorigenesis (A. Yang et al. 2000). Yet, the first characterization of Trp73^{-/-} mice surviving beyond this time did not reveal any signs of spontaneous tumorigenesis up to the age of 15 months (A. Yang et al. 2000), whereas a second characterization surprisingly reported a 60% incidence of

Establishment and characterization of preclinical mouse models for evaluation of oncogenic and tumor-suppressive properties of p53 family members

small lung adenocarcinoma in Trp73^{-/-} mice at the age of 10 months (Flores et al. 2005). Additionally, the median survival of Trp73^{+/-} mice in this report was significantly reduced to 14 months compared to wildtype animals. This accelerated mortality was accompanied by benign lung adenoma and malignant lung adenocarcinoma as well as lymphoma and hemangiosarcoma.

The initially conflicting observations made in cancer patients - on the one hand deletion or silencing of the TP73 locus, on the other hand overexpression of p73 in various tumors- can partially be explained by the N-terminal diversity of p73 (Figure 5). P73 isoforms are grossly divided into two subgroups based on the presence or absence of the N-terminal transactivation domain: the tumor suppressive full length isoform TAp73 and the tumor-promoting N-terminally truncated isoform Δ Np73. Both isoforms positively regulate each others' protein levels: the intronic promoter P2 within the TP73 locus contains a p53-responsive element which is bound and transactivated by TAp73 and p53, leading to Δ Np73 expression (Seelan et al. 2002; Grob et al. 2001b). Δ Np73, in turn, stabilizes TAp73 but not p53 protein (Slade et al. 2004). Yet, Δ Np73 interferes with both, p53- and TAp73-induced target gene expression in a dominant negative manner (see 1.3.4).

Independently from the intronic P2 promoter, additional N-terminally truncated isoforms Δ 2, Δ 2/3 and Δ N' are generated by alternative splicing of the TAp73-transcript, the latter leading to a protein being functionally identical to the Δ Np73 protein transcribed from P2 (M Kaghad et al. 1997; Ng et al. 2000; Stiewe, Zimmermann, et al. 2002). Moreover, C-terminal splicing variants α , β , γ , δ , ϵ , η and ζ further enlarge the diversity of p73 isoforms (De Laurenzi et al. 1998; M Kaghad et al. 1997), which allows a precise fine-tuning of p73's biological functions (Ueda et al. 1999; Murray-Zmijewski et al. 2006). Still, suitable antibodies for specific detection of the various isoforms are very restricted and thus, most expression analyses from human tumor samples have to be considered cautiously. More recent studies, however, revealed that both N-terminal isoforms are upregulated in cancer which goes in line with their mutual induction and stabilization. Regarding these data, TP73 is rather a "two-in-one" gene encoding for both, tumor suppressive as well as tumor promoting factors. Apart from mutual regulation of TAp73 and Δ Np73, protein levels and activity are also modulated by other factors. The p53 regulators Mdm2 and 4 also bind

to p73. However, this interaction does not result in proteasomal degradation but impedes p73-mediated transcription (Bálint et al. 1999). Protein stability of both N-terminal p73 isoforms is regulated by the E3 ubiquitin ligase Itch and the F-Box protein FBXO45 (Rossi et al. 2005; Peschiaroli et al. 2009). Moreover, Δ Np73 is degraded via the polyamine-induced antizyme pathway upon genotoxic stress (Dulloo et al. 2010).

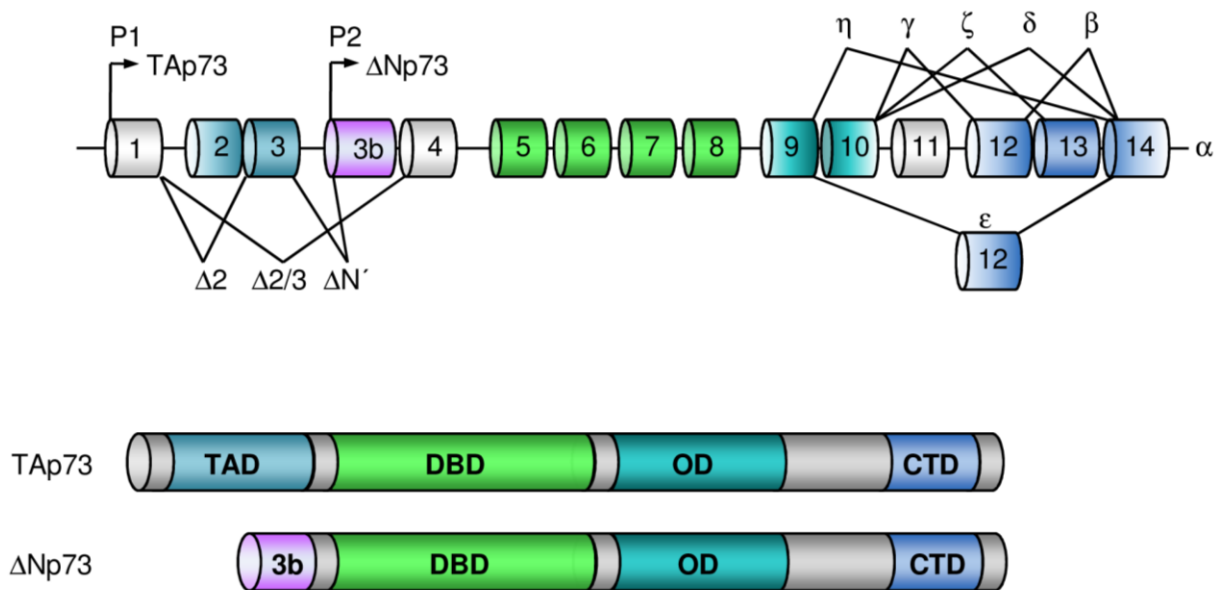


Figure 5: Isoforms of the TP73 gene

Structure of the TP73 locus encoding for p73 isoforms: N-terminal isoforms are derived either by alternative promoter usage (P1 for TAp73, P2 within exon 3b for Δ Np73) or alternative splicing ($\Delta 2$, $\Delta 2/3$ and $\Delta N'$), arrows indicate transcriptional start sites. Additional variation is given by alternative splicing of the C-terminus (α , β , γ , δ , ϵ , η and ζ). Transactivation domain (TAD), DNA-binding domain (DBD), oligomerization domain (OD) and C-terminal-domain (CTD), (adapted from Stiewe, Theseling, et al. 2002)

1.3.3 TAp73-a bird in the hand is worth two in the bush

Similar to p53, the N-terminal full-length isoform TAp73 exhibits primarily tumor-suppressive functions by induction of cell cycle arrest and proapoptotic genes (M Kaghad et al. 1997; C. a Jost et al. 1997; Yang, Kaghad, Wang, Gillett, Fleming, Do, et al. 1998). Even more, it has been shown that p53 requires TAp73 for DNA-damage induced apoptosis (Flores et al. 2002).

In contrast to the Trp73-knockout model which lacks both N-terminal isoforms, the isoform-specific TAp73-knockout revealed the tumor suppressive character of the full length isoform: loss of TAp73 resulted in enhanced tumor formation in 30% of heterozygous and 70% of homozygous knockout mice (Tomasini et al. 2008). Again, lung adenocarcinoma were the predominant tumor type observed

Establishment and characterization of preclinical mouse models for evaluation of oncogenic and tumor-suppressive properties of p53 family members in homozygous knockouts of TAp73, followed by (thymic) lymphoma. Further analyses exhibited a fundamental role of TAp73 in the maintenance of genomic stability as the loss of TAp73 entailed elevated genomic instability and aneuploidy in murine oocytes leading to female infertility. During mitosis and meiosis, the spindle assembly checkpoint (SAC) complex regulates the correct distribution and segregation of the sister chromatids. It impedes metaphase-to-anaphase transition until all kinetochores are properly attached to the spindle to ensure proper chromatid distribution to the daughter cells. TAp73 interacts with the SAC-component BubR1 directing its localization and activity and thus supports genomic stability (Tomasini et al. 2009).

Another feature of TAp73 is the repression of angiogenesis by downregulation of proinflammatory and proangiogenic cytokines (Stantic et al. 2015). Apart from limiting growth of the primary tumor - as reduced vascularization restricts oxygen and energy supply - this characteristic also confines invasion and metastasis. Moreover, TAp73 has directly been linked to interference with invasion and metastasis via expression of FOXO1 (Forkhead box protein F1)(Tamura et al. 2013).

Upon DNA damage, TAp73 induces a proapoptotic response in a cell cycle-dependent manner: during G1/S-phase transition, the tumor suppressor Rb (retinoblastoma protein) becomes inactivated by phosphorylation and releases the transcription factor E2F1 and the tyrosine kinase c-Abl. E2F1 subsequently binds to the P1 promoter upstream of exon 1 and transactivates transcription of TAp73 (Stiewe & Pützer 2000; Irwin et al. 2000; Seelan et al. 2002). DNA-damage activates c-Abl facilitating phosphorylation and stabilization of TAp73, eventually leading to induction of proapoptotic genes (Wang & Ki 2001; Agami et al. 1999; Gong et al. 1999).

However, as described above, TAp73 has also been found to be co-expressed with Δ Np73 in many tumors, which raises the question whether this is only a secondary effect of Δ Np73-mediated stabilization of TAp73 or whether malignant cells can even profit from TAp73 upregulation. In fact, depending on the context, TAp73 α can also execute pro-tumorigenic functions either by induction of cell cycle promoting genes (e.g. Cyclin D1) or by counteracting apoptosis (Subramanian et al. 2015; Koepfel et al. 2011; Nyman et al. 2005). P73 target genes have been identified which contain AP1 binding sites close to

their p73-binding motifs. Elevated levels of TAp73 α increasingly recruit c-Jun to these binding sites which is followed by enhanced induction of cancer-promoting genes (Subramanian et al. 2015; Koeppel et al. 2011). Moreover, TAp73 α impedes drug-induced apoptosis by interfering with Bax and caspase activation, but also mitochondrial dysfunction in small cell lung cancer cells (SCLC) (Nyman et al. 2005). In addition, hypoxia-mediated stabilization of TAp73 induces angiogenic genes leading to enhanced vascularization of tumors (Dulloo et al. 2015).

Taken together, most data prove that TAp73 can largely be considered as a tumor suppressor although it should not be forgotten that TAp73 also inherits pro-tumorigenic potential.

1.3.4 Δ Np73-the bad apple

High expression of the N-terminal truncated isoform Δ Np73 has been correlated with chemoresistance and poor prognosis in various cancer types (Müller et al. 2005; Concin et al. 2005; Dominguez et al. 2006). Moreover, recent work has linked Δ Np73 to promote skin cancer metastasis by induction of an EMT-like phenotype in melanoma cells (Steder et al. 2013). As a dominant negative inhibitor of TAp73 and p53, Δ Np73 competes with both factors for DNA-binding sites, thus preventing transcriptional activation of cell cycle arrest- and apoptosis-inducing genes (Figure 6). Additionally, Δ Np73 complexes TAp73 in transactivation-deficient hetero-oligomers, again interfering with its tumor suppressive function (Kartasheva et al. 2002; Zaika et al. 2002; Stiewe, Carmen C. Theseling, et al. 2002).

Accordingly, overexpression of Δ Np73 initiates immortalization in primary fibroblasts and even causes enhanced proliferation in E1A- or myc-immortalized cells (Petrenko et al. 2003). Moreover, Δ Np73 abrogates oncogene-induced senescence and cooperates with oncogenic Ras leading to malignant transformation and enhanced tumorigenicity of xenografts in nude mice. Likewise, the overexpression of Δ Np73 accelerates tumorigenicity of NIH3T3 fibroblasts, whereas the tumorigenic potential of E1A/Ras-transformed MEFs drops upon isoform-specific Δ Np73 loss (Stiewe, Zimmermann, et al. 2002; Wilhelm et al. 2010).

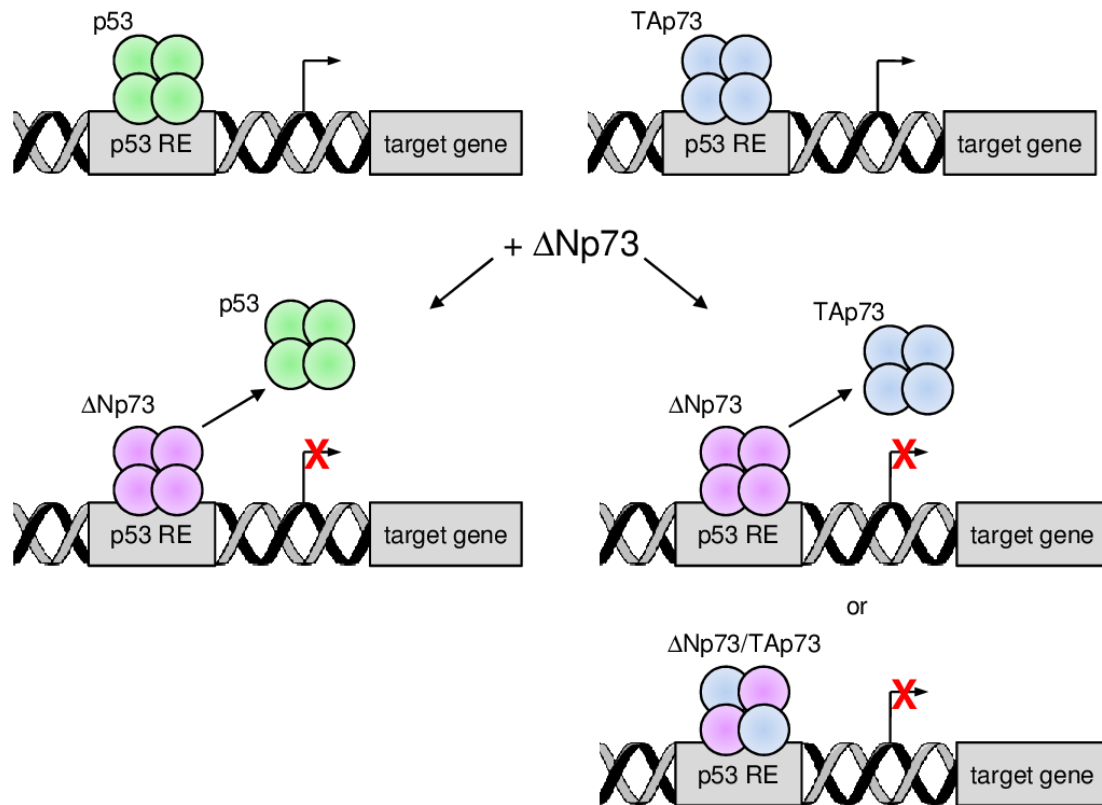


Figure 6: Dominant negative effect of $\Delta Np73$ on its family members p53 and TAp73

adapted from (Stiewe, Carmen C Theseling, et al. 2002)

Expectedly, the isoform-specific knockout in mice did not lead to enhanced tumorigenesis nor did $\Delta Np73^{-/-}$ mice display reduced survival for any other reason (Wilhelm et al. 2010). Yet, mild neurodegeneration has been observed, which is being reflected in reduced neuronal density and thickness of the motor cortex and underlines $\Delta Np73$'s anti-apoptotic function (Wilhelm et al. 2010). Supporting this finding, $\Delta Np73$ has been shown to prevent p53-induced cell death in sympathetic neurons (Pozniak et al. 2000). In myoblasts, $\Delta Np73$ also thwarts p53-induced cell death and, moreover, inhibits differentiation (Belloni et al. 2006; Cam et al. 2006).

In contrast, liver-specific overexpression of $\Delta 2/3$ causes a very high penetrance of hepatocellular liver adenoma which progress to hepatic adenocarcinoma in ~ 80% of mice (Tannapfel et al. 2008). Thus, $\Delta Np73$ inherits strong oncogenic potential which becomes fully deployed when supported by cooperative events. As p73 has been implicated not only in hepatocellular carcinoma but also in many other cancer types, a mouse model ubiquitously overexpressing $\Delta Np73$ is investigated here in order to better understand $\Delta Np73$'s role in tumorigenesis.

	Median survival	Tumor incidence	LOH
Trp53+/-	TFS: 18 months	Osteosarcoma (~30%) Lymphoma (~30%) Soft tissue sarcoma (~30%) Carcinoma (~10%)	50% (Donehower) 80-90% (Flores)
Trp53-/-	TFS: ~5 months	Lymphoma (~70%) Soft tissue sarcoma (~20%) Osteosarcoma (~10%)	
Trp73+/-	OS: 14 months (Flores)	Lung adenoma (40%) Squamous cell hyperplasia (30%) Lymphoma (12%) Sarcoma (12%) Lung adenocarcinoma (10%)	80-100% (Flores)
Trp73-/-	OS: ~ 25 days (Yang; Flores)	Lung adenocarcinoma (60% of mice surviving beyond 2 months, Flores) No tumors (Yang)	
TAp73+/-	OS: 22 months	Lymphoma (15%) Lung adenocarcinoma (5%) Colon carcinoma (5%) Sarcoma (5%)	66%
TAp73-/-	OS: 19 months	Lung adenocarcinoma (32%) Lymphoma (32%) Colon carcinoma (9%)	
Δ Np73-/-	Normal life span	None reported	
Alb p73 Δ 2/3	Not specified	Hepatic adenocarcinoma (80%)	

Table 1: Tumor incidence in mouse models of the p53-family

Median tumor-free survival (TFS), overall survival (OS) and tumor spectra of mouse models with hetero- and homozygous knockouts of individual members of the p53-family according to (Donehower et al. 1992; Flores et al. 2005; A. Yang et al. 2000; Wilhelm et al. 2010; Tomasini et al. 2008; Tannapfel et al. 2008).

1.4 Developmental defects in mouse models of the p53 family

The targeted deletion of various p53 family members in mice demonstrated an indispensable role for p53 and p73 in reproduction and development.

Breeding of heterozygous p53 knockout mice results in a largely normal mendelian ratio of genotypes with a slightly enhanced mortality of female p53-/- embryos during early development. These embryos die from exencephaly of the midbrain as neuronal overgrowth causes defects in neural tube closure (Sah et al. 1995). Still, p53-/- females show a reduced pregnancy rate accompanied by reduced litter size. Here, the implantation of embryos is severely disrupted by the absence of the p53-target LIF1 which prepares the uterus for blastocyst implantation into the endometrium (Hu et al. 2007).

Establishment and characterization of preclinical mouse models for evaluation of oncogenic and tumor-suppressive properties of p53 family members

Mice with a complete p73 knockout were generated by an exchange of exon 5 and 6 with a neomycin-resistance gene, rendering these mice deficient for both isoforms TA- and Δ Np73 (A. Yang et al. 2000). Although breeding of heterozygous Trp73 knockout mice leads to the expected ratio of genotypes, homozygous knockouts suffer from hippocampal dysgenesis, hydrocephalus, neuronal loss and strong immunological defects leading to a high mortality rate within the first weeks of life due to intracranial and gastrointestinal bleeding. Additionally, Trp73^{-/-} males reaching adulthood display a disorder in pheromonal perception due to neuronal loss in the vomeronasal organ. This deficit leads to an indifferent sexual interest in females and a lack of territorial behaviour against other males. In contrast, Trp73^{-/-} females fail to conceive most likely due to hormonal disorders (A. Yang et al. 2000).

	Prenatal defects	Postnatal defects	Infertility of -/- males	Infertility of -/- females
p53 ^{-/-}	Neural tube closure defects, slightly reduced number of -/- females	-	-	Disturbed uterine decidualization impede blastocyst implantation
Trp73 ^{-/-}	-	Hippocampal dysgenesis, Hydrocephalus, Intestinal hemorrhages, Immunological defects, 75% die within 2 months	Disturbed pheromone signaling (dysfunction of vomeronasal organ)	Hormonal imbalance
TAp73 ^{-/-}	-	Hippocampal dysgenesis	Disturbed germ cell differentiation and maturation	Reduced follicular pool size, Decreased ovulation, Genomic instability of oocytes
Δ Np73 ^{-/-}	-	-	-	-

Table 2: Developmental phenotypes and cause of infertility in mouse models of the p53-family

Data from (Tomasini et al. 2008; Holembowski, Kramer, Riedel, Sordella, Nemajerova, Dobbstein & Ute M Moll 2014; Inoue et al. 2014; A. Yang et al. 2000; Hu et al. 2007; Sah et al. 1995)

The generation of mice selectively deficient for only one of both isoforms helped to decipher their particular role in fertility and embryonic development. In mice with a specific knockout of TAp73, the neomycin resistance gene was used to substitute exons 2 and 3 thereby retaining the expression of Δ Np73 (Tomasini et al. 2008). Similar to Trp73^{-/-} mice, TAp73^{-/-} mice are characterized by hippocampal dysgenesis as well as infertility of both genders. Nevertheless, these mice show a much milder phenotype than Trp73^{-/-} mice as they do not display any signs of neuronal loss, enlarged ventricles or intracranial/gastrointestinal bleedings and thus survive much longer. In females, the loss of TAp73 leads to a reduced number of primordial and primary follicles resulting in a decreased ovulation rate. Additionally, the few ovulated oocytes are trapped under the bursa preventing them to reach the fallopian tubes and consequently the uterus. In vitro fertilization (IVF) of TAp73^{-/-} oocytes shows a normal fertilization but spindle abnormalities lead to an arrest in early cleavage leading to multinucleated blastomeres and abnormal blastocysts (Tomasini et al. 2008). Furthermore, it has been shown that maternal aging leads to the loss of p73 in oocytes resulting in the same poor oocyte quality. In contrast, male infertility is based on impaired germ cell differentiation and maturation in the testes leading to the loss of vital spermatids (Inoue et al. 2014; Holembowski, Kramer, Riedel, Sordella, Nemajerova, Dobbstein & Ute M Moll 2014).

Interestingly, the knockout of the Δ Np73 isoform did not lead to any developmental failures or infertile phenotypes whereas the overexpression of Δ Np73 leads to early embryonic lethality (Hüttinger-Kirchhof et al. 2006; Erster et al. 2006; Tissir et al. 2009; Wilhelm et al. 2010). The attempt to create a transgenic mouse strain overexpressing Δ Np73 repeatedly failed as the microinjection of constitutive promoter-driven Δ Np73 constructs in zygotes and their subsequent implantation in pseudopregnant mice did not lead to any viable transgenic litter. Further analyses revealed developmental failures at gastrulation stage as the embryos become absorbed at the implantation sites between E8.5 and E10 leaving empty uterine sacs. This strong phenotype is not unexpected taking into account that loss of p53 or p73 affects normal development and Δ Np73 acts as a pan-inhibitor on all p53 family members. Hence, the transgenic Δ Np73 mouse model used in this work has been created as a Cre-inducible expression model in order to circumvent embryonic lethality.

2 Material and Methods

2.1 Material

2.1.1 Mouse strains

Strain	Description	Background	Source
C57BL/6J	Inbred wildtype strain	C57BL/6J	Charles River
EF1α-ΔNp73α	Inducible (Cre/Lox) knockin of human Δ Np73 α under EF1 α promoter	FVB/N	Created in Stiewe lab
FVB/N (Taketo et al. 1991)	Inbred wildtype strain	FVB/N	
Gt(ROSA)26Sor^{tm1(cre/ERT)Brn} (Vooijs et al. 2001)	CreERT knockin at the ROSA26 locus; Cre recombinase is fused to the mutant estrogen hormone binding domain (ERT)	FVB/N	Anton Berns
Gt(ROSA)26Sor^{tm1(cre/ERT2)Tyj} (Ventura et al. 2007)	CreERT2 knockin at the ROSA26 locus; Cre recombinase is fused to the mutant estrogen hormone binding domain 2 (ERT2)	C57BL/6J	Provided by Stefan Gaubatz
Rag2^{tm1.1Flv} ; Il2rg^{tm1.1Flv} (Song et al. 2010)	Immunodeficiency caused by homozygous knockout of Rag2 and IL2 γ chain	BALB/C	Provided by Cornelia Brendel
Trp53^{tm1Brd} (Donehower et al. 1992)	Heterozygous Trp53 knockout	C57BL/6J	Allan Bradley

2.1.2 Cell lines

Cell line	Description	Source
B16-F10	Murine melanoma from skin of C57BL/6J	ATCC
HCT 116 p53^{-/-}	Human colorectal carcinoma from colon, p53 was inactivated by homologous recombination	Provided by Bert Vogelstein
HCT 116 p53^{+/+}	Human colorectal carcinoma from colon with endogenous wildtype p53	Provided by Bert Vogelstein
HEK 293T	Human embryonic kidney, contains SV40 large T antigen	ATCC
Hs 766T	Human pancreatic carcinoma from lymph node metastases	Provided by Matthias Lauth

MDA-MB-231	Human mammary adenocarcinoma from pleural effusion	Provided by Andreas Burchert
MEFs	Murine embryonic fibroblasts obtained at E14.5	Own establishment from timed matings
NCI-H187	Human small cell lung cancer (SCLC) from pleural effusion	Provided by Andreas Burchert
NCI-H69	Human small cell lung cancer (SCLC) from the lung	Provided by Andreas Burchert

2.1.3 Bacterial strains

The E.coli strains used in this work were ordered from Life Technologies.

Bacterial strain	Description
TOP10F'	F'[lacI ^q Tn10(tet ^R)] mcrA Δ(mrr-hsdRMS-mcrBC) φ80lacZΔM15 ΔlacX74 deoR nupG recA1 araD139 Δ(ara-leu)7697 galU galK rpsL(Str ^R) endA1 λ ⁻
DH10B	F ⁻ endA1 recA1 galE15 galK16 nupG rpsL ΔlacX74 φ80lacZΔM15 araD139 Δ(ara,leu)7697 mcrA Δ(mrr-hsdRMS-mcrBC) λ ⁻

2.1.4 Plasmids

Plasmid	Backbone	Insert	Source
pCLucIPZ-nsh	pCLucIPZ	<u>CLuc-IRES-Puro-nsh</u>	AG Stiewe
pENTR/D-TOPO ΔNp73α	pENTR/D-TOPO	ΔNp73α	AG Stiewe
pENTR/D-TOPO TAp73α	pENTR/D-TOPO	TAp73α	AG Stiewe
pENTR4 T2A	pENTR4	T2A	AG Stiewe
pGIPZ-nsh	pGIPZ	<u>GFP-IRES-Puro-nsh</u>	Dharmacon
pGLucIPZ-nsh	pGLucIPZ	<u>GLuc-IRES-Puro-nsh</u>	AG Stiewe
pGLucIPZ-shp53.1	pGLucIPZ	<u>GLuc-IRES-Puro-shp53.1</u>	AG Stiewe
pGLucIPZ-shp53.5	pGLucIPZ	<u>GLuc-IRES-Puro-shp53.5</u>	AG Stiewe
pInducer10 CLuc-nsh	pInducer10	CLuc-nsh	AG Stiewe
pInducer10 GLuc-nsh	pInducer10	GLuc-nsh	AG Stiewe
pInducer10 GLuc-shp73.3	pInducer10	GLuc-shp73.3	AG Stiewe
pInducer10 GLuc-shp73.5	pInducer10	GLuc-shp73.5	AG Stiewe
pInducer20	pInducer20		Stephen J. Elledge
pInducer20 ΔNp73α	pInducer20	DNp73a	This work
pInducer20 T2A	pInducer20	T2A	This work
pInducer20 TAp73α	pInducer20	TAp73a	This work
pMD2.G	pMD2.G	VSV-G	Didier Trono
psPAX2	psPAX2		Didier Trono

2.1.5 Oligonucleotides

2.1.5.1 siRNAs

The siRNAs are derived from Dharmacon/Thermo Scientific.

Name/Gen e	Target sequence (5' ► 3')	Modification	Supplier
nsi	UGGUUUACAUGUCGACUAA UGGUUUACAUGUUGUGUGA UGGUUUACAUGUUUUUCUGA UGGUUUACAUGUUUUUCCUA	OnTargetPlus Pool	Dharmacon
p73 si8	GGCCATGCCTGTTTACAAG	siGENOME	Dharmacon

2.1.5.2 shRNAs

The shRNAs are derived from the Pooled Human GIPZ Whole Genome Library (Thermo Scientific). Individual plasmids were picked from the pGIPZ plasmid library and shRNAs were cloned into pGLucIPZ or pCLucIPZ vectors via EcoRI/XhoI digestion and ligation.

shRNA #	shRNA (sense)- loop- shRNA (antisense) (5' ► 3')	Oligo ID
nsh	TCTCGCTTGGGCGAGAGTAAG- TAGTGAAGCCACAGATGTA- CTTACTCTCGCCCAAGCGAGA	
shp53.1	GGAGGATTTTCATCTCTTGTAT- TAGTGAAGCCACAGATGTA- ATACAAGAGATGAAATCCTCC	V2LHS217
shp53.5	CCCGGCGCACAGAGGAAGAGAA- TAGTGAAGCCACAGATGTA- TTCTCTTCTCTGTGCGCCGG	V3LHS333920
shp73.3	GGACTGGAAATTGTCAATATT- TAGTGAAGCCACAGATGTA- AATATTGACAATTTCCAGTCC	V2LHS-181826
shp73.5	CCGCACAGTTCGGCAGCTACA- TAGTGAAGCCACAGATGTA- TGTAGCTGCCGAAGTGTGCGG	V3LHS-330453

2.1.5.3 Primers

Primers and probes were designed with the GenScript Real-time PCR Primer Design tool (<https://www.genscript.com/ssl-bin/app/primer>) and tested for specificity by alignment to the human or murine genome using the BLAST alignment tool (http://blast.ncbi.nlm.nih.gov/Blast.cgi?CMD=Web&PAGE_TYPE=BlastHome).

Oligonucleotides were synthesized by Sigma-Genosys if not indicated otherwise.

Genotyping primers

Target	Forward primer (5' ► 3')	Reverse primer (5' ► 3')
CreERT or CreERT2 transgene	GCACGTTACCCGGCATCAAC	CGATGCAACGAGTGATGAGGTTTC
EF1 α - Δ Np73 α transgene	TAGGCCAGCTTGGCACTTG	TGGAGCTGGGTTGTGCGTA
Trp53 KO allele	CAGGCTAACCTAACCTACCAC	TGAAGAGCTTGGCGGCGAATG
Trp53 wt allele		ACAGCGTGGTGGTACCTTAT

qPCR and semiquantitative (sq) PCR primers

Target	Forward primer (5' ► 3')	Reverse primer (5' ► 3')
HA-Flag- Δ Np73	GTACCCATACGACGTCCCAG	TCATCTGGTCCATGGTGCCT
h Δ Np73 3'UTR	CAAACGGCCCCGCATGTTCCC	TTGAACTGGGCCGTGGCGAG
hGAPDH	AATGGAAATCCCATCACCATC T	CGCCCCACTTGATTTTGG
hp73 (sqRT)	GACGGAATTCACCACCATCCT	CCAGGCTCTCTTTCAGCTTCA
hp73 3'UTR	AGGCTGAGGAAGCTGAGTGA	CTGCAGATTTGCCTGGATTT
hTAp73 3'UTR	GGCTGCGACGGCTGCAGAGC	GCTCAGCAGATTGAACTGGGCCA TG
mActin	CCTGAGCGCAAGTACTCTGTG T	GCTGATCCACATCTGCTGGAA
mID4 ¹	AGGGTGACAGCATTCTCTGC	CCGGTGGCTTGTTTTCTCTTA
mITGB4 ¹	TTGCGACTACGAAATGAAGG	TGCGTCACCGTAGAAGAGAC
mJAG1 ¹	AAATGGCTGGAAAGGAAAGA	CGGGACACATGCACTTAAAC
mJAG2 ¹	GACATCAATCCCAACGACTG	TAGGCGTCACACTGGAACCTC
mKDR ¹	TGATTTACCTGGCACTCTC	TTTCACATCCCGGTTTACAA
mSerpB10 ¹	GAAGCAATAGATGGCCTGGA	TGTCTGCACTGGTCCACTTATC
mSerpB2 ¹	CACCACAAGAAACCCAGAGA	CTCCTGCTTGTGCCTGTAAA
mWnt7a ¹	CGCTGGGAGAGCGTACTG	CGATAATCGCATAGGTGAAGG

ChIP primers

Binding site	Forward primer (5' ► 3')	Reverse primer (5' ► 3')
mCdkn1a -1920 site	ATCCGAGGAGGAAGACTGG	TGCTTTGGAGAAGCTGTGAG
mCdkn1a -2850 site	CTGCATCAGTCCTCCCATC	ATGTTCTGAAGCCAGAAA

Digital PCR primers and probes

Unlike the probe design described before (2.1.5.3), GFP and viral integration sites were detected using short hydrolysis probes from the Universal Probe Library (UPL #149, Roche #04694350001). For target detection, a third primer

¹¹ 5% DMSO

was used composed of the particular forward primer sequence extended by the complementary sequence of the UPL #149 probe (White et al. 2009).

The VIC-labeled TaqMan Copy Number Reference Assay (Life Technologies #4458366) served as reference.

Target		Primers (5' ► 3')		Probe (5' ► 3') [dye] sequence [quencher]
CLuc	for	AGCTGAACGACTCTGCAATAG		[6FAM] TCGCCGGTCAAAGT GATCTTGATCA [BHQ1] or [JOE] TCGCCGGTCAAAGTG ATCTTGATCA [BHQ1]
	rev	CTTGTGGCACACGTTACATTTTC		
GFP	for	GATGAAGAGCACCAAAGGCG		UPL#149: [6FAM] <u>CCGCCGCT</u> [BHQ1]
	rev	GGTAGAAGCCGTAGCCCATC		
	UPL_for	<u>GGCGGCGAGATGAAGAGCACCAA</u> AGGCG		
GLuc	for	GATCGTCGACATTCCTGAGATT		[6FAM] TCCATGGGCTCCAA GTCCTTGAAC [BHQ1]
	rev	GATCGACCTGTGCGATGAA		
Viral integration	for	GGGCTAATTCACTCCCAACGA		UPL#149: [6FAM] <u>CCGCCGCT</u> [BHQ1]
	rev	CCTCTGGTTTCCCTTTCGCT		
	UPL_for	<u>GGCGGCGAGGGCTAATTCACTCC</u> CAACGA		

2.1.6 Antibodies

2.1.6.1 Primary antibodies

Antigen	Clone/ Order no	Host	Supplier	Western Blot	ChIP	IHC
p53	DO-1	mouse	Dr. B. Vojtesek	1:5000		1:1000
total p73	EP436Y	rabbit	Epitomics	1:500		1:1000
TAp73	A300-126A	rabbit	Bethyl	1:500		
ΔNp73	#986	rabbit	custom made by Eurogentec	1:300	20 µl	
Gaussia luciferase	401P	rabbit	NanoLights	1:1000		1:1000
β-actin	AC-15/ ab- 6276	mouse	Abcam	1:10000		

2.1.6.2 Secondary antibodies

Antigen	Linked to	Clone/ Order no	Host	Supplier	Western Blot	IHC
mouse IgG	HRP	NA9310	sheep	Amersham	1:5000	
rabbit IgG	HRP	NA9340	donkey	Amersham	1:5000	
mouse IgG	Alexa 680	A10038	goat	Molecular Probes	1:5000	
mouse IgG	Alexa 488	A11029	goat	Molecular Probes	1:5000	

mouse IgG	Biotin	EO46401	rabbit	Dako		1:500
rabbit IgG	Biotin	EO43201	goat	Dako		1:500

2.1.7 Chemicals

All chemicals were ordered from AppliChem, Carl Roth or Sigma unless indicated otherwise.

- Nutlin-3, racemic (cell culture) InSolution Nutlin-3 (Merck #444151)
- Nutlin-3, racemic (in vivo) (APAC Pharmaceutical #665451)
- Klucel (Fagron, Hydroxypropylcellulose GF)

2.1.8 Consumables

384 well qPCR plates	4titude
96 well plates, white, V-bottom	Greiner
cDNA Microarray Slides SurePrint G3 Mouse GE 8x60K	Agilent Technologies
Cuvettes for Bradford	Sarstedt
Digital PCR Chips QuantStudio 3D	Life Technologies
Electroporation cuvettes for bacteria 1 mm	Eurogentec
Eppendorf reaction tubes (1.5 & 2 ml)	Eppendorf
Experion RNA StdSens Analysis Kit	Biorad
Falcons (15 & 50 ml)	Sarstedt
Filters Filtropur 0.45 µm	Sarstedt
Microscope slides SuperFrost Plus	Thermo Fisher
Needles	Braun
Nitrocellulose Membrane Hybond ECL	Amersham
Pipette tips	Life Technologies
Syringes	Braun/BD
Tissue culture multi-well plates	Greiner
Tissue culture dishes	Sarstedt
Tissue Lyser Stainless Steel Beads 5 mm	Qiagen

2.1.9 Hardware and devices

Benchtop Tissue Processor TP1020	Leica
Binocular microscope SZ	Olympus
Tissue culture Hood MSC advantage	Thermo
Tissue culture Incubator HERAccl 240	Thermo
Tissue culture Incubator HERAccl 240i CO2 Incubator	Thermo
Centrifuge 5415R	Eppendorf
Centrifuge 5810R	Eppendorf
Centrifuge J2-21	Beckman
ChemiDoc MP	BioRad
Canon Eos 70D digital single lens reflex camera	Canon
Digital PCR Chip Loader QuantStudio 3D	Life Technologies
Digital PCR Chip Reader QuantStudio 3D	Life Technologies

DNA Microarray Slide Scanner	Agilent Technologies
Electrophoresis Chamber DNA Gels Biometra	Whatman
Electrophoresis Chamber Xcell 4 Sure Lock Midi Cell	Invitrogen
Electrophoresis Chamber Xcell Sure Lock Novex Mini Cell	Invitrogen
Electroporator Micro Pulser	BioRad
Embedding Cooling station EG 1150C	Leica
Embedding station EG 1150H	Leica
Freezer HERA Freeze TOP, -80°C	Thermo
In vivo Imaging System IVIS 50	Caliper
Isoflurane Vaporizer Dräger 19.1	Dräger
LabChip XT	Caliper
Luminometer Orion II	Berthold
Magnetic Mixer Ikamag REO	IKA
Microscope CKX41	Olympus
Microscope ICC 50HD	Leica
Microwave	Severin
Milli-Q Biocel	Millipore
Mouse restrainer	University Marburg
Needle RN 22/51/4 or RN 27/25/4	Hamilton
Photometer	Eppendorf
Power Supply Power Pac 200	BioRad
Power Supply Power Pac 300	BioRad
QIAcube	Qiagen
QIAxcel	Qiagen
Roller Mixer SRT2	Stuart
Rotary Microtome RM 2235	Leica
Scale PLB 1000-2	Kern
Sonopuls	Bandelin
Sonorex RK100	Bandelin
Special accuracy scale New Classic MS	Mettler Toledo
Spectrophotometer NanoDrop ND-1000	Nanodrop
Syringe for tumor cell injection 100µl	Hamilton
Tank Blot	PeqLab
Tank Blot Criterion Blotter	BioRad
Thermocycler GeneAmp PCR System 9700 with Flat Block	Life Technologies
Thermocycler Light Cycler 480 II	Roche
Thermocycler Mastercycler gradient	Eppendorf
Thermocycler Mx3005P	Stratagene
Thermomixer comfort	Eppendorf
Tissue Lyser LT	Qiagen
Gel iX Imagersystem	Intas
Vortexer REAX 2000	Heidolph

2.2 Methods

2.2.1 Molecular Biology

2.2.1.1 Genotyping PCR

For genotyping of genetically engineered mice, tail biopsies were taken at the age of 2-3 weeks and lysed over night at 65 °C in 200 µl PBNB buffer/60 µg proteinase K. Proteinase K was then inactivated by incubation at 95°C for 10 minutes. 1 µl of the lysed biopsy was taken for PCR. For primers see 2.1.5.3.

➤ EF1 α - Δ Np73 α :

21.5 µl	H ₂ O	
1 µl	tail biopsy	
0.6 µl	for primer [10 µM]	
0.6 µl	rev primer [10 µM]	
3 µl	HotStarTaq Plus buffer (10x)	
0.6 µl	dNTPs [10 mM]	
1.5 µl	DMSO	
0.2 µl	HotStarTaq Plus DNA Polymerase	

94°C	15 min	}	x 10, -0.5 °C/cycle
95°C	15 sec		
60°C	30 sec		
72°C	2 min		
95°C	15 sec	}	x 25
55°C	30 sec		
72°C	2 min		
4°C	forever		

1500 bp = floxed Δ Np73 transgene

450 bp = recombined Δ Np73 transgene

➤ CreERT/CreERT2:

14.75 µl	H ₂ O	
1 µl	tail biopsy	
1.25 µl	for primer [10 µM]	
1.25 µl	rev primer [10 µM]	
5 µl	GoTaq buffer (5x)	
0.5 µl	dNTPs [10 mM]	
0.25 µl	GoTaq DNA Polymerase	

95°C	2 min	}	x 30
95°C	30 sec		
64°C	30 sec		
72°C	1 min		
72°C	2 min		
4°C	forever		

300 bp = CreERT transgene

➤ Trp53:

8.25 µl H₂O
 1 µl tail biopsy
 0.75 µl for primer [10 µM]
 0.75 µl rev primer (wt) [10 µM]
 0.75 µl rev primer (KO) [10 µM]
 3 µl GoTaq buffer (5x)
 0.3 µl dNTPs [10 mM]
 0.2 µl GoTaq DNA Polymerase

94°C 3 min
 94°C 1 min
 58°C 30 sec
 72°C 1 min
 72°C 2 min
 4°C forever
 600 bp = p53 wt allele
 750 bp = p53 knockout allele

} x 30

The size of amplified products was assessed either by QIAxcel capillary electrophoresis with precast gel cartridges (Qiagen) or by agarose gel electrophoresis (2.2.1.2).

- PBNB buffer 50 mM KCl, 10 mM Tris HCl pH8.3, 2.5 mM MgCl₂ x 6H₂O, 0.45% NP-40, 0.45% Tween 20
- Proteinase K 20 mg/ml (AppliChem #A4392,0010)
- HotStarTaq Plus reagents (Qiagen #203605)
- GoTaq reagents (Promega #M3178)

2.2.1.2 Separation of nucleic acids by agarose gel electrophoresis

DNA fragments were resolved by size using agarose gel electrophoresis. Agarose was melted in 1x TAE buffer with a final concentration of 0.5-2% agarose, depending on expected fragment size. Lukewarm liquid gel was supplemented with ethidium bromide for visualization of DNA fragments and poured in a gel cast. DNA samples were supplemented with DNA loading buffer and fragments were separated under constant voltage in the gel in a gel chamber filled with 1x TAE buffer. UV light illuminated ethidium bromide intercalating in the DNA using Gel iX Imagersystem (Intas).

- Agarose NEEO Ultra Quality (Carl Roth #2267.4)
- 50x TAE 2 M Tris HCl, 1 M acetic acid, 50 mM EDTA pH 8.0
- Ethidium bromide 0.025% (Carl Roth #HP47.1)
- DNA loading buffer Loading Buffer DNA IV (AppliChem #A3481,0010)

➤ DNA ladder GeneRuler DNA Ladder Mix (Fermentas #SM0332)

2.2.1.3 Genomic DNA (gDNA) isolation from mammalian cells

Isolation and purification of gDNA derived from cell culture or murine tissue was conducted according to manufacturers protocol using either the peqGold tissue DNA Mini Kit (PeqLab #12-3096-01) or the QIAamp DNA blood Mini Kit (Qiagen #51104).

2.2.1.4 RNA Isolation from mammalian cell culture

For isolation of mRNAs from cell culture, cells were washed once with phosphate-buffered saline (PBS), then lysed directly on the cell culture dish by adding 600 µl RLT buffer (Qiagen #79216) and scraped from the dish. RNA was isolated from cell lysates with the RNeasy Mini Kit (Qiagen #74106) according to manufacturer's protocol using the QIAcube (Qiagen). RNA quality and yield were evaluated by spectrophotometric measurement (Nanodrop ND-1000).

2.2.1.5 RNA isolation from tissue

For murine tissue samples, mRNA was isolated using TRIzol (Life Technologies #15596026) in combination with the Tissue Lyser (Qiagen). Therefore, 10-30 mg of tissue were first stored at -80°C for 30 min for better tissue disruption. After addition of 1 ml TRIzol, tissue was comminuted by a 5 mm steel ball (Qiagen) on the Tissue Lyser for 2-6 minutes at 50 Hz depending on consistency of the tissue. 200 µl chloroform were added, samples were vortexed for 15 sec and incubated for 2-3 minutes. After centrifugation (15 min at 4°C and 12000 g), the mixture separated in 3 phases: the lower red phase containing protein, the interphase containing DNA and the upper aqueous phase containing RNA. The upper phase was then transferred carefully into a fresh tube. RNA was precipitated by adding 500 µl isopropanol. After centrifugation (10 min at 4°C and 12000 g), supernatant was discarded and the RNA pellet was washed with 1 ml 75% Ethanol and centrifuged (5 min at 4°C and 7500 g). The pellet was then air-dried and dissolved in 25 µl RNase free water at 55°C for 10 min. RNA quality and yield were determined by spectrophotometric measurement (Nanodrop ND-1000). For a more accurate analysis of mRNA quality and quantity in microarray samples, purified nucleic acids were evaluated with the Experion RNA StdSens Analysis Kit (Biorad

#700-7103). Only samples with a RQI ≥ 9 were used for Microarray experiments.

2.2.1.6 cDNA synthesis

To obtain cDNA for expression analysis in semiquantitative PCR or qPCR, RNA was reversely transcribed into cDNA with the Omniscript RT Kit (Qiagen #205111).

Reverse Transcriptase mix:

1 μ g	RNA
2 μ l	Buffer RT (10x)
2 μ l	dNTP Mix [10 mM]
2 μ l	Oligo-dT Primer
0.2 μ l	RNase Inhibitor
1 μ l	<u>Reverse Transcriptase</u>
ad 20 μ l with RNase free water	

For semiquantitative PCR, a control RT reaction without reverse transcriptase was prepared for every sample to exclude contamination by residual genomic DNA.

The RT reaction was then incubated at 37°C for one hour. cDNA was diluted 1:1 with RNase free water and used for qPCR or semiquantitative PCR.

2.2.1.7 qPCR

In qPCR, gene expression is analyzed by detection of amplification products at the end of every single amplification cycle. SYBR Green dye was used to quantify double-stranded amplicons. This fluorophore binds primarily to double-stranded DNA, independent from the DNA sequence. When complexed with DNA, the fluorophore can be excited by blue light, thereby emitting green light. Amplification and detection was performed on a Thermal LightCycler 480 (Roche).

For gene expression analysis on mRNA levels, RNA samples were prepared and cDNA was synthesized as described above (2.2.1.6). Each sample was measured in triplicates using the SYBR Green JumpStart Taq ReadyMix (Sigma #205111).

qPCR Mastermix:

5 μ l	2x SYBR Green Mix
0.2 μ l	for primer [10 μ M]
0.2 μ l	rev primer [10 μ M]
3.6 μ l	H ₂ O
0.05 μ l	VisiBlue dye (tebu bio, #K101)

Some primers were used with 5% DMSO to decrease unspecific binding of primers to DNA and to prevent secondary structure formation of primers/template, thereby enhancing target amplification (2.1.5.3).

First, the mastermix for each primer pair was pipetted in 384 well plates and then 1 μ l of diluted cDNA was added to every single well. For most target genes, qPCR was run on the Thermal LightCycler 480 with the following programs:

➤ qPCR standard cycler program:

	94°C	2 min	
amplification	{ 94°C 20 sec 60°C 20 sec 72°C 20 sec }	x 45	
melting curve	{ 95°C 15 sec 60°C 30 sec 60°C to 95°C (0.11°C/sec) continuous detection }		

➤ TAp73 qPCR cycler program:

	94°C	2 min	
touchdown	{ 94°C 20 sec 70°C 20 sec 72°C 20 sec }	x 10, -0.5°C/cycle	
amplification	{ 94°C 20 sec 65°C 20 sec 72°C 20 sec }	x 30	
melting curve	{ 95°C 15 sec 60°C 30 sec 60°C to 95°C (0.11°C/sec) continuous detection }		

➤ $\Delta Np73$ qPCR cyclers program:

	94°C 2 min	
touchdown	$\left\{ \begin{array}{l} 94^\circ\text{C} \ 20 \text{ sec} \\ 68^\circ\text{C} \ 20 \text{ sec} \\ 72^\circ\text{C} \ 20 \text{ sec} \end{array} \right\}$	x 10, -0.5°C/cycle
amplification	$\left\{ \begin{array}{l} 94^\circ\text{C} \ 20 \text{ sec} \\ 63^\circ\text{C} \ 20 \text{ sec} \\ 72^\circ\text{C} \ 20 \text{ sec} \end{array} \right\}$	x 30
melting curve	$\left\{ \begin{array}{l} 95^\circ\text{C} \ 15 \text{ sec} \\ 60^\circ\text{C} \ 30 \text{ sec} \\ 60^\circ\text{C} \text{ to } 95^\circ\text{C} \ (0.11^\circ\text{C}/\text{sec}) \text{ continuous detection} \end{array} \right.$	

The analysis of data is based on the $\Delta\Delta C_t$ method. Therefore, the thermal cycler measured the C_t value for each sample. This value represents the PCR cycle in which the detected fluorescent signal exceeds the background threshold. After calculation of the average of all triplicates, the ΔC_t value was calculated by subtraction of the C_t values of the target gene from C_t values of the reference gene (β -actin for mouse, GAPDH for human):

$$\Delta C_t = C_t[\text{target gene}] - C_t[\text{reference gene}]$$

In the next step, a reference sample is used for further calculations (e.g. untreated samples, input controls):

$$\Delta\Delta C_t = \Delta C_t[\text{sample}] - \Delta C_t[\text{reference sample}]$$

The standard deviation was calculated as follows:

$$\text{StDev} [\Delta C_t, \Delta\Delta C_t] = \sqrt{\text{StDev} [\text{target gene}]^2 + \text{StDev} [\text{reference gene}]^2}$$

To allow comparisons between different samples, linear values were calculated:

$$\begin{aligned} \text{relative expression} &= 2^{-\Delta\Delta C_t} \\ \pm \text{ error on relative expression} &= 2^{-(\Delta\Delta C_t \pm \text{StDev}[\Delta\Delta C_t])} \end{aligned}$$

2.2.1.8 Semiquantitative PCR

In contrast to qPCR, gene expression analysis by semiquantitative PCR is an endpoint analysis where the PCR product is quantified by agarose gel electrophoresis. To compare the amount of amplified DNA, it is an absolute

requirement to end the PCR during its exponential amplification phase before it reaches the plateau phase. Therefore, the number of amplification cycles must be adjusted carefully depending on the amount of transcripts in the sample. Semiquantitative PCR was performed for expression analysis of the HA-Flag- Δ Np73 α transgene in murine tissue and cells. RNA was isolated and reversely transcribed into cDNA (2.2.1.6). For detection of the transgenic mRNA, primers were used which bind within the region of the HA-Flag tag (forward primer) and the Δ Np73 α sequence (reverse primer). As the transgene encodes for the cDNA of Δ Np73, -RT controls were used to exclude contamination by genomic DNA additionally to DNase digestion performed during RNA purification (2.2.1.4 and 2.2.1.5)

semiquantitative PCR mix:

16 μ l H₂O
2 μ l HotStarTaq Plus buffer (10x)
0.4 μ l dNTPs [10mM]
0.4 μ l for primer [10 μ M]
0.4 μ l rev primer [10 μ M]
0.13 μ l HotStarTaqPlus DNA Polymerase (Qiagen)
1 μ l cDNA

Cycler program:

95°C	5 min	
95°C	30 sec	} x10, -0.5°C/cycle
62°C	30 sec	
72°C	1 min	
95°C	30 sec	
57°C	30 sec	
72°C	1 min	
72°C	2 min	
4°C	forever	

10 μ l per reaction were then loaded on a 1% agarose gel.

2.2.1.9 Two-color based Microarray

Expression analysis of the whole transcriptome was performed by cDNA Microarray analyses (Schulze & Downward 2001). Here, a whole library of oligonucleotides complementary to cDNAs is spotted on a solid phase (e.g. glass slide). Fluorescently labeled cDNAs of samples hybridize to the spotted oligonucleotides which are then detected in a microarray slide scanner.

Differential expression was evaluated on single gene level as well as for whole gene sets (GSEA) in canonical pathways.

Starting material was amplified and fluorescently labeled with Cy5-CTP by T7 RNA polymerase using the Quick Amp Labeling Kit (Agilent #5190-0444). The Universal Mouse Reference (Agilent # 740100) served as reference control and was labeled likewise with Cy3-CTP. The synthesized complementary RNAs (cRNAs) were purified with the RNeasy Mini Kit (Qiagen #74106) and then hybridized to SurePrint G3 Mouse GE 8x60K Microarray slides (Agilent #G4852A). Fluorescence intensities R (Cy5-red labeled samples) and G (Cy3-green labeled reference) were detected for every single probe on the Microarray with the slide scanner (Agilent #G2565CA) and processed with the Feature Extraction software tool (Agilent). Microarrays were performed in collaboration with the Genomics Unit Marburg (formerly Michael Krause).

Microarray analysis: differential expression on single-gene level

Data first underwent LOESS normalization to minimize intensity-dependent variations of the dyes (Y. H. Yang et al. 2002). For any further analysis normalized, log₂ transformed data were used. The quality of the microarrays was determined by MA plots. Therefore, M and A values for every single probe were calculated and plotted against each other in a graph.

M reflects the difference of the log intensity values, the expression:

$$M = \log_2 (R/G) = \log_2 (R) - \log_2 (G)$$

And A is the average log intensity:

$$A = \frac{1}{2} \log_2 (RG) = \frac{1}{2} (\log_2 (R) + \log_2 (G))$$

The samples were then divided in two groups: Δ Np73 high (rec- Δ Np73) and Δ Np73 low (LSL- Δ Np73 or CreERT) expressing cells. To exclude weak background signals, only probes were analyzed in which at least one sample showed an average intensity (A) ≥ 5 . Next, averages of log intensity values (M) for both groups were calculated and differential expression between both groups (log₂ fold change, log₂(FC)) was assessed to identify up- and down-regulated genes:

$$\log_2(\text{FC}) = M (\Delta\text{Np73 high}) - M (\Delta\text{Np73 low})$$

To get an overview, the ranked gene list of all differentially expressed genes which were significantly up- or downregulated by at least 2-fold ($\log_2(\text{FC}) \geq 1$ or ≤ -1 ; $p \leq 0.05$) was used to create a heatmap with the HeatMapImage module

from

Gene	Pattern
------	---------

(<http://www.broadinstitute.org/cancer/software/genepattern/modules>).

Microarray analysis: differential expression of whole gene sets (GSEA)

Gene set enrichment analysis was conducted to discover differentially regulated pathways from Microarray data (Subramanian et al. 2005). Using this computational method, a collection of samples belonging to two groups (e.g. ΔNp73 high versus ΔNp73 low expressing cells) is investigated for enrichment of genes from beforehand defined gene sets with common biological functions. Depending on whether the genes within a gene set are enriched rather at the top or the bottom of the rank-ordered gene list, a gene set is found to be up- or downregulated in one of the two groups. In this work, the curated gene sets of canonical pathways (C2.CP) from the Molecular Signature Database (MSigDB v4) were analyzed with default settings except the permutation type which was changed to "gene sets". Again, only probes with $A \geq 5$ for at least one sample were included in the analysis. The networks of significantly up- and downregulated gene sets with a p-value ≤ 0.005 and a false discovery rate (FDR) ≤ 0.1 were visualized by Cytoscape v 3.2.0 (Cline et al. 2007) using the Enrichment Map plugin v 2.0.1 (Merico et al. 2010).

2.2.1.10 Digital PCR

Digital PCR is used for exact quantification of DNA target sequences. Like in qPCR, primers are designed to produce a specific 50-150 bp amplicon of the target sequence. For further specificity, a fluorescently labeled probe is added to the PCR reaction, which is composed of a fluorescent dye at the 5' end and a corresponding quencher at the 3' end, comparable to TaqMan probes. During the amplification process, the probe binds specifically to the amplicon. When the polymerase exerts its 5'-to-3' exonuclease activity during amplification, the probe is degraded and the fluorophore released from the quencher, thereby emitting light.

In contrast to other (semi-) quantitative PCRs, digital PCR does not perform one single PCR reaction for one sample. With the here used QuantStudio3D Digital

PCR platform from Life Technologies, each sample is loaded on a QuantStudio3D Digital PCR Chip (#4485507) with 20000 independent nanoscale reaction wells, thus providing 20000 data points for one sample in one run. Unlike qPCR, emitted light does not have to reach a defined threshold in a linear range. Instead, the chip is read out in the QuantStudio 3D Digital PCR Instrument (#A25606) after the amplification process and every single reaction compartment is measured separately and either rated as “positive” or “negative” for light emission, like a binary code (→ digital PCR) (Baker 2012). Furthermore, the chip reader distinguishes two dyes, FAM and VIC, thus facilitating simultaneous quantification of two targets in one sample.

In this work, digital PCR was used to analyze the tumor composition from transplantation experiments in mice. For determination of the ratio between GLuc- and CLuc-positive cells, both targets were measured simultaneously in one reaction using a FAM-labeled GLuc and a JOE-labeled CLuc probe (2.1.5.3). In experiments with more than two targets, each target was quantified in a separate reaction. Apart from the FAM-labeled primer/probe mix detecting the target, a VIC-labeled primer/probe mix detecting murine Tfrc (Life Technologies #4458366) was employed as reference for relative quantification. Digital PCR was performed according to manufacturer’s protocol. Primer mixes contained a 10 μ M concentration of each primer, whereas probes were used in a 2.5 μ M concentration if not indicated otherwise.

➤ digital PCR mix for simultaneous GLuc/CLuc quantification:

7.5 μ l QuantStudio 3D digital PCR master mix (2x)
0.75 μ l Primer mix (GLuc_for, GLuc_rev, CLuc_for & CLuc_rev)
1.5 μ l Probe mix (FAM-GLuc & JOE-CLuc)
100 ng gDNA (human)
ad 15 μ l H₂O

➤ digital PCR mix with target specific probe and Tfrc reference:

7.5 μ l QuantStudio 3D digital PCR master mix (2x)
0.75 μ l Primer mix (for_primer & rev_primer)
1.5 μ l FAM-labeled probe
0.75 μ l VIC-labeled Tfrc reference assay
250 ng gDNA (murine)
ad 15 μ l H₂O

➤ digital PCR mix with UPL#149 probe and Tfrc reference:

7.5 µl QuantStudio 3D digital PCR master mix (2x)
1.73 µl Primer/Probe mix (see below)
0.75 µl VIC-labeled Tfrc reference assay
250 ng gDNA (murine)
ad 15 µl H₂O

➤ Primer/Probe mix:

3 µl for_primer
6 µl rev_primer
3 µl for_primer_UPL
5.25 µl VIC-labeled UPL#149 probe

The whole reaction was then loaded on the PCR chip and run under the following program:

digital PCR cycler program:

96°C	10 min	} x40
60°C	2 min	
98°C	30 sec	
60°C	2 min	
4°C	forever	

After readout in the chip reader, data were analyzed online with the QuantStudio 3D Analysis Suite Cloud Software (<https://www.lifetechnologies.com/iaam/loginDisplay>). For calculation of GLuc/CLuc ratios obtained from the same PCR reaction, absolute values (copies/reaction) were used:

$$G/C \text{ ratio in gDNA} = \frac{\text{GLuc (FAM) copies/reaction}}{\text{CLuc (VIC) copies/reaction}}$$

When FAM-labeled targets were measured in independent reactions, relative quantification was performed involving the VIC-labeled Tfrc reference:

$$\text{rel. [target]} = \frac{\text{target (FAM) copies/reaction}}{\text{Tfrc (VIC) copies/reaction}}$$

$$G/C \text{ ratio in gDNA} = \frac{\text{rel.[GLuc]}}{\text{rel.[CLuc]}}$$

2.2.1.11 Gateway cloning

The LR clonase II enzyme mix (Life Technologies #11791-100) was used for recombination of an entry clone, containing the gene of interest flanked by *attL* sites, and a destination vector containing *attR* sites. Recombination was performed according to manufacturer's guidelines. The product was then transformed into electrocompetent bacteria.

2.2.1.12 Transformation of *E.coli* by electroporation

To screen for desired clones and to propagate plasmid DNA, cloning products were transformed into electrocompetent bacteria. Frozen bacteria were thawed on ice and supplemented with 1-2 μ l of cloning product. Bacteria were then transferred into a chilled electroporation cuvette and pulsed with 1.8 kV in a Micropulser (BioRad). After addition of 0.5 ml pure LB medium, bacteria were incubated on a shaker for 30-60 minutes at 37°C and 300 rpm. 50-100 μ l of transformed bacteria were then plated on LB agar plates supplemented with antibiotics for selection of positive clones. Agar plates were incubated overnight at 37°C and clones were picked for small scale plasmid preparations (2.2.1.13).

- LB medium 5 g/l NaCl, 5 g/l yeast extract, 10 g/l Bactotryptone
- Agar Plates 1.5% agar-agar in LB medium either with Kanamycin (50 μ g/ml) or Ampicillin (100 μ g/ml)

2.2.1.13 Plasmid DNA isolation from bacteria

Small scale plasmid preparation

To obtain small amounts of plasmid DNA, e.g. to screen for correct clones by restriction digest or sequencing, small scale plasmid preparation was applied. Overnight cultures were inoculated with liquid LB containing antibiotics to maintain selective pressure for positive clones. Liquid cultures were then processed by alkaline lysis method. 2 ml of the overnight culture were centrifuged and resuspended in 300 μ l P1 Buffer. Addition of 300 μ l P2 Buffer lysed the bacteria for 5 min on ice. 300 μ l P3 buffer were added to neutralize the reaction. The suspension was then centrifuged (10 min at full speed) and supernatant was transferred into a fresh tube. DNA was precipitated with 700 μ l isopropanol and pelleted by centrifugation at full speed for 30 min at 4°C. The pellet was washed once with 70% ethanol, dried at 37 °C for 10-20 min and

resuspended in 50 µl ddH₂O. DNA yield and quality were assessed at the Nanodrop ND-1000.

- P1 buffer 50 mM Tris HCl pH 7.5, 10 mM EDTA pH 8.0, 100 µg/ml RNaseA
- P2 buffer 200 mM NaOH, 1% SDS
- P3 buffer 3 M KAc pH 5.5

Medium scale plasmid preparation

Medium scale plasmid preparations were used to obtain larger and cleaner amounts of plasmids, e.g. for cloning or transfection of eukaryotic cells. For this purpose, 100 ml liquid cultures were inoculated with small scale overnight precultures (see "Small scale plasmid preparation"). Lysis and purification was performed by anion-exchange technology using Nucleobond Xtra Midi Kit (Macherey-Nagel #740410.100) according to manufacturer's protocol.

Large scale plasmid preparation

Large scale preparations were needed for immunization of C57BL/6J mice with plasmid DNA. Here, 500 ml LB medium were inoculated with small scale overnight pre-cultures (see "Small scale plasmid preparation"). The liquid cultures were then purified via anion exchange-based EndoFree Plasmid Mega Kit (Qiagen #12381).

2.2.2 Proteinbiochemistry

2.2.2.1 Preparation of protein lysates

Tissue culture cells were washed once with chilled PBS and were harvested directly from tissue culture plates by adding NP-40 lysis buffer. To exclude cell debris, lysates were centrifuged for 5 min (4°C with 1500 rpm) and supernatant was transferred into a fresh tube.

For protein detection in organs, 20-30 mg of tissue were put in a 2 ml tube together with NP-40 lysis buffer and a 5 mm stainless steel bead (Qiagen). Tissue was then broken up on the Tissue Lyser (Qiagen) for 2 minutes at 50 Hz, centrifuged and supernatant was transferred into a fresh tube.

Total protein was quantified in a colorimetric assay using Bradford. The Coomassie blue dye in the acidic Bradford solution complexes proteins, thus turning from red to blue colour. This shifts the absorption maximum from 470 nm to 595 nm which is then measured in the photometer (Eppendorf).

- NP-40 lysis buffer 50 mM Tris, pH 8.0, 150 mM NaCl, 5 mM EDTA pH 8.0, 2% NP-40
- Protease Inhibitor 1 tablet cOmplete Protease Inhibitor Cocktail (Roche #04693116001) diluted in 5 ml ddH₂O
- Bradford reagent Quick Start Bradford 1x Dye Reagent (BioRad #500-0205)

2.2.2.2 Protein separation by SDS Page

For preparation of protein samples, 20-50 µg of protein were supplemented with Rotiload as sample reducing agent, denatured at 95°C for 5 min and then loaded on precast NuPAGE Novex 4-12% Bis-Tris Gels. For separation of proteins by size, gels were run under constant voltage (100-150 V) in NuPAGE SDS MOPS Running Buffer for 1-2 hrs.

- Rotiload 4x Rotiload 1 (Carl Roth #K929.1)
- SDS-Page gels NuPAGE® Novex® Bis-Tris Mini and Midi Gels (Life Technologies)
- Running buffer NuPAGE® MOPS SDS Running Buffer (Life Technologies)
- Protein ladder PageRuler Prestained Protein Ladder (Thermo Scientific #26616)

2.2.2.3 Protein detection by Western Blot

Proteins were transferred from SDS Page gels to nitrocellulose membranes (GE Healthcare #RPN303D) in XCell II Blotting modules. Tankblotting was performed in NuPAGE Transfer Buffer/15% methanol under approximately 100 V and constant ampere for 60-90 minutes, depending on protein size. All antibodies were diluted in TBST/5% nonfat dry milk if not indicated otherwise (2.1.6)

To avoid unspecific binding of primary antibodies, membranes were blocked in TBST/10% nonfat dry milk prior to overnight-incubation with the primary antibody at 4°C. After three washing steps in TBST, HRP- or fluorescence-coupled secondary antibodies were incubated for 1 hour at room temperature, again followed by 3 washing steps with TBST. Finally, chemiluminescent signals were detected either by X-Ray films or at the Gel Doc XR (Biorad). Fluorescent signals were imaged either at the Infrared Scanner Odyssey (LI-COR) or the Gel Doc XR (Biorad).

➤ Transfer buffer	NuPAGE® Transfer Buffer (Invitrogen)
➤ TBS	15 mM NaCl, 5 mM Tris HCl pH 7.5
➤ TBST	1x TBS with 0.1% Tween 20
➤ nonfat dry milk	Skim Milk Powder (Sigma #70166)
➤ HRP substrate	Western Bright Chemiluminescence Substrate Sirius (Biozym #541021)

2.2.2.4 Chromatin immunoprecipitation

Before harvesting the cells, cell culture medium was exchanged to make sure that cells are covered with 20 ml of medium. For fixation of cells, 1 ml PFA was added and incubated for 10 minutes. 2 ml of 2x glycine were added and after 5 minutes of incubation sample preparation continued at 4°C. Medium was removed and cells were washed twice with chilled PBS. 1.3 ml PBS/4% Protease Inhibitor was added and cells were scraped into a 2 ml Eppi. After centrifugation (5 minutes at 4°C and 700 g), pellets were stored at -80°C.

Cell pellets were dissolved in SDS Lysis Buffer/4% Protease Inhibitor with a final concentration of 2×10^7 cells per 1 ml. Samples were then sonicated in the bioruptor (Diagenode) for 9 cycles. After centrifugation (room temperature, 10000 g for 10 minutes), sheared chromatin was transferred in fresh reaction tubes as 100 µl aliquots.

For pre-clearing, 900 µl of Dilution Buffer and 30 µl of BSA-blocked Protein G Sepharose beads were added to the chromatin and subsequently incubated for 1 hour at 4°C on a rotating wheel. After short centrifugation, 950 µl of the pre-cleared chromatin was transferred into a fresh reaction tube and additional 10 µl were stored aside (4°C), serving as 1% input later on. Finally, the antibody was added for immunoprecipitation over night at 4°C on a rotating wheel.

On the following day, 55 µl of fresh sepharose beads were pre-blocked in BSA, added to the chromatin and incubated for 4 additional hours at 4°C on a rotating wheel. After centrifugation (1 min at 4°C at 3000 g), supernatant was removed using a syringe with a 27 g needle. Each sample and each input were then mixed with 100 µl 10% Chelex, vortexed and incubated at 99°C for 10 minutes. After protein digestion with 1 µl Proteinase K (20 µg/µl) for 30 minutes at 55°C, Proteinase K was inactivated for 10 minutes at 99°C. 80 µl of supernatant were transferred carefully into a fresh reaction tube, thereby avoiding any Chelex carry-over. For a second elution step, 120 µl H₂O were added to the Chelex, vortexed, centrifuged and supernatant was pooled with the previous 80 µl.

For qPCR, 1µl Chromatin was added to the PCR reaction (see 2.2.1.7).

- 18.5% PFA 18.5% PFA, 7 mM KOH, 5 ml H₂O
- Glycine 1.25 M Glycine
- SDS Lysis buffer 1% SDS, 10 mM EDTA, 50 mM Tris HCl pH 8.1
- Dilution buffer 0.01% SDS, 1.1% Triton X-100, 1.2 mM EDTA, 16.7 mM Tris HCl pH 8.1, 167 mM NaCl
- Beads Protein G Sepharose 4 Fast Flow (GE Healthcare #17-0618-05), 50% slurry
- Blocking buffer beads 0.5% BSA in PBS
- 10% Chelex Chelex 100 Resin (BioRad #142-1253) in 10 ml ddH₂O

2.2.2.5 Histopathology and Immunohistochemistry (IHC)

Tissue preparation and fixation

All tissues from experimental animals were fixed in 10% buffered Formalin shortly after necropsy for at least 2 days at 4°C. Tissues were first rinsed in tap water for 2 hrs and then dehydrated according to the following steps and subsequently embedded in paraffin:

Solution	Incubation
70% ethanol	90 min
80% ethanol	90 min
96% ethanol	90 min
1st isopropanol	90 min
2nd isopropanol	90 min
Roticlear	90 min
First paraffin (56°C)	4 hrs
Second paraffin (56°C)	4 hrs

Paraffin-embedded tissues were cut with a rotary microtome (Leica RM2235) to obtain sections of 5 µm thickness. Samples were then fixed to glass slides overnight at 37°C.

To prepare sections for further processing (hematoxylin/eosin (H&E) staining or immunohistochemistry (IHC)), specimen first underwent rehydration:

Solution	Incubation
1st Roticlear	10 min
2nd Roticlear	10 min
96% isopropanol	5 min
80% isopropanol	5 min
70% isopropanol	5 min

- 10% Formalin 10% neutral buffered Formalin pH 6.9 (Merck #100496)
- Roticlear (Carl Roth #A538)

H&E staining

For illustration of tissue structures, microscopic specimen were stained with H&E. Basic hematoxylin (Merck) was used to display cell nuclei in a blue color, whereas acidic eosin stains (Merck) the cytoplasm red. Fixed specimen (see "Tissue preparation and fixation") were first immersed in hematoxylin for 45 sec and after 10 min rinsing under fresh tap water treated eosin for 30 sec. Samples were then washed in 96% isopropanol for 5 min followed by 2x 5 min washing steps in xylol and finally mounted in Entellan (Merck). Images were taken with the Leica ICC50 camera and white balance was adjusted in Adobe Photoshop CS6. Histopathological examination of tumors was carried out by Prof. Dr. Andreas Rosenwald (Universität Würzburg).

- hematoxylin Mayer's hemalaun (Merck # 1092491000)
- eosin 0.5% aqueous Eosin-G solution 0.5% (Merck #1098441000)
- Entellan mounting medium (#107961)

Protein detection by immunohistochemistry

Antigen-retrieval was performed to retrieve epitopes which might be masked due to fixation and embedding procedures by incubation in 10 mM citrate buffer for 30 min in a steamer. Sections were cooled down slowly and immersed in tap water and distilled water. For double staining of sections, DAB (diaminobenzidine) and Fast Red were used for antigen detection respectively. To prevent cross reactions, primary antibodies originating from two different species were chosen. To avoid unspecific signals from endogenous alkaline phosphatases and peroxidases during antigen detection with Fast Red or DAB, 3% H₂O₂ (in aqua dest.) was used for blocking for 10 min. Washing steps always included two washing cycles with TBST and one cycle with TBS for 10 min each. All antibodies were diluted in Dako REAL antibody diluent. After incubation of the primary antibody over night at 4°C, specimen were washed and incubated for 30 min with the corresponding biotinylated IgG antibody. For signal amplification, specimen were incubated with streptavidin-coupled peroxidase for 30 minutes. Antigens were then visualized by subsequent substrate addition of DAB. Washing the samples with TBS stopped the reaction when brown signals were observed under the microscope.

For the second antigen detection, the whole procedure was repeated with the corresponding primary antibody. A secondary biotinylated IgG antibody was

added and after binding of streptavidin-tagged phosphatase for 30 minutes, detection of the second antigen followed by addition of Fast Red substrate for 3 minutes. Again, washing with distilled water stopped the reaction.

Counterstaining of sections was performed with Mayer's Hematoxylin (Merck) and sections were finally mounted in Mowiol. Again, image acquisition was performed with the Leica LCC50 camera and white balance was adjusted in Adobe Photoshop CS6.

- 10 mM citrate buffer 10 mM citric acid, 0.05% Tween 20, pH 6.0
- Blocking reagent Dual Endogenous Enzyme Blocking Reagent (Dako # S200380)
- TBST TBS/0.5% Tween 20
- TBS 5 mM Tris, 15 mM NaCl, pH 7.6
- Antibody diluent Dako REAL antibody diluent (#S202230-2)
- DAB DAB Plus Substrate Kit (Life Technologies #00-2020)
- Fast Red liquid Permanent Red Substrate-Chromogen (Dako #K064011-2)
- streptavidin-tagged peroxidase (KPL #71-00-38)
- streptavidin-tagged phosphatase (KPL #71-00-45)
- Mowiol 6 g Glycerol, 2.4 g Mowiol 4-88 (Carl Roth # 0713.1), 6 ml aqua dest, 12 ml Tris HCl pH 8.5

2.2.3 Cell biology

2.2.3.1 Cultivation of mammalian cells

All cells were kept in RPMI or DMEM supplemented with 10%FCS/PenStrep in cell culture incubators at 37°C with 5% CO₂ and 20% O₂. For subcultivation, cells were splitted every second or third day keeping cells at 60-90% confluency. Therefore, cells were dispersed in 2x Trypsin-EDTA solution or Accutase for 5-15 min at 37°C. Addition of full cell culture medium inactivated Trypsin/Accutase and cell suspensions were splitted in a 1:5 -1:10 ratio.

For cryopreservation, cells in subconfluent state were taken up in cryopreservation medium containing 20% FBS and 10% DMSO. Cells were then slowly cooled down to -80°C in an isopropanol-filled cryopreservation container (Nalgene). For long-term storage, cells were transferred to liquid nitrogen tanks.

- PBS 1x Dulbecco's phosphate buffered saline, no calcium, no magnesium (Life Technologies #14190)
- Trypsin-EDTA 2x Trypsin-EDTA in PBS (Sigma Aldrich #T4174)

- Accutase Accutase solution (Sigma Aldrich #A6964)
- DMEM Dulbecco's Modified Eagle Medium (Life Technologies #41966)
- RPMI RPMI-1640 Medium, GlutaMAX (Life Technologies #61870)
- PenStrep Penicillin/Streptomycin (Life Technologies #15140-122)
- FBS (Sigma Aldrich #F0804)
- Full medium DMEM or RPMI/1% PenStrep/10% FBS
- Cryopreservation medium DMEM/1% PenStrep/20% FBS/10% DMSO

2.2.3.2 Preparation of murine embryonic fibroblasts (MEFs)

MEFs were isolated from E14.5 embryos from timed matings. First, embryos were decapitated and the liver was removed. The remains were then minced with a surgical scissor and further dispersed in 2x Trypsin-EDTA solution for 30 min at the thermomixer at 800 rpm and 37°C. Cells were then plated on 15 cm plates in full medium and medium was exchanged the following day. For genotyping of the embryo, the liver was lysed in PBDN buffer/Proteinase K and used for genotyping PCR (2.2.1.1). To achieve recombination and thus expression of the Δ Np73-transgene, cells were treated with 1 μ M 4OHT (4-Hydroxytamoxifen) for 5 days.

- 4OHT stock solution 1 mM 4OHT (Sigma H7904) in 99% ethanol

2.2.3.3 Manipulation of cells

Transient transfection of siRNAs

Transient transfection of cells was performed using Lipofectamine RNAiMax (Life Technologies #13778150). Suspension cells were detached by Accutase and seeded on 6 well plates with 5-7x 10⁵ cells per well in 3.4 ml full medium. For transfection, 4 μ l 20 μ M siRNA and 10 μ l RNAiMax transfection reagent were diluted in 300 μ l OptiMEM each. After 5 min incubation, both reactions were mixed and incubated for 20 min prior to addition to cell suspensions.

Establishment of stable cell lines by lentiviral transduction

Lentiviral constructs were used to introduce shRNAs or cDNAs into human and murine cell lines. To obtain virions, 293T cells served as virus-producing cell line. Depending on the amount of required virus, 293T cells were seeded either on 10 or 15 cm cell culture dishes (3.5x 10⁶ or 0.75x 10⁷ cells). Next day, cells were transfected with Arrest-In transfection reagent (Open Biosystems). Therefore, full medium was exchanged by DMEM/10% FBS (8 ml/10 cm dish,

12 ml/15 cm dish) and the plasmid DNA of lentiviral vector, envelope and packaging plasmids were diluted in pure DMEM (1 ml for 10 cm dish, 3,85 ml for 15 cm dish). As DNA is employed in a 1:5 ratio to Arrest-In transfection reagent, 70,8 µl or 128,8 µl Arrest-In were diluted in the same volume of DMEM like the DNA. Diluted DNA and diluted Arrest-In were then mixed and incubated for 20 min at room temperature prior to addition to cells.

➤ plasmids for 10 cm cell culture dish:

6.9 µg 2nd generation lentiviral vector
2.07 µg pMD2.g
5.19 µg pSPAX2
14.16 µg DNA

➤ plasmids for 15 cm cell culture dish:

18.1 µg 2nd generation lentiviral vector
6.37 µg pMD2.g
11.73 µg pSPAX2
36.56 µg DNA

The transfection medium was exchanged by full medium 6 hours later. Medium containing the lentivirus was collected 2 and 3 days after transfection, filtered through a 0.45 µm filter and purified and concentrated via PEG (polyethyleneglycol) precipitation (Kutner et al. 2009). Therefore, filtered tissue culture medium was pooled and supplemented with the following components (indicated volumes refer to 1 ml of collected cell culture medium):

250 µl 50% PEG₈₀₀₀ (autoclaved)
106.4 µl 4M NaCl (autoclaved)
114.2 µl PBS

For precipitation of the virus, the mixture was stored at 4°C for 1.5 hours and inverted every 20-30 min. After incubation, the precipitated lentivirus was centrifuged (10 min at 4°C at 7000 g) and the white precipitate was dissolved in 50 mM Tris HCl pH 7.4 (5.9 µl per ml of collected supernatant). After vortexing for 20 seconds, lentiviral aliquots were stored at -80 °C.

For stable transduction of established cell lines, 2.5-3.5x 10⁴ cells were seeded on 6 well plates the day before infection. Before spin infection, full medium was exchanged by full medium containing polybrene (8 µg/ml) for higher infection

efficiency. After addition of 0.1-1 μ l purified virus, cells were centrifuged for 1 hour at 37°C and 1500 rpm. The medium was exchanged the next day and 2-3 days after infection, Puromycin- (1 μ g/ml) or Genitacin- (500 μ g/ml) selection was started.

- Arrest-In (Thermo Scientific)
- Puromycin (Life Technologies, #A1113803)
- Genitacin (Life Technologies, #10131035)

2.2.3.4 Luminescent cell viability assay

The CellTiter-Glo assay (Promega #G7571) was used for assessment of viable cells in cell culture. This assay measures metabolically active cells by quantitation of present ATP: an ATP-dependent luciferase reaction produces a luminescent signal proportional to abundant ATP. The emitted light was then quantified in the Orion II luminometer (Berthold). For this assay, cells were seeded in triplicates on 96-well plates and were measured according to manufacturer's protocol. For analysis, the background value (medium only) was subtracted from all samples and values were normalized to untreated controls.

2.2.3.5 Monitoring of luciferase-labeled tumor cells

Gaussia luciferase (GLuc) converts its substrate coelenterazine to coelenteramide via oxidative decarboxylation, thereby emitting blue light at a wavelength of ~480 nm. A similar enzymatic reaction is executed by Cypridina luciferase (CLuc) when it encounters its substrate Cypridina luciferin (also called Vargulin) leading to Cypridina oxyluciferin. Here, the emitted wavelength is slightly shorter, ~460 nm. The enzymatic reaction of both luciferases is ATP- and cofactor-independent (Figure7).

All quantitative measurements of Luciferase activities were performed in a Berthold Luminometer Orion II with indicated dilutions of substrate stock solutions. As the enzyme activity of GLuc shows flash kinetics, all measurements in the Berthold Luminometer were performed under reproducible conditions by automated injection of substrate stock solutions and detection of luciferase activity (GLuc for 10 sec, CLuc for 5 sec). Coelenterazine (PJK) was prepared as a 10 mM stock solution in acidified ethanol, whereas Cypridina luciferin (NEB) was prepared according to manufacturer's protocol.

To monitor GLuc and CLuc activity in cell culture supernatant, cells were seeded in triplicates on 96-well plates. Complete medium was collected several

times per week in 96-well PCR plates and was either measured directly after sample collection or stored at -20°C for long-term experiments. Frozen samples were thawed and shaken on a Thermomixer for 5 min at 600 rpm before measurement. Depending on the amount of luciferases within the samples, the supernatant was diluted 1:10-1:200 in PBS to guarantee measurement in the linear range of detection. 5 μl of each sample were provided in white 96-well plates with V-bottom (Greiner) and measured separately for GLuc and CLuc activity in the luminometer.

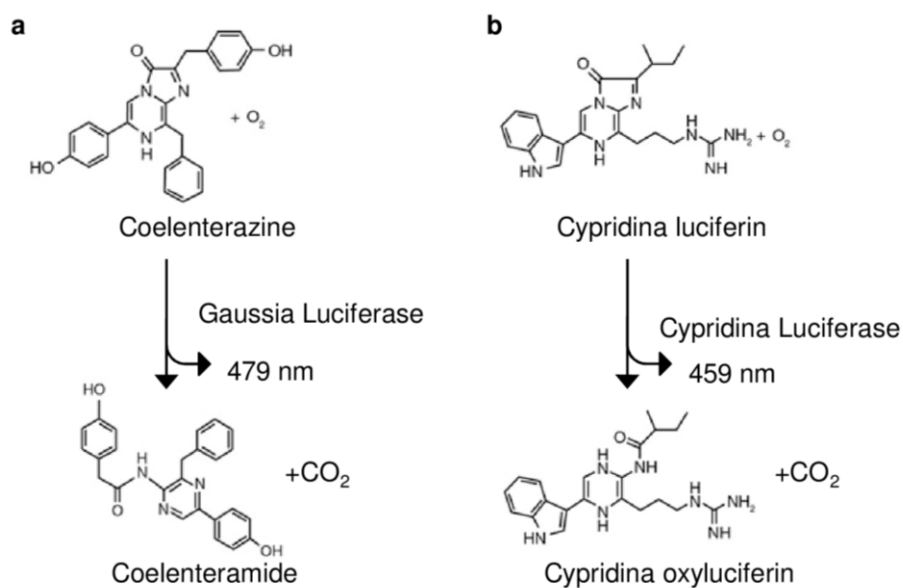


Figure 7: Enzymatic reactions of Gaussia Luciferase and Cypridina Luciferase
Luciferases specifically oxidize their particular substrates Coelenterazine (a) or Cypridina luciferin (b) thereby emitting a bioluminescent signal (adapted from NEB).

For luciferase activity in cell culture medium, the coelenterazine stock solution was used 1:500 in PBS with an injection volume of 50 μl , Cypridina luciferin with the same dilution in Cypridina Buffer/PBS (1:5) with an injection volume of 25 μl .

- Coelenterazine Stock solution 10 mM Coelenterazine (PJK # 102172)
in Ethanol/120 mM HCl
- Cypridina luciferin (NEB # E3309L)

2.2.4 Animal experiments

Animal housing, breeding and experiments of all laboratory animals used in this study were conducted in the animal facilities of the Philipps University Marburg in accordance with the Regional Board Giessen. Breeding and housing of CreERT⁻, ΔNp73 ⁻ and p53^{-/-} mice was performed under basic hygienic standards whereas mice involving transplantation experiments were bred

under specific pathogen free (SPF) conditions in the facility "IMT". Improving social behavior, mice were kept in groups when possible and cages were enriched with nesting material.

All animal experiments subjected to approval were performed according to regulations and guidelines of the German Protection of Animals Act and were approved by the Regional Board Giessen.

Notifiable and approved animal experiments:

Reg. Number	Title
V54-19c2015h01MR20/27 A1/2009 and A46/2012	Breeding and housing of transgenic mice
V54-19c2015h01MR20/27 Nr.61/2012	Establishment of a dual luciferase shRNA assay for validation of tumor relevant genes in mouse models
V54-19c2015h01MR20/27 Nr.83/2014	Monitoring syngenic tumors with secreted luciferases

2.2.4.1 Breeding of mice

Mice of the immunodeficient Rag2^{tm1.1Flv};Il2rg^{tm1.1Flv} strain were mated among each other to maintain the homozygous double-knockout of the Rag2- and IL2rg-alleles. All other strains were bred in heterozygous matings with the respective wildtype inbred strain FVB/N or C57BL/6J (2.1.1).

2.2.4.2 Induction of the EF1 α - Δ Np73 transgene

For induction of the Δ Np73 transgene, LSL- Δ Np73 mice were mated with CreERT mice. Litters obtained from these matings were intraperitoneally injected with 1 mg tamoxifen for 5 consecutive days at the age of 4-6 weeks to induce recombination and thus to turn on transgene-expression.

- Tamoxifen 10 mg/ml tamoxifen (Sigma #T5648) in 95% Corn oil/5% Ethanol

2.2.4.3 Survival analysis of transgenic mice

Overall (OS) and tumor-free (TFS) survival analyses were performed using Prism 6 (GraphPad). Tumor-free mice were censored to assess tumor-free survival (TFS).

2.2.4.4 Transplantation of established tumor cell lines

All xenograft experiments were conducted in immunodeficient Rag2^{tm1.1Flv};Il2rg^{tm1.1Flv} mice. Human cancer cells HCT 116, MDA-MB-231 or Hs

766T were prepared in ice-cold PBS (1×10^7 cells/ml) and 100 μ l cell suspension were injected subcutaneously or intravenously into the tail vein of mice. Concerning syngenic/allogenic transplantations of murine B16-F10, 2×10^5 cells were injected intravenously into Rag2^{tm1.1Flv};Il2rg^{tm1.1Flv} or C57BL/6J mice. Health condition of experimental animals was monitored daily and mice were sacrificed by cervical dislocation upon reaching endpoint criteria.

2.2.4.5 Monitoring of luciferase-labeled tumor cells in vivo

Luciferase activity in plasma

For quantitative measurement of luciferase activities in vivo, plasma/blood samples were collected from experimental animals by punctuation of the tail vein. For each animal and time point, 20 μ l of whole blood were collected and mixed with 0.5 IE heparin to prevent coagulation. To obtain plasma, solid blood components were separated from liquid blood components by centrifugation (15 min, 3600 g, 4°C). Samples were then stored in 96-well PCR plates at -20°C until the end of the experiment. Again, depending on luciferase amounts, samples were diluted 1:10-1:100 in PBS for repeated measurements. For each luciferase, 2x 5 μ l diluted plasma were taken for analysis. GLuc activity was determined by injection of 100 μ l coelenterazine (1:200 in PBS), whereas for CLuc activity 25 μ l Cypridina luciferin (1:200 in Cypridina Buffer/PBS (1:5)) were sufficient.

- Heparin Heparin Natrium 5000 (Ratiopharm PZN 3029820)
- Coelenterazine stock solution see 2.2.3.5
- Cypridina stock solution see 2.2.3.5

Luciferase activity in tumor lysates

To determine the G/C activity ratios in transplanted tumors, whole tumors were excised from mice and coarsely chopped with scissors, followed by further shearing with a teflon pestle. Together with a 5 mm stainless steel bead (Qiagen), 10-20 mg of tissue were then transferred to a precooled 2 ml tube. After addition of 100 μ l Passive Lysis Buffer (Promega, #E1941), the samples were finely mashed in the Tissue Lyser (Qiagen) for 2 min with 40 Hz. Again, 2x 5 μ l of the crude tissue lysate were taken for quantification of luciferase activities in the luminometer under the same conditions as described for plasma samples.

Bioluminescence imaging (BLI)

All bioluminescent imaging procedures were performed with the Xenogen IVIS 50 (Caliper). As emission spectra of both luciferases overlap, it is not possible to image both luciferases simultaneously. Moreover, since CLuc signals are much more stable than GLuc signals, all experimental animals/tumors/tissues were first imaged for GLuc activity. Only upon exclusion of any residual bioluminescent GLuc-signal, CLuc activity was measured.

The Xenogen IVIS 50 is equipped with a highly sensitive CCD Camera with a quantum efficiency of over 85% between 500-700 nm. During acquisition, the camera was kept at -90°C to reduce noise and dark charge signals. Within one experiment, all acquisition parameters were kept constant. Immunodeficient mice injected with luciferase expressing tumor cells were bred on BALB/C background. Using albino mice prevented disturbing absorption of bioluminescent signal by skin pigmentation. As light emitted from tumors in vivo was expected to be partially absorbed by surrounding tissue and hemoglobin, pictures were acquired with medium binning (CCD resolution). The sensitivity was further enhanced by keeping F/Stop at 1, although these parameters further reduced resolution. For imaging of tumors ex vivo, the CCD resolution was kept on low binning.

BLI in vivo

Prior to BLI of experimental animals with GLuc and CLuc expressing metastases, mice were anesthetized in an isoflurane-flooded chamber. Inhalational anesthesia was maintained during the whole BLI procedure. Therefore, the IVIS 50 was equipped with an isoflurane vaporizer (Dräger 19.1) and used with 1-1.5 vol% of isoflurane/O₂ at a flow rate of 50-100 ml/min. Anesthetic depth was checked by toe pinch reflex. To prevent cooling of mice during anesthesia, the sample stage of the Xenogen IVIS 50 was heated to 37°C. For imaging of whole mice, the sample stage was moved to position B (field of view 7.5 x 7.5 cm). To prevent corneal damage, eyes were covered with eye ointment (Bepanthen). When mice showed no response to foot pad pinches anymore, GLuc substrate coelenterazine (11.8 µl stock solution with 78.2 µl PBS, \triangleq 50 µg) was injected into the tail vein and imaged instantly with an acquisition time of 5 min. Since the exposure time was sufficient to convert the whole coelenterazine to coelenteramide, CLuc activity was imaged shortly

afterwards. Cypridina luciferin was also injected into the tail vein (100 μ l of Custom VLuc injectable (Targeting Systems) 1:500 in Cypridina Substrate Dilution Buffer) and imaged immediately with the same acquisition time as for GLuc. After imaging procedure, animals were allowed to wake up again under red light to prevent cooling. Mice were sacrificed by cervical dislocation the next day, as GLuc and CLuc activities were meant to be measured either by BLI of tumors *ex vivo* and/or by measurement of tumor lysates in the luminometer. This time interval guaranteed absence of any residual CLuc signal from *in vivo* BLI.

- Isoflurane (Baxter PZN 6497131)

BLI *ex vivo*

After mice were dispatched by cervical dislocation, organs/tumors were excised and stored in ice-cold PBS in 24-well plates. Like BLI *in vivo*, GLuc was imaged first. Therefore 24-well plates were supplemented with 1 ml of coelenterazine (1:1000 in PBS) per well, tumors/organs were transferred to the wells as quickly as possible and were subsequently imaged with 1 sec exposure time on sample stage position C (field of view 10x 10 cm). As emitted light from excised tumors is not absorbed by surrounding tissue, exposure time was strongly reduced compared to *in vivo* BLI. After acquisition of GLuc activity, organs/tumors were bathed in PBS for at least 1 hr. To image CLuc activity, the imaging procedure was repeated with Cypridina Luciferin (1:1000 in Cypridina Buffer/PBS (1:5)). For quantification of BLI results, each well was marked as a region of interest (ROI) and total counts of every ROI were determined for calculation of G/C ratios of every single organ/tumor.



3 Results

3.1 Establishment of an assay to monitor the dynamics of clonal tumor evolution in vivo using secreted luciferases

3.1.1 Characterization of combined applications of GLuc and CLuc in vitro

The aim of this study was the establishment of an assay that uses two secreted luciferases to label two distinct cell populations and monitor their development over a certain period of time. Therefore, the luciferases Gaussia luciferase (GLuc) and Cypridina luciferase (CLuc) were chosen as they are known to be secreted from cells and exhibit very high sensitivity (Nakajima et al. 2004; Tannous et al. 2005).

For constitutive expression of luciferases, cells were stably transduced with the lentiviral constructs pGLucIPZ or pCLucIPZ, encoding for either one luciferase, a puromycin selection marker and a short hairpin RNA (shRNA) (Figure 8a). Initially, for an in depth evaluation of this reporter system, only constructs with a non-silencing shRNA (nsh) were used. In following experiments, functional shRNAs were used in order to perform comparative analysis of pointedly manipulated cell populations (Figure 14).

At first, the luciferases were tested for their emission spectra to ensure proper bioluminescent signal detection in the luminometer and the bioluminescent imaging system. Therefore, the supernatants of transduced cells were supplemented with their particular luciferase substrate coelenterazine (for GLuc) or Cypridina luciferin (for CLuc) and emitted wavelengths were detected in a spectrofluorophotometer. The emission curves of both luciferases largely overlap displaying emission peaks in the blue spectrum at a wavelength of 459 nm for CLuc and 479 nm for GLuc, respectively (Figure 8b). Accordingly, bioluminescent signals from both luciferases are readily detected by standard luminometers, but both luciferases have to be measured in separate reactions as the overlap of emission spectra renders the distinct detection of both enzymatic reactions within one reaction impossible.

Since both luciferases were planned to be used in a dual luciferase assay, the substrate specificity of both enzymes had to be assessed to exclude cross reactivities. Thus, luciferase-expressing HCT 116 cells were either mixed with

each other or with parental cells (Figure 8c). Again, luciferase activities were measured in cell culture supernatants by addition of substrates. The bioluminescent signal was then quantified in a luminometer as relative light units per second (RLU/s). Supernatant from parental cells exhibited only very low background levels of luciferase activity, whereas GLuc activity was detected exclusively in mixtures containing GLuc transduced cells as well as CLuc activity was only obtained from cell mixtures containing CLuc transduced cells, reflecting a high substrate specificity (Figure 8c). Additionally, luciferase activities in GLuc/CLuc mixtures were equal to activities in mixtures with parental cells, thus demonstrating that there is no cross reactivity or mutual inhibition in combined applications of both luciferases.

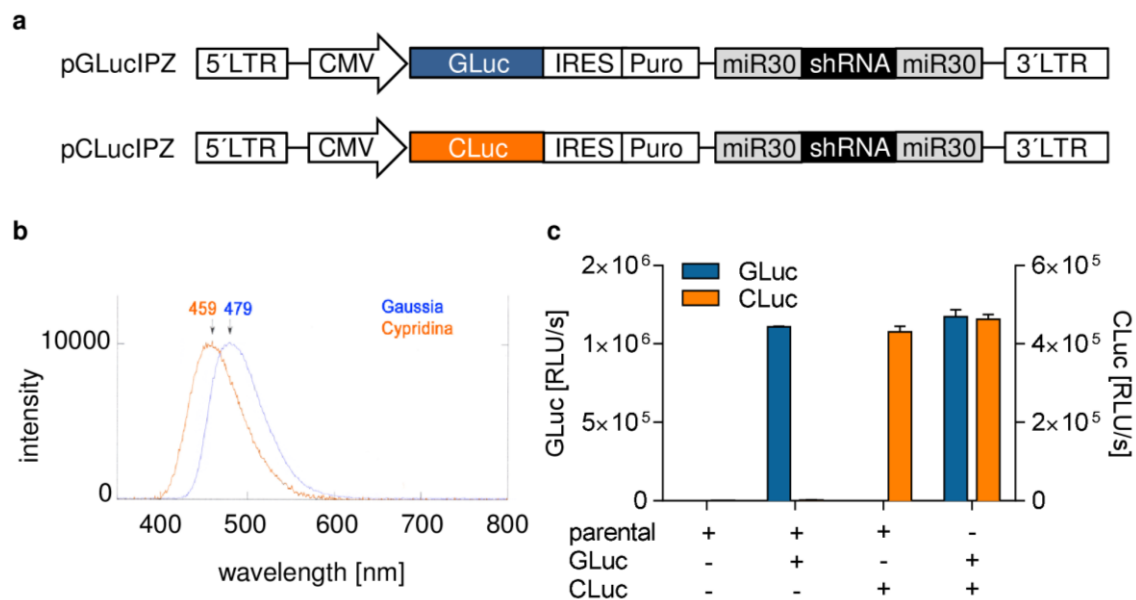


Figure 8: Specificity of Gaussia and Cypridina luciferase

a) Lentiviral constructs pGLucIPZ and pCLucIPZ for stable transduction of eukaryotic cells to express secreted luciferases in combination with a selection marker (Puro) and an shRNA; 5' long terminal repeats (5'LTR), cytomegalovirus promoter (CMV), Gaussia luciferase (GLuc), Cypridina luciferase (CLuc), internal ribosomal entry site (IRES), puromycin resistance (Puro), miR30 structure (miR30), short hairpin RNA (shRNA), 3' long terminal repeats (3'LTR).

b) Emission spectrum of enzymatic reaction of Gaussia luciferase converting coelenterazine to coelenteramide (GLuc) and Cypridina luciferase converting Cypridina luciferine to Cypridina oxyluciferine (CLuc).²

c) Specificity of luciferases: parental, GLuc- and CLuc- expressing HCT 116 were mixed in a 1:1 ratio as indicated at the bottom of the graph; activity of both luciferases was measured by addition of corresponding substrates (mean + s.d.), RLU/s relative light units per second, n=3.

²experiment performed by Dr. Frithjof Scheer

A major characteristic of Gaussia and Cypridina luciferase is their secretion from cells. As the luciferases were ultimately planned to be measured in the blood stream of mice being transplanted with luciferase labeled cells, the availability of the luciferases in the surrounding milieu had to be determined. To assess to which extend luciferases are transported out of the cell, GLuc- and CLuc-transduced cells were seeded at similar cell numbers and cultured for 1 day. Cells were lysed in a volume equal to the collected supernatant (see 2.2.3.5) and equal volumes of cell lysates and supernatants were tested for luciferase activity. The calculation of the cell/supernatant ratio revealed that approximately 1/3 of GLuc remains within the cells, whereas only 1/30 of CLuc is retained in the cells (Figure 9a). This result ensured sufficient luciferase abundance in the extracellular milieu.

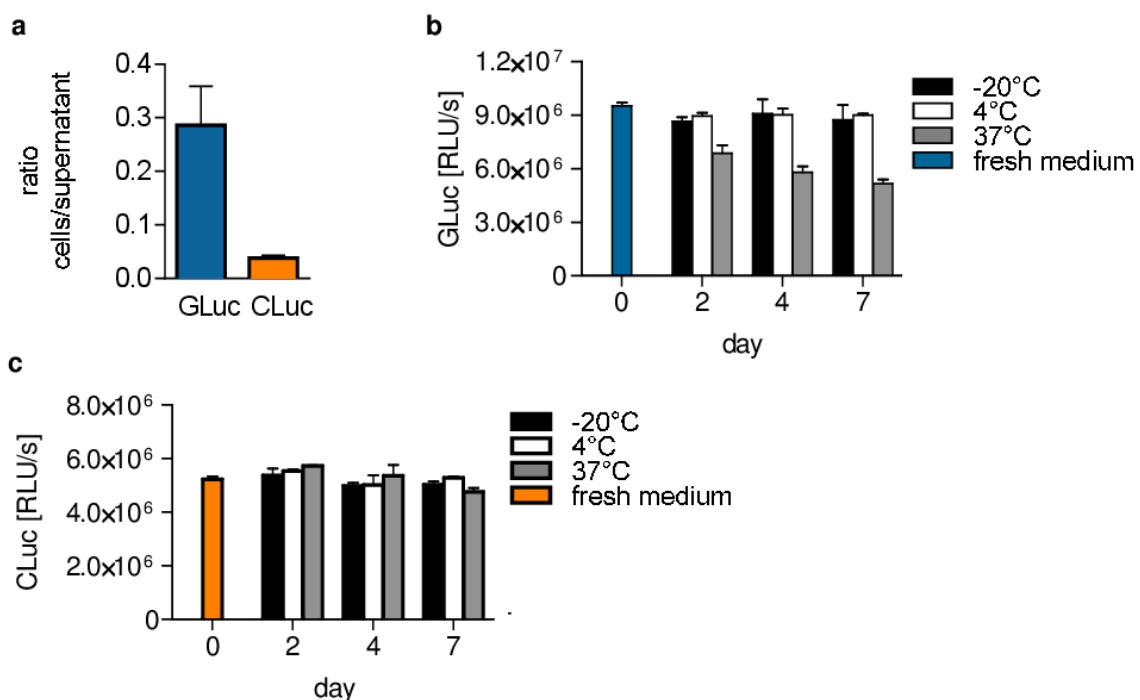


Figure 9: Stability of Gaussia and Cypridina luciferase in cell culture supernatant
HCT 116 cells were stably transduced with pGLucIPZ or pCLucIPZ for stable expression of luciferases.

a) Ratio of luciferase activities (mean + s.d.) in equal volumes of lysed cells and conditioned medium (24 hours); luciferase assay was performed to calculate relative retention of luciferases within the cells, n=2.

b)+c) GLuc (b) and CLuc (c) activity (mean + s.d.) in complete medium of luciferase expressing cells upon different storage conditions, n=3.³

For optimization of the experimental handling procedure, luciferase stability was tested upon different storage conditions. The GLuc activity in the supernatant of GLuc-positive cells remained stable for one week when stored at 4°C or -20°C

³experiment performed by Mirjam Hefter

but dropped to approximately 50% upon storage at 37°C (Figure 9b). CLuc showed an even higher stability, as the activity remained stable not only at 4°C and -20°C but even upon storage at 37°C (Figure 9c). Based on these results, luciferase-containing cell culture supernatant was stored at -20°C in the following experiments.

It has already been shown that luciferase activity of GLuc-transduced cells directly correlates with the cell number (Tannous 2009). However, this has not been evaluated for CLuc yet. Therefore, luciferase expressing HCT 116 cells were seeded at cell numbers ranging from 5000-50000 cells and luciferase activity was measured in the supernatant on the following day. Calculation of the Pearson's correlation coefficient r revealed a correlation of cell numbers and corresponding luciferase activities not only for GLuc ($r=0.9827$) but also for CLuc ($r=0.9993$) at a highly significant level (Figure 10a). In a further

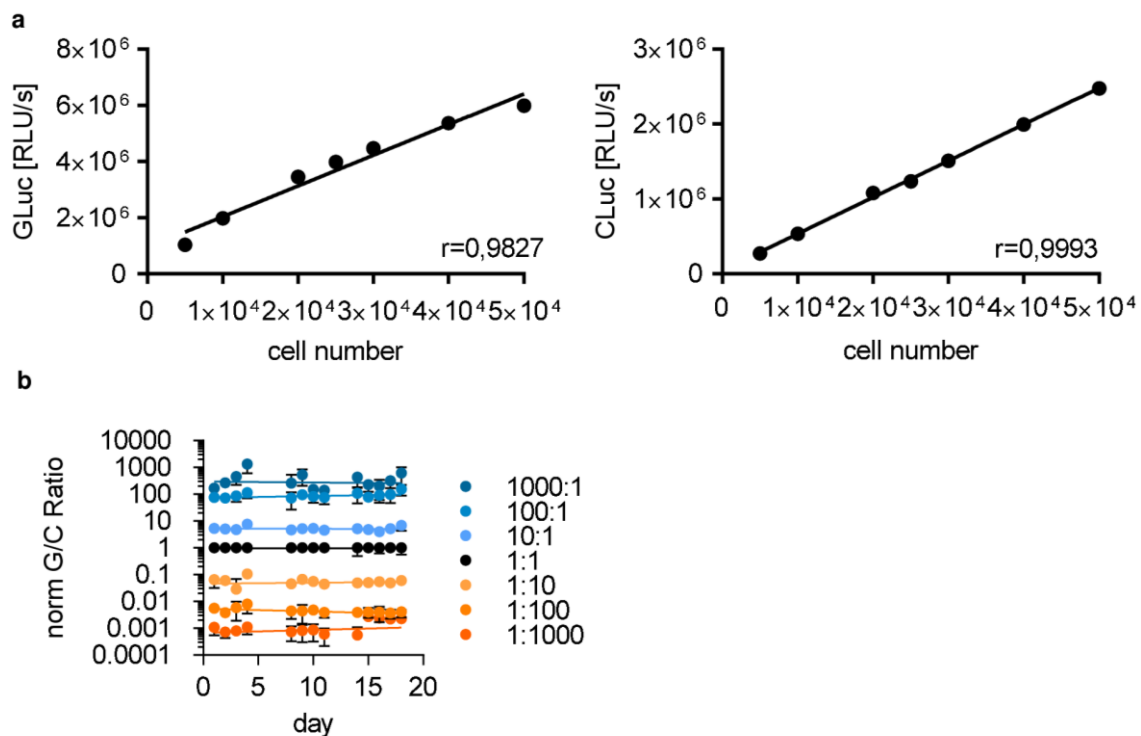


Figure 10: Luciferase activity directly correlates with cell number

HCT 116 cells stably transduced with pGLucIPZ or pCLucIPZ were seeded at different cell numbers/ratios and analyzed for luciferase activity.

a) GLuc (left graph) and CLuc (right graph) activities (mean \pm s.d.) correlate directly with cell numbers shown by Pearson's correlation coefficient (r), $p < 0.0001$, $n=3$.⁴

b) Normalized GLuc/CLuc activity ratios (mean \pm s.d.) from supernatant of GLuc/CLuc cell mixtures of different ratios (1000:1-1:1000), ratios of each day were normalized to the corresponding average G/C ratio of the 1:1 mixture, $n=3$.⁵

⁴experiment performed by Joël Charles

⁵experiment performed by Maximilian Kleint

experiment, GLuc- and CLuc- expressing HCT 116 cells were seeded in different ratios ranging from 1000:1 to 1:1000 to investigate whether GLuc/CLuc ratios remain stable over time even at very extreme ratios of both luciferases. Therefore, supernatant was collected regularly in the course of passaging cell mixtures for 18 days and G/C ratios were calculated from luciferase activities. Indeed, the measured GLuc/CLuc activity ratios remained stable over time and moreover reflected the actually seeded cell ratios, thus suggesting that none of the luciferases affects proliferation (Figure 10b).

3.1.2 Characterization of combined GLuc/CLuc applications in vivo

After characterization of GLuc and CLuc for dual applications in cell culture experiments, the luciferases were further investigated for tumor cell monitoring by blood sampling or bioluminescent imaging (BLI).

Firstly, the luciferases were tested for their substrate specificity when being secreted into the blood stream instead of cell culture medium. Therefore, GLuc- or CLuc-expressing HCT 116 cells were injected subcutaneously into mice and plasma was investigated for GLuc- and CLuc-activity upon outgrowth of tumors. Mice without transplants served as controls to assess unspecific background signal. Only the plasma of mice injected with GLuc-positive cells revealed a strong luciferase activity when supplemented with GLuc substrate coelenterazine, whereas the addition of CLuc substrate Cypridina luciferin exhibited a luminescent signal only in plasma from mice injected with CLuc-positive cells (Figure 11a). As the detected luciferase activities exceeded the background signals by 3 orders of magnitude, both luciferases were considered to be specific not only in cell culture medium but also in plasma samples. Secondly, specificity was tested for BLI. Accordingly, GLuc-labeled cells were injected into the right and CLuc-labeled cells into the left flank of the very same mouse. When tumors reached a size of approximately 3-4 mm, the GLuc substrate coelenterazine was injected intravenously followed by BLI. Here, only the GLuc-labeled tumor cells exhibited a bioluminescent signal (Figure 11b, middle panel). After confirmation that the enzymatic reaction between GLuc and its substrate was complete, the substrate Cypridina luciferin was injected intravenously followed by BLI. This time, the bioluminescent signal was restricted to the CLuc expressing tumor (Figure 11b, right panel). Hence, the BLI demonstrated the substrate specificity of both luciferases in vivo, as the

injection of the substrates led to a very specific bioluminescent signal restricted to the particular tumor (Figure 11b).

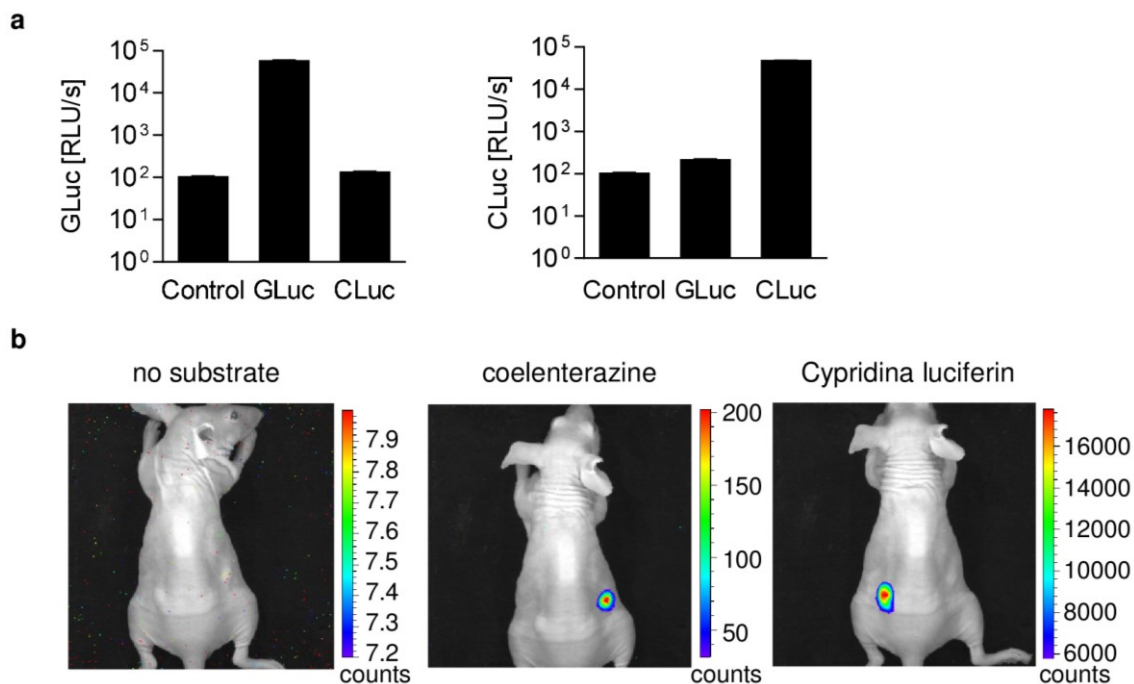


Figure 11: Luciferase specificity in vivo

a) Luciferase activities in plasma of mice 3 weeks after transplantation of GLuc- or CLuc-expressing HCT 116 cells or of mice without transplants (control); each bar shows luciferase activities (mean \pm s.d.) of one representative mouse.⁶

b) Pseudocolour images overlaid with grayscale photographs obtained from bioluminescent imaging (BLI) of a single representative mouse injected subcutaneously with GLuc- (right flank) and CLuc- (left flank) labeled HCT 116; imaging was performed with the IVIS50 after administration of either Coelenterazine (substrate for GLuc) or Cypridina luciferin (substrate for CLuc); scalebar represents the counts (raw amplitude of detected signal).

For optimization of experimental procedures, the luciferases were investigated for stability and potential interference with blood/plasma components ex and in vivo. For this purpose, supernatant from luciferase expressing cells was mixed either with PBS - serving as positive control - or freshly prepared blood or plasma from non-injected control mice. The mixtures were then tested for their luciferase activities at the indicated time points after mixing (Figure 12a). Time point zero exhibits a low background signal of approximately 100 RLU/s for the different solvents (PBS, blood, plasma) before the luciferases were added. Regardless of the solvent, both luciferases exhibited stable activity for at least one hour. Moreover, the activities in PBS and plasma were comparable to each other, whereas the intensities in the blood samples were reduced to a tenth

⁶experiment performed by Mirjam Hefter

most likely due to light absorption by the presence of hemoglobin. Thus, for all further experiments involving measurement of luciferase activities in the bloodstream of mice, plasma samples were used instead of whole blood.

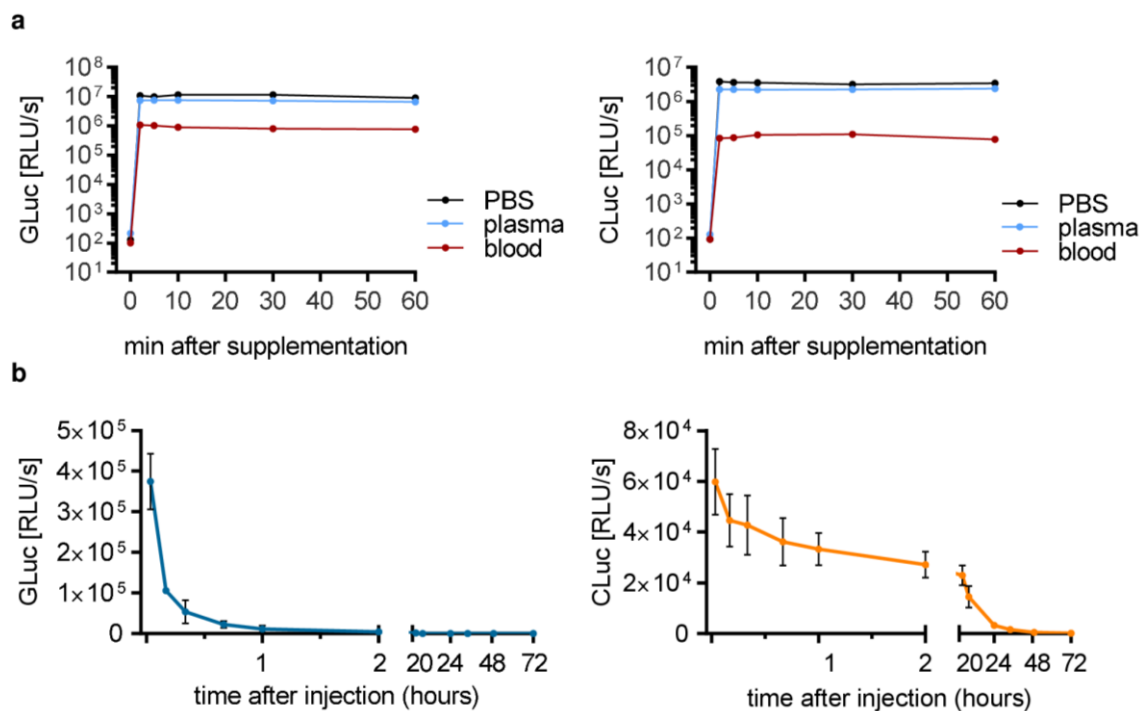


Figure 12: Stability of luciferases ex vivo and in vivo

a) Stability of luciferases in PBS, plasma or whole blood ex vivo; luciferase containing cell culture supernatant was mixed with indicated solvents and measured for luciferase activity after indicated timepoints, n=2.

b) Luciferase activities (mean \pm s.d.) of mice injected intravenously with luciferase containing supernatant, plasma samples were collected at indicated timepoints to assess the half-life of the luciferases in vivo ($T_{1/2}$ (GLuc) = 10 minutes; $T_{1/2}$ (CLuc) = 90 minutes), n=3.

To determine the half-life of the luciferases in vivo, the supernatant from GLuc- and CLuc-labeled cells was injected into the right tail vein of mice and plasma samples were withdrawn from the left tail vein at the indicated time points (Figure 12b). Luciferase activities were measured simultaneously at the end of the experiment. Gaussia luciferase exhibited a short half-life of approximately 10 minutes, whereas Cypridina luciferase is slightly more stable with a half life of approximately 90 minutes. Considering these results, the luciferases provide enough stability in vivo for reliable quantification of enzymatic activity in blood samples as they are not immediately metabolized (e.g. by the liver) and eliminated from the organism (e.g. the kidneys). Additionally, it can be assumed that the relatively short half-life prevents strong accumulation of either one

luciferase thus preventing falsification of the actual abundance of luciferase-labeled tumor cells and providing sensitive monitoring of dynamic processes. Addressing the sensitivity of the luciferases in vivo, GLuc- and CLuc-labeled HCT 116 cells were subcutaneously injected into mice at different GLuc/CLuc ratios (1:1000-1000:1) and plasma samples were collected during the whole course of the experiment. The luciferase activities in mice injected with equal amounts of GLuc- and CLuc-labeled cells (1:1) increased similarly and exponentially over the time (Figure 13a). Additionally, the increase of both luciferase activities run parallel with the increase of the tumor volume measured by a caliper, hereby underlining that the luciferases are suitable as a direct measure for luciferase-labeled tumor cells in vivo. Notably, the detection of GLuc and CLuc activities is much more sensitive than the caliper measurements as luciferases are detectable approximately 1 week before tumors become palpable. Considering the luciferase activity ratios measured in the plasma of mice injected with different cell ratios, the correlation of injected and measured ratios reveals a high sensitivity of luciferases even at very high dilutions of the luciferases (Figure13b).

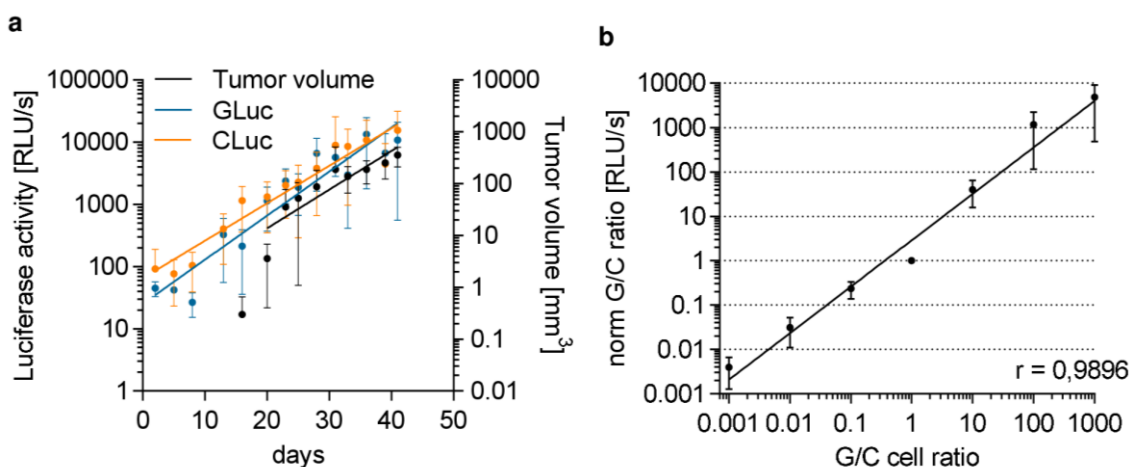


Figure 13: Sensitivity of luciferases in vivo

a) Luciferase activities in plasma (mean \pm s.d.) of mice injected subcutaneously with GLuc- and CLuc-labeled HCT 116 mixed in a 1:1 ratio; tumor volume was measured in parallel by a caliper, n=10.⁷

b) Normalized G/C ratios (mean of 5 animals on 5 different days \pm s.d.) in the plasma of mice injected subcutaneously with GLuc- and CLuc-labeled HCT 116 cells in different ratios (1:1000-1000:1); correlation of data calculated by Pearson's correlation coefficient (r), n=5 per group.⁸

⁷experiment performed by Mirjam Hefter

⁸experiment performed by Maximilian Kleint

These promising results demonstrate high specificity and sensitivity of both luciferases in combined applications not only in cell culture but also in vivo.

3.1.3 Monitoring shRNA-induced heterogeneity of tumors under chemotherapy

To test the dual luciferase assay for its applicability in an experimental setting, tumor cells were transduced with the previously mentioned lentiviral constructs carrying either a non-silencing shRNA or shRNAs targeting p53 (Figure 14). Introduction of these constructs into cells expressing p53 leads to cell populations differing in their p53-expression. Mixing of these cell populations differing in their p53-status mimics the heterogeneous composition of a tumor. The cell mixtures were then put under selective pressure by chemotherapy to monitor the influence of the p53 status on the therapeutic response. In detail, HCT 116 cells - expressing wildtype p53 -were stably transduced with constructs carrying either CLuc combined with a non-silencing shRNA (CLuc-nsh), GLuc with a non-silencing shRNA (GLuc-nsh) or GLuc with two independent shRNAs targeting p53 (GLuc-shp53.1 and GLuc-shp53.5). Cells were then treated with nutlin-3, an Mdm2 antagonist, which induces p53 stabilization and subsequent cell cycle arrest and apoptosis (further details: see 1.3.1)(Vassilev et al. 2004).

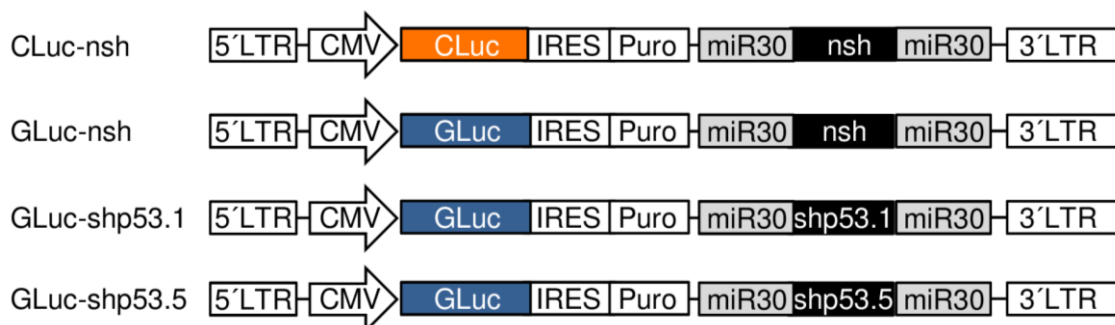


Figure 14: Lentiviral pGLucIPZ and pCLucIPZ constructs for comparative analyses of cell populations differing in their p53-status

For detailed description of the constructs see Figure 8a; pGLucIPZ and pCLucIPZ are abbreviated as pGLuc and pCLuc, respectively.

First, knockdown efficiencies of the shRNAs directed against p53 were tested by Western Blot. Compared to control cells transduced with GLuc- and CLuc-nsh constructs, the p53 protein levels were markedly reduced in GLuc-shp53.1 cells and even more in -shp53.5 cells (Figure 15a). Accordingly, nutlin-3-mediated stabilization of p53 led to a strongly reduced number of viable GLuc-

and CLuc-nsh control cells within 3 days, whereas GLuc-shp53.1 and -shp53.5 cells showed a less pronounced effect due to p53 knockdown (Figure 15b).

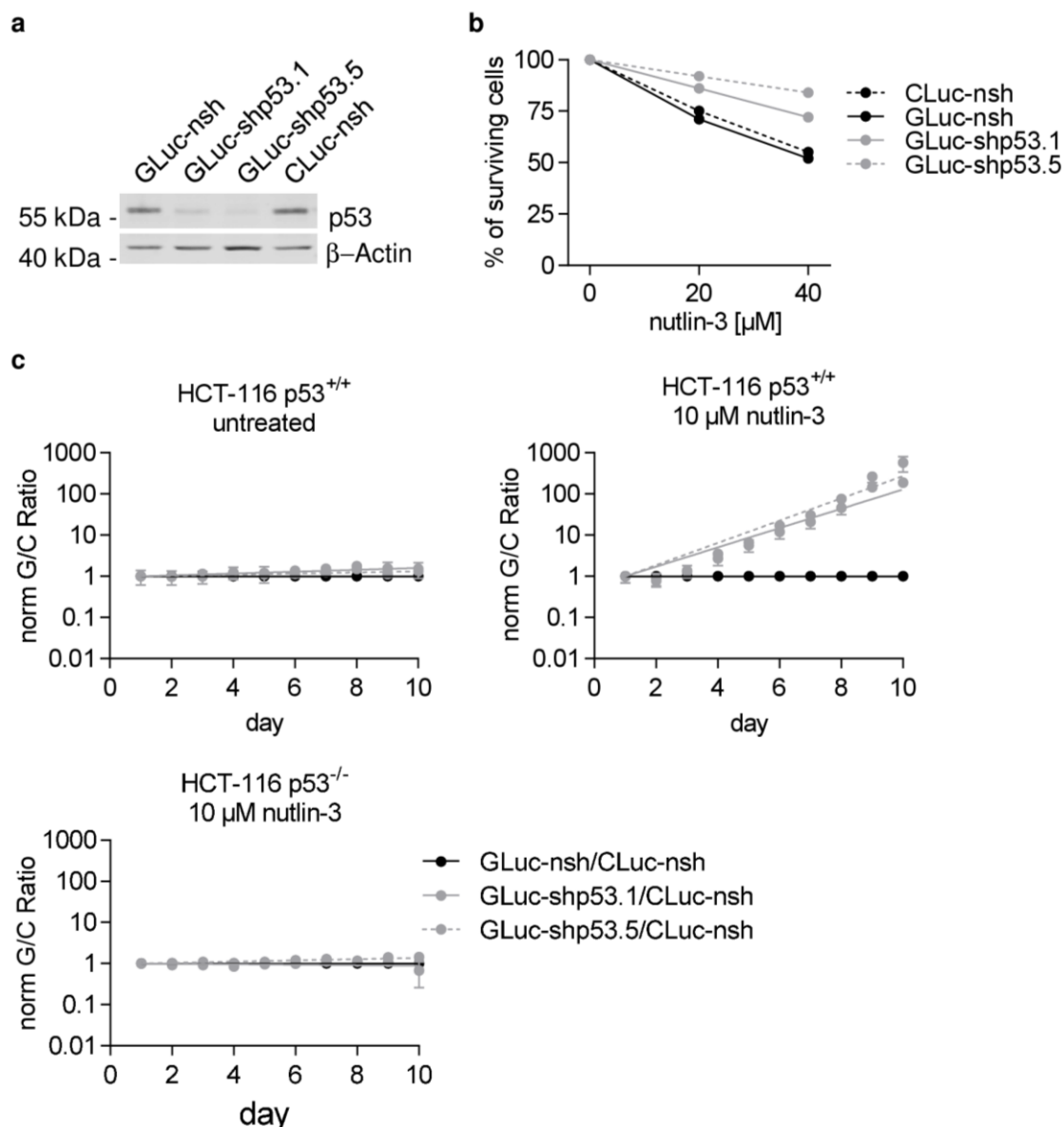


Figure 15: Monitoring shRNA-induced heterogeneity of HCT 116 under nutlin-3 therapy in vitro

a) Western Blot of HCT 116 cells stably transduced with GLuc-nsh, GLuc-shp53.1, GLuc-shp53.5 and CLuc-nsh for knockdown efficiencies of shRNAs against p53; β -actin served as loading control; for lentiviral constructs see Figure 14.

b) Cell viability assay of stably transduced HCT 116 cells upon 3 days of nutlin-3 treatment at indicated concentrations, values (mean) were normalized to untreated cells, n=3

c) Normalized G/C activity ratios (mean \pm s.d.) of untreated HCT 116 cells (upper left), nutlin-3 treated HCT 116 cells (upper right) or nutlin-3 treated isogenic HCT 116 p53^{-/-} (lower left), n=3.⁹

To test whether this effect can also be monitored by the dual luciferase assay established in this work, CLuc-nsh cells were either mixed with GLuc-nsh cells

⁹experiment performed by MirjamHefter

or with GLuc-shp53.1 or -shp53.5 cells and seeded for cell culture experiments. The cell mixtures were then either left untreated (normal full medium) or were treated with 10 μ M nutlin-3. The supernatant was collected regularly during 10 days at indicated time points and was replaced either by fresh medium or nutlin-3 supplemented medium (Figure 15c, upper images). At the end of the experiment all supernatants were measured in one run and the G/C ratios were normalized to the G/C ratios of the GLuc-nsh/CLuc-nsh control mixture of each day. Under normal conditions, the knockdown of p53 in HCT 116 had no effect on cell proliferation as the ratios of all three groups remained stable during the course of the experiment (Figure 15c, upper left image). The G/C ratios of the nutlin-3 treated GLuc-nsh/CLuc-nsh mixture also remained stable over time, as both cell populations responded similarly to the treatment (Figure 15c, upper right image). However, nutlin-3 treatment led to an increase of the G/C ratios in cell mixtures of CLuc-nsh cells with GLuc-shp53.1 or -shp53.5 cells. In detail, p53-depleted cells are not affected by nutlin-3 and thus proliferate at a normal rate, whereas p53 becomes stabilized in CLuc-nsh cells leading to cell cycle arrest and apoptosis. A control experiment with isogenic HCT 116 p53^{-/-} cells transduced with the same constructs and treated with the same conditions confirmed that this effect is indeed p53-dependent as the p53-shRNAs had no effect on the G/C ratios (Figure 15c, lower image).

To assess whether the dual luciferase assay is also suitable for the monitoring of therapeutic effects in vivo, a mixture of CLuc-nsh and GLuc-shp53.5 HCT 116 was engrafted subcutaneously into mice. Two weeks after tumor cell injection, mice were treated either with vehicle (2% Klucel/0.2 % Tween-80) or nutlin-3 (200mg/kg) twice daily. Up to this timepoint, the luciferase activities in the plasma of both groups developed equally (Figure 16a+b). This development remained unchanged in the vehicle treated cohort as both luciferase activities increased similarly. In contrast to that, the administration of nutlin-3 led to an overgrowth of GLuc-shp53 cells over CLuc-nsh cells (Figure 16a). Additionally, the calculation of the G/C activity ratio in plasma displays a two-fold increase upon 10 days of nutlin-3-treatment, whereas the ratio in the vehicle group remained unchanged (Figure 16b). Thus, the growth advantage of p53-depleted cells over p53-proficient cells under nutlin-3 therapy is also detectable in plasma. Furthermore, the G/C activity ratios in tumor lysates also revealed a

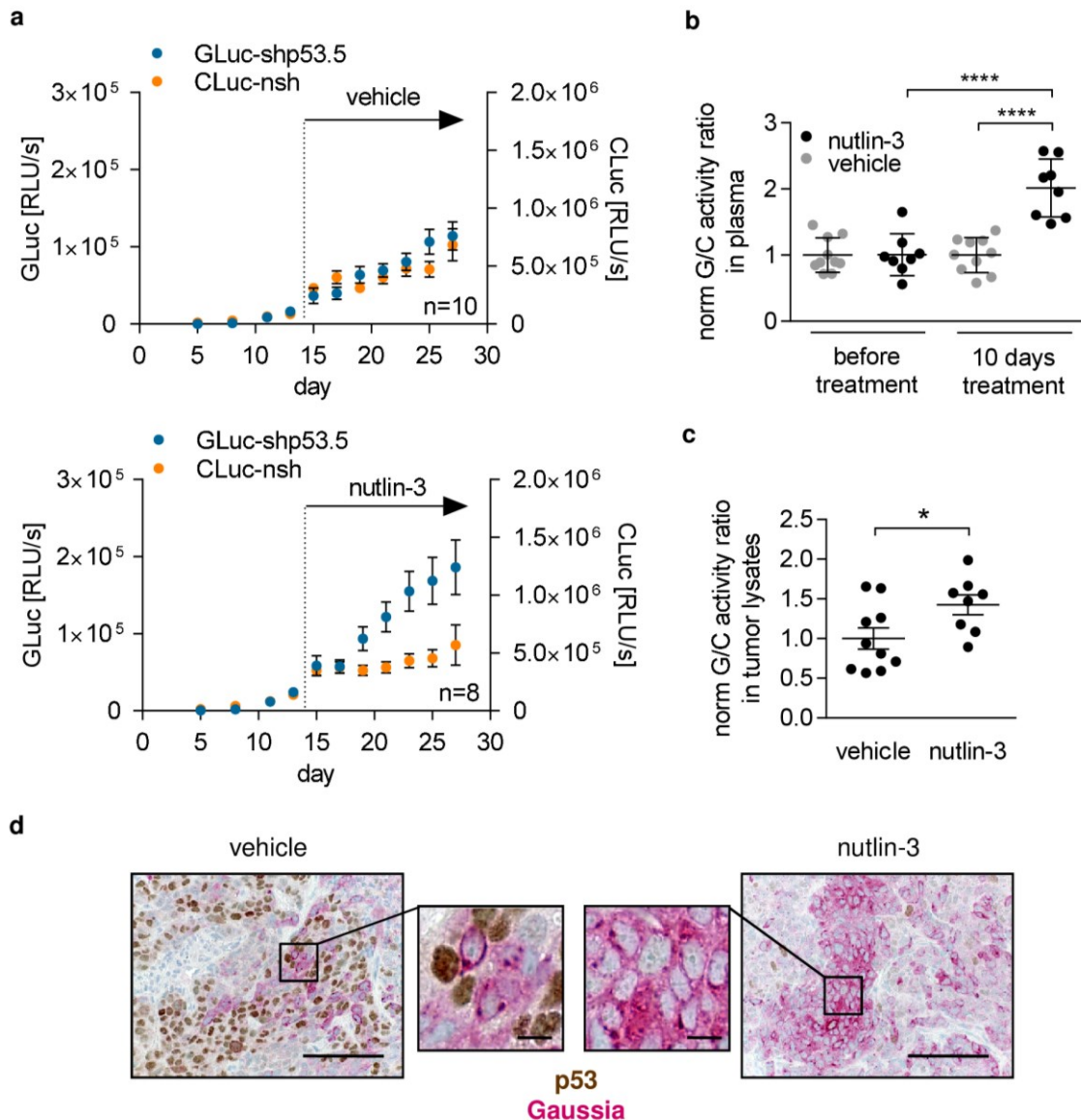


Figure 16: Monitoring shRNA induced heterogeneity of HCT 116 under nutlin-3 therapy

a) Luciferase activities (mean \pm s.e.m.) in plasma of mice injected subcutaneously with a 1:1 mixture of CLuc-nsh and GLuc-shp53.5 HCT 116; vehicle control (2%Klucel/0.2% Tween-80) or nutlin-3 (200 mg/kg body weight) were administered orally twice daily starting on day 13; tumor growth curves were analyzed by two-way-ANOVA ($p^{**}<0.005$).

b) Normalized G/C ratios (mean \pm s.d.) from plasma samples before and after vehicle/nutlin-3 treatment; one-way ANOVA corrected for multiple comparisons by Bonferroni ($p^{****}<0.00005$).

c) Normalized G/C ratios (mean \pm s.d.) from tumor lysates of vehicle/nutlin-3 treated mice; one-tailed Mann-Whitney t-test ($p^*<0.05$).

d) Immunohistochemical double stainings of representative tumors after vehicle/nutlin-3 treatment; tumors were stained for p53 (DAB, brown) and Gaussia luciferase (Fast Red, red); scale bars 200 μ m (lower magnification) and 10 μ m (higher magnification).

significantly 1.5-fold higher abundance of GLuc-shp53.5 cells in nutlin-3 treated samples compared to vehicle treated samples (Figure 16c). To evaluate tumor compositions independently from luciferase activities, immunohistochemical (IHC) stainings for GLuc and p53 were performed in tumors excised from vehicle- and nutlin-3-treated mice. Tumors from the control group showed a balanced composition of Gaussia-positive/p53-negative (GLuc-shp53.5) and Gaussia-negative/p53-positive (CLuc-nsh) cells, whereas tumors from nutlin-3 treated mice were depleted from Gaussia-negative/p53-positive (CLuc-nsh) cells consisting mostly of Gaussia-positive/p53-negative (GLuc-shp53.5) cells (Figure 16d). Hence, IHC double stainings for GLuc and p53 were able to confirm the results from luciferase measurements in plasma in an independent readout.

3.1.4 Application of the GLuc/CLuc assay in experimental metastasis

In a further approach, the applicability of the dual luciferase assay was tested in a setting of experimental metastasis. For this purpose, the breast cancer cell line MDA-MB-231 was chosen. Upon injection into the tail vein of mice, these cells leave the blood stream in the capillary bed of the lungs and colonize the lung tissue resulting in the formation of metastases. MDA-MB-231 cells harbor an endogenous p53 mutation (R280K, hereinafter mutp53) which is a key player for the metastatic phenotype of this cell line (Adorno et al. 2009).

For evaluation of the GLuc/CLuc assay in this context, MDA-MB-231 cells were stably transduced with the same constructs as shown above (CLuc-nsh, GLuc-nsh, GLuc-shp53.1 or GLuc-shp53.5, Figure 14) to confer a stable knockdown of the metastasis-promoting mutp53 in comparison to the non-targeting shRNA. All constructs simultaneously express secreted luciferase reporters GLuc and CLuc as indicated. The knockdown efficiencies of the two independent shRNAs were confirmed by Western Blot (Figure 17a). Independent of the co-expressed luciferase, the MDA-MB-231 cells carrying the control shRNA showed a high abundance of p53 protein, whereas the introduction of shp53.1 reduced p53 to barely detectable levels, an effect even more pronounced by the shp53.5. Additionally, the cells were tested for their Gaussia protein levels to ensure comparable infection efficiencies with equal amounts of the reporter being expressed among the three cell populations GLuc-nsh, GLuc-shp53.1 and

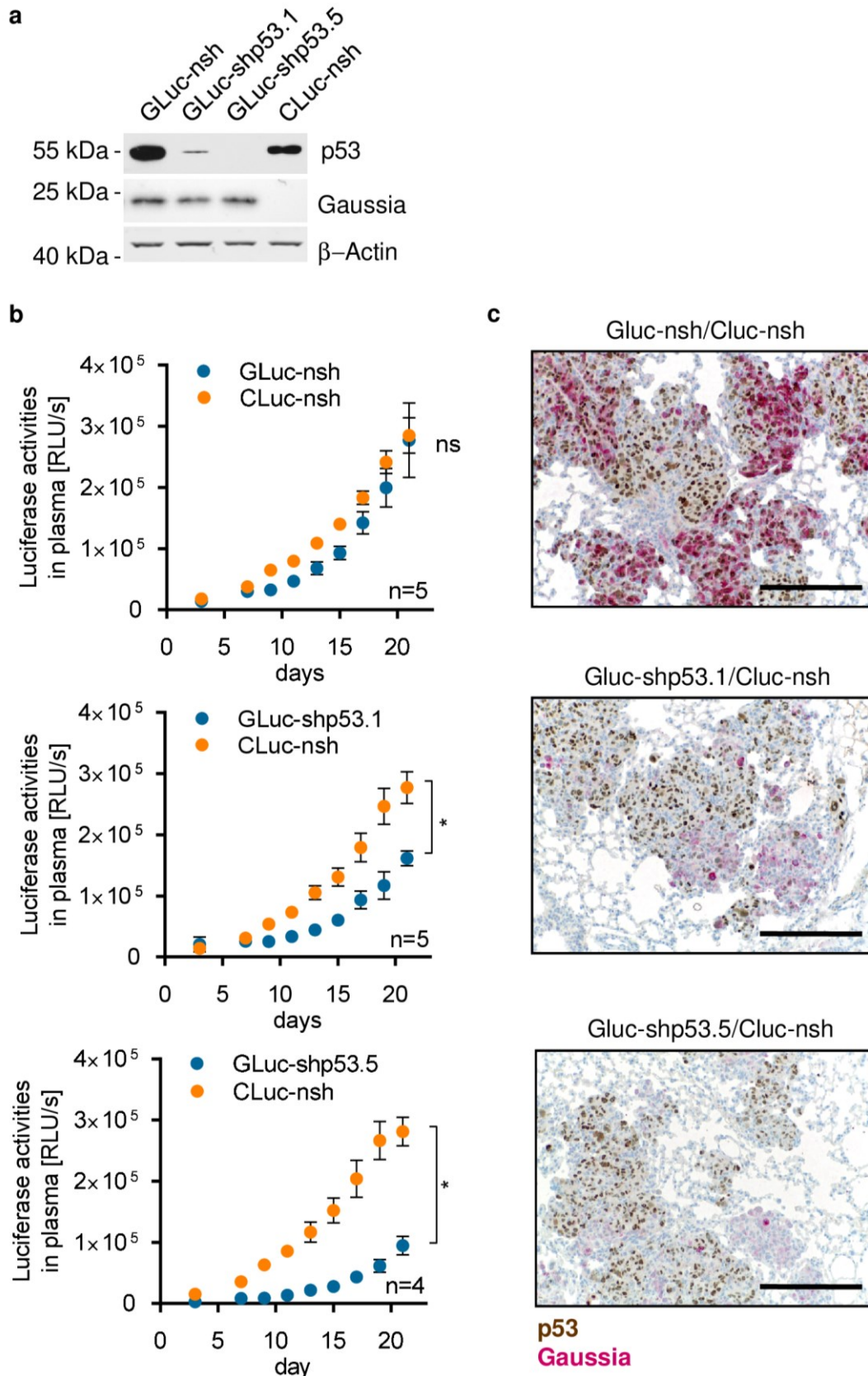


Figure 17: Monitoring clonal evolution in metastasis

a) Western Blot of MDA-MB-231 cells stably transduced with GLuc-nsh, GLuc-shp53.1, GLuc-shp53.5 and CLuc-nsh to compare infection rate (by expression levels of Gaussia luciferase) and knockdown efficiencies of shRNAs against p53; β -actin served as loading control.

b) Luciferase activities in the plasma of mice injected intravenously with MDA-MB-231 cell mixtures (GLuc-nsh/CLuc-nsh, GLuc-shp53.1/CLuc-nsh and GLuc-shp53.5/CLuc-nsh); GLuc and CLuc activities (means \pm s.e.m.) are plotted on the same axis; Two-way-ANOVA shows a statistically significant underrepresentation of GLuc-shp53.1 and GLuc-shp53.5 cells compared to CLuc-nsh cells ($p^* < 0.01$), $n=5$ ($n=4$ for shp53.5).

c) IHC double stainings of representative lung metastases for p53 (DAB, brown) and Gaussia luciferase (Fast Red, red); scale bars 200 μ m.

GLuc-shp53.5 (Figure 17a). Finally, CLuc-nsh cells were mixed in a 1:1 ratio either with GLuc-nsh, GLuc-shp53.1 or GLuc-shp53.5 cells and injected into the tail vein of immunodeficient mice for lung colonization. To monitor the extent of total tumor burden of cells with and without mutp53, blood samples were taken three times per week. The parallel increase of GLuc and CLuc in the plasma of GLuc-nsh/CLuc-nsh injected mice showed an equal growth of both cell populations in the injected mice (Figure 17b, top). In case of GLuc-shp53.1/CLuc-nsh and GLuc-shp53.5/CLuc-nsh engrafted mice the GLuc activities in the plasma increased to a much lesser extent than the CLuc activities due to mutp53 depletion (Figure 17b, middle and bottom). This effect was statistically significant for both GLuc constructs targeting p53, although the loss of metastatic growth was even more pronounced in GLuc-shp53.5 cells caused by a stronger knockdown efficiency of shp53.5 (Figure 17a). Immunohistochemical double stainings of explanted lungs for p53 and Gaussia luciferase confirmed the results obtained from the plasma activities (Figure 17c). The lung metastases of GLuc-nsh/CLuc-nsh injected mice display an equal distribution of GLuc-positive and -negative MDA-MB-231 cells, all being positive for mutp53. Metastases of GLuc-shp53.1/CLuc-nsh and GLuc-shp53.5/CLuc-nsh engrafted mice are also positive for mutp53 but negative for GLuc, thus representing CLuc-nsh cells. GLuc-positive cells without mutp53 are hardly detectable in those sections, hence confirming the reduced metastatic potential of cells lacking mutp53.

The intravenous injection of these tumor cells might, besides lung colonization, also facilitate the colonization of other organs, e.g. the liver or the lymph nodes. To detect the tumor cells not only in the lungs but also in other organs, mice underwent BLI. Therefore, mice were injected with the GLuc substrate coelenterazine and imaged for bioluminescent signals one day before mice were sacrificed (Figure 18a). The bioluminescent signal of GLuc-nsh cells was restricted to the lungs, whereas GLuc-labeled cells depleted from mutp53 were

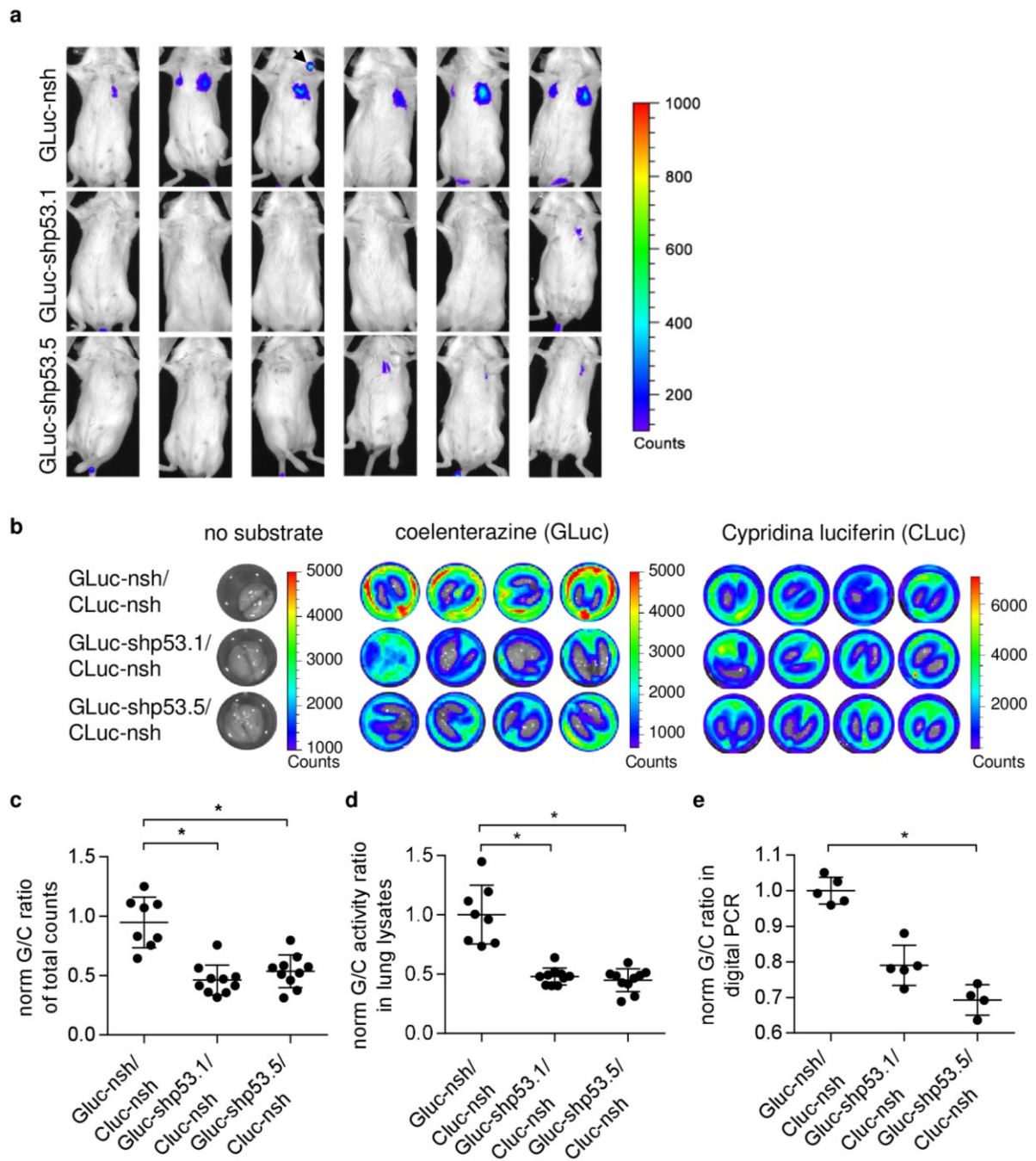


Figure 18: Detection of metastasis by bioluminescent imaging in a competitive GLuc/CLuc assay

a) In vivo BLI for GLuc activity upon intravenous injection of coelenterazine in mice 20 days upon injection of MDA-MB-231 cell mixtures (GLuc-nsh/CLuc-nsh, GLuc-shp53.1/CLuc-nsh and GLuc-shp53.5/CLuc-nsh); scalebar represents the counts.

b) Ex vivo BLI of metastasized lungs explanted from a) before substrate administration (left), upon bathing in coelenterazine (middle) and after bathing in Cypridina luciferin (right); scalebar represents the counts.

c) Normalized G/C ratio generated from BLI data in b) (mean \pm s.d., non-parametrical Kruskal-Wallis test and Dunn's post test for multiple comparisons, $p^* < 0.01$) of total counts from b); data normalized to mean G/C ratio of control mixture.

d) Normalized G/C activity ratio of lung lysates (mean \pm s.d., non-parametrical Kruskal-Wallis test and Dunn's post test for multiple comparisons, $p^* < 0.01$)

e) Normalized G/C ratio of gDNA from lung lysates (mean \pm s.d., non-parametrical Kruskal-Wallis test and Dunn's post test for multiple comparisons, $p^* < 0.01$) measured by digital PCR.

barely detectable in BLI. In one case, the signal seems to arise additionally from a lymph node (Figure 18a, arrow). Imaging of CLuc upon injection of Cypridina luciferin did not lead to any useful data, since at this stage of tumor burden the CLuc content in the blood stream exceeds the amount of CLuc at the tumor site leading to an overall illumination of the experimental animals (data not shown). This observation might be a result of CLuc stability in vivo (Figure 12b) and the highly efficient secretion of CLuc, resulting in very low levels of intracellular luciferase (Figure 9a). In addition, ex vivo imaging of explanted lungs confirmed the results from BLI in vivo: the strongest signal was obtained from GLuc-positive cells containing mutp53 (Figure 18b, middle). In contrast to the GLuc signal, the CLuc imaging showed an equal abundance of CLuc positive cells in all three groups as all CLuc-nsh cells had the same mutp53 status (Figure 18b, right). To obtain statistically evaluable results from these imaging procedures, the total counts of emitted light within a defined region of interest (ROI) of every single lung were used to calculate corresponding G/C ratios. These ratios were significantly reduced in lungs from mice injected with GLuc-shp53.1/CLuc-nsh or GLuc-shp53.5/CLuc-nsh cell mixtures, as the GLuc-shp53 cells lacking metastasis-promoting mutp53 are strongly underrepresented compared to mutp53 proficient GLuc-nsh or CLuc-nsh cells (Figure 18c).

The same lungs were washed to prevent background signals from residual substrates and homogenized tissue was used for additional quantification of luciferase activities in the luminometer. The normalized G/C ratios of lung lysates reflect the previously obtained results with comparable differences in G/C ratios and significance (Figure 18d).

Finally, the genomic DNA (gDNA) of the tumor bearing lungs was extracted to investigate the clonal composition of the tumors by digital PCR. This measurement is totally independent from the luciferase activities as this method quantifies the copies of integrated luciferase sequences within the gDNA of the tumor cells (Figure 18e). The GLuc/CLuc gDNA ratio, assessed by digital PCR, gave a similar result as the evaluations of the luciferase activities in ex vivo BLI or tumor lysates (Figure 18c, d), demonstrating that the measurement of GLuc and CLuc luciferase activities indeed reflects the clonal composition of a tumor.

3.1.5 Expanding the GLuc/CLuc assay to an inducible system for knockdown of essential tumor genes

The lentiviral constructs used in this work were created to provide stable and continuous expression of luciferases and shRNAs. Yet, if the applied experimental shRNA targets a gene being essential for the survival or the proliferation of the cell, the transduced cells will immediately die or be unable to proliferate, thus making it impossible to proceed with further experiments. To overcome this problem, the luciferases were cloned into the backbone of the tetracycline (tet)-inducible lentiviral vector pInducer10 (Figure 19a). Upon integration of the lentiviral particles into the hosts' genome, the puromycin-resistance gene is steadily expressed and allows the selection for stably transduced cells. Additionally, the reverse tetracycline transactivator3 (rtTA3) is present but not functional until tetracycline is added. Under normal conditions, neither the luciferases nor the shRNAs are expressed. In presence of tetracycline, rtTA3 binds to the tetracycline responsive element (TRE2) leading to a transient expression of the luciferases and the shRNAs as long as tetracycline is present.

3.1.5.1 Knockdown of p73 reduces tumorigenicity in Hs 766T cells

As p73 has been shown to be highly upregulated in many different tumor entities (Yokomizo et al. 1999; Casciano et al. 2002; Concin et al. 2004; Zaika et al. 2002), we investigated whether this overexpression is essential for the tumorigenicity in such tumor cells. As a model we used the pancreatic cancer cell line Hs 766T, which exhibits high expression levels of both N-terminal isoforms TAp73 and Δ Np73. In order to test whether p73-depletion leads to proliferative disadvantages in these cells, cells were transduced with pInducer10 constructs expressing either GLuc or CLuc combined with a non-coding shRNA (nsh) or GLuc coupled to two different shRNAs targeting p73 (Figure 19a). Upon transduction with the aforementioned constructs, cells were tested for the knockdown efficiency of the introduced shRNAs. Experiments proved 5 days of tetracycline treatment to be enough to obtain a strong reduction of TA and Δ Np73 levels in GLuc-shp73.3 or GLuc-shp73.5 cells compared to control cells with GLuc-nsh or CLuc-nsh (Figure 19b). As the p73 expression of all cell lines remained on the same level in absence of tetracycline, the inducible system is considered to be non-leaky.

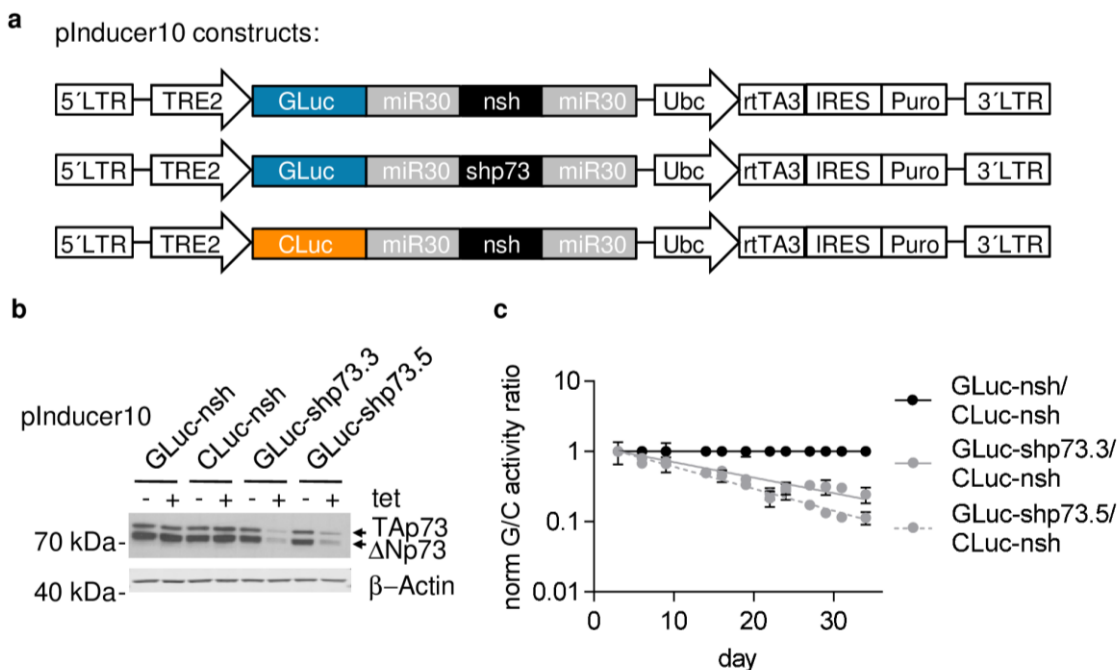


Figure 19: Inducible luciferase reporter constructs for evaluation of essential tumor genes

pInducer10 lentiviral constructs were designed for tetracycline (tet)-inducible expression of luciferases and shRNA for evaluation of TP73 as an essential gene in the pancreatic cancer cell line Hs 766T harboring high levels of p73.

a) pInducer10 lentiviral constructs for inducible luciferase and shRNA expression; 5'long terminal repeats (5'LTR), tetracycline responsive element 2 (TRE2), Gaussia/Cypridina Luciferase gene (GLuc/CLuc), miR30 structure (miR30), non-silencing shRNA (nsh), shRNA targeting p73 (shp73), Ubiquitin C promoter (Ubc), reverse tetracycline transactivator 3(rtTA3), internal ribosomal entry site (IRES), puromycin resistance gene (Puro), 3'long terminal repeats (3'LTR).

b) Knockdown efficiency of lentiviral constructs \pm 5 days tetracycline treatment (2mg/ml) in Hs 766T cells detected by an antibody against total p73; β -actin served as loading control.

c) Normalized G/C activity ratios (mean \pm s.d.) of stably transduced Hs 766T cell mixtures seeded in a 1:1 ratio as indicated in the figure legend (GLuc-nsh/CLuc-nsh, GLuc-shp73.3/CLuc-nsh and GLuc-shp73.5/CLuc-nsh); for induction of luciferases and shRNAs cells were treated continuously with tetracycline (2mg/ml), n=3.

To analyze whether the knockdown of p73 has an impact on the survival/proliferation of the Hs 766T cells, CLuc-nsh cells were mixed in a 1:1 ratio either with GLuc-nsh cells (control) or with GLuc-shp73.3 or GLuc-shp73.5 cells and seeded in cell culture. During the course of the experiment the cells were treated continuously with tetracycline and the medium was collected several times per week. At the end of the experiment, the luciferase activities of all collected supernatants were measured and G/C ratios were calculated and normalized to the GLuc-nsh/CLuc-nsh ratio. The decrease of the G/C ratio in cell mixtures containing GLuc-shp73 cells demonstrated a strong growth

disadvantage towards CLuc-nsh control cells (Figure 19c). Thus, the inducible expression system for GLuc and CLuc proved valuable to identify p73 as an essential factor for Hs 766T cells.

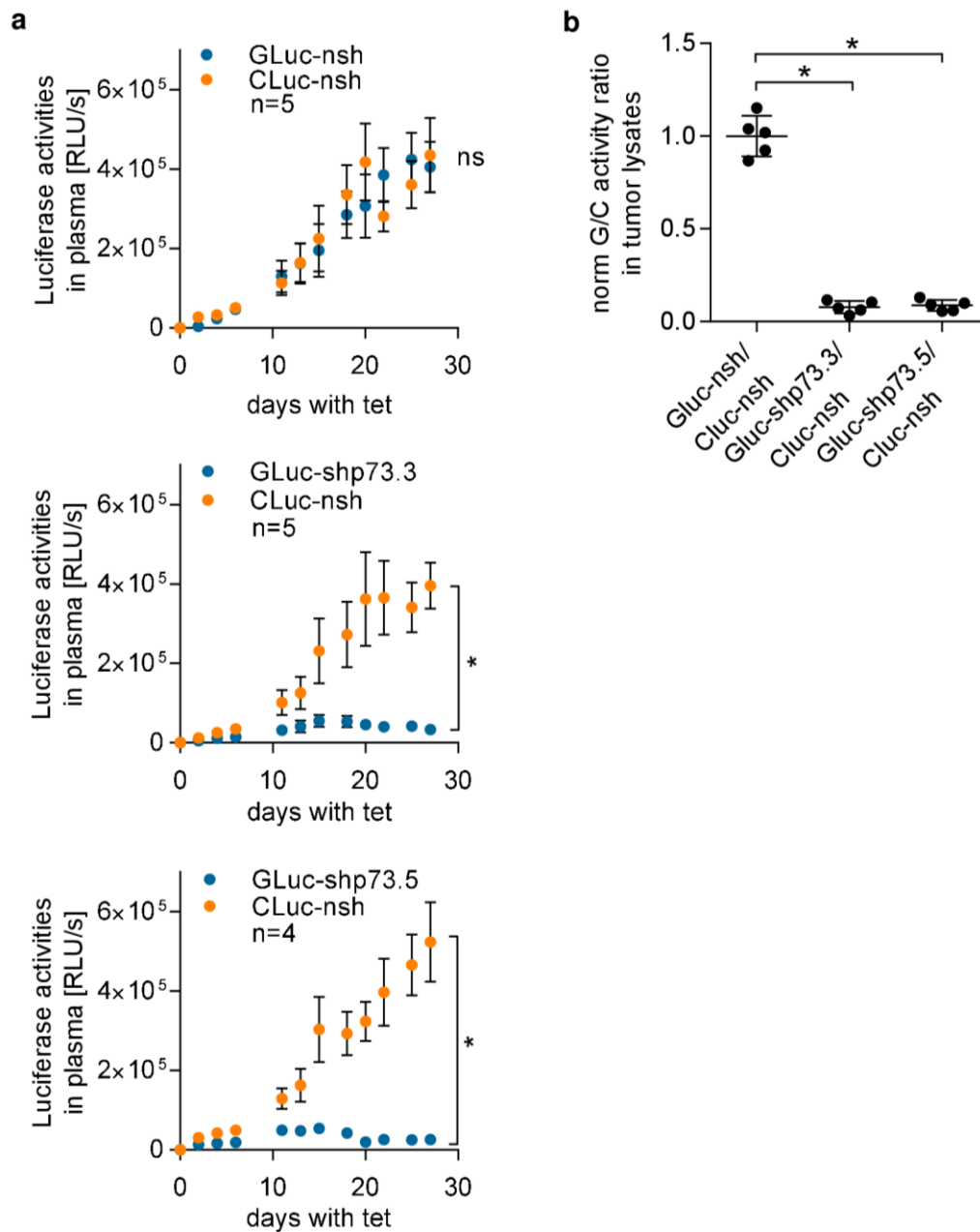


Figure 20: Inducible constructs validate p73 as essential tumor gene in Hs 766T for tumorigenicity in vivo

a) Luciferase activities in the plasma mice injected subcutaneously with indicated mixtures of Hs 766T (means \pm s.e.m, Two-way-ANOVA($p^* < 0.01$)); mice received tetracycline from day of injection on; GLuc and CLuc activities are plotted on the same axis; $n=5$ ($n=4$ for shp73.5).

b) Normalized G/C activity ratio of lysates from explanted tumors (mean \pm s.d., non-parametrical Kruskal-Wallis test and Dunn's post test for multiple comparisons, $p^* < 0.05$).

To see whether p73 is also essential for the tumorigenicity of this cell line, the same cell mixtures were injected subcutaneously into immunodeficient mice and blood samples were collected several times per week. Beginning with the day of tumor engraftment, tetracycline was given to the mice via the drinking water to induce the knockdown of p73 and simultaneous expression of the luciferase reporters. The luciferase activities in the plasma of mice injected with the control mixture (GLuc-nsh/CLuc-nsh) revealed a parallel increase of both luciferases to the same extent (Figure 20a, upper graph) and thus a comparable tumorigenicity of both cell populations independent from the luciferases being expressed. In contrast to that, the GLuc activity of p73-depleted cells remained on a very low level in mice injected with GLuc-shp73.3/CLuc-nsh or GLuc-shp73.5/CLuc-nsh cells, whereas the CLuc activities increased to the same extent as in the control cohort (Figure 20a middle and lower graph). Even with small group sizes of 4-5 animals the growth-inhibitory effect of p73-depletion was proven to be significant. The G/C activity ratios in lysed tumors from this experiment confirmed this result: the normalized ratios display a significant underrepresentation of GLuc-labeled cells when p73 was depleted (Figure 20b). Taken together, the dual luciferase assay was successfully improved for the monitoring of growth-inhibiting effects provided by inducible silencing of essential genes in cell culture experiments as well as in vivo applications, which was demonstrated by the identification of p73 being an essential factor for tumorigenicity in Hs 766T cells.

3.1.5.2 Reintroduction of p73 isoforms identifies Δ Np73 as essential tumor factor in Hs 766T

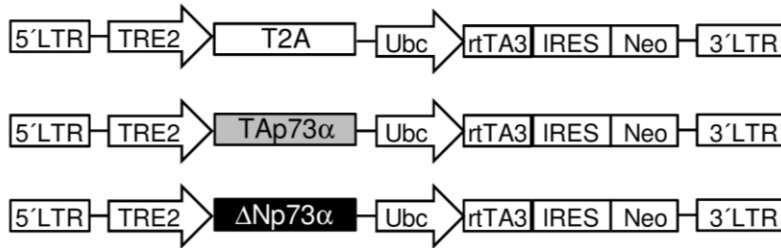
The previously shown data demonstrated a growth promoting effect of p73 in Hs 766T cells. Still, it remained unclear whether both N-terminal isoforms are essential for this phenotype or whether the presence of one of these isoforms is sufficient. For this purpose, TAp73 α and Δ Np73 α were reintroduced into p73-depleted Hs 766T either separately or in combination with each other. This was carried out by lentiviral transduction of GLuc-shp73.3 cells with pInducer20 constructs (Figure 21a). As the shRNA p73.3 binds to the 3'UTR of p73 transcripts, it targets only endogenous but not the reintroduced p73 cDNAs. Integration of pInducer20 constructs in Hs 766T cells allows transient expression of p73 isoforms in the presence of tetracycline.

Results

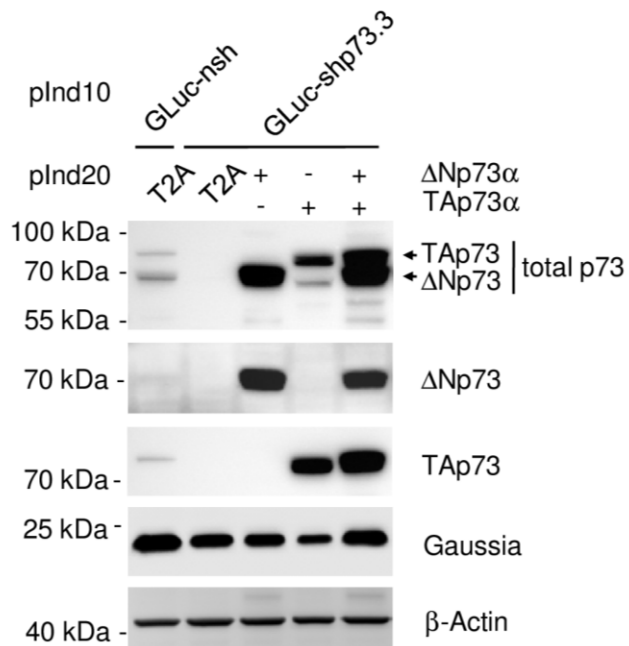
a pInducer10 constructs:



pInducer20 constructs:



b



c

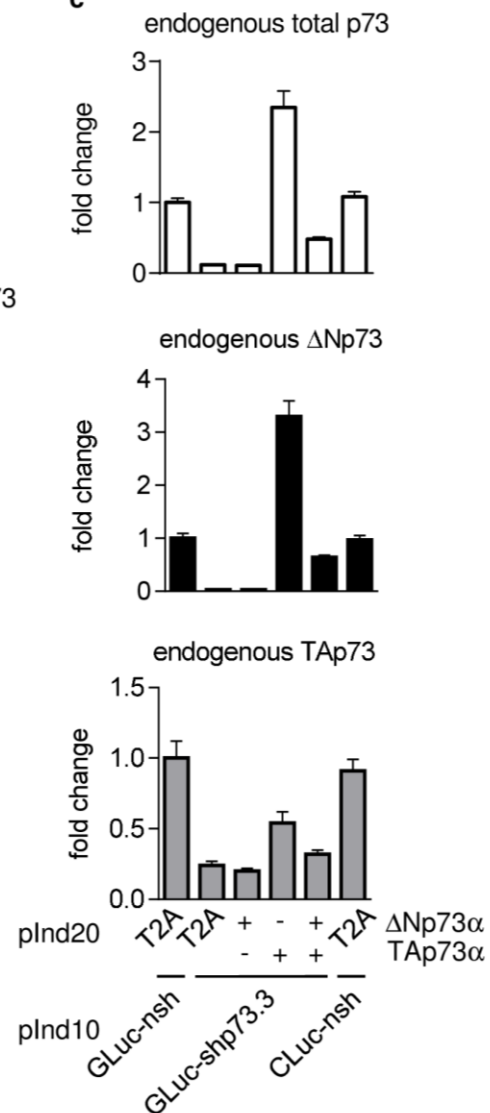


Figure 21: Dissecting the function of N-terminal isoforms in Hs 766T by reintroduction of TA and ΔNp73α in p73-depleted cells

GLuc-shp73.3 Hs 766T were additionally transduced with pInducer20 constructs for inducible expression of Δ Np73 α , TAp73 α , Δ Np73 α +TAp73 α or empty vector (T2A)

a) Lentiviral constructs pInducer10 (description see Figure 19) for tet-inducible luciferase- and shRNA expression and pInducer20 for tet-inducible expression of p73 isoforms or empty vector.

b) p73 protein levels in Hs 766T carrying constructs as indicated above detected by Δ Np73- or TAp73-specific or total p73 antibody; Gaussia levels were also detected from cell lysates; β -actin served as loading control; cells received tetracycline (2 mg/ml) for 5 days.

c) qPCR for endogenous p73 expression in the same cells as in b).

Additionally, pInducer20 carries a neomycin-resistance gene allowing for selection of successfully transduced cells. To obtain cells expressing both isoforms, GLuc-shp73.3 cells were first reintroduced with TAp73 α , underwent neomycin-selection and were finally transduced with the Δ Np73 α vector. As the constructs for both isoforms harbor the same selection marker, single cell clones were picked and investigated for their TA and Δ Np73 content upon tetracycline- treatment (Figure 21b+c). The T2A sequence, a 54 bp sequence encoding for the self-cleaving 2a peptide, served as an empty vector control.

Firstly, Hs 766T cells were analyzed for their p73 expression levels upon reintroduction of p73-isoforms. Therefore, Western Blots were performed to assess the protein levels of total, Δ N and TAp73 (Figure 21b). Independent from the isoform, the reintroduction of p73 led to a strong overexpression exceeding the physiological p73 levels in Hs 766T. However, the Δ Np73 levels of the GLuc-shp73.3/ Δ Np73 α and GLuc-shp73.3/ Δ Np73 α +TAp73 α were comparable to each other, which is also true for TAp73 levels in GLuc-shp73.3/TAp73 α and GLuc-shp73.3/ Δ Np73 α +TAp73 α cells (Figure 21b). Unexpectedly, the detection of total p73 further revealed a reconstitution of Δ Np73 to basal levels in GLuc-shp73.3/TAp73 α cells although only TAp73 α was reintroduced. This result raised the question, whether the knockdown conferred by the pGLuc-shp73.3 construct was still present in these cells. Hence, Gaussia luciferase was detected by Western Blot in order to assess the abundance of the GLuc-shp73.3 construct (Figure 21b). Compared to the other cell lines, GLuc was slightly reduced in GLuc-shp73.3/ Δ Np73 α +TAp73 α cells, but still present.

Based on this indefinite result, qPCR experiments were performed to re-assess the p73-knockdown efficiencies in the different cell populations (Figure 21c). To exclude detection of reintroduced cDNAs, primers were used specifically

detecting endogenous p73. As expected, shp73.3 displayed a high knockdown-efficiency in the empty vector control (GLuc-shp73.3/T2A), an effect which was also observed in Δ Np73 α -reconstituted Hs 766T. Yet, the reintroduction of TAp73 α caused a strong upregulation of endogenous p73 compared to basal levels in GLuc-nsh/T2A cells (Figure 21c, upper panel). Isoform-specific PCR revealed that this induction is primarily caused by the upregulation of endogenous Δ Np73 (Figure 21c, middle panel). Considering this result, the abundance of Δ Np73 protein in GLuc-shp73.3/TAp73 α cells is most likely caused by TAp73-mediated activation of the Δ Np73 promoter as was previously reported (Grob et al. 2001a; Kartasheva et al. 2002) rather than by the loss of the knockdown efficiency. This assumption was further supported by the finding that the combined reintroduction of both isoforms reconstituted endogenous Δ Np73 almost to basal levels (Figure 21c, middle panel), whereas GLuc-expression confirmed high abundance of the GLuc-shp73.3 construct (Figure 21b).

After reconstitution of N-terminal p73 isoforms, a dual luciferase assay was performed in cell culture to see whether the restoration of the different p73 isoforms rescues the proliferative phenotype in p73-depleted Hs 766T. Therefore, CLuc-nsh/T2A cells were mixed in a 1:1 ratio either with GLuc-nsh/T2A cells (basal levels of p73), with GLuc-shp73.3/T2A cells (no p73), with GLuc-shp73.3/ Δ Np73 α cells (high Δ Np73), with GLuc-shp73.3/TAp73 α cells (TAp73 high, Δ Np73 basal) or with GLuc-shp73.3/ Δ Np73 α +TAp73 α (high TAp73 and high Δ Np73). Again, cells were kept under tetracycline during the course of the experiment and supernatants were collected several times per week. The G/C ratios of each mixture were normalized to the G/C ratio of the control mix (GLuc-nsh/T2A+CLuc-nsh/T2A). As expected from previous results (Figure 19), the G/C ratio of GLuc-shp73.3/T2A+CLuc-nsh/T2A diminished over time due to p73-depletion in GLuc-expressing cells (Figure 22). The overexpression of Δ Np73 α in GLuc-shp73.3 cells was able to rescue the growth disadvantage as the G/C ratios remained stable during the course of the experiment. In contrast to that, the G/C ratios in GLuc-shp73.3/TAp73 α mixtures declined much faster than in GLuc-shp73.3/T2A

mixtures, thus indicating an additional growth-inhibitory effect of TAp73 α in GLuc-shp73.3 cells. Surprisingly, the simultaneous overexpression of both isoforms had no effect on the proliferation of GLuc-shp73.3 cells.

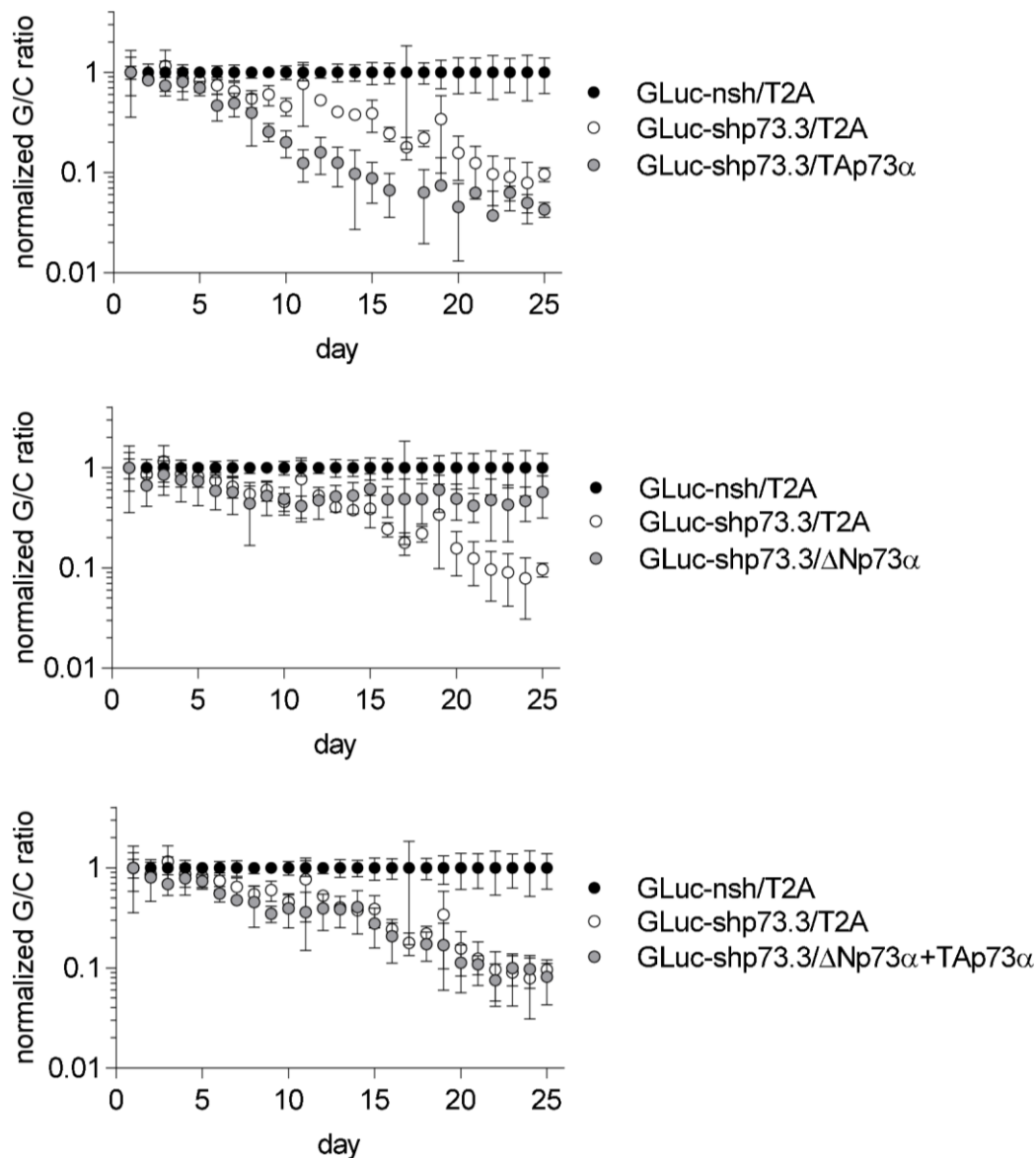


Figure 22: Δ Np73 α restores cell growth in p73-depleted Hs 766T cells

Normalized G/C activity ratios (mean \pm s.d.) of stably transduced Hs 766T cell mixtures seeded in a 1:1 ratio; CLuc-nsh/T2A cells were either mixed with GLuc-nsh/T2A, GLuc-shp73.3/T2A, GLuc-shp73.3/TAp73 α (upper graph), GLuc-shp73.3/ Δ Np73 α (middle graph), or GLuc-shp73.3/ Δ Np73 α +TAp73 α (lower graph) cells; for induction of luciferases, shRNAs and cDNAs cells were treated continuously with tetracycline (2 mg/ml), n=3

3.1.6 Low immunogenicity of luciferases in immunocompetent mice

Up to this point, all experiments of the dual luciferase assay *in vivo* were performed by xenotransplantation of luciferase-labeled human cancer cells into immunodeficient $Rag2^{tm1.1Flv};Il2rg^{tm1.1Flv}$ mice. In order to use these luciferases in future experiments for the monitoring of endogenously growing tumors in transgenic mice possessing a fully functional immune system, the luciferases were investigated for their potential to provoke an immune response, which might result in an experimental bias due to the rejection of luciferase expressing cells. Therefore, syngenic transplantations of luciferase labeled B16-F10 melanoma cells were conducted in immunocompetent C57BL/6J mice.

Lentiviral constructs:

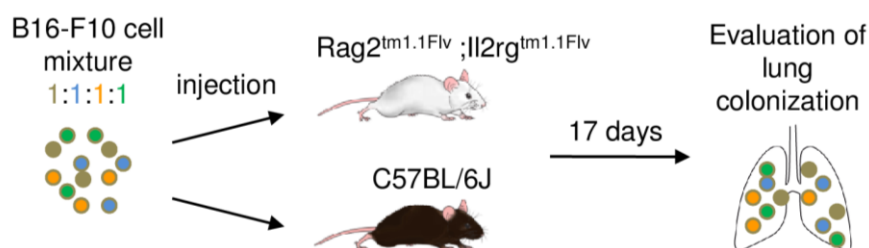
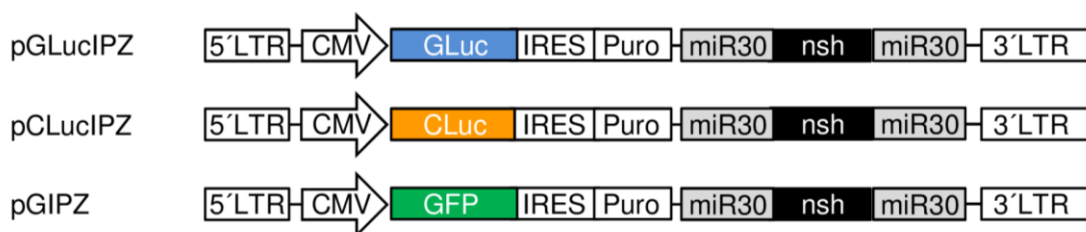


Figure 23: Experimental setup for evaluation of immunogenic properties of GLuc and CLuc

B16-F10 melanoma cells were stably transduced with the lentiviral constructs pGLucIPZ, pCLucIPZ or pGIPZ (upper scheme) and a 1:1:1:1 mixture of parental (brown), pGLucIPZ (blue), pCLucIPZ (orange) and pGIPZ (green) transduced cells was injected intravenously into immunodeficient $Rag2^{tm1.1Flv};Il2rg^{tm1.1Flv}$ mice and immunocompetent C57BL/6J mice; 17 days after tumor cell application, mice were sacrificed and lungs excised for further analyses.

Prior to transplantation, the cells were stably transduced with lentiviral pGLucIPZ or pCLucIPZ constructs encoding either for GLuc or CLuc, a puromycin selection marker and a non-coding shRNA (Figure 23). To exclude immunogenic effects of the selection marker or the shRNA, an additional construct was used which carries a GFP sequence in place of the luciferases (pGIPZ), as GFP is known to be poorly immunogenic (Skelton et al. 2001). Parental cells served as an additional control to rule out any immunological

effects caused by the lentiviral transduction of the cells. As B16-F10 cells have been shown to colonize the lungs upon tail vein injection (Fidler & Nicolson 1978), a 1:1:1:1 mixture of parental, pGLucIPZ, pCLucIPZ and pGIPZ cells was injected intravenously into immunocompetent C57BL/6J mice to obtain lung metastases. The very same cell mixture was also injected into immunodeficient $Rag2^{tm1.1Flv};Il2rg^{tm1.1Flv}$ mice to compare tumor burden and tumor composition of both groups.

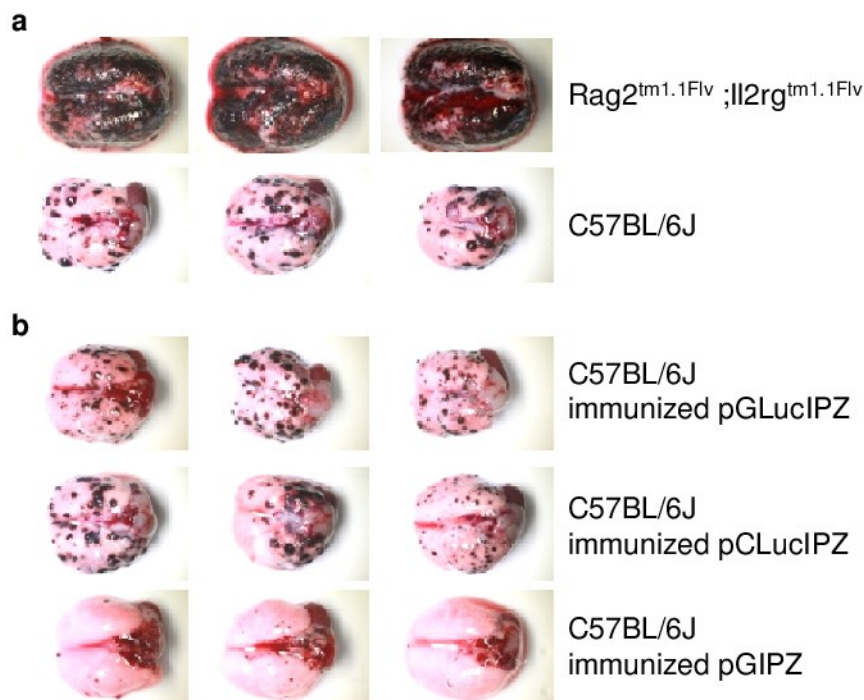


Figure 24: Syngenic transplantation of luciferase-labeled B16-F10 cells in immunocompetent C57BL/6J mice

Representative photographs of lungs from mice injected intravenously with B16-F10 melanoma cells (melanin-expressing metastases in dark brown); Immunodeficient ($Rag2^{tm1.1Flv};Il2rg^{tm1.1Flv}$) and immunocompetent (C57BL/6J) mice were injected intravenously with a 1:1:1:1 mixture of parental, pGLucIPZ-, pCLucIPZ- or pGIPZ-transduced B16-F10 cells; C57BL/6J mice were either untreated (a) or inoculated by intramuscular injection (b) of pGLucIPZ, pCLucIPZ or pGIPZ plasmid DNA 3 weeks prior to tumor cell injection (immunized pGLucIPZ, pCLucIPZ or pGIPZ).

Due to highly expressed melanin pigment, B16-F10 metastases were easily detectable. At first sight, lungs from immunodeficient $Rag2^{tm1.1Flv};Il2rg^{tm1.1Flv}$ mice displayed a much higher tumor burden compared to lungs excised from immunocompetent C57BL/6J mice (Figure 24a). In order to investigate whether this observation was a result of tissue rejection caused by luciferase- or GFP-expression, the tumor compositions were investigated by copy number quantification of GLuc, CLuc and GFP by digital PCR (Figure 25). To assess exclusively transduced B16-F10 cells, the copy number of lentiviral integration

Results

sites in B16-F10 cells was also quantified by digital PCR (Figure 25a-c) and used for normalization. Assuming that the reduced tumor cell abundance in lungs obtained from C57BL/6J mice was indeed caused by an immune response against one or both luciferases, the proportion of the affected cell population(s) would be underrepresented in samples from C57BL/6J mice. Thus, the normalized copy numbers of GLuc and/or CLuc would be reduced, whereas the copy numbers of GFP would be elevated. In fact, lung lysates from immunocompetent C57BL/6J mice did not show any significant underrepresentation of GLuc-, CLuc-, or GFP-positive cells compared to those from immunodeficient mice (Figure 25a-c). Thus, the similar tumor compositions of both cohorts rejected the initial hypothesis of an immunogenic effect of the luciferases.

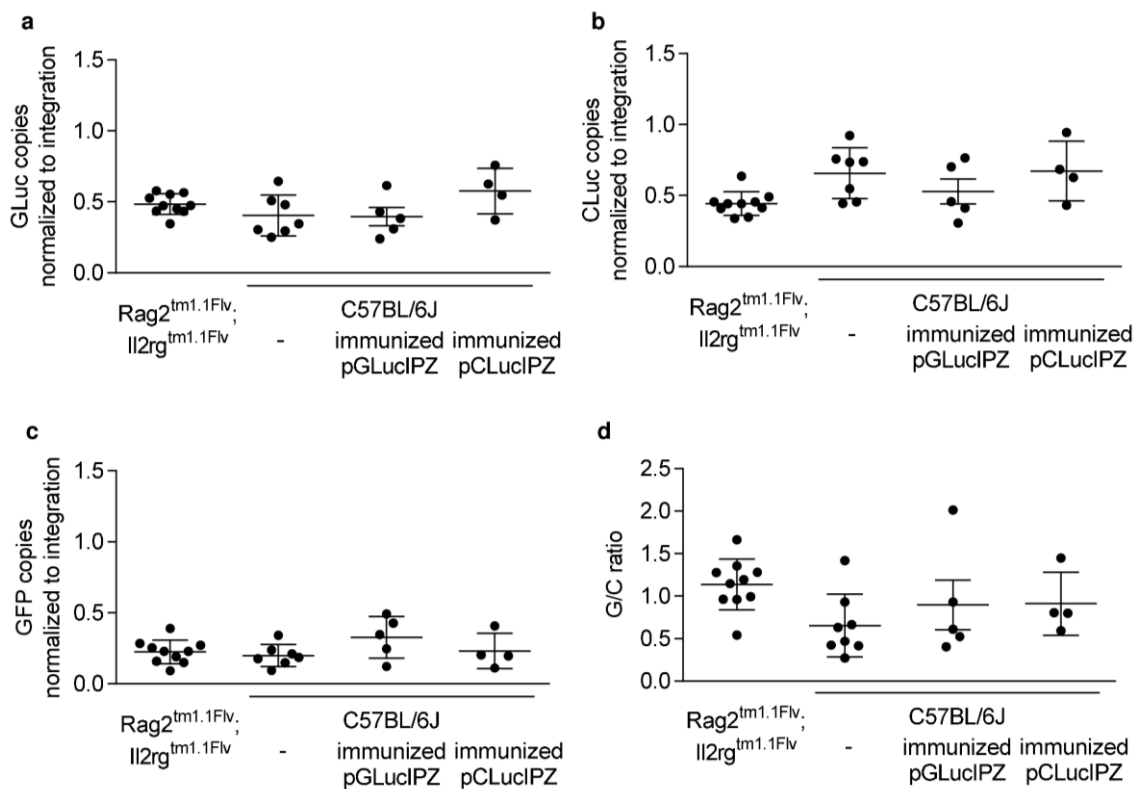


Figure 25: Immunotolerance of C57BL/6J mice against *Gaussia* and *Cypridina* luciferase

Digital PCR of gDNA from lungs lysates (Figure 24); The transferrin receptor gene (*Tfrc*) served as reference for relative quantification; samples with < 3% transduced B16-F10 content (measured by relative quantification of integration sites by digital PCR) were excluded from analyses.

a-c) Normalized copy numbers of GLuc (a), CLuc (b) and GFP (c) (mean ± s.d., no significant differences detected by non-parametrical Kruskal-Wallis test and Dunn's post test for multiple comparisons) in gDNA of lung lysates.

d) G/C ratio of copy numbers (mean \pm s.d., no significant differences detected by non-parametrical Kruskal-Wallis test and Dunn's post test for multiple comparisons, $p^* < 0.05$).

However, as mice were sacrificed 17 days after tumor cell transplantation, this short time period might be not sufficient to induce tissue rejection by the immune system. In order to ascertain the previous finding of immunotolerance towards GLuc and CLuc, three additional cohorts of C57BL/6J mice were inoculated with plasmid DNA of pGLucIPZ, pCLucIPZ or pGIPZ vectors 3 weeks before administration of the B16-F10 cell mixture. Like a vaccination, the intramuscular injection of the plasmid DNA leads to a first immune response against the injected plasmid-encoded protein (Danko et al. 1997) and thus triggers an enhanced immune reaction as soon as the organism encounters the same antigen for a second time-in this case by injection of the luciferase- or GFP-expressing B16-F10. Yet, macroscopic investigation of isolated lungs revealed no difference between untreated C57BL/6J mice and mice being vaccinated with pGLucIPZ or pCLucIPZ, reinforcing previous results of immunotolerance towards GLuc and CLuc. Unexpectedly, the vaccination with the low-immunogenic GFP-vector strongly reduced the tumor burden. Lungs from pGIPZ-immunized mice had to be excluded from further analyses, as the abundance of tumor cells -and consequently GLuc/CLuc/GFP copy numbers- fell below the detection limits of digital PCR.

Neither pGLucIPZ- nor pCLucIPZ-inoculated mice showed any significant reduction of luciferase-labeled cells. (Figure 25b). The vaccination of C57BL/6J mice with pGLucIPZ did not further reduce the G/C ratio, neither did the vaccination with pCLucIPZ increase the ratio (Figure 25d) as would be expected in case of an enhanced immune response. Taken together, neither GLuc nor CLuc induced any significant immune response in the C57BL/6J inbred strain that could cause an experimental bias when using these secreted luciferases for monitoring tumors in immunocompetent mice.

3.2 Characterization of a mouse model overexpressing oncogenic Δ Np73

Within the p73 family, full length TAp73 is considered to execute tumor suppressive functions, whereas N-terminally truncated Δ Np73 presumably exerts oncogenic functions (see 1.3.2). This finding was further underlined by the results obtained from tumorigenicity studies in Hs 766T, as the growth-

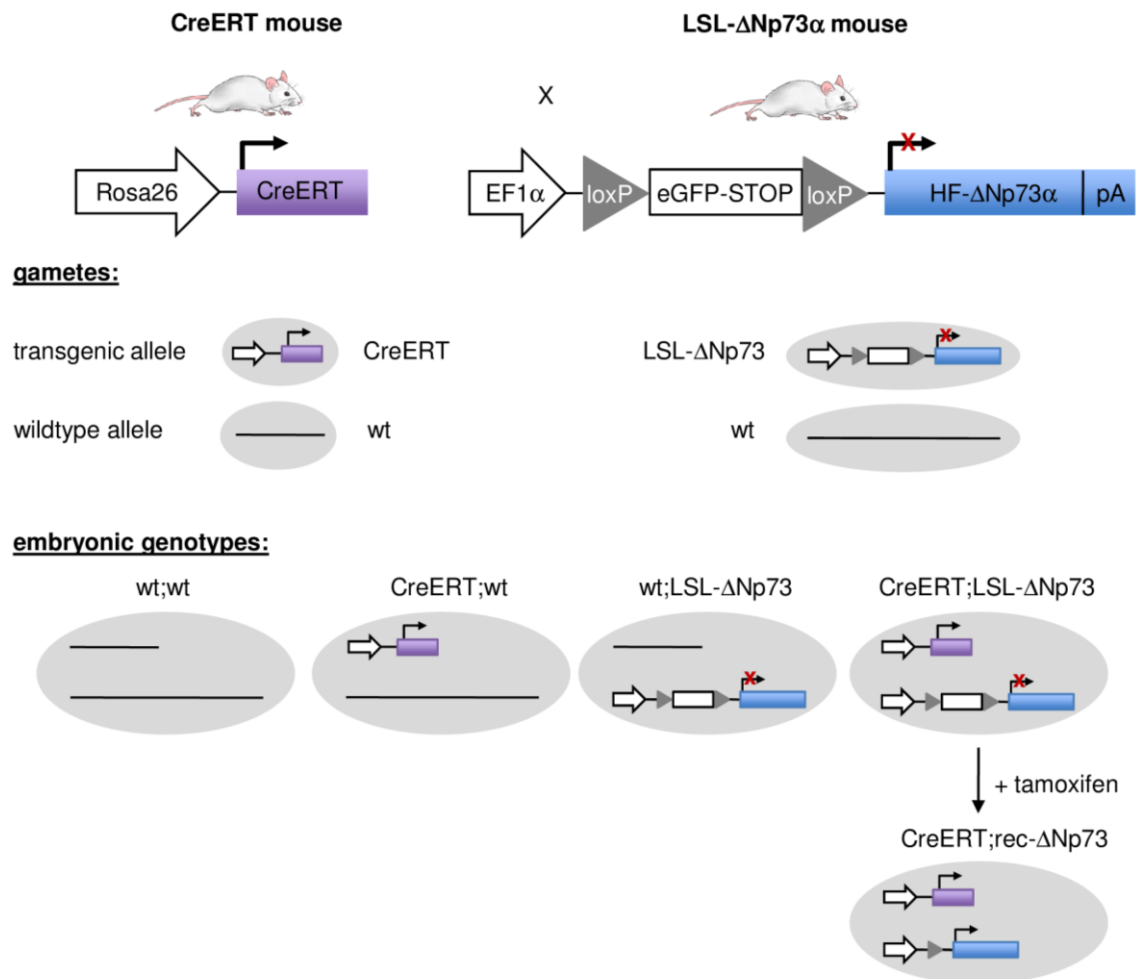


Figure 26: Breeding scheme for induction of the Δ Np73 transgene

Heterozygous CreERT transgenic mice were mated with heterozygous LSL- Δ Np73 transgenic mice to obtain Δ Np73 overexpressing litter. Schematic transgenic constructs for both strains are shown below the mice; Rosa26 locus for ubiquitous expression (Rosa26), Cre recombinase fused to the tamoxifen-inducible estrogen receptor (CreERT), promoter of elongation factor 1 α (EF1 α), recognition sites for Cre recombinase (loxP), enhanced green fluorescent protein (eGFP), stop cassette (STOP), human HA-Flag-tagged Δ Np73 α (HF- Δ Np73 α), poly-adenosine-monophosphate tail (pA); Below the constructs the potential gametes carrying either the transgenic or wildtype allele are depicted as well as embryonic genotypes (wt;wt, CreERT;wt, wt;LSL- Δ Np73, CreERT;LSL- Δ Np73); treatment of double transgenic progeny (CreERT;LSL- Δ Np73) with tamoxifen leads to recombination of the loxP sites thus enabling Δ Np73 expression (CreERT;rec- Δ Np73).

inhibitory effect of p73-depletion in these cells was amplified by reintroduction of TAp73 α , whereas the reintroduction of Δ Np73 α restored cell growth (3.1.5.2). Additionally, Δ Np73 has been found to be upregulated in various tumor types (see 1.3.2). To further decipher the distinct role of Δ Np73 in tumorigenesis, a Δ Np73-overexpressing mouse model was characterized in this thesis. The attempt to create a mouse model overexpressing Δ Np73 constitutively failed repeatedly as no founder mice could be obtained (Hüttinger-Kirchhof et al. 2006). As a consequence, an inducible mouse model was deployed, which provides inducible Δ Np73 expression by the Cre-loxP system (Figure 26+Figure 27).

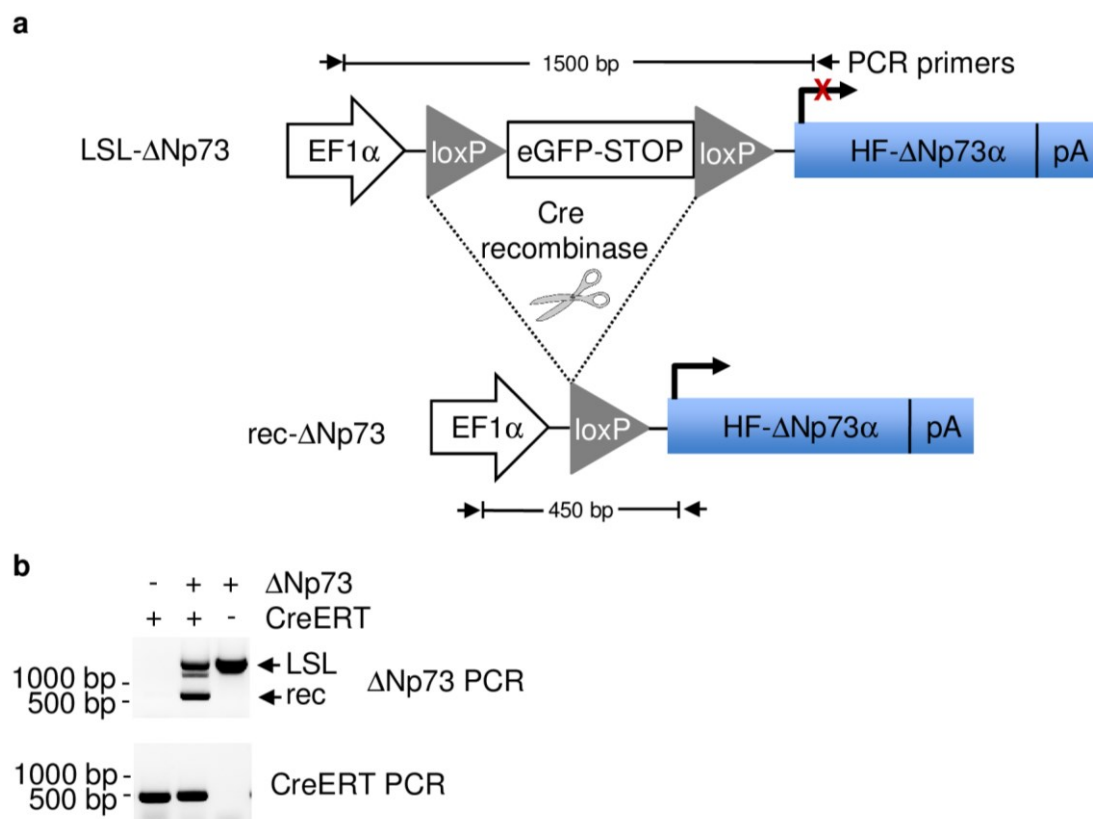


Figure 27: Inducible recombination of the Δ Np73-transgene by the Cre-loxP system

a) Scheme of the Δ Np73 transgene before (upper graph) and after (lower graph) recombination; arrows indicate primer binding sites and fragment size in genotyping PCR.

b) Genotyping PCR of single and double transgenic MEFs from timed matings of LSL-HF- Δ Np73 and CreERT transgenic mice; recombination was achieved by 5 days 4-hydroxytamoxifen (4OHT) treatment of MEFs and verified by PCR product size (floxed allele 1500 bps, recombined 450 bps).

The CreERT strain used in this work yields a Cre recombinase transgene inserted into the murine ROSA26 locus, thereby providing constitutive

expression of the transgene (Badea et al. 2003). The Cre recombinase is fused to a modified murine estrogen receptor (ERT), which retains the recombinase in the cytoplasm due to interactions with heat shock proteins. Upon administration of the anti-estrogen tamoxifen, the enzyme is released and translocates to the nucleus where it catalyzes the recombination of loxP sites.

The EF1 α - Δ Np73 α mouse strain (short: LSL- Δ Np73) carries a transgene composed of three major parts: an HA-Flag-tagged human Δ Np73 α transgene (HF- Δ Np73 α), an EF1 α promoter to drive transgene expression and a loxP-STOP-loxP (LSL) cassette which prevents Δ Np73 expression under normal conditions (Figure 27). To induce Δ Np73 expression, LSL- Δ Np73 mice were crossbred with CreERT mice. Administration of tamoxifen to double transgenic mice (CreERT;LSL- Δ Np73) induced Cre-mediated recombination of the loxP sites, thereby eliminating the LSL cassette. The recombined state of the transgene is further referred to as rec- Δ Np73.

3.2.1 Impact of the Δ Np73-transgene on murine embryonic fibroblasts

First, in order to verify the functionality of this mouse model, the recombination, expression and functionality of the transgene were tested in MEFs obtained from timed matings of CreERT with LSL- Δ Np73 mice (Figure 26). MEFs of all four possible genotypes - either wildtype for both transgenes (wt;wt), single transgenic for one of both transgenes (CreERT;wt or wt;LSL- Δ Np73) or for both transgenes (CreERT;LSL- Δ Np73) were treated with 4-hydroxytamoxifen (4OHT) to achieve recombination of the floxed allele in double transgenic cells (Figure 27a). Genotyping PCR (for primer binding sites see Figure 27a) demonstrated that 4OHT-treatment had no impact on the floxed Δ Np73 allele in single transgenic MEFs, whereas double transgenic MEFs exhibited recombination of the loxP sites, thus eliminating the stop cassette (Figure 27b).

3.2.1.1 Validation of the Δ Np73-transgene expression and functionality in MEFs

All genotypes of MEFs were investigated specifically for mRNA-expression of the HA-Flag- Δ Np73 α -transgene by reverse transcription-qPCR using primers which bind within the HA-Flag-tag sequence (forward primer) and Δ Np73 α (reverse primer). 4OHT-treated double transgenic MEFs displayed a high

abundance of the HF- Δ Np73 α transcript, whereas neither 4OHT-treated wildtype and single transgenic MEFs nor untreated double transgenic MEFs exhibited any Δ Np73 expression (Figure 28a). This expression pattern was further confirmed on protein level, as p73 protein was detected exclusively in rec- Δ Np73 MEFs (Figure 28b).

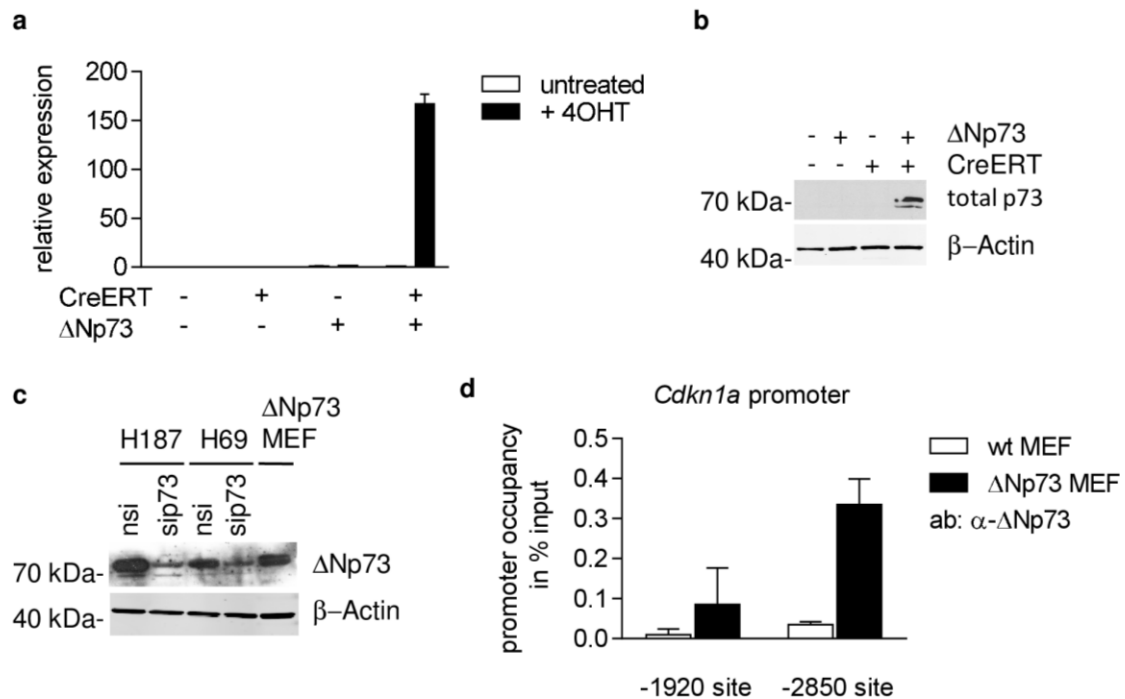


Figure 28: Expression and functionality of the Δ Np73-transgene in MEFs

MEFs of all genotypes were treated with 1 μ M 4OHT for 5 days.

a) Relative expression of the HA-Flag- Δ Np73 α -transgene (mean \pm s.d.) assessed by qPCR in wildtype, single and double transgenic MEFs (untreated or treated with 4OHT); data normalized to untreated wildtype MEFs.

b) Representative Western Blot for total p73 expression in single and double transgenic MEFs; β -Actin served as loading control.

c) Representative Western Blot for comparative protein expression analysis of Δ Np73 levels in CreERT; Δ Np73 MEFs (Δ Np73 MEF) and human small cell lung cancer cell lines H187 and H69 treated with a non-silencing control siRNA (nsi) or an siRNA targeting p73 (sip73); β -actin served as loading control.

d) ChIP analysis for evaluation of Δ Np73 binding ability to chromatin in Δ Np73 MEFs (mean % of input \pm s.d.) at the -1920 site (negative control) and the -2850 site (established p73 binding site) of the murine *Cdkn1a* promoter; ChIP was performed with a Δ Np73-specific antibody, n=2.

Moreover, to evaluate whether p73-expression in rec- Δ Np73 MEFs is in a physiological range, protein levels were compared with small cell lung cancer cell lines (SCLC) H187 and H69 which are known to exhibit high p73 expression. In parallel, the specificity of detected bands was verified by siRNA-induced depletion of p73 in SCLC samples (sip73). Western Blot analysis

clearly demonstrated that, even if overexpressed, the level of the transgene is physiological (Figure 28c).

In order to assess whether the expressed human Δ Np73-transgene is functional in murine cells, chromatin immunoprecipitation (ChIP) was performed in rec- Δ Np73 and wildtype (negative control) MEFs. Δ Np73 bound effectively (0.35% of input) to the known p53-response element at the -2850 region within the *Cdkn1a* promoter whereas only poor binding was observed at the -1920 region which served as negative control (Figure 28d). Thus, it can be assumed that the Δ Np73 transgene is able to execute its function as a transcription factor and, as a consequence, to regulate gene expression.

3.2.1.2 Whole transcriptome analysis of Δ Np73-overexpressing MEFs

In order to investigate the effects of the Δ Np73-transgene on global gene expression, cDNA microarray analysis was performed. The expression profiles of 4 independent rec- Δ Np73 MEFs were compared with those from 4 independent single transgenic MEFs (2 LSL- Δ Np73 and 2 CreERT). Δ Np73-regulated genes were identified by calculation of the fold change of log₂-transformed ($\log_2(\text{FC})$) data from rec- Δ Np73 versus control MEFs (see 2.2.1.9). The differential regulation of all genes being up- or downregulated by at least 2-fold was then visualized in a heatmap (Figure 29a). Expectedly, *Trp73* was found on top of the upregulated genes in rec- Δ Np73 MEFs and semiquantitative PCR -specifically amplifying the HF- Δ Np73a transcript- ascribed this result to transgene expression (Figure 29b).

To identify biological processes regulated by Δ Np73, microarray data were evaluated by Gene Set Enrichment Analysis (GSEA) and interactions of regulated canonical pathways were visualized in an enrichment map (Figure 30). As Δ Np73 is known to exert oncogenic functions, it was not expected to find replication- and mitosis-related gene sets to be repressed in rec- Δ Np73 MEFs. On single gene level, the reduced expression of mitosis-promoting genes like *CENPA*, *TGFB3*, *CCNB1* and *CCNB2* in rec- Δ Np73 MEFs supported this finding (Figure 29a). Related to replication, gene sets annotated with DNA-repair and chromosome maintenance were also negatively regulated by Δ Np73.

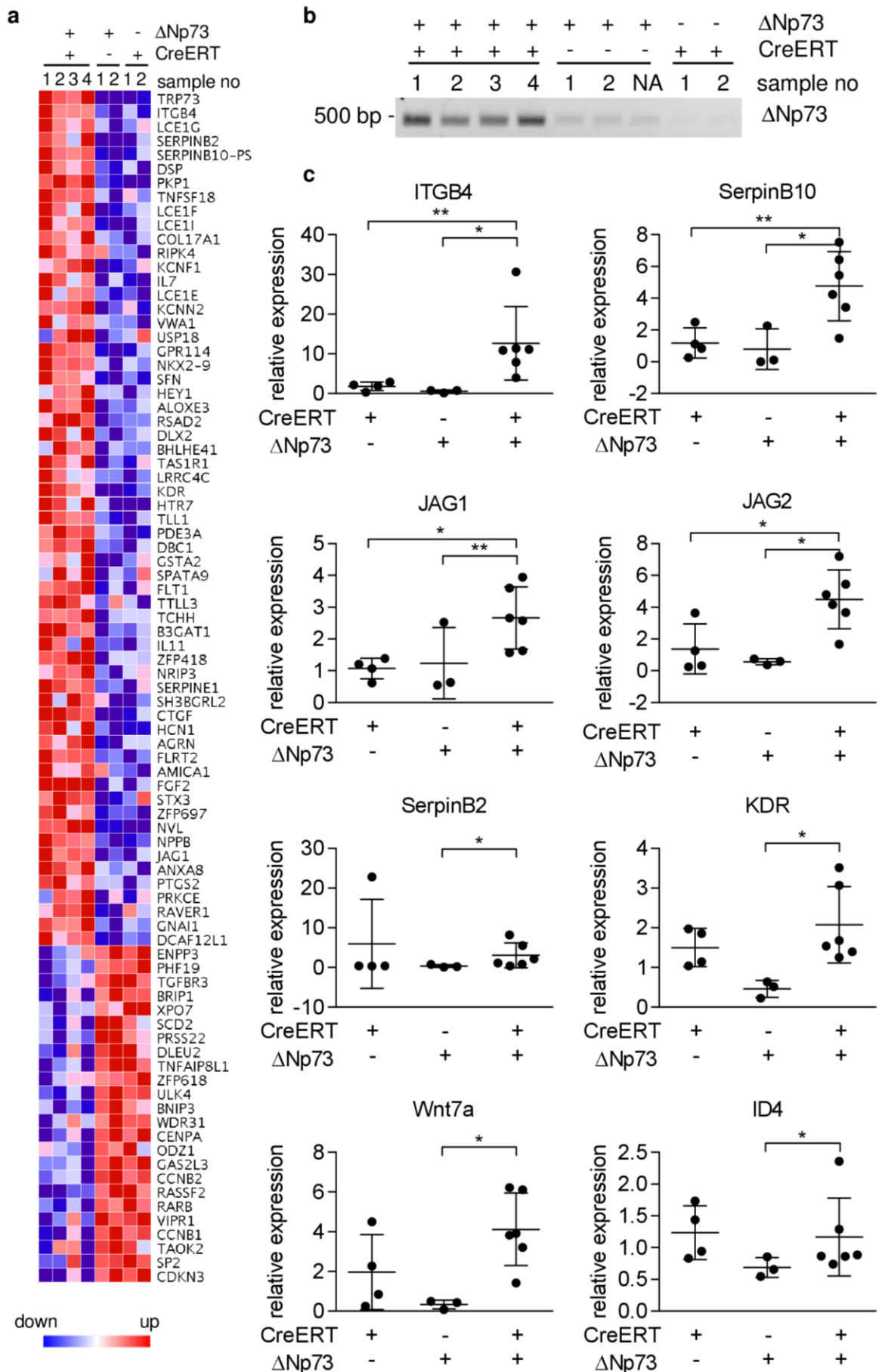


Figure 29: Differentially regulated genes in Δ Np73-overexpressing MEFs

Results

a) Heatmap of up- (red) and downregulated (blue) genes ($\log_2(\text{FC}) > 1$ or < -1 , $p\text{-val} \leq 0.05$) in 4 independent double transgenic (rec Δ Np73;CreERT) versus 4 independent single transgenic (LSL- Δ Np73 or CreERT) control MEFs obtained from Microarray analysis.

b) Semiquantitative PCR for quantification of HA-Flag- Δ Np73 expression in MEFs from a); one LSL- Δ Np73 MEF was not analyzed (NA) in a).

c) Validation of selected Δ Np73-induced genes by qPCR (one-tailed t-test, $*p\text{-val} \leq 0.05$, $**p \leq 0.05$).

Apart from this, Δ Np73 repressed metabolic pathways, especially those involved in glycolysis and gluconeogenesis.

Ultimately, cancer-promoting characteristics of Δ Np73 were identified after consideration of the pathways which were induced by Δ Np73. In detail, migration- and cell adhesion-related gene sets were upregulated, thus connecting high Δ Np73 levels with enhanced metastasis (Figure 30). Within these pathways, the transmembrane receptor integrin $\beta 4$ (ITGB4) was one of the commonly regulated factors and additionally the most upregulated gene next to Trp73. QPCR in MEFs further confirmed this result, as ITGB4 was highly upregulated in rec- Δ Np73 cells (Figure 29c).

In summary, these data suggest that Δ Np73 exerts its oncogenic function rather by induction than by repression and accordingly further validation experiments focused exclusively on Δ Np73-induced factors (Figure 29c).

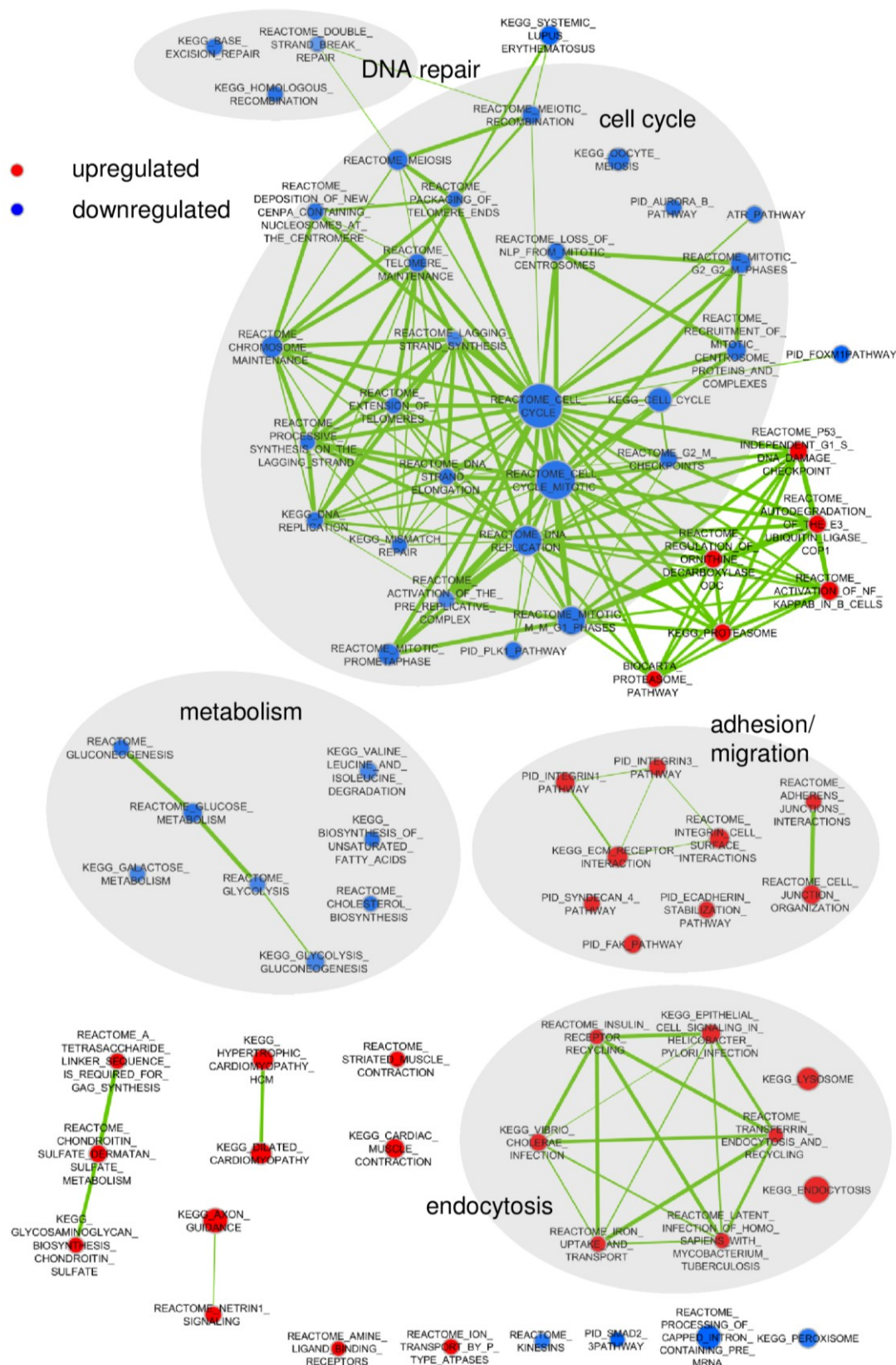


Figure 30: Gene Set Enrichment Analyses of $\Delta Np73$ -overexpressing MEFs
Up- (red nodes) and downregulated (blue nodes) canonical pathways computed by GSEA of microarray data from rec- $\Delta Np73$ MEFs; Enrichment map was created by integration of GSEA results in Cytoscape (Cutoff p-value ≤ 0.005 , FDR ≤ 0.1); The size of nodes reflects the number of regulated genes in a particular gene set, the thickness

of connecting lines in green represent the number of commonly regulated genes between two gene sets.

3.2.2 Expression analysis of the Δ Np73-transgene in murine organs

For analysis of Δ Np73-overexpressing mice, LSL- Δ Np73 mice were mated with CreERT mice. Double transgenic pups were subjected to tamoxifen treatment for 5 consecutive days at the age of 4-6 weeks for recombination of the loxP-flanked STOP cassette in front of the transgene (Figure 26). Single transgenic siblings were treated likewise to serve as control mice.

Two weeks after the last tamoxifen application, mice were sacrificed and genomic DNA was isolated from different organs to verify recombination efficiency in whole animals by genotyping PCR. The tamoxifen treatment of double transgenic mice led to a complete recombination (rec- Δ Np73) in almost every organ, except the brain, which might be limited due to the blood-brain-barrier (Figure 31a). In contrast, single transgenic floxed mice kept their floxed allele (LSL- Δ Np73).

To test whether the recombination subsequently leads to transcription of the Δ Np73-transgene, mRNA was isolated from organs and analyzed using semiquantitative PCR. Most organs show a strong upregulation of the Δ Np73 transcript in rec- Δ Np73 samples compared to LSL- Δ Np73 (Figure 31b). Occasionally, signals were also detected in some organs derived from LSL- Δ Np73 mice (e.g. testis, brain and lung) which is most likely due to contamination with genomic DNA as the PCR is not able to distinguish between genomic DNA or cDNA from transcripts. In contrast to elevated mRNA levels of the transgene, protein levels were barely detectable in most organs of rec- Δ Np73 mice (Figure 31c). Only testes showed a strong Δ Np73 expression which was also confirmed by immunohistochemistry (Figure 31d). While the spermatozoa-nourishing Sertoli cells within the seminiferous tubules, testosterone-producing Leydig cells between the tubules and mature spermatozoa were negative for p73, it was found to be highly expressed throughout all developmental stages of male germ cells including spermatogonia, spermatocytes and spermatids.

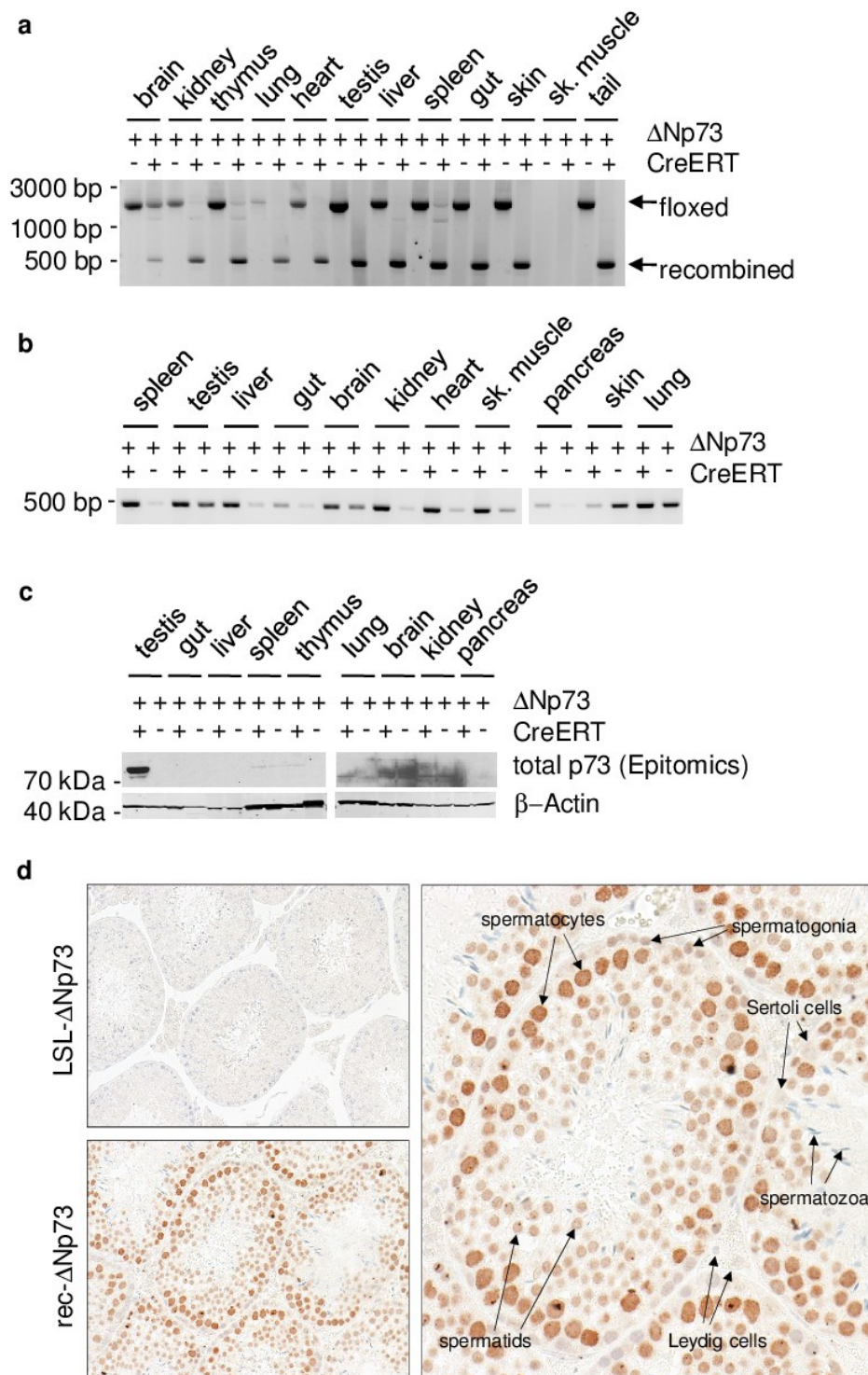


Figure 31: ΔNp73 expression in organs of transgenic mice

Recombination of the floxed allele and transgene expression was evaluated in ΔNp73;CreERT transgenic mice after application of tamoxifen for 5 consecutive days

a) Genotyping PCR for the floxed and recombined ΔNp73 allele in different organs/tissue of single and double transgenic mice, (sk. muscle = skeletal muscle); for primer binding sites see Figure 27a).

b) Semiquantitative PCR for HA-Flag-ΔNp73 expression.

c) Protein levels of total p73 in different organs of LSL- and rec-ΔNp73 mice, β-actin served as loading control.

d) Immunohistochemical staining of p73 in the testis of LSL- and rec-ΔNp73 mice (200x magnification); different cell types are highlighted by arrows.

3.2.3 Reproductive defects of Δ Np73 transgenic mice

3.2.3.1 Infertility of Δ Np73-overexpressing males

The high expression of Δ Np73 throughout the testes of rec- Δ Np73 mice raised the question whether this overexpression has any effects on fertility. Therefore, 9 matings were set up, each consisting of two wildtype females and one rec- Δ Np73 male. The transgenic males used for these breeding experiments were obtained from matings of CreERT mice with LSL- Δ Np73 mice. As described before (see Figure 27), pups have been treated with tamoxifen to achieve recombination. Additionally, 10 single transgenic male siblings (5 CreERT and 5 LSL- Δ Np73) were used for control mating trios (Figure 32a). When fertility studies started, all mice were between 6-8 weeks of age to ensure sexual maturity and exclude age-related effects. Furthermore, all matings were set up at the same time to prevent seasonal effects on the mating behavior of rec- Δ Np73 and control males. From 9 mating triplets in total, none of the rec- Δ Np73 males produced any litter. The Δ Np73-overexpressing males showed absolutely

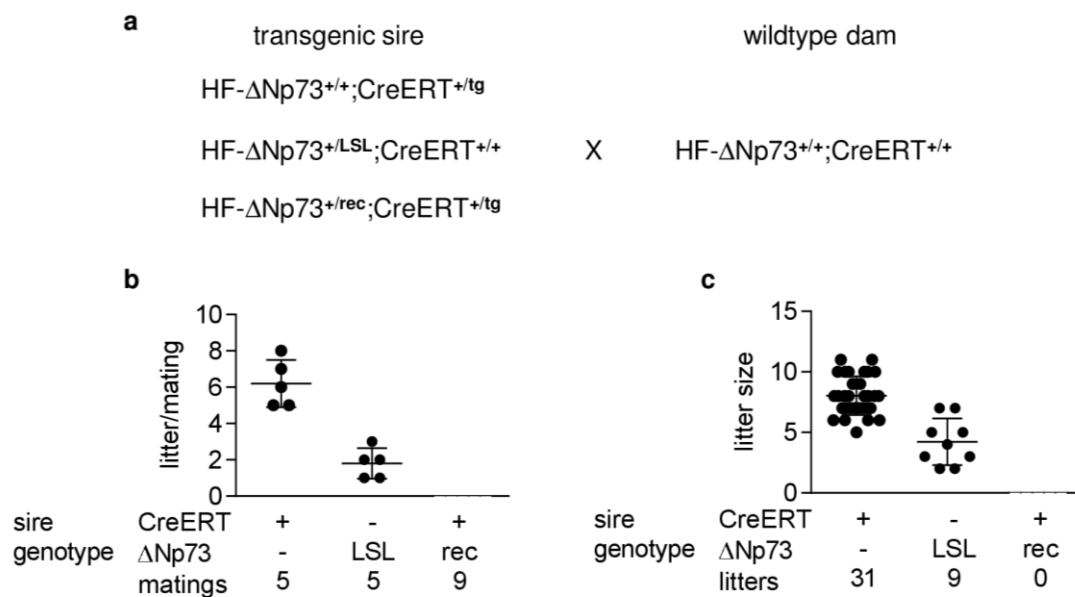


Figure 32: Infertility of Δ Np73-overexpressing males

Single and double transgenic males were treated with tamoxifen to induce Δ Np73 expression; 6-8 week old males were mated with two FVB/N females each for 6 months; genotypes of males are depicted below each graph, "LSL" and "rec" define status of the Δ Np73-transgene; the numbers below the graphs display the total numbers of matings (b) and litters (c).

a) Breeding scheme of transgenic males with wildtype females.

b) Number of litters per mating (mean \pm s.d.); 9 rec- Δ Np73 males failed completely to produce any litter.

c) Litter size of matings (mean \pm s.d.).

normal mating behavior, including scenting and mounting of the females, but none of the females gave birth to any pups, whereas single transgenic males produced on average 6 (CreERT sires) and 2 (LSL- Δ Np73 sires) litters per mating (Figure 32b). Beside the total amount of litters, LSL- Δ Np73 single transgenic males averaged 4 pups per litter opposing an average litter size of 8 pups from CreERT males (Figure 32c). However, although the amount of litters and the corresponding litter size from LSL- Δ Np73 males was reduced compared to CreERT matings, genotyping of the offspring arising from these matings exhibited a completely expected mendelian ratio of genotypes, half wildtype, half transgenic (Figure 33).

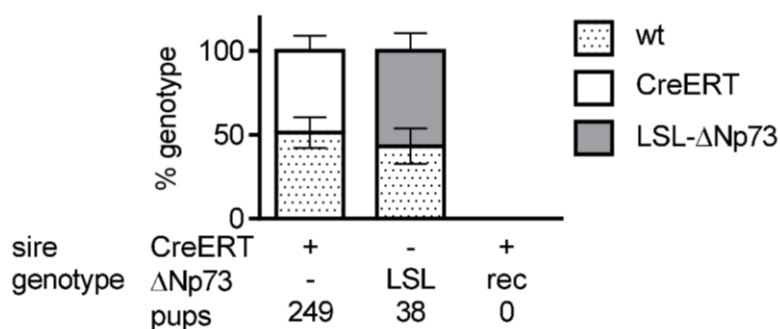


Figure 33: Genotype distribution of litters from CreERT and LSL- Δ Np73 males
 Frequency of transgene transmission of pups from mating experiments in Figure 32 (mean of each litter \pm s.d.).

3.2.3.2 Embryonic lethality of Δ Np73-overexpressing offspring from rec- Δ Np73 females

The same fertility tests were performed with Δ Np73-overexpressing females. 5 rec- Δ Np73 females were mated with 1 wildtype male each. For control matings, single transgenic (either CreERT or LSL- Δ Np73) siblings were mated with wildtype males (Figure 34a). Again, all matings were set up with mice of 6-8 weeks of age for 6 months.

In contrast to Δ Np73-overexpressing males, rec- Δ Np73 females did not display enhanced Δ Np73-expression in their reproductive organs (data not shown) and were able to breed. Rec- Δ Np73 dams delivered on average 5 times compared to single transgenic dams which delivered 6 (CreERT) and 7 (LSL- Δ Np73) times (Figure 34b). Despite the comparable amount of litters, the litter size from rec- Δ Np73 females was significantly reduced compared to control matings (Figure 34c). All pups arising from these matings were genotyped and the obtained fractions of genotypes were compared to the expected mendelian ratio. The

offspring from single transgenic dams showed the expected 1:1 distribution of transgenic and wildtype mice (Figure 35b). In contrast to that, the progeny of rec- Δ Np73 dams displayed an unexpected distribution of genotypes. Here, two transgenic alleles are involved, resulting in four different possible combinations of transgenic and wildtype alleles with equal likelihood (1:1:1:1): the oocyte is either completely wildtype, single transgenic for CreERT or rec- Δ Np73 or double transgenic harboring one CreERT and one rec- Δ Np73 allele (Figure 35a+b). Genotyping of rec- Δ Np73-derived pups revealed a strong underrepresentation of mice carrying a recombined Δ Np73 allele. In total, only two mice with a rec- Δ Np73 allele were born, whereas the remaining 66 animals were either completely wildtype or single transgenic for CreERT (Figure 35b).

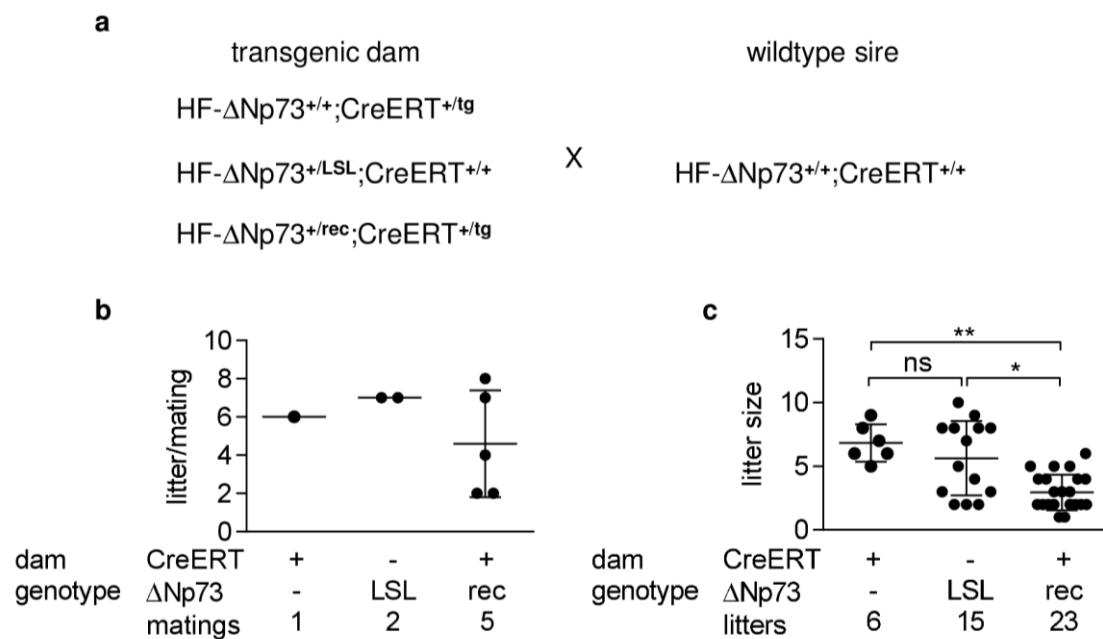


Figure 34: Δ Np73-overexpressing females deliver viable litters of reduced size
 Single and double transgenic females were treated with tamoxifen to induce Δ Np73 expression; 6-8 week old FVB/N males were mated with two transgenic females each; genotypes of dams are depicted below each graph, "LSL" and "rec" define the status of the Δ Np73-transgene; the numbers below the graphs display the total numbers of matings (b) and litters (c)
 a) Breeding scheme of transgenic dams with wildtype males.
 b) Number of litters per mating (mean \pm s.d.).
 c) Litter size of matings (mean \pm s.d.); Kruskal Wallis test corrected for multiple comparisons with Dunn's post test, p^{**}<0.005, p^{*}<0.05, ns = non-significant.

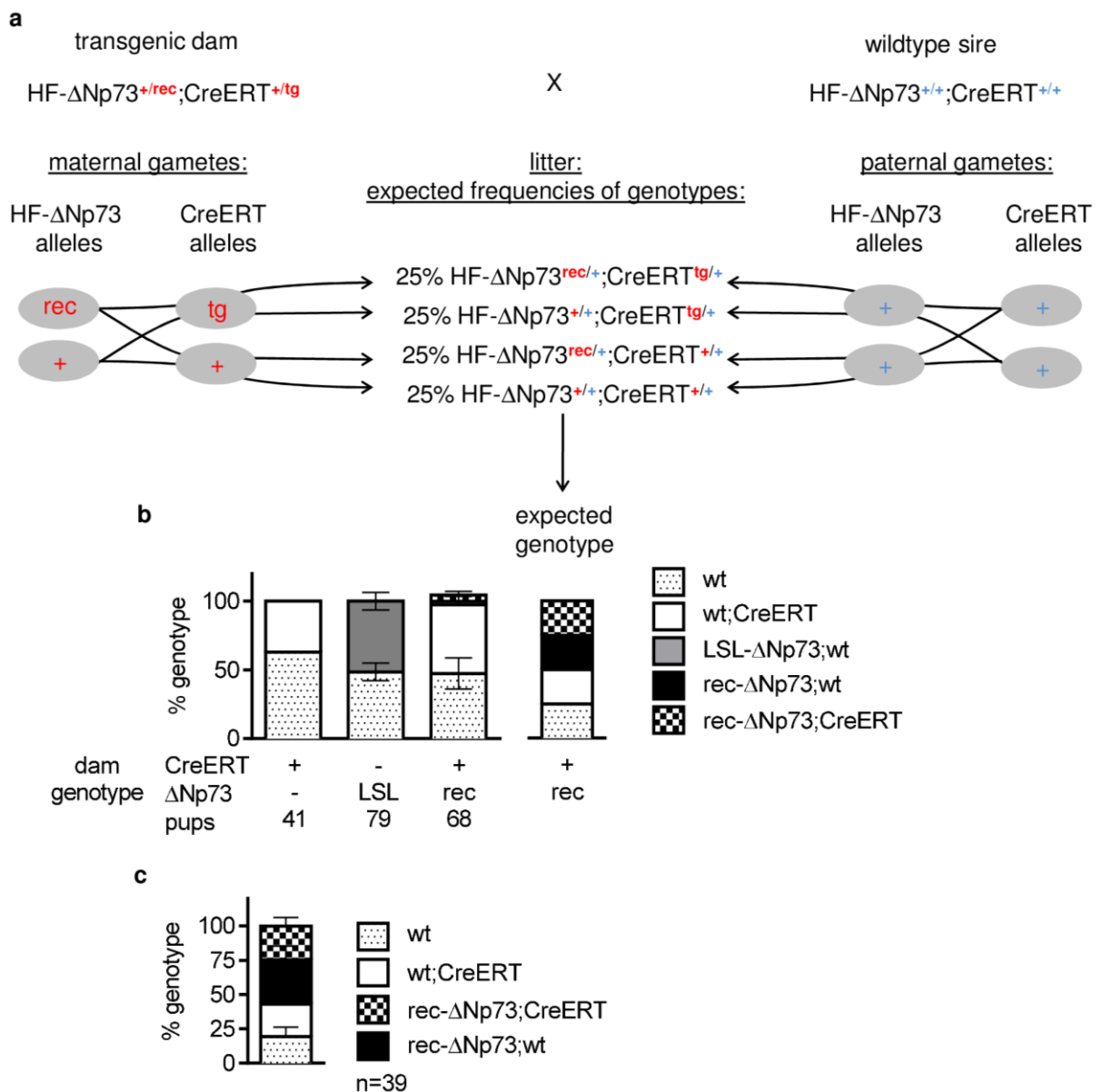


Figure 35: Δ Np73 overexpression leads to embryonic lethality

Genotyping of litters obtained from single and double transgenic dams

a) Scheme of gametes in matings of Δ Np73-overexpressing dams (red) with wildtype sires (blue); genotypes of the progeny are expected to occur at the same rate (25% each).

b) Genotyping results of pups from matings of single and double transgenic females (mean of each mating \pm s.d.); „expected genotype“ reflects expected mendelian ratio from matings of Δ Np73-overexpressing females as described in a); genotypes of dams are depicted below the graphs, numbers reflect the number on genotyped pups.

c) Genotyping results of pups obtained from matings of the two rec- Δ Np73 females from the previous mating experiment (b) with wildtype males.

As rec- Δ Np73 dams gave birth to an expected extent of pups being wildtype or transgenic for CreERT, the lack of rec- Δ Np73 pups must be due to the genetic status of the embryos and not the status of the dams. This result confirms former findings of embryonic lethality caused by the overexpression of Δ Np73

(see 1.3.4). Nevertheless, there were two females born with the double transgenic status $rec-\Delta Np73; CreERT$. These were further mated with wildtype males and their litters underwent genotyping as well. Surprisingly, these females were able to deliver $rec-\Delta Np73$ positive mice in the expected mendelian ratio (Figure 35c).

In sum, the mouse model being created for ubiquitous overexpression of $\Delta Np73$ exhibited only barely detectable $\Delta Np73$ protein levels in most organs. However, the high $\Delta Np73$ expression within the testis shed new light on $\Delta Np73$ as an important factor in reproductive biology, which was further emphasized by the high mortality rate of $\Delta Np73$ -overexpressing embryos.

3.2.4 $\Delta Np73$ -overexpressing mice lack a tumorigenic phenotype

The $\Delta Np73$ -strain was developed to investigate potential oncogenic properties of $\Delta Np73$ during tumor formation in long-term studies. Therefore, $\Delta Np73$ -overexpressing mice were bred as described before (see 3.2.2) and single transgenic siblings were used as control groups, independent of gender. All mice were treated with tamoxifen and were subsequently monitored for medical conditions. Mice were euthanized reaching endpoint criteria (tumor size exceeding 1 cm^3 , ulcerating tumors, heavily impaired motility, cachexy, lethargy or bowel prolapse). After autopsy of animals, organs were prepared for histological analysis. The Kaplan-Meier curves of these mice display a slight disadvantage of $rec-\Delta Np73$ mice in overall (OS) and tumor-free (TFS) survival before the median survival is reached: control mice exhibited prolonged survival compared to $rec-\Delta Np73$ mice at the age between 400 and 650 days (Figure 36). Nevertheless, these observable trends did not reach statistical significance, which was also confirmed by the median OS/TFS of the three different groups: half of $rec-\Delta Np73$ mice were dead after 673/812 days, $LSL-\Delta Np73$ after 687/845 days and $CreERT$ mice after 653/801 days. Comparison of tumor incidence between the groups revealed no tumor-promoting effect of $\Delta Np73$ in this mouse model.

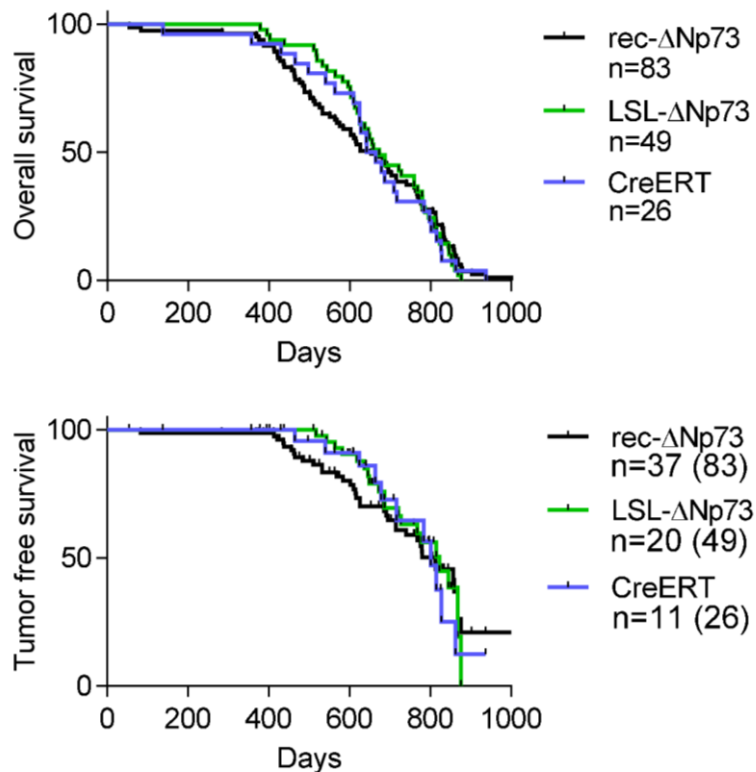


Figure 36: Overexpression of $\Delta Np73$ has no effect on overall or tumor-free survival

Kaplan-Meier Plot for overall survival (OS, upper) and tumor-free survival (TFS, lower) of double and single transgenic mice; all mice received tamoxifen for 5 consecutive days at the age of 4-5 weeks; tumor-free animals were censored for TFS; the size of all cohorts included in the analysis are given in the legend, numbers in brackets show number of mice before censoring; log-rank test does not detect significant differences in OS nor in TFS between single and double transgenic mice.

3.2.5 Impact of the $\Delta Np73$ -transgene on the tumor phenotype of the p53-knockout mouse model

Carcinogenesis is caused by multiple genetic alterations. Thus, the overexpression of an oncogene like $\Delta Np73$ may not be sufficient to induce malignant cell growth but requires additional inactivation of a tumor suppressor gene. As the $\Delta Np73$ -transgenic strain did not show shortened lifespan due to enhanced tumor formation, we aimed to investigate whether $\Delta Np73$ overexpression has an impact on the tumor phenotype of heterozygous p53-knockout mice ($p53^{+/-}$).

To generate $p53^{+/-}$ mice with concomitant $\Delta Np73$ overexpression and corresponding control animals, breedings were performed in two steps (Figure 37). First, $p53^{+/-}$ mice were interbred with CreERT mice to obtain CreERT; $p53^{+/-}$ mice. These animals were then further crossed with LSL- $\Delta Np73$ mice to obtain LSL- $\Delta Np73$;CreERT; $p53^{+/-}$ mice which were then treated with tamoxifen for

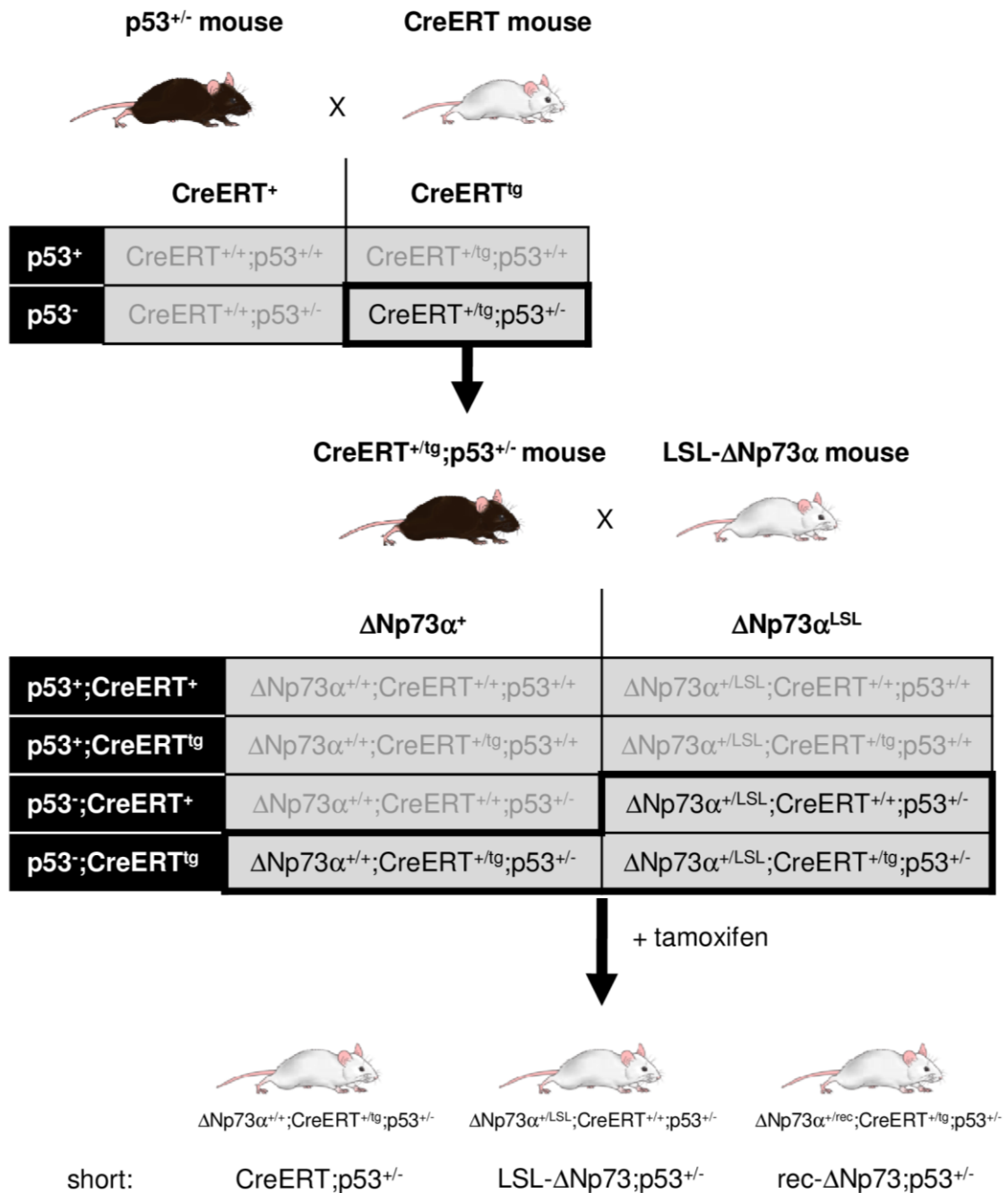


Figure 37: Breeding scheme for p53^{+/-} mice overexpressing ΔNp73

Heterozygous p53 knockout mice (p53^{+/-}) were mated with heterozygous CreERT mice (CreERT^{+/tg}, += wildtype allele, tg= transgenic allele) to obtain CreERT-expressing mice with a heterozygous p53 knockout (CreERT^{+/tg};p53^{+/-}); crossbreeding of CreERT^{+/tg};p53^{+/-} mice with heterozygous LSL-ΔNp73α mice was performed to obtain p53^{+/-} mice additionally carrying the CreERT or the LSL-ΔNp73α transgene alone (ΔNp73α^{+/+};CreERT^{+/tg};p53^{+/-} and (ΔNp73α^{+/LSL};CreERT^{+/+};p53^{+/-}) or both transgenes (ΔNp73α^{+/LSL};CreERT^{+/tg};p53^{+/-}); tamoxifen treatment of these mice led to recombination of the LSL-ΔNp73α allele (→rec-ΔNp73α) and thus induced the overexpression of the transgene.

recombination of the LSL cassette (short: rec-ΔNp73;p53^{+/-}). LSL-ΔNp73;p53^{+/-} and CreERT;p53^{+/-} siblings from these matings were treated likewise and

served as control groups. Like in 3.2.4, the health status of mice was monitored regularly and mice were sacrificed reaching endpoint criteria.

In the context of a heterozygous knockout of p53, Δ Np73-overexpressing mice exhibited a significantly reduced OS and TFS compared to control groups (Figure 38). Furthermore, autopsy and pathological examination showed that Δ Np73 increased the tumor burden and shifted the tumor spectrum towards lymphoma and lung tumors at the expense of soft tissue tumors (Figure 39). Histopathology identified the lung tumors as adenoma, low and high grade adenocarcinoma as well as papillary adenocarcinoma which is an unusual phenotype for p53 knockout mice (Figure 40a).

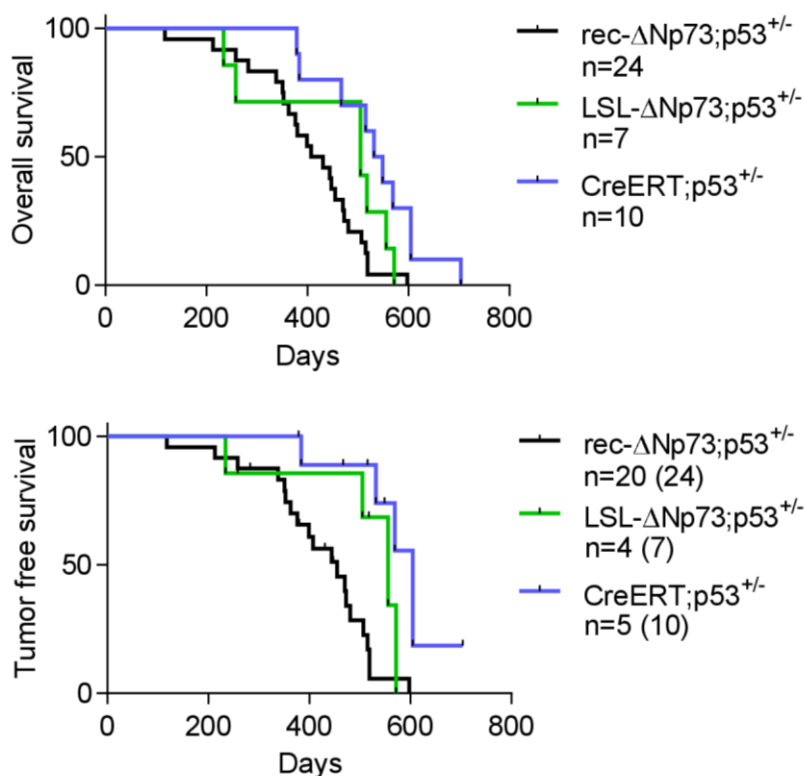


Figure 38: Overexpression of Δ Np73 reduces survival of p53^{+/-} mice

Kaplan-Meier Plot for overall survival (OS, left) and tumor-free survival (TFS, right) of rec- Δ Np73;p53^{+/-}, LSL- Δ Np73;p53^{+/-} and CreERT;p53^{+/-} mice; all mice received tamoxifen for 5 consecutive days at the age of 4-5 weeks; tumor-free animals were censored for TFS; the size of all cohorts included in the analysis are given in the legend, numbers in brackets show number of mice before censoring; Log-rank test detected a significant difference in OS ($p < 0.005$) as well as in TFS ($p < 0.0005$).

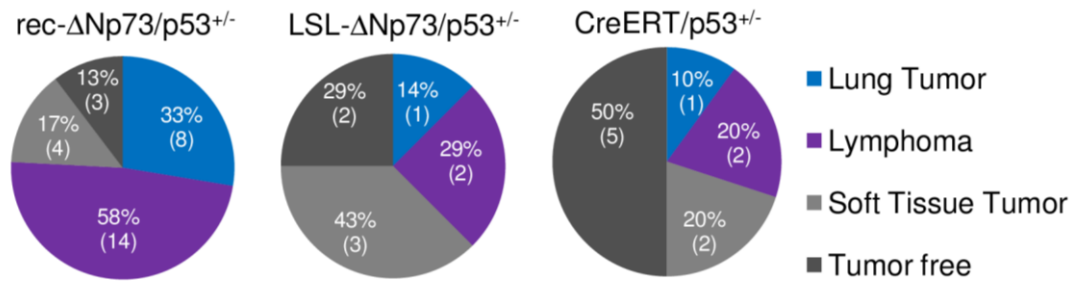


Figure 39: ΔNp73 alters the tumor spectrum of p53^{+/-} mice

Pie charts reflecting the tumor incidence and type of rec-ΔNp73;p53^{+/-}, LSL-ΔNp73/p53^{+/-} and CreERT/p53^{+/-} mice; values in brackets depict number of affected mice.

The mice in this experiment harbor a heterozygous knockout for p53. With progressing disease, tumor cells often lose the second allele leading to a survival advantage of the knockout cells. As ΔNp73 has been shown to inhibit p53 it was predicted that rec-ΔNp73 mice do not show loss of heterozygosity (LOH) and retain the p53 wildtype allele (Stiewe, Zimmermann, et al. 2002; Stiewe, Carmen C. Theseling, et al. 2002; Kartasheva et al. 2002; Zaika et al. 2002). To test whether LOH occurred within the lung tumors which arose from rec-ΔNp73/p53^{+/-} mice, genomic DNA was isolated from tumor samples and genotyped for p53 (Figure 40b). Most tumors showed prominent signals for the p53 knockout allele but only weak signals for the wildtype allele. Weak signals for the wildtype allele are most likely the result of stromal contamination rather than p53-maintenance in tumor cells arguing for an unexpectedly frequent loss of heterozygosity also in the presence of rec-ΔNp73.

Taken together, the ΔNp73 mouse model by itself lacks a tumor-promoting phenotype which might be based on low expression of the transgene in most organs. Yet, the crossbreeding of ΔNp73 mice with the p53^{+/-} strain demonstrated that the supportive deregulation of further tumor-relevant factors endorses ΔNp73 to carry out its oncogenic potential.

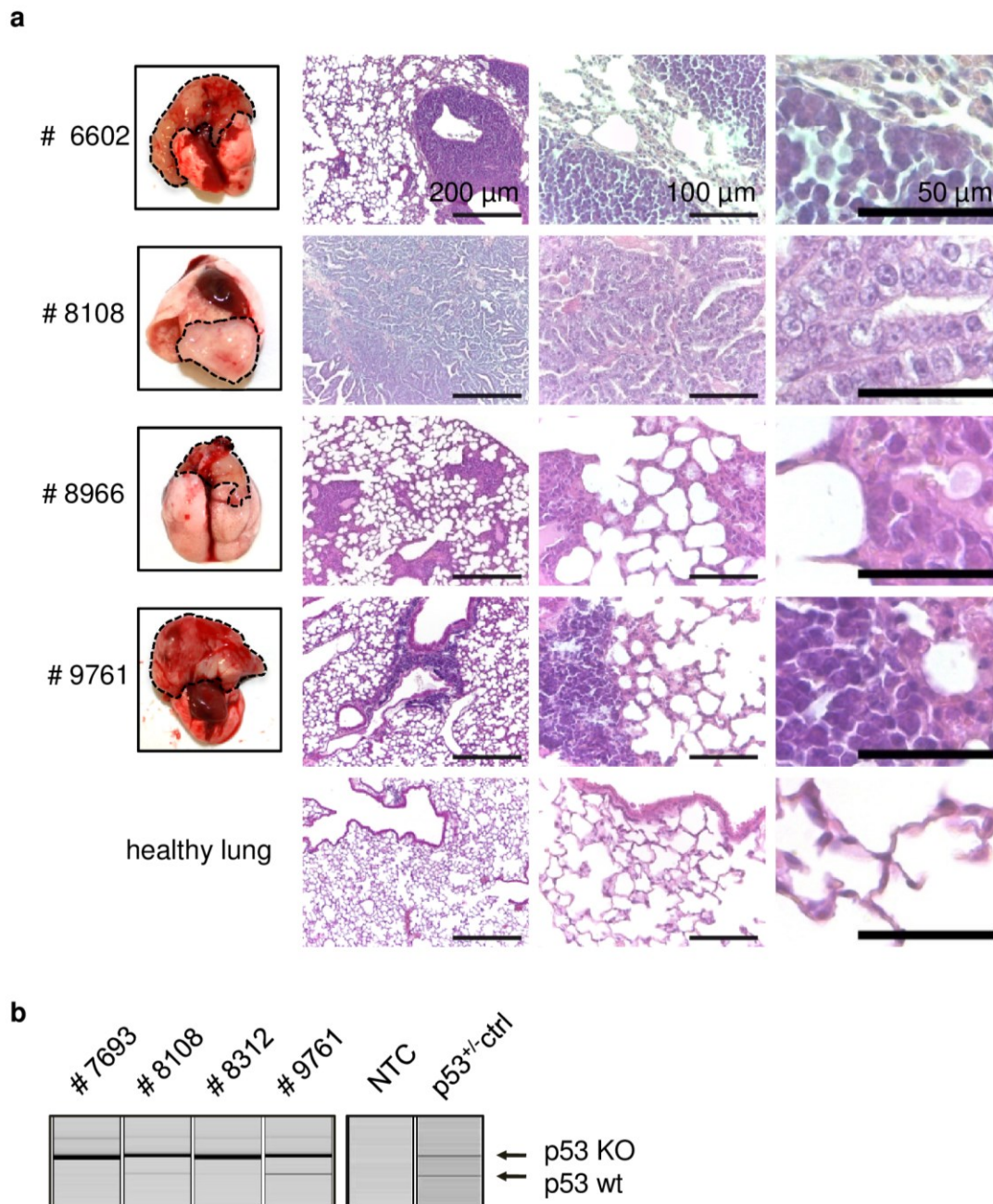


Figure 40: Analysis of lung tumors from $rec-\Delta Np73/p53^{+/-}$ mice

a) Left panel: exemplary photographs of tumor-bearing lungs from $rec-\Delta Np73;p53^{+/-}$ mice (eartag #6602 high grade carcinoma, #8108 papillary adenocarcinoma, #8966 high grade carcinoma, #9761 carcinoma); dashed lines encircle tumor tissue; right panels: corresponding hematoxylin & eosin (H&E) stainings of lung tumors from the left panel in different magnifications; bars depict size; H&E's at the bottom represent healthy lung tissue.

b) Loss of heterozygosity (LOH) analysis for p53 status by genotyping PCR of a panel of lung tumors from $rec-\Delta Np73;p53^{+/-}$ mice; NTC (non-template control), $p53^{+/-}$ ctrl (tail biopsy from a genotyped healthy $p53^{+/-}$ mouse, positive control); upper band reflects the knockout allele, lower band the wildtype allele.



4 Discussion

4.1 A dual luciferase assay to monitor tumor heterogeneity in solid tumors in vivo

It is crucial to understand the processes regulating tumor heterogeneity as the abundance of tumor cells with differing mutational status cause tumor progression, promote metastasis and, worst of all, therapy resistance. In patients, tumor development and composition, e.g. during cancer treatment or relapse, can be investigated by sequencing of circulating tumor DNA or cells. However, this method is not applicable for research in mouse models for human cancer as the required blood volumes exceed murine blood volume. Here, we developed a system which allows the monitoring of two different tumor cell populations of solid tumors in vivo using secreted luciferases (Charles et al. 2014). Additionally, this system allows targeted genetic manipulation of the tumor cells by application of shRNAs helping to identify and validate the oncogenic or tumor suppressive potential of individual genes. Previous methods use fluorescent markers to monitor growth dynamics by flow cytometry either in cell culture or in blood samples of mouse xenografts (Zuber et al. 2011). Nevertheless, in vivo applications remained restricted to hematological malignancies, as tumor cell composition of solid tumors in mice cannot be assessed by blood samples.

4.1.1 Limitations of imaging techniques for solid tumors in small experimental animals

Various imaging techniques like MRT (magnetic resonance tomography), CT (computed tomography) and PET (positron emission tomography) have been proven very useful in the clinics to discover, locate and monitor cancerous masses in patients (www.cancer.gov, www.cancer.org). Further refined in their spatial resolution, these techniques became also applicable tools to monitor solid tumor growth in mouse models of human cancer (Balaban & Hampshire 2001; Puaux et al. 2011). Both, MRT and CT display high resolution (Table 3) and deliver 3-dimensional information about tumor location and volume with a detection limit of ~1mm in tumor size. MRT uses a strong magnetic field in order to excite the tissue to emit radio waves and is very accurate in distinguishing soft tissues. In contrast, CT measures tissue-absorption of X-Rays and the poor

Method	MRT	PET-CT/ PET-MRT	CT	BLI	FLI
Spatial resolution	100µm	1-2mm	150µm	1-10mm depending on tissue depth and luciferase expression	1-10mm depending on tissue depth and fluorescent marker expression
Reporter gene	-	-	-	Luciferase	Fluorescent marker
Detection limits (diameter)	1mm	<1mm	<1mm	<1mm	2mm
Analysis time	3hrs/mouse	3hrs/mouse	30min/mouse	30-60min/mouse depending on luciferase kinetics	30min/mouse
Equipment costs	1-2 million US \$	0.4-1.2 million US \$	Not specified	<0.5 million US \$	<0.5 million US \$
Main advantages	High resolution, anatomy, tumor size and morphology	Detection of non-palpable tumors, measures tumor cell metabolism, tumor localization	High resolution, anatomy, tumor size and morphology	Detection of nonpalpable tumors, relative measure of tumor size, up to 5 mice can be measured simultaneously	Up to 5 mice can be measured simultaneously
Main disadvantages	Low throughput, respiratory motion makes imaging challenging	High background in some regions (brain, bladder)	Poor contrast of soft tissue, Radiation damage	Light emission dependent on tissue depth and substrate availability	Light emission dependent on tissue depth, autofluorescence of tissue

Table 3: Main characteristics of imaging techniques used in experimental animals (adapted from (Piaux et al. 2011; Wessels et al. 2007)

contrast in soft tissues often needs to be enhanced by application of contrast agents. Moreover, the combination of MRT or CT with PET can give additional information on the metabolic activity, proliferation and angiogenesis within a

tumor (Yao et al. 2012). This is achieved by administration of radioactively labelled sugars, fluorothymidines or antibodies against VEGF (vascular endothelial growth factor) which accumulate in metabolically highly active, fast proliferating and highly vascularized tumors. Finally, monoclonal antibodies targeting tumor-specific markers are also used in PET to locate cancerous tissue.

A different approach to monitor tumor growth in small experimental animals is optical imaging by detection of bioluminescent (BLI) or fluorescent (FLI) signals (Puaux et al. 2011). In contrast to the aforementioned methods, this technique requires constitutive expression of luciferases or fluorescent markers to label the cells of interest. Hence, the sensitivity of this assay strongly depends on enzymatic activity (BLI), expression and stability of the applied reporters. Moreover, the detection limit depends on tissue depth and emitted wavelengths as emitted light is attenuated by the surrounding tissue. Additionally, tissue autofluorescence and absorption of exciting light signals render sensitivity of FLI more susceptible to tissue depth than sensitivity of BLI (Puaux et al. 2011). In fact, BLI and PET jointly inherit the highest sensitivity for solid tumor detection in small experimental animals as both of them are capable to detect microscopic tumors, whereas MRI and FLI require larger tumor volumes (Puaux et al. 2011). Notably, the luciferases GLuc and CLuc used in this work display up to a 1000-fold higher sensitivity compared to other commonly used luciferases like Firefly or Renilla luciferase (Tannous et al. 2005; Tanahashi et al. 2001). Therefore, these luciferases are remarkably useful to detect small tumor volumes.

Still, the means of BLI using these two highly sensitive luciferases remains limited: The emitted light from the enzymatic reaction of both luciferases with their respective substrate emits light in the blue spectrum. Depending on the depth of the tumor within the body, the blue light becomes absorbed by the surrounding tissue it has to pass through on its way to the CCD camera sensor which makes BLI in vivo less suitable for quantification of tumor volumes. To circumvent this problem, the used GLuc and CLuc could be substituted by luciferases emitting red light (e.g. red-shifted Firefly luciferase), thus preventing absorption of bioluminescent signals by the tissues. Yet another critical disadvantage for BLI is the high secretion rate and stability of Cypridina

luciferase. Even a small tumor mass of CLuc-labelled cells secretes such a high rate of CLuc that the signal from the tumor is drowned out by circulating luciferases in the blood stream. There are several reasons which might account for this problem. On the one hand, CLuc is secreted at a much higher rate than GLuc, on the other hand, CLuc has a prolonged half-life in vivo. Both characteristics can lead to the accumulation of CLuc in the blood stream and thus perturb the signal-to-noise ratio. In addition, absorption of bioluminescent signals from blood vessels close to the body surface is much lower than from the inner body mass, which further elevates the background signal. Nevertheless, BLI of GLuc is a versatile tool to locate GLuc-labelled metastases *ex vivo* which can be detected in isolated organs at the end of an experiment. However, plasma samples remain the first choice to monitor tumor growth in experimental animals over time by luciferase activities.

4.1.2 Combined applications of GLuc and CLuc to monitor tumor composition

Both luciferases, GLuc and CLuc, are commonly used markers in a large set of applications in biological and biomedical research, e.g. as markers for transcriptional activity, for protein-protein interactions or simply for labelling tumor cells to assess cell growth (Wu et al. 2007; Remy & Michnick 2006; Tannous 2009). Previous work demonstrated that both luciferases can be used in combination with each other to study promoter activities in cell culture assays over time (Wu et al. 2007). Yet, this study did not investigate the applicability for comparative tumor cell quantification *in vivo*. Such an approach has been performed using only GLuc, providing multiplexing by tagging GLuc with different epitopes (van Rijn et al. 2013). Strikingly, this epitope-tagging allows reliable detection of up to 6 different transplanted cell populations by blood sampling. As the quantification for each cell population relies on GLuc activity, the signals have to be separated by ELISA (Enzyme-linked immunosorbent assay): 96-well plates are coated with antibodies directed against the respective tags which specifically bind their particular epitope-tagged GLuc. Although this approach offers the opportunity to monitor more than 2 different cell populations *in vivo*, it is not possible to perform BLI -as all cells are labelled with the same

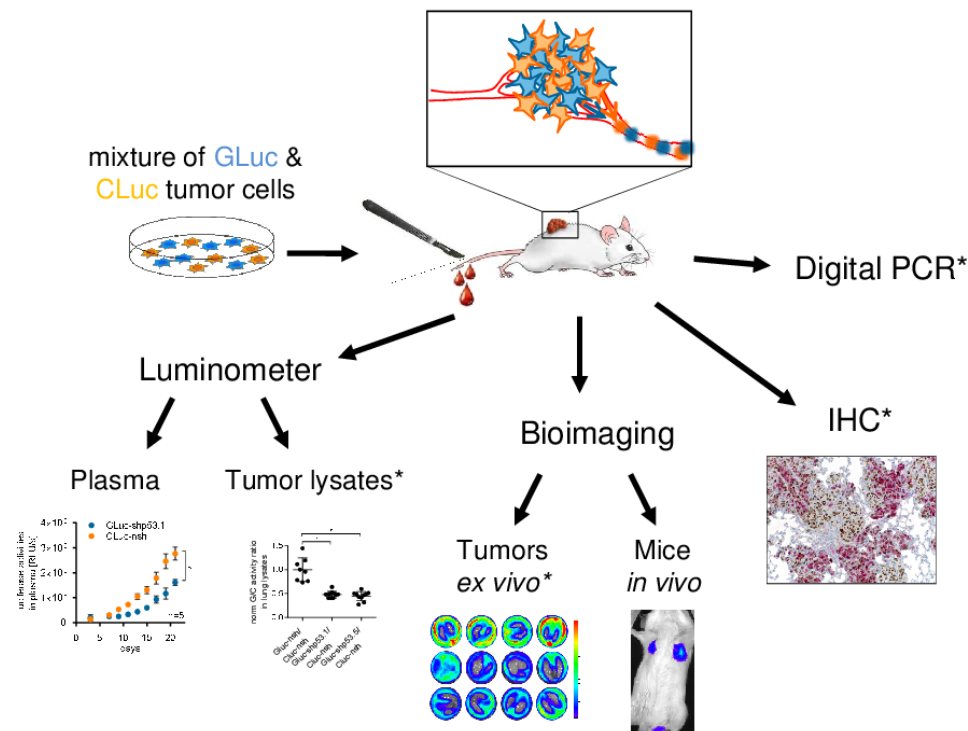


Figure 41: Experimental read-outs for in vivo applications of GLuc and CLuc

Tumor compositions are assessed in the luminometer, the bioluminescent imager, by IHC or digital PCR. The luminometer and bioluminescent imager measure luciferase activities. IHC detects presence/absence of luciferases on protein level, digital PCR quantifies copy numbers of luciferases in genomic DNA. *applications for endpoint analyses.

luciferase- and, even more important, the ELISA-based differentiation is very costly and labour-intensive.

A recent publication demonstrated that the combination of the two luciferases GLuc and CLuc is an excellent tool to monitor different cell populations simultaneously in the blood stream of transplanted mice (Bovenberg et al. 2013), very similar to the results achieved in the scope of this work (Charles et al. 2014). Beyond, they used SEAP (secreted embryonic alkaline phosphatase) as an additional bioluminescent blood reporter for a third tumor cell population. Blood sampling of mice inoculated with differentially labelled therapy-responsive and -resistant glioma cells prove the applicability of this multiplexed reporter assay. Consistent with our findings, the markers reveal high sensitivity, substrate specificity, short half-life and absence of mutual inhibition or activation, thus facilitating reliable tumor cell quantification and monitoring of dynamic processes in vivo in a minimally invasive manner. Standing out from Bovenberg's approach, we endowed our lentiviral constructs for tumor cell

labelling additionally with shRNAs to permit targeted constitutive or inducible genetic manipulation.

4.1.3 Endpoint analyses confirm results from luciferase activities in plasma samples

In order to confirm results obtained from plasma samples from long-term experiments, additional read-outs were established for endpoint analyses of isolated tumors (Figure 41). As mentioned above, BLI is very applicable for evaluation for tumor tissue ex vivo. The calculated GLuc:CLuc activity ratios of RLU's detected by the CCD sensor are comparable to luciferase activities in final plasma samples. Moreover, these values are consistent with GLuc:CLuc activity ratios from homogenized tumors measured in the luminometer. Thus, the quantification of bioluminescent signals from plasma samples as well as tumor tissue delivers very precise and reliable results to evaluate tumor burden. Beyond these read-outs, further methods were established in order to evaluate results independently from luciferase activities. Immunohistochemistry reveals information about tumor composition by presence or absence of GLuc-labelled cells. Moreover, double-staining can give additional information about GLuc-positive and -negative cell populations within a tumor. Immunodetection of p53, for example, confirmed knockdown-efficiencies of shRNAs directed against p53 whereas p53 was readily detectable in control cells. Thus, tumor cell populations can also be investigated for potential deregulation of downstream effectors of genetically manipulated targets like p53 to get deeper insight into their mode of action during tumor progression, resistance mechanisms and metastasis. Another measure for tumor composition independent from luciferase activity is conducted by digital PCR. This method quantifies the copy numbers of both luciferases in the gDNA from tumor lysates. The calculation of GLuc:CLuc abundance is consistent with measures relying on luciferase activities.

4.1.4 Application of GLuc and CLuc provide refinement and reduction of animal experiments

The high sensitivity of luciferases massively contributes to the refinement of animal experiments as demanded by Russell and Burch (The principles of humane experimental technique). As the collection of data points begins only a

few days after transplantation and blood samples can confidently be collected three times per week, experiments can be terminated to an earlier time point without losing reliability of results. Admittedly, the duration of the experiment depends on the strength of the investigated effect. Here, another exceptional advantage of the invented method becomes clear: the application of two luciferases allows simultaneous monitoring of two different cell populations, the exploratory cell line and a control cell line (e.g. nsh-transduced or therapy-sensitive cell line). This allows normalization to control cells by calculation of the ratios of both cell populations. Compared to ordinary xenograft experiments in which tumor size of one cell population is assessed by caliper measurements, such a normalization reduces the variance of data points to a minimum.

Additionally to the advantage of refinement, this feature also strongly reduces the number of test animals in two different ways, again supporting the 3R's from Russell and Burch. On the one hand, cohorts of animals transplanted with control cells are to be discontinued, thereby reducing the amount of test animals to 50 % as the control cells are transplanted together with the exploratory cells. On the other hand, the low variance of values (σ^2) alleviates the capability to detect statistically significant differences on the significance level α , thus allowing a reduction of group sizes (n) without losing statistical power:

$$n = \frac{z^2 \times \sigma^2}{ME^2}$$

(n=group size, z=standard score for which cumulative probability is $1 - \alpha$ (or $1 - \frac{\alpha}{2}$), σ^2 =variance, ME=margin of error).

4.1.5 Evaluation of essential genes by tet-inducible genetic manipulation

The lentiviral constructs to label tumor cells with luciferases were designed to facilitate targeted genetic manipulation by shRNAs. While this is an excellent tool to study enhanced tumor progression upon knockdown of a tumor suppressor like p53, the knockdown of oncogenic factors is likely to cause problems in experimental setups as cells forfeit their growth or survival advantage. Here, the invention of a tetracycline-inducible system facilitated

timed knockdown of essential genes which allows propagation of stably transduced cells to obtain sufficient cell numbers for experiments.

4.1.6 Identification of p73 as an essential factor for cell growth in Hs 766T cells

High p73 expression in various cancer types clearly implicates p73 in tumorigenesis and raises the question whether p73 is an essential factor whose abundance is indispensable for survival and tumorigenicity of cancer cells. In fact, application of the dual luciferase assay with the inducible system identified p73 as an essential factor in Hs 766T pancreatic adenocarcinoma cells. The knockdown of total p73 lead to a severely impaired cell growth compared to control cells both in cell culture and in vivo.

4.1.6.1 An unlikely couple: growth-inhibitory TAp73 versus growth-promoting Δ Np73

Early studies of p73 levels in patient-derived tumors did not discriminate between N-terminally truncated and full-length isoforms (Tokuchi et al. 1999; Yokomizo et al. 1999; Zaika et al. 1999). More recent studies, however, reveal an upregulation of both isoforms whereby Δ Np73 levels frequently exceed TAp73 levels (Zaika et al. 2002; Tomasini et al. 2008). This finding is reasonable with respect to the opposing functions of both isoforms as Δ Np73's oncogenic features are able to outweigh TAp73's tumor suppressive functions. The reintroduction of full length and N-terminally truncated p73 isoforms support the previous findings: TAp73 exerts an additional growth-inhibitory effect whereas Δ Np73 rescues cell growth to a normal level. Interestingly, the reintroduction of both isoforms was not able to re-establish cell growth. Here, a very precise fine tuning of both isoforms would be beneficial in order to investigate at which ratio of isoforms the tumor suppressive or tumor promoting function prevails. However, such a fine tuning is very complex. The reintroduction of TAp73, for example, triggers expression of endogenous Δ Np73 (Seelan et al. 2002). But as TAp73 protein levels still exceed Δ Np73 by far, the growth inhibitory effect of the full length isoform superimposes Δ Np73's tumor promoting function.

Similar experiments conducted in small cell lung cancer cells with high levels of p73 failed to prove a universal essential tumorigenic function for total p73. Here, the loss of p73 had only minor effects on cell growth (Grit Pattschull, data not shown). Thus, the function of p73 is considered to be cell context dependent.

4.1.7 Perspectives of the dual luciferase assay beyond transplantation experiments

The dual luciferase assay is a unique method which facilitates monitoring of two different cell populations in transplanted solid tumors in vivo. The highly sensitive system was proven to capture differences in cell growth in order to evaluate differences in (shRNA-induced) tumorigenesis, chemosensitivity and metastasis of different cell populations, but applications in remote disciplines like developmental biology or immunology are also conceivable. Raw data as well as normalization to control cells by calculation of GLuc:CLuc ratios deliver highly reliable results. Moreover, this cost-effective method is distinguished by very simple operating procedure and enables refinement of animal experiments as well as substantial reduction in test animal numbers.

Still, transplantation experiments of human cancer cell lines or patient-derived xenografts into immunocompromised mice are limited in their scientific validity (Kerbel n.d.). On the one hand, the immune system affects tumor growth in different ways and its absence might distort results (Richmond & Su 2008). On the other hand, application of cancer cells allows investigation of malignant cells of progressed state but early stages of cancer development are barely examinable. Thus, monitoring of endogenous tumor formation by secreted luciferases would be a highly convenient method to investigate the role of individual factors in tumor development. For example, luciferases could be applied in (genetically engineered) mouse models which use somatic gene delivery by viral infection or hydrodynamic injection of naked DNA for tumor induction (e.g. intratracheal infection for lung cancer models, intraductal infection of pancreas, prostate and mammary fat pad or hydrodynamic gene delivery for hepatocellular carcinoma) (Russell et al. 2003; Wang et al. 2006; Leow et al. 2005; José et al. 2013; Rodriguez et al. 2014). Viruses used for tumor induction have to be equipped with luciferase sequences to label the developing tumor cells, thus facilitating a simple but precise monitoring of tumor development or therapeutic responses by blood sampling.

4.1.8 Immune tolerance of GLuc and CLuc pave the way for monitoring of endogenous tumors

Self-evidently, a substantial prerequisite of such experimental setups is the immune tolerance towards the applied luciferases GLuc and CLuc. Syngenic transplantations of luciferase-labelled B16-F10 melanoma cells into immunocompetent mice illustrate immune tolerance for both luciferases. The composition of GLuc-, CLuc- or GFP-labelled B16-F10 cells was found to be similar among groups of transplanted immunocompromised, immunocompetent C57BL/6J and GLuc- or CLuc-vaccinated mice. Nevertheless, the applied viral constructs have to be considered carefully: Overall, tumors in immunocompetent mice developed worse than in immunodeficient mice. Such a general tumor cell rejection is unlikely to be caused by common tissue rejection as B16-F10 cells display comparable tumorigenicity in C57BL/6J mice and various immunocompromised strains (Seo et al. 2011; Ohira et al. 1994). In contrast, the lentiviral vector backbone or the viral integration itself might provoke an immune response against transduced cells leading to a reduced overall tumor burden (Brown et al., 2007; Sushrusha Nayak M S Roland W Herzog, 2011). This is also supported by the finding, that transplants expressing lentiviral-delivered GFP rather provoke an immune response than transplants from GFP-transgenic mice do (Yang et al. 2014). Thus, tissue rejection is rather caused by lentiviral constructs than by the fluorescent protein itself. Hence, the luciferases GLuc and CLuc are suitable markers for future experiments to monitor tumor development in immunocompetent mice but gene delivery has to be chosen carefully.

4.2 The Δ Np73 α -knockin model: developmental disorders, reproductive failure and tumor progression

p73 is clearly implicated in cancer, but the TP73 encodes for a whole range of N- and C-terminal isoforms which makes it difficult to fully understand the role of p73 in tumor development (Ueda et al. 1999; Yang & McKeon 2000). A coarse division of this protein family based on the presence or absence of the transactivation domain distinguishes tumor suppressive and oncogenic isoforms. Mouse models of isoform-specific Trp73 knockouts confirm tumor suppressive characteristics of TAp73 as these mice exhibit reduced survival due to enhanced spontaneous tumor formation (Tomasini et al. 2008). Consistent with Δ Np73's reputation as a tumor-promoting factor, the loss of Δ Np73 does not increase tumor formation (Wilhelm et al. 2010) whereas liver-specific overexpression of Δ Np73 leads to high penetrance of hepatocellular carcinoma (Tannapfel et al. 2008). However, the role of Δ Np73 in tumor formation in other tissues remains uncertain thus demanding for a mouse model with ubiquitous overexpression of Δ Np73.

4.2.1 Impaired transgene expression in organs of Δ Np73 α -knockin mice

Previous attempts to generate an ubiquitously Δ Np73-overexpressing mouse model have failed as transgenic embryos already died in utero, most likely due to embryonic lethal defects caused by Δ Np73 (Erster et al. 2006; Hüttinger-Kirchhof et al. 2006). To circumvent this problem, a Cre-inducible mouse model was established for investigation of spontaneous tumor formation caused by elevated levels of Δ Np73. Although tamoxifen treatment induced recombination very efficiently, protein was hardly abundant. Apart from the testis, Δ Np73 protein was barely detectable in any organ-neither with p73-specific antibodies nor with antibodies recognizing the HA- or Flag-tags (data not shown).

4.2.2 ... based on epigenetic silencing?

A reason for this observation might be epigenetic silencing of the transgene. Methylation of CpG islands within a promoter region causes a very compact chromatin structure which obstructs the access of transcription factors to this gene locus. Hence, the genes located in this region are transcriptionally repressed. Such epigenetic modifications are preserved during mitotic cell

divisions. Interestingly, these DNA methylations are largely removed during zygote formation and become re-established in blastocyst stage (Wu & Zhang 2012). In detail, male primordial germ cells erase their somatic methylation imprints for complete reorganization and paternal-specific imprinting during spermatogenesis (del Mazo et al. 1994; Rousseaux et al. 2005). During this process, hypomethylated and hyperacetylated histone modifications allow expression of genes which are usually silenced in the somatic cells of the organism. Thus, gene repression can be reversed during germ cell development which goes in line with the strong $\Delta Np73$ expression which was restricted to spermatogonia, spermatocytes and spermatids. In addition, spermatozoa, which are of advanced developmental stage, again failed to express $\Delta Np73$, further supporting the idea of epigenetic silencing as spermatozoa display a very condensed chromatin structure.

One explanation for epigenetic silencing of $\Delta Np73\alpha$ is the insertion site of the transgene within the murine genome. The location of the transgene in the here characterized mouse model is unknown. Thus, it is possible that the transgene has been inserted into a CpG-rich genomic region which causes hypermethylation of the EF1 α promoter and, as a consequence, repression of the $\Delta Np73\alpha$ transgene. The creation of a novel mouse strain by targeted insertion of the transgene into a genomic region which is not targeted by epigenetic modifications, e.g. the ROSA26 locus, could help to circumvent this problem in future studies.

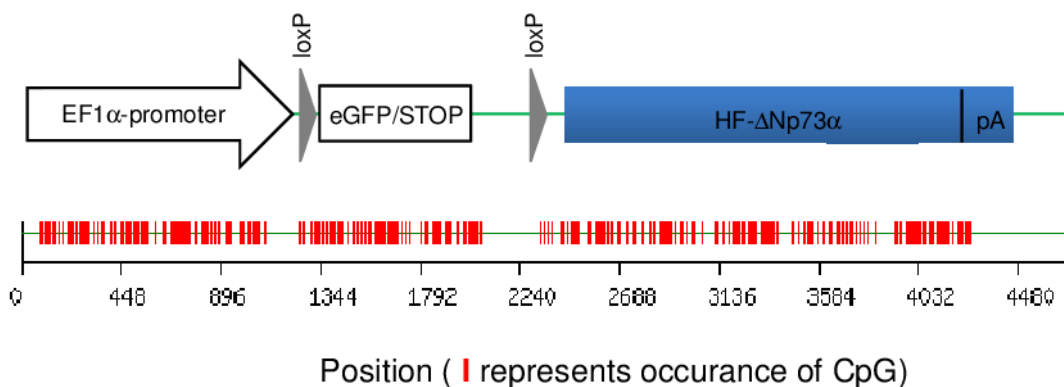


Figure 42: CpG-rich HA-Flag- $\Delta Np73\alpha$ transgene
 Localization of CpGs (lower graph, analyzed at <http://bitgene.com/gene-analysis>) in the HA-Flag-DNp73 transgenic construct (upper graph).

Independent from the location, the CpG content of a transgene itself is able to cause hypermethylation of CpG islands within the upstream promoter and, as a consequence, can lead to transcriptional silencing due a compact chromatin structure (Chevalier-Mariette et al. 2003). Although the here used EF1 α promoter is the promoter of a widely-expressed gene, it also contains a CpG island. Usually, this CpG island is protected from methylation, but hypermethylation of a downstream CpG-rich transgene is able to affect the methylation status of the promoter. Like naturally occurring CpG methylation, transgene repression is temporarily reversed during germ cell development. In fact, the Δ Np73 α transgene has been found to be a CpG-rich sequence which would explain the largely poor expression profile in this mouse model and, moreover, the strong protein abundance in germ cells (Figure 42).

4.2.3 Δ Np73 α aggravates tumorigenic phenotype of p53 \pm mice

Survival studies of the Δ Np73 α -strain failed to detect enhanced spontaneous tumor formation. Certainly, the low levels of Δ Np73 protein in most tissues might account for the lack of a phenotype to exert an oncogenic function as pan-inhibitor of the tumor suppressive p53 family members. Nevertheless, it is also conceivable that a single genetic insult given by Δ Np73 overexpression is insufficient to induce spontaneous tumor formation in the absence of other genetic alterations. Supporting this notion, overexpression of Δ Np73 α significantly reduces the life span of p53-haploinsufficient mice due to accelerated tumor formation. Moreover, Δ Np73 α alters the tumor spectrum observed in heterozygous p53 mice leading to increased lymphoma, lung adenoma and carcinoma occurrence.

Interestingly, TP73 has been found to be frequently silenced in samples from lymphoma patients (Corn et al. 1999; Kawano et al. 1999). Moreover, p73 loss in a myc-driven lymphoma mouse model revealed enhanced dissemination of malignant B-cells, although it had no influence on tumor onset (Nemajerova et al. 2010). Likewise, studies on irradiation-induced tumorigenesis of p53 \pm and p53 \pm /p73 \pm mice failed to detect accelerated lymphomagenesis upon p73 reduction (Perez-Losada et al. 2005). This suggests that TAp73's tumor suppressive function is probably less critical for lymphomagenesis but rather for impeding progression of the disease by nodular spread. In fact,

histopathological examination discovered disseminated lymphoma in 5 out of 16 lungs derived from $\text{rec}\Delta\text{Np73/p53}^{\pm}$ mice opposing 1 lymphoma in 7 investigated $\text{LSL-}\Delta\text{Np73/p53}^{\pm}$ lungs (data not shown). Finally, the metastatic signature of ΔNp73 -overexpressing MEFs identified by whole transcriptome analyses also support the idea of ΔNp73 being a driver for dissemination.

Apart from lymphoma, clinical data also provide evidence for p73 being involved in lung cancer. In NSCLC (non-small cell lung cancer) p73 haploinsufficiency correlates with p53 mutation (Nicholson et al. 2001). Moreover, expression analyses of patient-derived tumors on TAp73 and ΔNp73 confirmed an increased $\Delta\text{Np73:TAp73}$ ratio (Lo lacono et al. 2011). Accordingly, the TAp73^{-/-} mouse model demonstrated that loss of TAp73 in lung tissue coincides with genomic instability and a high incidence of lung adenocarcinoma (Tomasini et al. 2008). Therefore, it is likely that the neoplastic growth in lungs of $\Delta\text{Np73/p53}^{\pm}$ mice stems from the dominant negative function of $\Delta\text{Np73}\alpha$ over TAp73, which enforces genomic instability. In contrast, the inhibitory effect of ΔNp73 on p53 remains unclear as LOH studies revealed a loss of the remaining p53 allele in lung tumors. If ΔNp73 sufficiently inhibited p53, the loss of the second allele would not further promote tumor progression, like it has been observed in the mouse model with liver-specific ΔNp73 expression (Tannapfel et al. 2008). Here, hepatocellular carcinoma retained wildtype p53 being indicative for a dominant negative effect of ΔNp73 over p53. Yet, if ΔNp73 had no other function beyond p53-inhibition, this would not explain the accelerated tumor incidence in $\Delta\text{Np73}\alpha/\text{p53}^{\pm}$ mice compared to p53^{\pm} mice. Thus, the oncogenic function of ΔNp73 in lung tumor and lymphoma induction in this mouse model is rather attributed to the dominant negative effect over TAp73 than p53.

4.2.4 Dysregulation of p73 causes male infertility

The observed $\Delta\text{Np73}\alpha$ expression in the testes of transgenic mice raised the question, whether elevated levels of ΔNp73 affect the fertility in males. Indeed, mating experiments revealed a complete infertility in these mice. Interestingly, Trp73^{\pm} and TAp73^{-/-} males also fail to produce litter (A. Yang et al. 2000; Tomasini et al. 2008) whereas ΔNp73 is dispensable as ΔNp73^{\pm} mice exhibit only limited reproductive failure (Tissir et al. 2009; Wilhelm et al. 2010).

However, the common feature of reproductive failure in different mouse models of the p73 family is -at least partially, of different origin. Trp73^{-/-} males lose their sexual interest in mature females due to impaired pheromonal perception in the vomeronasal organ. In contrast, TAp73^{-/-} specific knockouts as well as Δ Np73-overexpressing males show completely normal mating behaviour which indicates that the reproductive failure is not solely attributable to the absence of TAp73 in the vomeronasal organ. Apart from disturbed mating behaviour, 6 weeks old Trp73^{-/-} and also TAp73^{-/-} males suffer on a complete loss of spermatids and spermatozoa in the seminiferous tubules (Inoue et al. 2014)(Holembowski, Kramer, Riedel, Sordella, Nemajerova, Dobbelstein & Ute M Moll 2014). In part, this phenotype is caused by structural abnormalities of Sertoli cells which disrupt the blood-testis-barrier and the attachment of developing germ cells in the nursing pockets. Moreover, in wildtype mice TAp73 is highly expressed in spermatogonia and spermatids where it strictly controls the expression of peptidases, protease inhibitors, receptors and integrins (Inoue et al. 2014; Holembowski, Kramer, Riedel, Sordella, Nemajerova, Dobbelstein & Ute M. Moll 2014). As a consequence of TAp73 loss, adhesion- and migration-related molecules are upregulated which subsequently leads to a premature detachment of germ cells from the germ epithelium and finally to apoptosis. A very similar expression profile was observed in Δ Np73 MEFs indicating that male infertility in Δ Np73 α -overexpressing males is based on the dominant negative effect of Δ Np73 over TAp73. Yet, in contrast to the loss of TAp73 or total p73, the overexpression of Δ Np73 α for up to three months did not induce any morphological changes in the testes. Thus, it needs further investigation to clarify which additional functions, beyond inhibition of TAp73, are carried out by Δ Np73 that shatter reproductive processes. Here, it should be considered that Δ Np73-overexpressing males are completely infertile - meaning that the dysfunction is not restricted to the haploid germ cells that carry the Δ Np73 allele, but also either affects the haploid germ cells which carry the wildtype allele or the germ cells before separation of the homologous chromosomes in meiosis. This suggests a hormonal deregulation affecting all germ cells going in line with the finding that TAp73^{-/-} males have decreased progesterone levels (Inoue et al. 2014).

4.2.5 p73 is essential for embryonic development

In contrast to the complete infertility of $\Delta Np73$ males, the fertility of $\Delta Np73\alpha$ -overexpressing females is only partially restricted as they deliver at a normal rate but with reduced litter size. Genotyping of pups revealed that embryos emerging from $\Delta Np73$ -transgenic oocytes die in utero, confirming previous data from approaches which failed to obtain transgenic mice constitutively overexpressing $\Delta Np73$ (Hüttinger-Kirchhof et al. 2006; Erster et al. 2006). Embryos developing from zygotes being microinjected with a $\Delta Np73$ construct failed to develop beyond gastrulation stage (Erster et al. 2006). In fact, if $\Delta Np73$ -induced embryonic lethality is mediated by inhibition of TAp73, the defect is likely to occur even at an earlier developmental stage: loss of TAp73 impairs ovulation and causes spindle abnormalities in in vitro fertilized oocytes which abrogates the embryonic preimplantation development (Tomasini et al. 2008). Thus, genomic integrity in oocytes might be undermined by $\Delta Np73$ by interference with TAp73. During these fertility studies, two females were born carrying a recombined $\Delta Np73\alpha$ allele. These animals delivered, like their mothers, at a normal rate albeit giving birth to pups also carrying the $\Delta Np73\alpha$ transgene at a completely normal mendelian ratio. Apparently $\Delta Np73$ -induced embryonic lethality was circumvented in these animals, probably by silencing of the transgene.

Considering the results from $Trp73^{-/-}$, $TAp73^{-/-}$, $\Delta Np73^{-/-}$ and $\Delta Np73\alpha$ overexpressing mouse models, TAp73 is absolutely essential for both, male fertility and embryonic development, whereas the loss of $\Delta Np73$ exhibits only minimally perturbed fertility. Conversely, high abundance of $\Delta Np73$ is considered to interfere with developmental programs orchestrated by TAp73 thus leading to similar reproductive defects as observed in $TAp73^{-/-}$ mice. As $p53^{-/-}$ mice show only minor defects in developmental programs, it is rather unlikely that $\Delta Np73$'s inhibitory function on p53 is involved in reproductive and developmental defects of $\Delta Np73\alpha$ mice.

4.2.6 $\Delta Np73\alpha$ -overexpressing MEFs exhibit a metastatic signature

Whole transcriptome analysis of $\Delta Np73\alpha$ -transgenic MEFs found many factors relevant for epithelial-to-mesenchymal-transition (EMT) to be upregulated. EMT is crucial for numerous developmental processes, yet is has also been

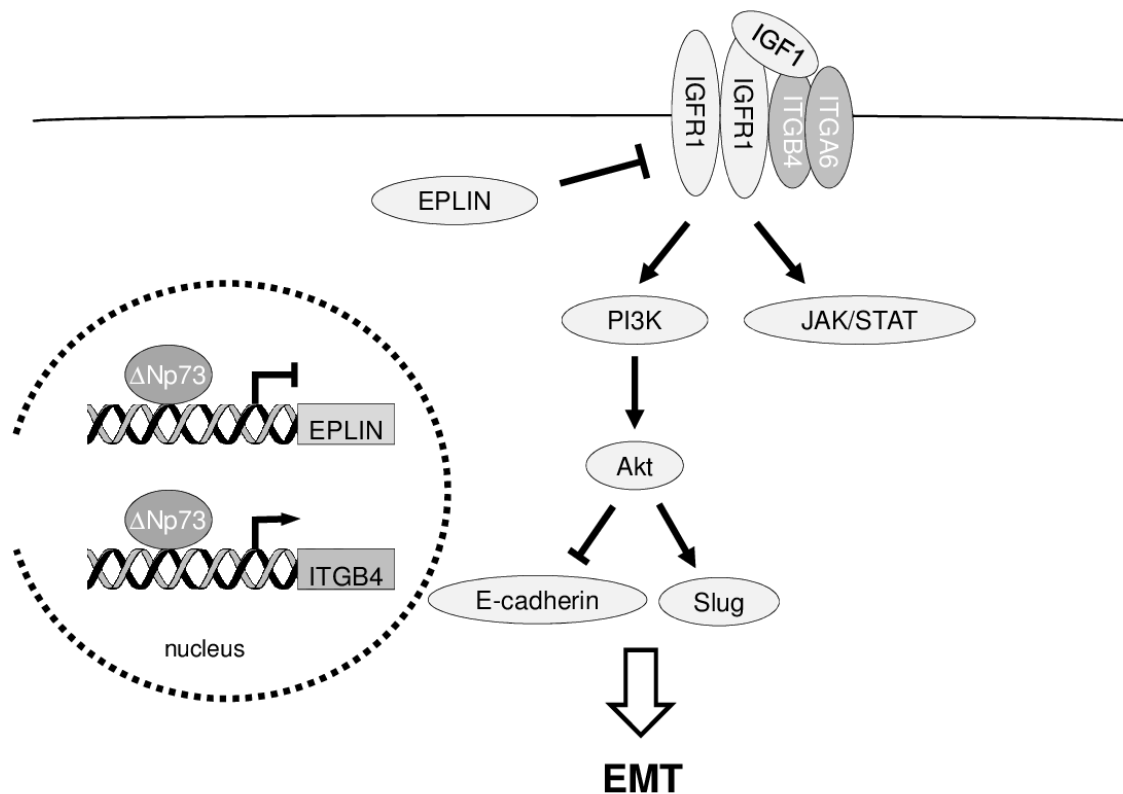
described as an essential part of metastasis (Thiery 2002). During EMT, epithelial cells undergo morphological changes leading to loss of cell polarity and cell-cell-adhesions. The dissociation from tissue represents the first step in metastasis. After detachment from the tumor, cells may enter the lymph or the blood stream which conveys them to the capillaries of more or less distant sites of the organism (Fidler 2003; Chambers et al. 2002). Depending on trafficking molecules, the metastatic cancer cells leave the blood stream or lymph and enter a new niche where they establish metastases.

4.2.7 Δ Np73 α induces factors involved in migration and EMT

Several factors involved in migration and metastasis were upregulated in Δ Np73 α MEFs. Among them, integrin β 4 (ITGB4) inherited the highest expression with a 12-fold induction compared to single transgenic control MEFs. The β 4 subunit of the integrin receptor forms heterodimers with α 6 subunits and adheres to laminins. The attachment of epithelial cells to the extracellular mass (ECM) can either be stable or transient. In the former case, α 6 β 4 integrins are localized in hemidesmosomes to anchor epithelial cells to the basement membrane, whereas in the latter case the integrins are concentrated in cell protrusions, thereby promoting migration (Rabinovitz et al. 1999). A recent publication showed that Δ Np73 fosters metastasis in melanoma cells by downregulation of EPLIN, a negative regulator of the IGFR1-Akt/STAT3 pathway (Steder et al. 2013). In the absence of EPLIN, IGFR1 becomes phosphorylated leading to activation of PI3K and JAK/STAT pathway. Particularly the phosphorylation of Akt entails changes of Slug and E-Cadherin levels eliciting an EMT-like phenotype (Grille et al. 2003; Fenouille et al. 2012). In addition, ITGB4 promotes anchorage-independent growth by association with IGFR1 and activation of the PI3K pathway (Fujita et al. 2012; Bon et al. 2006). These data suggest that Δ Np73 triggers IGFR1-mediated metastasis not only by downregulation of EPLIN but also by induction of ITGB4 (Figure 43).

Apart from ITGB4, Microarray data also revealed an upregulation of the plakin family members desmoplakin (Dsp) and plakophilin 1 (Pkp1). Plakins are cytoskeletal crosslinkers which connect cytoskeletal structures like actin-filaments to junctional complexes at the membrane (Belkin & Stepp 2000). These migration-related factors have been associated with invasive carcinoma

and poor prognosis in patients of various cancer types, e.g. osteosarcoma, basal like breast cancer, oral squamous cell carcinoma, pancreatic ductal carcinoma and lung cancer (Wan et al. 2010; Lu et al. 2008; Nagata et al. 2013; Damhofer et al. 2013; Zheng et al. 2013; Hsu et al. 2013).



adapted from
Steder et al., 2013
Fujita et al., 2012

Figure 43: Δ Np73 regulates PI3K pathway inducing EMT

Δ Np73 fosters metastasis by downregulation of EPLIN, a negative regulator of the IGFR1/Akt/STAT3 pathway (Steder et al. 2013). Under anchorage-independent conditions, Integrin α 6 β 4 associates with IGFR1 and IGF1 and promotes survival (Fujita et al. 2012). This signalling pathway might also be regulated by Δ Np73, as the Integrin α 6 β 4-subunit ITGB4 is induced by Δ Np73.

The Notch ligands JAG 1 and 2 were also upregulated by Δ Np73 α . This signalling cascade is involved in many developmental processes, especially neurogenesis (Mark 1995; de la Pompa et al. 1997). Like many factors regulating developmental programs, JAG1 and 2 are also involved in cancer progression. Both factors promote EMT as a driver for metastasis in breast (JAG1) and lung cancer (JAG2) (Sethi et al. 2011; Shao et al. 2015; Yang et al. 2011). Moreover, JAG1 expression has been correlated with poor survival in

breast cancer and head and neck cancer patients (Reedijk et al. 2005; Lin et al. 2010).

In addition, several Serine Protease Inhibitors (Serpins) were recently connected with brain metastasis in lung and breast cancer (Valiente et al. 2014).

Thus, many factors being upregulated in $\Delta\text{Np73}\alpha$ MEFs exhibit metastasis-promoting function. Although it has not been investigated whether ΔNp73 directly activates these genes, some of them have been found to be regulated by p53 family members. ITGB4, for example, is repressed by p53 and activated by TAp63 and TAp73 (Bon et al. 2009). Hence, the upregulation of ITGB4 might be a consequence of the dominant negative effect of ΔNp73 on p53. In contrast, JAG1 and 2 are known to be induced by all tumor suppressive p53 family members, predominantly by p63 and p73 (Sasaki et al. 2002). Thus, the upregulation of Notch-ligands by ΔNp73 seems to be inconsistent and requires further investigation.

The metastasis-promoting effect of $\Delta\text{Np73}\alpha$ on single gene level is further supported by GSEA analyses as 6 gene sets annotated with migration and metastasis were found to be upregulated. As an completely unexpected result, a great number of gene sets annotated with cell cycle progression were downregulated in samples with high ΔNp73 expression. As ΔNp73 exerts tumor-promoting functions, it was supposed to rather induce than to suppress cell division. However, this effect might be dependent on the cellular context. For these analyses, primary murine embryonic fibroblasts were used. In contrast to established cancer cell lines, these cells do not carry additional tumorigenic mutations which might support oncogenic ΔNp73 in enhanced proliferation. A single genetic alteration as the overexpression of $\Delta\text{Np73}\alpha$ is most likely not sufficient to overcome the safety mechanisms protecting the cells from aberrant growth. On the contrary, ΔNp73 might trigger oncogene-induced senescence in these cells, although β -Gal staining did not support this idea (data not shown). Finally, fibroblasts are of mesenchymal and not of epithelial origin and the impact of ΔNp73 might very well be cell context dependent. The upregulation of ΔNp73 in human cancers and its correlation with poor prognosis is prevalently based on carcinomas, a cancer type of epithelial origin.

Taken together, the microarray analyses of transgenic MEFs uncovered a metastatic signature induced by $\Delta Np73$ which is phenotypically supported by enhanced dissemination of lymphoma in $\Delta Np73;p53+/-$ mice. Migration and invasion assays of transgenic MEFs might validate these findings. Moreover, the role of validated targets like ITGB4, JAG1 and JAG2 in EMT and migration can also be investigated in such assays by targeted inhibition of these factors. Microarray analyses of the testis of TAp73 $^{-/-}$ mice revealed an expression profile of migratory genes which is quite similar to the profile obtained from $\Delta Np73\alpha$ MEFs (Holembowski, Kramer, Riedel, Sordella, Nemajerova, Dobbstein & Ute M. Moll 2014). Although the analyses were made in two completely different cell types, the strong conformity indicates that the dysregulated migratory signature in $\Delta Np73$ MEFs is mostly based on its dominant negative effect over TAp73. Even more, it can be assumed that it is exactly this signature that interferes with embryonic development and spermatogenesis but supports metastasis.

References

- Adorno, M. et al., 2009. A Mutant-p53/Smad complex opposes p63 to empower TGFbeta-induced metastasis. *Cell*, 137(1), pp.87–98. Available at: <http://www.ncbi.nlm.nih.gov/pubmed/19345189> [Accessed August 29, 2014].
- Agami, R. et al., 1999. Interaction of c-Abl and p73alpha and their collaboration to induce apoptosis. *Nature*, 399(6738), pp.809–813.
- Aoubala, M. et al., 2011. p53 directly transactivates $\Delta 133p53\alpha$, regulating cell fate outcome in response to DNA damage. *Cell death and differentiation*, 18(2), pp.248–58. Available at: <http://dx.doi.org/10.1038/cdd.2010.91> [Accessed February 25, 2016].
- Ayers, G.D. et al., 2010. Volume of preclinical xenograft tumors is more accurately assessed by ultrasound imaging than manual caliper measurements. *Journal of ultrasound in medicine : official journal of the American Institute of Ultrasound in Medicine*, 29(6), pp.891–901. Available at: <http://www.pubmedcentral.nih.gov/articlerender.fcgi?artid=2925269&tool=pmcentrez&rendertype=abstract> [Accessed January 25, 2016].
- Badea, T.C., Wang, Y. & Nathans, J., 2003. A noninvasive genetic/pharmacologic strategy for visualizing cell morphology and clonal relationships in the mouse. *The Journal of neuroscience : the official journal of the Society for Neuroscience*, 23(6), pp.2314–22. Available at: <http://www.ncbi.nlm.nih.gov/pubmed/12657690> [Accessed March 10, 2015].
- Baker, M., 2012. Digital PCR hits its stride. *Nature Methods*, 9(6), pp.541–544. Available at: <http://dx.doi.org/10.1038/nmeth.2027>.
- Balaban, R.S. & Hampshire, V.A., 2001. Challenges in Small Animal Noninvasive Imaging. *ILAR Journal*, 42(3), pp.248–262. Available at: <http://ilarjournal.oxfordjournals.org/content/42/3/248.abstract> [Accessed June 1, 2016].
- Bálint, E., Bates, S. & Vousden, K.H., 1999. Mdm2 binds p73 alpha without targeting degradation. *Oncogene*, 18(27), pp.3923–3929.
- Belkin, A.M. & Stepp, M.A., 2000. Integrins as receptors for laminins. *Microscopy Research and Technique*, 51(3), pp.280–301.
- Belloni, L. et al., 2006. DNp73alpha protects myogenic cells from apoptosis. *Oncogene*, 25(25), pp.3606–3612.
- Bettegowda, C. et al., 2014. Detection of circulating tumor DNA in early- and late-stage human malignancies. *Science translational medicine*, 6(224), p.224ra24. Available at: <http://stm.sciencemag.org/content/6/224/224ra24.long> [Accessed July 10, 2014].
- Bon, G. et al., 2006. Loss of $\alpha 4$ integrin subunit reduces the tumorigenicity of MCF7 mammary cells and causes apoptosis upon hormone deprivation. *Clinical Cancer Research*, 12(11 I), pp.3280–3287.
- Bon, G. et al., 2009. Negative regulation of $\alpha 4$ integrin transcription by homeodomain-interacting protein kinase 2 and p53 impairs tumor progression. *Cancer Research*, 69(14), pp.5978–5986.
- Bourdon, J.-C. et al., 2005. p53 isoforms can regulate p53 transcriptional

- activity. *Genes & development*, 19(18), pp.2122–37. Available at: <http://genesdev.cshlp.org/content/19/18/2122.long> [Accessed February 15, 2016].
- Bovenberg, M.S.S. et al., 2013. Multiplex blood reporters for simultaneous monitoring of cellular processes. *Analytical chemistry*, 85(21), pp.10205–10. Available at: <http://www.pubmedcentral.nih.gov/articlerender.fcgi?artid=3858835&tool=pmcentrez&rendertype=abstract>.
- Bringold, F. & Serrano, M., 2000. Tumor suppressors and oncogenes in cellular senescence☆. *Experimental Gerontology*, 35(3), pp.317–329. Available at: <http://www.sciencedirect.com/science/article/pii/S0531556500000838> [Accessed January 31, 2016].
- Brown, B.D. et al., 2007. In vivo administration of lentiviral vectors triggers a type I interferon response that restricts hepatocyte gene transfer and promotes vector clearance. *Blood*, 109(7), pp.2797–2805.
- Cam, H. et al., 2006. P53 Family Members in Myogenic Differentiation and Rhabdomyosarcoma Development. *Cancer Cell*, 10(4), pp.281–293.
- Canman, C.E., 1998. Activation of the ATM Kinase by Ionizing Radiation and Phosphorylation of p53. *Science*, 281(5383), pp.1677–1679. Available at: <http://www.sciencemag.org/cgi/doi/10.1126/science.281.5383.1677> [Accessed October 29, 2014].
- Casciano, I. et al., 2002. Expression of DNp73 is a molecular marker for adverse outcome in neuroblastoma patients. *Cell Death and Differentiation*, pp.246–251.
- Cavallaro, U. & Christofori, G., 2004. Cell adhesion and signalling by cadherins and Ig-CAMs in cancer. *Nature reviews. Cancer*, 4(2), pp.118–32. Available at: <http://dx.doi.org/10.1038/nrc1276> [Accessed December 6, 2015].
- Chambers, A.F., Groom, A.C. & MacDonald, I.C., 2002. Metastasis: Dissemination and growth of cancer cells in metastatic sites. *Nature Reviews Cancer*, 2(8), pp.563–572. Available at: <http://www.nature.com/doi/10.1038/nrc865> [Accessed June 12, 2016].
- Charles, J.P. et al., 2014. Monitoring the dynamics of clonal tumour evolution in vivo using secreted luciferases. *Nature communications*, 5, p.3981. Available at: <http://www.pubmedcentral.nih.gov/articlerender.fcgi?artid=4059931&tool=pmcentrez&rendertype=abstract>.
- Chevalier-Mariette, C. et al., 2003. CpG content affects gene silencing in mice: evidence from novel transgenes. *Genome biology*, 4(9), p.R53.
- Chung, E. et al., 2009. Secreted Gaussia luciferase as a biomarker for monitoring tumor progression and treatment response of systemic metastases. *PLoS one*, 4(12), p.e8316. Available at: <http://www.pubmedcentral.nih.gov/articlerender.fcgi?artid=2789383&tool=pmcentrez&rendertype=abstract> [Accessed October 31, 2014].
- Cline, M.S. et al., 2007. Integration of biological networks and gene expression data using Cytoscape. *Nature protocols*, 2, pp.2366–2382.
- Como, C.J. Di et al., 1999. p73 Function Is Inhibited by Tumor-Derived p53 Mutants in Mammalian Cells p73 Function Is Inhibited by Tumor-Derived p53 Mutants in Mammalian Cells. , 19(2).
- Concin, N. et al., 2005. Clinical relevance of dominant-negative p73 isoforms for responsiveness to chemotherapy and survival in ovarian cancer: Evidence for a crucial p53-p73 cross-talk in vivo. *Clinical Cancer Research*, 11(23),

- pp.8372–8383.
- Concin, N. et al., 2004. Transdominant Δ TAp73 Isoforms Are Frequently Up-regulated in Ovarian Cancer. Evidence for Their Role as Epigenetic p53 Inhibitors in Vivo. *Cancer Research*, 64(24), pp.2449–2460.
- Corn, P.G. et al., 1999. Transcriptional Silencing of the p73 Gene in Acute Lymphoblastic Leukemia and Burkitt ' s Lymphoma Is Associated with 5 ' CpG Island Methylation Advances in Brief Burkitt ' s Lymphoma Is Associated with 5 □ CpG Island Methylation 1. , (410), pp.3352–3356.
- Countries, I. of M. (US) C. on C.C. in L.M.-I., Sloan, F.A. & Gelband, H., 2007. Cancer Causes and Risk Factors and the Elements of Cancer Control. Available at: <http://www.ncbi.nlm.nih.gov/books/NBK54025/> [Accessed January 31, 2016].
- Damhofer, H. et al., 2013. Assessment of the stromal contribution to Sonic Hedgehog-dependent pancreatic adenocarcinoma. *Molecular oncology*, 7(6), pp.1031–42. Available at: <http://www.pubmedcentral.nih.gov/articlerender.fcgi?artid=3838447&tool=pmcentrez&rendertype=abstract> [Accessed June 17, 2015].
- Danko, I. et al., 1997. High expression of naked plasmid DNA in muscles of young rodents. *Human molecular genetics*, 6(9), pp.1435–43. Available at: <http://www.ncbi.nlm.nih.gov/pubmed/9285779>.
- Danovi, D. et al., 2004. Amplification of Mdmx (or Mdm4) directly contributes to tumor formation by inhibiting p53 tumor suppressor activity. *Molecular and cellular biology*, 24(13), pp.5835–43. Available at: <http://www.pubmedcentral.nih.gov/articlerender.fcgi?artid=480894&tool=pmcentrez&rendertype=abstract> [Accessed February 25, 2016].
- DeSantis, C.E. et al., Cancer treatment and survivorship statistics, 2014. *CA: a cancer journal for clinicians*, 64(4), pp.252–71. Available at: <http://www.ncbi.nlm.nih.gov/pubmed/24890451> [Accessed September 24, 2015].
- Dominguez, G. et al., 2006. Δ TAp73 upregulation correlates with poor prognosis in human tumors: Putative in vivo network involving p73 isoforms, p53, and E2F-1. *Journal of Clinical Oncology*, 24(5), pp.805–815.
- Donehower, L. a, 1996. The p53-deficient mouse: a model for basic and applied cancer studies. *Seminars in cancer biology*, 7(5), pp.269–78. Available at: <http://www.ncbi.nlm.nih.gov/pubmed/9110404>.
- Donehower, L., Harvey, M. & Slagle, B., 1992. Mice deficient for p53 are developmentally normal but susceptible to spontaneous tumours. *Nature*, 356. Available at: <http://www.nature.com/nature/journal/v356/n6366/abs/356215a0.html> [Accessed October 15, 2014].
- Dulloo, I. et al., 2015. Hypoxia-inducible TAp73 supports tumorigenesis by regulating the angiogenic transcriptome. *Nature cell biology*, 17(4), pp.511–23. Available at: <http://dx.doi.org/10.1038/ncb3130> [Accessed March 5, 2016].
- Dulloo, I. et al., 2010. The antiapoptotic DeltaNp73 is degraded in a c-Jun-dependent manner upon genotoxic stress through the antizyme-mediated pathway. *Proceedings of the National Academy of Sciences of the United States of America*, 107(11), pp.4902–4907.
- Eales, K.L., Hollinshead, K.E.R. & Tennant, D.A., 2016. Hypoxia and metabolic adaptation of cancer cells. *Oncogenesis*, 5, p.e190. Available at: <http://dx.doi.org/10.1038/oncsis.2015.50> [Accessed February 4, 2016].

- Erster, S. et al., 2006. Deregulated expression of DeltaNp73alpha causes early embryonic lethality. *Cell death and differentiation*, 13(1), pp.170–3. Available at: <http://www.ncbi.nlm.nih.gov/pubmed/16110322> [Accessed October 15, 2014].
- Fenouille, N. et al., 2012. The epithelial-mesenchymal transition (EMT) regulatory factor SLUG (SNAI2) is a downstream target of SPARC and AKT in promoting melanoma cell invasion. *PloS one*, 7(7), p.e40378. Available at: <http://www.ncbi.nlm.nih.gov/pubmed/22911700> [Accessed June 12, 2016].
- Fidler, I.J., 2003. Timeline: The pathogenesis of cancer metastasis: the “seed and soil” hypothesis revisited. *Nature Reviews Cancer*, 3(6), pp.453–458. Available at: <http://www.nature.com/doifinder/10.1038/nrc1098> [Accessed June 12, 2016].
- Fidler, I.J. & Nicolson, G.L., 1978. Tumor cell and host properties affecting the implantation and survival of blood-borne metastatic variants of B16 melanoma. *Israel journal of medical sciences*, 14(1), pp.38–50. Available at: <http://www.ncbi.nlm.nih.gov/pubmed/632082> [Accessed February 27, 2015].
- Flores, E.R. et al., 2002. p63 and p73 are required for p53-dependent apoptosis in response to DNA damage. *Nature*, 416(6880), pp.560–4. Available at: <http://dx.doi.org/10.1038/416560a> [Accessed February 21, 2016].
- Flores, E.R. et al., 2005. Tumor predisposition in mice mutant for p63 and p73: evidence for broader tumor suppressor functions for the p53 family. *Cancer cell*, 7(4), pp.363–73. Available at: <http://www.ncbi.nlm.nih.gov/pubmed/15837625> [Accessed October 15, 2014].
- Ford, J. & Hanawalt, P., 1997. Expression of wild-type p53 is required for efficient global genomic nucleotide excision repair in UV-irradiated human fibroblasts. - PubMed - NCBI. *The Journal of biological chemistry*, 272, pp.28073–80. Available at: <http://www.ncbi.nlm.nih.gov/pubmed/9346961> [Accessed February 25, 2016].
- Frese, K.K. & Tuveson, D.A., 2007. Maximizing mouse cancer models. *Nature reviews. Cancer*, 7(9), pp.645–58. Available at: <http://www.ncbi.nlm.nih.gov/pubmed/17687385> [Accessed November 16, 2015].
- Fujita, M. et al., 2012. Cross-talk between integrin $\alpha 6\beta 4$ and Insulin-like Growth Factor-1 Receptor (IGF1R) through direct $\alpha 6\beta 4$ binding to IGF1 and subsequent $\alpha 6\beta 4$ -IGF1-IGF1R ternary complex formation in anchorage-independent conditions. *Journal of Biological Chemistry*, 287(15), pp.12491–12500.
- Fulda, S., 2009. Tumor resistance to apoptosis. *International journal of cancer. Journal international du cancer*, 124(3), pp.511–5. Available at: <http://www.ncbi.nlm.nih.gov/pubmed/19003982> [Accessed February 22, 2016].
- Gaidon, C. et al., 2001. A subset of tumor-derived mutant forms of p53 down-regulate p63 and p73 through a direct interaction with the p53 core domain. *Molecular and cellular biology*, 21(5), pp.1874–87. Available at: http://www.pubmedcentral.nih.gov/articlerender.fcgi?artid=86759&tool=pmc_entrez&rendertype=abstract.
- Gerlinger, M. & Swanton, C., 2010. How Darwinian models inform therapeutic failure initiated by clonal heterogeneity in cancer medicine. *British journal of*

- cancer*, 103(8), pp.1139–43. Available at:
<http://dx.doi.org/10.1038/sj.bjc.6605912> [Accessed February 23, 2016].
- Gong, J.G. et al., 1999. The tyrosine kinase c-Abl regulates p73 in apoptotic response to cisplatin-induced DNA damage. *Nature*, 399(6738), pp.806–9. Available at: <http://www.ncbi.nlm.nih.gov/pubmed/10391249> [Accessed April 14, 2015].
- Graeber, T.G. et al., 1994. Hypoxia induces accumulation of p53 protein, but activation of a G1-phase checkpoint by low-oxygen conditions is independent of p53 status. *Molecular and Cellular Biology*, 14(9), pp.6264–6277. Available at:
http://mcb.asm.org/content/14/9/6264.abstract?ijkey=26dcc1e7aa12c5d96a2488417a8b95b5da198f1c&keytype2=tf_ipsecsha [Accessed January 13, 2016].
- Greaves, M. & Maley, C.C., 2012. Clonal evolution in cancer. *Nature*, 481(7381), pp.306–13. Available at:
<http://www.pubmedcentral.nih.gov/articlerender.fcgi?artid=3367003&tool=pmcentrez&rendertype=abstract> [Accessed July 9, 2014].
- Greenblatt, M.S. et al., 1994. Mutations in the p53 Tumor Suppressor Gene : Clues to Cancer Etiology and Molecular Pathogenesis Mutations in the p53 Tumor Suppressor Gene : Clues to Cancer Etiology and Molecular Pathogenesis. , pp.4855–4878.
- Greenman, C. et al., 2007. Patterns of somatic mutation in human cancer genomes. *Nature*, 446(7132), pp.153–8. Available at:
<http://dx.doi.org/10.1038/nature05610> [Accessed December 16, 2015].
- Grille, S.J. et al., 2003. The protein kinase Akt induces epithelial mesenchymal transition and promotes enhanced motility and invasiveness of squamous cell carcinoma lines. *Cancer research*, 63(9), pp.2172–8. Available at:
<http://www.ncbi.nlm.nih.gov/pubmed/12727836> [Accessed June 12, 2016].
- Grob, T.J. et al., 2001a. Human delta Np73 regulates a dominant negative feedback loop for TAp73 and p53. *Cell death and differentiation*, 8(12), pp.1213–23. Available at: <http://www.ncbi.nlm.nih.gov/pubmed/11753569> [Accessed March 12, 2015].
- Grob, T.J. et al., 2001b. Human delta Np73 regulates a dominant negative feedback loop for TAp73 and p53. *Cell death and differentiation*, 8(12), pp.1213–23. Available at:
<http://www.nature.com/cdd/journal/v8/n12/full/4400962a.html> [Accessed March 12, 2015].
- Hanahan, D. & Weinberg, R. a., 2011. Hallmarks of cancer: The next generation. *Cell*, 144(5), pp.646–674. Available at:
<http://dx.doi.org/10.1016/j.cell.2011.02.013>.
- Vander Heiden, M.G., Cantley, L.C. & Thompson, C.B., 2009. Understanding the Warburg effect: the metabolic requirements of cell proliferation. *Science (New York, N.Y.)*, 324(5930), pp.1029–33. Available at:
<http://science.sciencemag.org/content/324/5930/1029.abstract> [Accessed July 11, 2014].
- Hermeking, H. & Eick, D., 1994. Mediation of c-Myc-induced apoptosis by p53. *Science*, 265(5181), pp.2091–2093. Available at:
<http://science.sciencemag.org/content/265/5181/2091.abstract> [Accessed February 25, 2016].
- Holembowski, L., Kramer, D., Riedel, D., Sordella, R., Nemajerova, A., Dobbstein, M. & Moll, U.M., 2014. Tap73 is essential for germ cell

- adhesion and maturation in testis. *Journal of Cell Biology*, 204(7), pp.1173–1190.
- Holembowski, L., Kramer, D., Riedel, D., Sordella, R., Nemajerova, A., Dobbstein, M. & Moll, U.M., 2014. TAp73 is essential for germ cell adhesion and maturation in testis. *The Journal of cell biology*, 204(7), pp.1173–90. Available at: <http://www.pubmedcentral.nih.gov/articlerender.fcgi?artid=3971741&tool=pmcentrez&rendertype=abstract> [Accessed October 20, 2014].
- Hoppe-seyler, F. & Butz, K., 1993. function in HeLa cervical carcinoma cells by Repression of Endogenous p53 Transactivation Function in HeLa Cervical Carcinoma Cells by Human Papillomavirus Type 16 E6 , Human mdm-2 , and Mutant p53.
- Hsu, Y.L. et al., 2013. Galectin-1 promotes lung cancer tumor metastasis by potentiating integrin $\alpha 6 \beta 4$ and Notch1/Jagged2 signaling pathway. *Carcinogenesis*, 34(6), pp.1370–1381.
- Hu, W. et al., 2007. p53 regulates maternal reproduction through LIF. *Nature*, 450(7170), pp.721–724.
- Hüttinger-Kirchhof, N. et al., 2006. The p53 family inhibitor DeltaNp73 interferes with multiple developmental programs. *Cell death and differentiation*, 13(1), pp.174–7. Available at: <http://www.ncbi.nlm.nih.gov/pubmed/16341031> [Accessed September 1, 2014].
- Lo Iacono, M. et al., 2011. p63 and p73 Isoform Expression in Non-small Cell Lung Cancer and Corresponding Morphological Normal Lung Tissue. *Journal of Thoracic Oncology*, 6(3), pp.473–481. Available at: <http://linkinghub.elsevier.com/retrieve/pii/S1556086415322000> [Accessed June 10, 2016].
- Ichimiya, S. et al., 1999. P73 At Chromosome 1P36.3 Is Lost in Advanced Stage Neuroblastoma But Its Mutation Is Infrequent. *Oncogene*, 18(4), pp.1061–1066.
- Inoue, S. et al., 2014. TAp73 is required for spermatogenesis and the maintenance of male fertility. *Proceedings of the National Academy of Sciences of the United States of America*, 111(5), pp.1843–8. Available at: <http://www.pubmedcentral.nih.gov/articlerender.fcgi?artid=3918781&tool=pmcentrez&rendertype=abstract> [Accessed October 22, 2014].
- Irwin, M. et al., 2000. Role for the p53 homologue p73 in E2F-1-induced apoptosis. *Nature*, 407(6804), pp.645–8. Available at: <http://www.ncbi.nlm.nih.gov/pubmed/11034215> [Accessed February 25, 2016].
- Issaeva, N. et al., 2004. Small molecule RITA binds to p53, blocks p53-HDM-2 interaction and activates p53 function in tumors. *Nature medicine*, 10(12), pp.1321–8. Available at: <http://www.ncbi.nlm.nih.gov/pubmed/15558054> [Accessed February 23, 2016].
- Jacks, T. et al., 1994. Tumor spectrum analysis in p53-mutant mice. , 4(1), pp.1–7.
- Jenkins, D.E. et al., 2003. Bioluminescent imaging (BLI) to improve and refine traditional murine models of tumor growth and metastasis. *Clinical & experimental metastasis*, 20(8), pp.733–44. Available at: <http://www.ncbi.nlm.nih.gov/pubmed/14713107> [Accessed February 24, 2016].
- José, A. et al., 2013. Intraductal delivery of adenoviruses targets pancreatic tumors in transgenic Ela-myc mice and orthotopic xenografts. *Oncotarget*,

- 4(1), pp.94–105. Available at:
<http://www.pubmedcentral.nih.gov/articlerender.fcgi?artid=3702210&tool=pmcentrez&rendertype=abstract>
<http://www.ncbi.nlm.nih.gov/pubmed/23328228>.
- Jost, C.A., Marin, M.C. & Kaelin, W.G., 1997. p73 is a simian [correction of human] p53-related protein that can induce apoptosis. *Nature*, 389(6647), pp.191–4. Available at: <http://dx.doi.org/10.1038/38298> [Accessed February 25, 2016].
- Jost, C. a, Marin, M.C. & Kaelin, W.G., 1997. P73 Is a Simian [Correction of Human] P53-Related Protein That Can Induce Apoptosis. *Nature*, 389(6647), pp.191–194.
- Kaghad, M. et al., 1997. Monoallelically Expressed Gene Related to p53 at 1p36, a Region Frequently Deleted in Neuroblastoma and Other Human Cancers. *Cell*, 90(4), pp.809–819. Available at:
<http://www.cell.com/article/S0092867400805401/fulltext> [Accessed February 25, 2016].
- Kaghad, M. et al., 1997. Monoallelically expressed gene related to p53 at 1p36, a region frequently deleted in neuroblastoma and other human cancers. *Cell*, 90(4), pp.809–19. Available at:
<http://www.ncbi.nlm.nih.gov/pubmed/9288759> [Accessed March 19, 2015].
- Kang, Y. & Massagué, J., 2004. Epithelial-mesenchymal transitions: twist in development and metastasis. *Cell*, 118(3), pp.277–9. Available at:
<http://www.cell.com/article/S0092867404007020/fulltext> [Accessed January 8, 2016].
- Karin, M., 2006. Nuclear factor-kappaB in cancer development and progression. *Nature*, 441(7092), pp.431–6. Available at:
<http://dx.doi.org/10.1038/nature04870> [Accessed July 10, 2014].
- Kartasheva, N.N. et al., 2002. p53 induces the expression of its antagonist p73 Δ N, establishing an autoregulatory feedback loop. *Oncogene*, 21(31), pp.4715–4727. Available at:
<http://www.ncbi.nlm.nih.gov/pubmed/12101410> [Accessed March 12, 2015].
- Kastan, M. et al., 1991. Participation of p53 protein in the cellular response to DNA damage. - PubMed - NCBI. *Cancer research*, 51, pp.6304–6311. Available at: <http://www.ncbi.nlm.nih.gov/pubmed/1933891> [Accessed February 25, 2016].
- Kawano, S. et al., 1999. Loss of p73 gene expression in leukemias/lymphomas due to hypermethylation. *Blood*, 94(3), pp.1113–20. Available at:
<http://www.ncbi.nlm.nih.gov/pubmed/10419905> [Accessed June 10, 2016].
- Kay, B.K., Williamson, M.P. & Sudol, M., 2000. The importance of being proline: the interaction of proline-rich motifs in signaling proteins with their cognate domains. *FASEB journal : official publication of the Federation of American Societies for Experimental Biology*, 14(2), pp.231–41. Available at:
<http://www.ncbi.nlm.nih.gov/pubmed/10657980> [Accessed March 17, 2015].
- Kerbel, R.S., Human tumor xenografts as predictive preclinical models for anticancer drug activity in humans: better than commonly perceived-but they can be improved. *Cancer biology & therapy*, 2(4 Suppl 1), pp.S134-9. Available at: <http://www.ncbi.nlm.nih.gov/pubmed/14508091> [Accessed June 10, 2016].
- Kim, N.W. et al., 1994. Specific association of human telomerase activity with

- immortal cells and cancer. *Science (New York, N. Y.)*, 266(5193), pp.2011–5. Available at: <http://www.ncbi.nlm.nih.gov/pubmed/7605428> [Accessed December 11, 2015].
- Knudson, A.G., 1971. Mutation and cancer: statistical study of retinoblastoma. *Proceedings of the National Academy of Sciences of the United States of America*, 68(4), pp.820–3. Available at: <http://www.pubmedcentral.nih.gov/articlerender.fcgi?artid=389051&tool=pmcentrez&rendertype=abstract> [Accessed October 21, 2015].
- Koepfel, M. et al., 2011. Crosstalk between c-Jun and TAp73alpha/beta contributes to the apoptosis-survival balance. *Nucleic acids research*, 39(14), pp.6069–85. Available at: <http://www.pubmedcentral.nih.gov/articlerender.fcgi?artid=3152320&tool=pmcentrez&rendertype=abstract> [Accessed March 5, 2016].
- Kutner, R.H., Zhang, X.-Y. & Reiser, J., 2009. Production, concentration and titration of pseudotyped HIV-1-based lentiviral vectors. *Nature protocols*, 4(4), pp.495–505.
- de la Pompa, J.L. et al., 1997. Conservation of the Notch signalling pathway in mammalian neurogenesis. *Development (Cambridge, England)*, 124(6), pp.1139–1148.
- De Laurenzi, V. et al., 1998. Two new p73 splice variants, gamma and delta, with different transcriptional activity. *The Journal of experimental medicine*, 188(9), pp.1763–8. Available at: <http://www.pubmedcentral.nih.gov/articlerender.fcgi?artid=2212516&tool=pmcentrez&rendertype=abstract> [Accessed March 19, 2015].
- Leek, R.D. et al., 1999. Necrosis correlates with high vascular density and focal macrophage infiltration in invasive carcinoma of the breast. *British journal of cancer*, 79(5–6), pp.991–5. Available at: <http://www.pubmedcentral.nih.gov/articlerender.fcgi?artid=2362675&tool=pmcentrez&rendertype=abstract> [Accessed February 22, 2016].
- Lees-miller, S.P. et al., 1992. Human DNA-Activated Protein Kinase Phosphorylates Serines 15 and 37 in the Amino-Terminal Transactivation Domain of Human p53. , 12(11), pp.5041–5049.
- Leow, C.C., Wang, X. De & Gao, W.Q., 2005. Novel method of generating prostate-specific Cre-loxP gene switching via intraductal delivery of adenovirus. *Prostate*, 65(1), pp.1–9.
- Levrero, M. et al., 2000. The p53 / p63 / p73 family of transcription factors : overlapping and distinct functions. , 1670, pp.1661–1670.
- Li, F.P. & Fraumeni, J.F., 1969. Soft-tissue sarcomas, breast cancer, and other neoplasms. A familial syndrome? *Annals of internal medicine*, 71(4), pp.747–52. Available at: <http://www.ncbi.nlm.nih.gov/pubmed/5360287> [Accessed February 26, 2016].
- Lin, J.-T. et al., 2010. Association of high levels of Jagged-1 and Notch-1 expression with poor prognosis in head and neck cancer. *Annals of surgical oncology*, 17(11), pp.2976–2983.
- Lowe, S.W. & Ruley, H.E., 1993. Stabilization of the p53 tumor suppressor is induced by adenovirus 5 E1A and accompanies apoptosis. *Genes & Development*, 7(4), pp.535–545. Available at: http://genesdev.cshlp.org/content/7/4/535.abstract?ijkey=7a7a30568800149b8a0f0b68c9bb826ae3d329bc&keytype=tf_ipsecsha [Accessed February 25, 2016].
- Lu, S. et al., 2008. Analysis of integrin beta4 expression in human breast

- cancer: association with basal-like tumors and prognostic significance. *Clinical cancer research : an official journal of the American Association for Cancer Research*, 14(4), pp.1050–1058.
- Malkin, D. et al., 1990. Germ line p53 mutations in a familial syndrome of breast cancer, sarcomas, and other neoplasms. *Science*, 250(4985), pp.1233–1238. Available at: <http://science.sciencemag.org/content/250/4985/1233.abstract> [Accessed February 26, 2016].
- Maltzman, W. & Czyzyk, L., 1984. UV irradiation stimulates levels of p53 cellular tumor antigen in nontransformed mouse cells. *Molecular and Cellular Biology*, 4(9), pp.1689–1694. Available at: http://mcb.asm.org/content/4/9/1689.abstract?ijkey=f8cefe7c62bc1700a6da398524148457ac2a5071&keytype2=tf_ipsecsha [Accessed January 20, 2016].
- Mantovani, A. et al., 2008. Cancer-related inflammation. *Nature*, 454(7203), pp.436–44. Available at: <http://dx.doi.org/10.1038/nature07205> [Accessed July 10, 2014].
- Mark, E., 1995. Notch signaling. , 10193(1994).
- del Mazo, J. et al., 1994. DNA methylation changes during mouse spermatogenesis. *Chromosome research : an international journal on the molecular, supramolecular and evolutionary aspects of chromosome biology*, 2(2), pp.147–52. Available at: <http://www.ncbi.nlm.nih.gov/pubmed/8032673> [Accessed June 23, 2015].
- Merico, D. et al., 2010. Enrichment map: A network-based method for gene-set enrichment visualization and interpretation. *PLoS ONE*, 5(11).
- Milner, J. & Medcalf, E.A., 1991. Cotranslation of Activated Mutant ~ 53 with Wild Type Drives the Wild-Type p53 Protein into the Mutant Conformation. , 65, pp.765–774.
- Moll, U.T.E.M. et al., 1995. Wild-type p53 protein undergoes cytoplasmic sequestration in undifferentiated neuroblastomas but not in differentiated tumors. , 92(May), pp.4407–4411.
- Morelli, M.P. et al., 2015. Characterizing the patterns of clonal selection in circulating tumor DNA from patients with colorectal cancer refractory to anti-EGFR treatment. *Annals of oncology : official journal of the European Society for Medical Oncology / ESMO*, 26(4), pp.731–6. Available at: <http://www.ncbi.nlm.nih.gov/pubmed/25628445> [Accessed February 23, 2016].
- Müller, M. et al., 2005. TAp73/Delta Np73 influences apoptotic response, chemosensitivity and prognosis in hepatocellular carcinoma. *Cell death and differentiation*, 12(12), pp.1564–1577.
- Mundt, H.M. et al., 2010. Dominant negative (DeltaN) p63alpha induces drug resistance in hepatocellular carcinoma by interference with apoptosis signaling pathways. *Biochemical and biophysical research communications*, 396(2), pp.335–41. Available at: <http://www.sciencedirect.com/science/article/pii/S0006291X10007734> [Accessed February 25, 2016].
- Murray-Zmijewski, F., Lane, D.P. & Bourdon, J.-C., 2006. p53/p63/p73 isoforms: an orchestra of isoforms to harmonise cell differentiation and response to stress. *Cell death and differentiation*, 13(6), pp.962–72. Available at: <http://www.ncbi.nlm.nih.gov/pubmed/16601753> [Accessed March 19, 2015].

- Nagata, M. et al., 2013. ITGA3 and ITGB4 expression biomarkers estimate the risks of locoregional and hematogenous dissemination of oral squamous cell carcinoma. *BMC cancer*, 13(1), p.410. Available at: <http://www.pubmedcentral.nih.gov/articlerender.fcgi?artid=3844399&tool=pmcentrez&rendertype=abstract>.
- Nakajima, Y. et al., 2004. cDNA cloning and characterization of a secreted luciferase from the luminous Japanese ostracod, *Cypridina noctiluca*. *Bioscience, biotechnology, and biochemistry*, 68(February 2015), pp.565–570.
- Navin, N.E., 2014. Cancer genomics: one cell at a time. *Genome Biology*, 15(8), p.452. Available at: <http://www.pubmedcentral.nih.gov/articlerender.fcgi?artid=4281948&tool=pmcentrez&rendertype=abstract> [Accessed September 2, 2014].
- Nemajerova, A. et al., 2010. Loss of p73 promotes dissemination of Myc-induced B cell lymphomas in mice. *The Journal of clinical investigation*, 120(6), pp.2070–80. Available at: <http://www.ncbi.nlm.nih.gov/pubmed/20484818> [Accessed June 10, 2016].
- Ng, S.W. et al., 2000. Analysis of p73 in human borderline and invasive ovarian tumor. *Oncogene*, 19(15), pp.1885–90. Available at: <http://www.nature.com/onc/journal/v19/n15/full/1203512a.html> [Accessed March 19, 2015].
- Nicholson, S.A. et al., 2001. Alterations of p14ARF, p53, and p73 genes involved in the E2F-1-mediated apoptotic pathways in non-small cell lung carcinoma. *Cancer research*, 61(14), pp.5636–43. Available at: <http://www.ncbi.nlm.nih.gov/pubmed/11454718> [Accessed June 10, 2016].
- Nordling, C.O., 1953. A new theory on cancer-inducing mechanism. *British journal of cancer*, 7(1), pp.68–72.
- Nowell, P.C., 1976. The clonal evolution of tumor cell populations. *Science (New York, N.Y.)*, 194(4260), pp.23–8. Available at: <http://www.ncbi.nlm.nih.gov/pubmed/959840> [Accessed February 8, 2015].
- Nyman, U. et al., 2005. Full-length p73alpha represses drug-induced apoptosis in small cell lung carcinoma cells. *The Journal of biological chemistry*, 280(40), pp.34159–69. Available at: <http://www.ncbi.nlm.nih.gov/pubmed/16087678> [Accessed March 6, 2016].
- Ohira, T. et al., 1994. In vitro and in vivo growth of B16F10 melanoma cells transfected with interleukin-4 cDNA and gene therapy with the transfectant. *Journal of cancer research and clinical oncology*, 120(11), pp.631–635.
- Oliner, J.D. et al., 1992. Amplification of a gene encoding a p53-associated protein in human sarcomas.pdf. *Nature*, 358(July), pp.80–83.
- Olsson, E. et al., 2015. Serial monitoring of circulating tumor DNA in patients with primary breast cancer for detection of occult metastatic disease. *EMBO molecular medicine*, 7(8), pp.1034–47. Available at: <http://www.pubmedcentral.nih.gov/articlerender.fcgi?artid=4551342&tool=pmcentrez&rendertype=abstract> [Accessed December 1, 2015].
- Pereira, E. et al., 2015. Personalized Circulating Tumor DNA Biomarkers Dynamically Predict Treatment Response and Survival In Gynecologic Cancers. *PloS one*, 10(12), p.e0145754. Available at: <http://journals.plos.org/plosone/article?id=10.1371/journal.pone.0145754> [Accessed February 23, 2016].
- Perez-Losada, J. et al., 2005. p63 and p73 do not contribute to p53-mediated lymphoma suppressor activity in vivo. *Oncogene*, 24(35), pp.5521–5524.

- Available at: <http://www.nature.com/doi/10.1038/sj.onc.1208799> [Accessed June 10, 2016].
- Peschiaroli, a et al., 2009. The F-box protein FBXO45 promotes the proteasome-dependent degradation of p73. *Oncogene*, 28(35), pp.3157–3166. Available at: <http://dx.doi.org/10.1038/onc.2009.177>.
- Petrenko, O., Zaika, A. & Moll, U.M., 2003. Δ Np73 Facilitates Cell Immortalization and Cooperates with Oncogenic Ras in Cellular Transformation In Vivo DNp73 Facilitates Cell Immortalization and Cooperates with Oncogenic Ras in Cellular Transformation In Vivo. *Molecular and Cellular Biology*, 23(16), pp.5540–5555.
- Pozniak, C.D. et al., 2000. An anti-apoptotic role for the p53 family member, p73, during developmental neuron death. *Science (New York, N.Y.)*, 289(5477), pp.304–306.
- Puau, A.-L. et al., 2011. A comparison of imaging techniques to monitor tumor growth and cancer progression in living animals. *International journal of molecular imaging*, 2011, p.321538. Available at: <http://www.pubmedcentral.nih.gov/articlerender.fcgi?artid=3216304&tool=pmcentrez&rendertype=abstract>.
- Quaresma, M., Coleman, M.P. & Rachet, B., 2015. 40-year trends in an index of survival for all cancers combined and survival adjusted for age and sex for each cancer in England and Wales, 1971–2011: a population-based study. *The Lancet*, 385(9974), pp.1206–1218. Available at: <http://www.thelancet.com/article/S0140673614613969/fulltext> [Accessed November 2, 2015].
- Rabinovitz, I., Toker, A. & Mercurio, A.M., 1999. Protein kinase C-dependent mobilization of the $\alpha 5 \beta 1$ integrin from hemidesmosomes and its association with actin-rich cell protrusions drive the chemotactic migration of carcinoma cells. *Journal of Cell Biology*, 146(5), pp.1147–1159.
- Reedijk, M. et al., 2005. High-level coexpression of JAG1 and NOTCH1 is observed in human breast cancer and is associated with poor overall survival. *Cancer Research*, 65(18), pp.8530–8537.
- Remy, I. & Michnick, S.W., 2006. A highly sensitive protein-protein interaction assay based on Gaussia luciferase. *Nature Methods*, 3(12), pp.977–979. Available at: <http://www.nature.com/doi/10.1038/nmeth979> [Accessed June 9, 2016].
- Richmond, A. & Su, Y., 2008. Mouse xenograft models vs GEM models for human cancer therapeutics. *Disease models & mechanisms*, 1(2–3), pp.78–82. Available at: <http://www.ncbi.nlm.nih.gov/pubmed/19048064> [Accessed June 10, 2016].
- van Rijn, S. et al., 2013. Functional multiplex reporter assay using tagged Gaussia luciferase. *Scientific reports*, 3, p.1046. Available at: <http://www.pubmedcentral.nih.gov/articlerender.fcgi?artid=3541509&tool=pmcentrez&rendertype=abstract> [Accessed November 11, 2014].
- Rodriguez, E. et al., 2014. Versatile and enhanced tumour modelling in mice via somatic cell transduction. *Journal of Pathology*, 232(4), pp.449–457.
- Rossi, M. et al., 2005. The ubiquitin-protein ligase Itch regulates p73 stability. *The EMBO journal*, 24(4), pp.836–848.
- Rousseaux, S. et al., 2005. Establishment of male-specific epigenetic information. *Gene*, 345(2), pp.139–153.
- Russell, T.D. et al., 2003. Transduction of the mammary epithelium with adenovirus vectors in vivo. *Journal of virology*, 77(10), pp.5801–5809.

- Sah, V.P. et al., 1995. A subset of p53-deficient embryos exhibit exencephaly. *Nature genetics*, 10(2), pp.175–180.
- Sakaguchi, K. et al., 1998. DNA damage activates p53 through a phosphorylation-acetylation cascade. *Genes & Development*, 12(18), pp.2831–2841. Available at: <http://www.genesdev.org/cgi/doi/10.1101/gad.12.18.2831> [Accessed November 11, 2014].
- Sasaki, Y. et al., 2002. The p53 family member genes are involved in the Notch signal pathway. *Journal of Biological Chemistry*, 277(1), pp.719–724.
- Scaffidi, P., Misteli, T. & Bianchi, M.E., 2002. Release of chromatin protein HMGB1 by necrotic cells triggers inflammation. *Nature*, 418(6894), pp.191–5. Available at: <http://dx.doi.org/10.1038/nature00858> [Accessed December 20, 2015].
- Schultz, J. et al., 1997. SAM as a protein interaction domain involved in developmental regulation. *Protein science : a publication of the Protein Society*, 6(1), pp.249–53. Available at: <http://www.pubmedcentral.nih.gov/articlerender.fcgi?artid=2143507&tool=pmcentrez&rendertype=abstract> [Accessed February 25, 2016].
- Schulze, a & Downward, J., 2001. Navigating gene expression using microarrays--a technology review. *Nature cell biology*, 3(August), pp.E190–E195.
- Schwab, M., Praml, C. & Amler, L.C., 1996. Genomic instability in 1p and human malignancies. *Genes, chromosomes & cancer*, 16(4), pp.211–29. Available at: <http://www.ncbi.nlm.nih.gov/pubmed/8875235> [Accessed April 23, 2015].
- Seelan, R.S. et al., 2002. The human p73 promoter: characterization and identification of functional E2F binding sites. *Neoplasia (New York, N.Y.)*, 4(3), pp.195–203. Available at: <http://www.pubmedcentral.nih.gov/articlerender.fcgi?artid=1531693&tool=pmcentrez&rendertype=abstract> [Accessed March 19, 2015].
- Seo, S.H. et al., 2011. The effects of mesenchymal stem cells injected via different routes on modified IL-12-mediated antitumor activity. *Gene therapy*, 18(5), pp.488–495. Available at: <http://dx.doi.org/10.1038/gt.2010.170>.
- Serrano, M. et al., 1997. Oncogenic ras provokes premature cell senescence associated with accumulation of p53 and p16INK4a. *Cell*, 88(5), pp.593–602. Available at: <http://www.ncbi.nlm.nih.gov/pubmed/9054499> [Accessed April 22, 2015].
- Sethi, N. et al., 2011. Tumor-Derived Jagged1 Promotes Osteolytic Bone Metastasis of Breast Cancer by Engaging Notch Signaling in Bone Cells. *Cancer Cell*, 19(2), pp.192–205. Available at: <http://dx.doi.org/10.1016/j.ccr.2010.12.022>.
- Shao, S. et al., 2015. Notch1 signaling regulates the epithelial–mesenchymal transition and invasion of breast cancer in a Slug-dependent manner. *Molecular Cancer*, 14(1), pp.1–17. Available at: <http://www.molecular-cancer.com/content/14/1/28>.
- Shay, J., Pereira-Smith, O. & Wright, W., 1991. A role for both RB and p53 in the regulation of human cellular senescence. - PubMed - NCBI. *experimental cell research*, 196, pp.33–39. Available at: <http://www.ncbi.nlm.nih.gov/pubmed/1652450> [Accessed February 25, 2016].

- Shay, J.W., 2001. Telomerase and cancer. *Human Molecular Genetics*, 10(7), pp.677–685. Available at: <http://hmg.oxfordjournals.org/content/10/7/677.full> [Accessed November 15, 2015].
- Shieh, S.-Y. et al., 1997. DNA Damage-Induced Phosphorylation of p53 Alleviates Inhibition by MDM2. *Cell*, 91(3), pp.325–334. Available at: <http://linkinghub.elsevier.com/retrieve/pii/S009286740080416X>.
- Shyr, D. & Liu, Q., 2013. Next generation sequencing in cancer research and clinical application. *Biological procedures online*, 15(1), p.4. Available at: <http://biologicalproceduresonline.biomedcentral.com/articles/10.1186/1480-9222-15-4> [Accessed December 16, 2015].
- Siolas, D. & Hannon, G.J., 2013. Patient-derived tumor xenografts: transforming clinical samples into mouse models. *Cancer research*, 73(17), pp.5315–9. Available at: <http://www.pubmedcentral.nih.gov/articlerender.fcgi?artid=3766500&tool=pmcentrez&rendertype=abstract> [Accessed February 24, 2016].
- Skelton, D., Satake, N. & Kohn, D.B., 2001. The enhanced green fluorescent protein (eGFP) is minimally immunogenic in C57BL/6 mice. *Gene therapy*, 8, pp.1813–1814.
- Slade, N. et al., 2004. DeltaNp73 stabilises TAp73 proteins but compromises their function due to inhibitory hetero-oligomer formation. *Cell death and differentiation*, 11(3), pp.357–60. Available at: <http://dx.doi.org/10.1038/sj.cdd.4401335> [Accessed March 5, 2016].
- Song, J. et al., 2010. A mouse model for the human pathogen Salmonella typhi. *Cell host & microbe*, 8(4), pp.369–376.
- Stantic, M. et al., 2015. TAp73 suppresses tumor angiogenesis through repression of proangiogenic cytokines and HIF-1 α activity. *Proceedings of the National Academy of Sciences*, 112(1), pp.220–225. Available at: <http://www.pnas.org/lookup/doi/10.1073/pnas.1421697112>.
- Steder, M. et al., 2013. DNp73 exerts function in metastasis initiation by disconnecting the inhibitory role of EPLIN on IGF1R-AKT/STAT3 signaling. *Cancer cell*, 24(4), pp.512–27. Available at: <http://www.ncbi.nlm.nih.gov/pubmed/24135282> [Accessed September 1, 2014].
- Stiewe, T., Zimmermann, S., et al., 2002. Transactivation-deficient DeltaTA-p73 acts as an oncogene. *Cancer research*, 62(13), pp.3598–3602.
- Stiewe, T. & Pützer, B.M., 2002. Role of p73 in malignancy: tumor suppressor or oncogene? *Cell death and differentiation*, 9(3), pp.237–245.
- Stiewe, T. & Pützer, B.M., 2000. Role of the p53-homologue p73 in E2F1-induced apoptosis. *Nature genetics*, 26(4), pp.464–9. Available at: <http://www.ncbi.nlm.nih.gov/pubmed/11101847> [Accessed February 25, 2016].
- Stiewe, T., Theseling, C.C. & Pützer, B.M., 2002. Transactivation-deficient Delta TA-p73 inhibits p53 by direct competition for DNA binding: implications for tumorigenesis. *The Journal of biological chemistry*, 277(16), pp.14177–85. Available at: <http://www.jbc.org/content/277/16/14177> [Accessed March 19, 2015].
- Stiewe, T., Theseling, C.C. & Pützer, B.M., 2002. Transactivation-deficient Δ TA-p73 inhibits p53 by direct competition for DNA binding. Implications for tumorigenesis. *Journal of Biological Chemistry*, 277(16), pp.14177–14185.
- Strano, S. et al., 2002. Physical interaction with human tumor-derived p53

- mutants inhibits p63 activities. *The Journal of biological chemistry*, 277(21), pp.18817–26. Available at: <http://www.ncbi.nlm.nih.gov/pubmed/11893750> [Accessed November 5, 2014].
- Subramanian, A. et al., 2005. Gene set enrichment analysis: a knowledge-based approach for interpreting genome-wide expression profiles. *Proceedings of the National Academy of Sciences of the United States of America*, 102, pp.15545–50. Available at: <http://www.ncbi.nlm.nih.gov/pubmed/16199517>.
- Subramanian, D., Bunjobpol, W. & Sabapathy, K., 2015. Interplay between TAp73 Protein and Selected Activator Protein-1 (AP-1) Family Members Promotes AP-1 Target Gene Activation and Cellular Growth. *The Journal of biological chemistry*, 290(30), pp.18636–49. Available at: <http://www.jbc.org/content/early/2015/05/27/jbc.M115.636548> [Accessed March 5, 2016].
- Sushrusha Nayak M S Roland W Herzog, 2011. Progress and prospects: immune responses to viral vectors. by S Nayak, R W Herzog. *Gene Therapy*, 17(3), pp.295–304.
- Taketo, M. et al., 1991. FVB/N: an inbred mouse strain preferable for transgenic analyses. *Proceedings of the National Academy of Sciences of the United States of America*, 88(6), pp.2065–2069.
- Tamura, M. et al., 2013. Forkhead transcription factor FOXF1 is a novel target gene of the p53 family and regulates cancer cell migration and invasiveness. *Oncogene*, 33(October 2012), pp.1–10. Available at: <http://www.ncbi.nlm.nih.gov/pubmed/24186199>.
- Tanahashi, Y. et al., 2001. Continuous measurement of targeted promoter activity by a secreted bioluminescence reporter, Vargula hilgendorffii luciferase. *Analytical biochemistry*, 289(2), pp.260–6. Available at: <http://europepmc.org/abstract/med/11161320> [Accessed June 2, 2016].
- Tannapfel, A. et al., 2008. Autonomous growth and hepatocarcinogenesis in transgenic mice expressing the p53 family inhibitor DNp73. *Carcinogenesis*, 29(1), pp.211–8. Available at: <http://www.ncbi.nlm.nih.gov/pubmed/17984115> [Accessed October 28, 2014].
- Tannous, B. a, 2009. Gaussia luciferase reporter assay for monitoring biological processes in culture and in vivo. *Nature protocols*, 4(4), pp.582–91. Available at: <http://www.pubmedcentral.nih.gov/articlerender.fcgi?artid=2692611&tool=pmcentrez&rendertype=abstract> [Accessed October 22, 2014].
- Tannous, B. a. et al., 2005. Codon-optimized gaussia luciferase cDNA for mammalian gene expression in culture and in vivo. *Molecular Therapy*, 11(3), pp.435–443.
- Thiery, J.P., 2002. Epithelial–mesenchymal transitions in tumour progression. *Nature Reviews Cancer*, 2(6), pp.442–454. Available at: <http://www.nature.com/doi/10.1038/nrc822> [Accessed June 12, 2016].
- Tibbetts, R.S. et al., 1999. A role for ATR in the DNA damage-induced phosphorylation of p53 A role for ATR in the DNA phosphorylation of p53. , pp.152–157.
- Tie, J. et al., 2015. Circulating tumor DNA as an early marker of therapeutic response in patients with metastatic colorectal cancer. *Annals of oncology : official journal of the European Society for Medical Oncology / ESMO*, 26(8), pp.1715–22. Available at:

- <http://www.ncbi.nlm.nih.gov/pubmed/25851626> [Accessed January 17, 2016].
- Tissir, F. et al., 2009. DeltaNp73 regulates neuronal survival in vivo. *Proceedings of the National Academy of Sciences of the United States of America*, 106(39), pp.16871–6. Available at: <http://www.pubmedcentral.nih.gov/articlerender.fcgi?artid=2757832&tool=pmcentrez&rendertype=abstract>.
- Tokuchi, Y. et al., 1999. The expression of p73 is increased in lung cancer, independent of p53 gene alteration. *British journal of cancer*, 80(10), pp.1623–1629.
- Tomasini, R. et al., 2008. TAp73 knockout shows genomic instability with infertility and tumor suppressor functions. *Genes & development*, 22(19), pp.2677–91. Available at: <http://www.pubmedcentral.nih.gov/articlerender.fcgi?artid=2559903&tool=pmcentrez&rendertype=abstract> [Accessed September 1, 2014].
- Tomasini, R. et al., 2009. TAp73 regulates the spindle assembly checkpoint by modulating BubR1 activity. *Proceedings of the National Academy of Sciences of the United States of America*, 106(3), pp.797–802.
- Ueda, Y. et al., 1999. New p73 variants with altered C-terminal structures have varied transcriptional activities. *Oncogene*, 18(35), pp.4993–8. Available at: <http://www.ncbi.nlm.nih.gov/pubmed/10490834> [Accessed March 19, 2015].
- Vakkila, J. & Lotze, M.T., 2004. Inflammation and necrosis promote tumour growth. *Nature reviews. Immunology*, 4(8), pp.641–8. Available at: <http://dx.doi.org/10.1038/nri1415> [Accessed February 22, 2016].
- Valiente, M. et al., 2014. Serpins promote cancer cell survival and vascular Co-option in brain metastasis. *Cell*, 156(5), pp.1002–1016.
- Vassilev, L.T. et al., 2004. In vivo activation of the p53 pathway by small-molecule antagonists of MDM2. *Science (New York, N.Y.)*, 303(5659), pp.844–8. Available at: <http://www.ncbi.nlm.nih.gov/pubmed/14704432> [Accessed July 10, 2014].
- Ventura, A. et al., 2007. Restoration of p53 function leads to tumour regression in vivo. *Nature*, 445(7128), pp.661–665.
- Vooijs, M., Jonkers, J. & Berns, A., 2001. A highly efficient ligand-regulated Cre recombinase mouse line shows that LoxP recombination is position dependent. *EMBO Reports*, 2(4), pp.292–297.
- Wan, X. et al., 2010. NIH Public Access. , 28(38), pp.3401–3411.
- Wang, J.Y. & Ki, S.W., 2001. Choosing between growth arrest and apoptosis through the retinoblastoma tumour suppressor protein, Abl and p73. *Biochemical Society transactions*, 29(Pt 6), pp.666–673.
- Wang, Z. et al., 2006. Widespread and stable pancreatic gene transfer by adeno-associated virus vectors via different routes. *Diabetes*, 55(4), pp.875–884.
- Wessels, J.T. et al., 2007. In vivo imaging in experimental preclinical tumor research--a review. *Cytometry. Part A : the journal of the International Society for Analytical Cytology*, 71(8), pp.542–9. Available at: <http://www.ncbi.nlm.nih.gov/pubmed/17598185> [Accessed April 27, 2016].
- White, R. a et al., 2009. Digital PCR provides sensitive and absolute calibration for high throughput sequencing. *BMC genomics*, 10, p.116.
- Wilhelm, M.T. et al., 2010. Isoform-specific p73 knockout mice reveal a novel role for delta Np73 in the DNA damage response pathway. *Genes &*

- development*, 24(6), pp.549–60. Available at:
<http://www.pubmedcentral.nih.gov/articlerender.fcgi?artid=2841333&tool=pmcentrez&rendertype=abstract> [Accessed September 1, 2014].
- Wu, C., Suzuki-Ogoh, C. & Ohmiya, Y., 2007. Dual-reporter assay using two secreted luciferase genes. *BioTechniques*, 42(3), pp.290–292. Available at:
<http://www.biotechniques.com/article/000112428> [Accessed June 9, 2016].
- Wu, H. & Zhang, Y., 2012. Early embryos reprogram DNA methylation in two steps. *Cell Stem Cell*, 10(5), pp.487–489. Available at:
<http://dx.doi.org/10.1016/j.stem.2012.04.012>.
- Wurdinger, T. et al., 2008. A secreted luciferase for ex vivo monitoring of in vivo processes. *Nature methods*, 5(2), pp.171–3. Available at:
<http://www.pubmedcentral.nih.gov/articlerender.fcgi?artid=2699561&tool=pmcentrez&rendertype=abstract> [Accessed October 21, 2014].
- Yang, A., Kaghad, M., Wang, Y., Gillett, E., Fleming, M.D., Do, V., et al., 1998. Encodes Multiple Products with Transactivating, Death-Inducing, and Dominant-Negative Activities. , 2, pp.305–316.
- Yang, A. et al., 2010. Genome-wide mapping indicates that p73 and p63 Co-occupy target sites and have similar DNA-binding profiles in vivo. *PLoS ONE*, 5(7).
- Yang, A. et al., 2002. On the shoulders of giants: p63, p73 and the rise of p53. *Trends in Genetics*, 18(2), pp.90–95. Available at:
<http://linkinghub.elsevier.com/retrieve/pii/S0168952502025957> [Accessed November 3, 2014].
- Yang, A., Kaghad, M., Wang, Y., Gillett, E., Fleming, M.D., Dötsch, V., et al., 1998. p63, a p53 Homolog at 3q27–29, Encodes Multiple Products with Transactivating, Death-Inducing, and Dominant-Negative Activities. *Molecular Cell*, 2(3), pp.305–316. Available at:
<http://www.cell.com/article/S1097276500802750/fulltext> [Accessed February 25, 2016].
- Yang, A. et al., 2000. p73-deficient mice have neurological, pheromonal and inflammatory defects but lack spontaneous tumours. , 25(1997), pp.99–103.
- Yang, A. & McKeon, F., 2000. P63 and P73: P53 mimics, menaces and more. *Nature reviews. Molecular cell biology*, 1(3), pp.199–207. Available at:
<http://dx.doi.org/10.1038/35043127> [Accessed June 2, 2016].
- Yang, M. et al., 2000. Whole-body optical imaging of green fluorescent protein-expressing tumors and metastases. *Proceedings of the National Academy of Sciences of the United States of America*, 97(3), pp.1206–11. Available at:
<http://www.pubmedcentral.nih.gov/articlerender.fcgi?artid=15570&tool=pmcentrez&rendertype=abstract> [Accessed February 9, 2016].
- Yang, Y. et al., 2011. The Notch ligand Jagged2 promotes lung adenocarcinoma metastasis through a miR-200 - Dependent pathway in mice. *Journal of Clinical Investigation*, 121(4), pp.1373–1385.
- Yang, Y.H. et al., 2002. Normalization for cDNA microarray data: a robust composite method addressing single and multiple slide systematic variation. *Nucleic acids research*, 30(4), p.e15.
- Yang, Z. et al., 2014. Options for tracking GFP-Labeled transplanted Myoblasts using in Vivo Fluorescence imaging: implications for tracking stem cell fate. *BMC biotechnology*, 14(1), p.55. Available at:
<http://www.ncbi.nlm.nih.gov/pubmed/24919771>.
- Yao, R., Lecomte, R. & Crawford, E.S., 2012. Small-Animal PET: What Is It,

- and Why Do We Need It? Available at:
<https://www.acsu.buffalo.edu/~rutaoyao/2012-jnmt-animalPET.pdf>
[Accessed June 1, 2016].
- Yokomizo, a et al., 1999. Overexpression of the wild type p73 gene in human bladder cancer. *Oncogene*, 18(July 1998), pp.1629–1633.
- Yonish-Rouach, E. et al., 1991. Wild-type p53 induces apoptosis of myeloid leukaemic cells that is inhibited by interleukin-6. - PubMed - NCBI. *Nature*, 353, pp.345–347. Available at:
<http://www.ncbi.nlm.nih.gov/pubmed/1852210> [Accessed February 25, 2016].
- Yu, J. et al., 1999. Identification and classification of p53-regulated genes. *Proceedings of the National Academy of Sciences*, 96(25), pp.14517–14522. Available at: <http://www.pnas.org/content/96/25/14517.full>
[Accessed February 25, 2016].
- Zaika, A.I. et al., 2002. DeltaNp73, a dominant-negative inhibitor of wild-type p53 and TAp73, is up-regulated in human tumors. *The Journal of experimental medicine*, 196(6), pp.765–780.
- Zaika, a I. et al., 1999. Overexpression of the wild type p73 gene in breast cancer tissues and cell lines. *Cancer research*, 59, pp.3257–3263.
- Zender, L. et al., 2008. An oncogenomics-based in vivo RNAi screen identifies tumor suppressors in liver cancer. *Cell*, 135(5), pp.852–64. Available at:
<http://www.pubmedcentral.nih.gov/articlerender.fcgi?artid=2990916&tool=pmcentrez&rendertype=abstract> [Accessed February 24, 2016].
- Zheng, Y. et al., 2013. A Rare Population of CD24+ITGB4+Notchhi Cells Drives Tumor Propagation in NSCLC and Requires Notch3 for Self-Renewal. *Cancer Cell*, 24(1), pp.59–74. Available at:
<http://dx.doi.org/10.1016/j.ccr.2013.05.021>.
- Zhu, J. et al., 1998. The potential tumor suppressor p73 differentially regulates cellular p53 target genes. *Cancer research*, 58(22), pp.5061–5. Available at: <http://www.ncbi.nlm.nih.gov/pubmed/9823311> [Accessed February 25, 2016].
- Zuber, J. et al., 2011. An integrated approach to dissecting oncogene addiction implicates a Myb-coordinated self-renewal program as essential for leukemia maintenance. *Genes & development*, 25(15), pp.1628–40. Available at:
<http://www.pubmedcentral.nih.gov/articlerender.fcgi?artid=3182026&tool=pmcentrez&rendertype=abstract> [Accessed February 19, 2016].

Abbreviations

4OHT	4-hydroxytamoxifen
AP1	Activator protein 1
ATM	Ataxia Telangiectasia mutated
ATP	Adenosine triphosphate
ATR	ATM-Rad3-related
Bax	Bcl-2 associated X protein
BLI	Bioluminescent imaging
bp	Base pairs
BubR1	Bub1-related protein kinase
c-Abl	Abelson murine leukemia viral oncogene homolog 1
CCNB1/2	Cyclin B1/2
Cdkn1a	Cyclin-dependent kinase inhibitor 1a
cDNA	Complementary DNA
CENPA	Centromere protein A
ChIP	Chromatin immune precipitation
CIS	Carcinoma in situ
CLuc	Cypridina luciferase
CpG	Cytosine phosphatidyl Guanine
Cre	Cre recombinase
cRNA	Complementary DNA
CT	Computed tomography
CTD	C-terminal domain
CTP	Cytidine triphosphate
DAB	Diaminobenzidine
DBD	DNA-binding domain
DMEM	Dulbecco's modified eagle's medium
DMSO	Dimethyl sulfoxide
DNA	Deoxyribonucleic acid
DNA-PK	DNA-dependent protein kinase
Dsp	Desmoplakin
E	Embryonic stage
E.coli	Escherichia coli
E-Cadherin	Epithelial Cadherin
ECM	Extracellular mass
EDTA	Ethylendiamtetraacetic acid
EF1 α	Elongation factor 1 α
ELISA	Enzyme linked immunosorbent assay
EMT	Epithelial to mesenchymal transition
EPLIN	Epithelial protein lost in neoplasm
ERT	Tamoxifen-inducible Estrogen receptor
FAM	Carboxyfluorescein
FBXO45	F-box only protein 45
FLI	Fluorescent imaging
FOXO1	Forkhead Box Protein 1
GADD45	Growth arrest and DNA-damage inducible gene 45
GAPDH	Glyceraldehyde 3-phosphate dehydrogenase
gDNA	Genomic DNA
GFP	Green fluorescent protein
GLuc	Gaussia luciferase
H&E	Hematoxylin and eosin

HA	hemagglutinin
Hp73	Human p73
HRP	Horseradish peroxidase
hrs	Hours
IE	International unit
IGFR1	Insulin like growth factor receptor 1
IgG	Immunoglobulin G
IHC	Immunohistochemistry
IL2	Interleukin 2
IRES	Internal ribosomal entry site
ITCH	Itchy E3 ubiquitin protein ligase
IVF	In vitro fertilization
JOE	Carboxy dichloro Dimethoxyfluorescein
KO	Knock out
LB	Luria broth medium
LIF1	Ligase interacting factor 1
LOH	Loss of heterozygosity
LSL	Lox-Stop-lox
LTR	Long terminal repeats
MDM2	Mouse double minute 2
MDM4	Mouse double minute 4
MEFs	Murine embryonic fibroblasts
mID4	Murine inhibitor of DNA binding 4
miRNA	Micro RNA
miTGB4	Murine integrin beta 4
mJAG1/2	Murine jagged1/2
mKDR	Murine kinase insert domain receptor
mRNA	Messenger RNA
MRT	Magnetic resonance tomography
MRT	Magnetic resonance tomography
mSerp	Murine Serpin Family Member
myc	Myelocytomatosis Viral Oncogene
n	Number
N-Cadherin	Neuronal Cadherin
nsh	Non-silencing shRNA
nsi	Non-silencing siRNA
OD	Oligomerization domain
OS	Overall survival
PBS	Pospho-buffered saline
PCAF	P300/CBP associated factor
pCLucIPZ/GLucIPZ	CLuc-IRES-Puro/ GLuc-IRES-Puro
PCR	Polymerase chain reaction
PEG	Polyethylene glycol
PET	Positron emission tomography
PI3K	Phosphatidylinositol Bisphosphate 3-Kinase
Pkp1	Plakophilin 1
PR	Proline-rich region
Puma	P53 upregulated mediator of apoptosis
Puro	Puromycin
Puro	puromycin
qPCR	Quantitative real-time PCR
r	Pearsons correlation coefficient r
Rag2	Recombination activating gene 2

Abbreviations

RB	Retinoblastoma protein
RE	Response element
RFP	Red fluorescent protein
RITA	Reactivation of p53 and induction of tumor cell apoptosis
RLU	Relative light units
RNA	Ribonucleic acid
RNAi	RNA interference
ROI	Region of interest
ROS	Reactive oxygen species
Rpm	Rounds per minute
RPMI	Roswell park memorial institute medium
rtTA	Reverse tetracycline transactivator
s	Second
s.d.	Standard deviation
SAC	Spindle assembly checkpoint
SAM	Sterile alpha motif
SCLC	Small cell lung cancer
SDS	Sodium dodecyl sulfate
SEAP	Secreted embryonic alkaline phosphatase
shRNA	Short hairpin RNA
siRNA	Small interfering RNA
SPF	Specific pathogen free
sqRT	Semiquantitative PCR
STAT3	Signal transducer and activator of transcription 3
T2A	Self-cleaving 2a peptide
TAD	Transactivation domain
TAE	Trisacetate EDTA
TAp63	Transactivating p63
TAp73	Transactivating p73
TBS	Tris-buffered saline
tet	Tetracycline
Tfrc	Transferrin receptor gene
TFS	Tumor free survival
TGFB3	Transforming growth factor Beta 1
TRE	Tetracycline responsive element
UTR	Untranslated region
UV-radiation	Ultra violet light radiation
VEGF	Vascular endothelial growth factor
VLuc	Vargula luciferin (alternative name for Cypridina luciferin)
Wnt	Wingless type
wt	Wildtype
Δ Np73	DeltaNp73

Publications

Scientific Presentations

Fuchs J, Charles JP, Hefter M, Vischedyk JB, Kleint M, Vogiatzi F, Schaefer JA and Stiewe T: Monitoring the dynamics of clonal tumour evolution in vivo using secreted luciferases. University of Giessen and Marburg Lung Center Meeting 2014 (Talk)

Fuchs J, Charles JP, Hefter M, Vischedyk JB, Kleint M, Vogiatzi F, Schaefer JA and Stiewe T: Monitoring the dynamics of clonal tumour evolution in vivo using secreted luciferases. 7th Junior Scientists Meeting: Young Scientists meet Experience, Reisenburg/Günzburg, 2014 (Poster)

Fuchs J, Charles JP, Hefter M, Vischedyk JB, Kleint M, Vogiatzi F, Schaefer JA and Stiewe T: Monitoring the dynamics of clonal tumour evolution in vivo using secreted luciferases. International Conference on From Omics to Novel Therapies in Cancer, MKFZ Charité Berlin, 2014 (Talk)

Fuchs J, Charles JP, Hefter M, Vischedyk JB, Kleint M, Vogiatzi F, Schaefer JA and Stiewe T: Generation of a Dual Luciferase shRNA Competition Assay. TRR17 Graduate School Retreat, Pommersfelden, 2013 (Talk)

Fuchs J, Charles JP, Hefter M, Schaefer JA and Stiewe T: Generation of a Dual Luciferase shRNA Competition Assay. TRR17 Graduate School Retreat, Monastery Schöntal, 2012 (Talk)

Fuchs J, Hüttinger N, Stiewe T: Characterizing a Δ Np73-overexpressing mouse model. SFB TRR17/Loewe Joint Symposium, Rothenburg 2011 (Poster)

Fuchs J and Stiewe T: Characterization of the transgenic Δ Np73 mouse model. Autumn School "The Puzzling World of Cancer", Würzburg 2010 (Poster)

Scientific Publications

Vogiatzi F., Brandt D. T., Schneikert J., Fuchs J., Grikscheit K., Wanzel M., Pavlakis E., Charles J.P., Timofeev O., Nist A., Mernberger M., Kantelhardt E. J., Siebolts U., Bartel F., Jacob R., Rath A., Moll R., Grosse R. and Stiewe, T. (2016). Mutant p53 promotes tumor progression and metastasis by the endoplasmic reticulum UDPase ENTPD5. *Proceedings of the National Academy of Sciences of the United States of America*, 113(52), E8433–E8442. <http://doi.org/10.1073/pnas.1612711114>

Charles JP, Fuchs J, Hefter M, Vischedyk JB, Kleint M, Vogiatzi F, Schaefer JA, Nist A, Timofeev O, Wanzel M and Stiewe T (2014), *Monitoring the dynamics of clonal tumour evolution in vivo using secreted luciferases*. *NATURE COMMUNICATIONS*, 5:3981. doi: 10.1038/ncomms4981

Meinel FG, Schwab F, Yaroshenko A, Velroyen A, Bech M, Hellbach K, Fuchs J, Stiewe T, Yildirim AÖ, Bamberg F, Reiser MF, Pfeiffer F and Nikolaou K, *Lung tumors on multimodal radiographs derived from grating-based X-ray imaging - A feasibility study*. *Physica Medica*, 12/2013. doi: 10.1016/j.ejmp.2013.11.001

List of Academic Teachers

My academic teachers at the Fridericiana University Karlsruhe were Mrs. and Mr.:

Bastmeyer, Blattner, Bentrop, Bertl, Bräse, Buschmann, Cato, Drumm, Fenske, Foitzik, Frey, Götz, Kadelka, Krug, Müller, Pankratz, Paulsen, Puchta, Radius, Rieder, Seyfried, Sleeman, Stinnesbeck, Spitzmueller, Sures, Taraschewski, Uetz, Wedlich, Weg-Remers, Weisenseel, Zöllner.

My academic teacher at the Philipps University Marburg was Mr. Stiewe.

Acknowledgements

Firstly, my deepest gratitude is dedicated to Prof. Dr. Thorsten Stiewe giving me the opportunity to work on such challenging as well as pioneering research projects. Thank you for making this work possible.

Moreover, I would like to thank the whole Stiewe lab, former and present members, for your support in each and every possible way. It was an exceptional experience to work and share life with such a well attuned, creative and caring team. Anne, the time we spent on poetry slams, music, cooking, drinks, conversations and laughs frequently saved my motivation, not to forget your infinite support in the lab and correcting this work. Thank you for being a friend! Anna and Tini, you were much more than an invincible party committee. Anna, thank you for all the laughs, your nordic sarcasm and bluntness. Tini, thank you for sharing not only work but also life. There is nothing better than greek families. And there is no better hair stylist than you. Siggi, Geli, Martina and Björn, thank you for infinite support and laughs in professional as well as personal matters. Joel, your creativity frequently eased (lab) routine. Also thank you for jointly working on the luciferase project. Mirjam, Jonas and Max, it was a pleasure to work together with so motivated people to drive forward the luciferase project. Lucas and Marco, thank you for your support in bioinformatic analyses and for your patience in deepening my bioinformatic comprehension.

Last but not least, I also want to mention my family. Thank you for always putting your confidence in me and in the paths I pursued so far. Tobi, Mutti and Papa, it means a lot to me that you always back me.

